Titre: Title:	Direct-write microfabrication and characterization of single-chamber micro solid oxide fuel cells with coplanar electrodes
Auteur: Author:	Melanie Kuhn
Date:	2009
Type:	Mémoire ou thèse / Dissertation or Thesis
Référence: Citation:	Kuhn, M. (2009). Direct-write microfabrication and characterization of single-chamber micro solid oxide fuel cells with coplanar electrodes [Thèse de doctorat, École Polytechnique de Montréal]. PolyPublie. https://publications.polymtl.ca/8287/

UNIVERSITÉ DE MONTRÉAL

DIRECT-WRITE MICROFABRICATION AND CHARACTERIZATION OF SINGLE-CHAMBER MICRO SOLID OXIDE FUEL CELLS WITH COPLANAR ELECTRODES

MELANIE KUHN

DÉPARTEMENT DE GÉNIE MÉCANIQUE

ÉCOLE POLYTECHNIQUE DE MONTRÉAL

THÈSE PRÉSENTÉE EN VUE DE L'OBTENTION

DU DIPLÔME DE PHILOSOPHIAE DOCTOR (Ph.D.)

(GÉNIE MÉCANIQUE)

AVRIL 2009

Your file Votre référence
ISBN: 978-0-494-49420-2
Our file Notre référence
ISBN: 978-0-494-49420-2

UNIVERSITÉ DE MONTRÉAL

ÉCOLE POLYTECHNIQUE DE MONTRÉAL

Cette thèse intitulée:

DIRECT-WRITE MICROFABRICATION AND CHARACTERIZATION OF SINGLE-CHAMBER MICRO SOLID OXIDE FUEL CELLS WITH COPLANAR ELECTRODES

présentée par: KUHN Melanie

en vue de l'obtention du diplôme de: Philosophiae Doctor

a été dûment acceptée par le jury d'examen constitué de:

Mme ROSS Annie, Ph.D., présidente

M. THERRIAULT Daniel, Ph.D., membre et directeur de recherche

M. VENGALLATORE Srikar, Ph.D., membre et codirecteur de recherche

M. TURENNE Sylvain, Ph.D., membre

Mme KESLER Olivera, Sc.D., membre

Dedication

I dedicate this work to my parents, Axel and Ursula Kuhn, for all their encouragement and support.

Acknowledgements

I wish to thank my supervisor Prof. Daniel Therriault and co-supervisor Prof. Srikar Vengallatore for the interesting subject and the opportunity to work in the fascinating field of single-chamber solid oxide fuel cells. I am very grateful for their continued support throughout the course of this project as well as the many interesting discussions. Their guidance and scientific input have been of great value in completing this project and for my academic development. Additionally, I am thankful for the many opportunities to present my work at national and international conferences.

Funding for this project was provided by the Fonds Québécois de la Recherche sur la Nature et les Technologies (FQRNT) and the Canadian Foundation for Innovation. Additionally, a doctoral research scholarship was granted by the FQRNT.

I would like to thank Prof. Michel Meunier from the Department of Engineering Physics at École Polytechnique for the close collaboration between our research groups and for giving me the possibility of using their single-chamber testing setup. Without this testing station many of the results presented in this work would not have been possible. Therefore I also thank Jean-Paul Lévesque and Yves Drolet for their technical support with the testing setup.

I would like to express my thanks to Dr. Teko W. Napporn, who introduced me to single-chamber solid oxide fuel cells and helped me to understand the working principles of these fuel cells. His expertise in the field and his enthusiasm and inspiring manner were of immense benefit for the realization of this work.

I would like to thank Prof. Jennifer A. Lewis for having given me the opportunity to work in her laboratory at the Department of Materials Science and Engineering at the University of Illinois at Urbana-Champaign during a two-month visit. I also thank Dr. Ranjeet B. Rao for his help with the fabrication of viscoelastic inks.

I wish to thank my current and past group members, especially Dr. Christian Fauteux, Louis Laberge-Lebel, Nicolas Lourdel, Aurélie Mougeot and Cécile Czulewycz, for their friendship and colleagueship.

I would like to extend my thanks to my friends in Germany for maintaining our friendship despite the long distance and for their various visits here in Montreal.

I would also like to thank Guillaume Lambotte for his support and encouragement, especially during the difficult moments. I additionally thank him for helping me with the thermodynamic calculations. I am thankful for the great time we spent together in Canada.

Finally, I wish to thank my parents for their encouragement and continued support over the past years.

Résumé

Les piles à combustible à oxyde solide à chambre unique « single-chamber solid oxide fuel cells » (SC-SOFCs) éliminent les problèmes liés au scellement nécessaire dans les SOFCs conventionnelles grâce à l'utilisation d'un mélange de combustible et d'oxydant, et sont une approche prometteuse pour la simplification de la conception des piles. Le principe de fonctionnement est basé sur la sélectivité des électrodes pour l'oxydation du combustible à l'anode et la réduction de l'oxydant à la cathode. Le mode d'opération en chambre unique permet le développement de nouvelles configurations de piles comme les SC-SOFCs avec électrodes coplanaires où l'anode et la cathode sont situées sur le même côté d'un substrat d'électrolyte. La miniaturisation de la largeur des électrodes et de la distance entre les anodes et cathodes adjacentes mène à une réduction de la résistance ohmique de la pile et une amélioration de sa performance. Cependant, le fonctionnement de ces SC-microSOFCs (SC-μSOFCs) n'est pas encore complètement compris, notamment à cause du manque de techniques de microfabrication appropriées.

L'objectif principal de cette thèse est d'évaluer la méthode d'écriture directe pour la fabrication de SC-μSOFCs avec électrodes coplanaires, ainsi que de caractériser les propriétés des piles fabriquées dans le but d'approfondir les connaissances sur cette technologie. L'écriture directe consiste en l'extrusion du matériau d'électrode sous forme d'encre à travers une micro-aiguille et sa déposition assistée par robot sur l'électrolyte suivant une forme désirée. Les encres ont été fabriquées à partir de matériaux d'électrodes conventionnellement employés dans les SOFCs en adaptant à l'écriture directe des encres utilisées pour l'épandage. Des structures de micro-électrodes coplanaires de différentes géométries et tailles ont ainsi été réalisées. En revanche, le comportement newtonien des encres entraîne de légères variations des dimensions des électrodes et de la distance inter-électrode. L'élaboration d'encres viscoélastiques a permis d'améliorer la stabilité dimensionnelle des électrodes et de mieux contrôler leur largeur et espacement.

Dans un deuxième temps, la caractérisation électrochimique des piles avec des électrodes coplanaires interdigitées a été effectuée à 700°C dans un mélange

méthane-air. Des voltages en circuit ouvert autour de 0,8 V et des puissances électriques de quelques mW/cm^2 ont été mesurés, confirmant ainsi la faisabilité de SC-μSOFCs avec électrodes coplanaires par écriture directe et l'utilisation de telles piles pour des applications de piles à combustible de quelque mW.

Ensuite, les limites de la miniaturisation de telles micro-piles à combustible ont été étudiées en utilisant des piles constituées d'une seule ligne par électrode. En dessous d'une largeur critique, la génération d'un voltage et d'une puissance électrique n'est pas possible à cause de la petite surface active des électrodes qui empêche un gradient stable de pression partielle d'oxygène de s'établir entre les micro-électrodes. Cette limite à la miniaturisation peut être compensée en créant des structures d'électrodes interdigitées. Des largeurs inférieures à la taille critique permettent de réduire la résistance ohmique tandis que l'utilisation de plusieurs lignes par électrode augmente la surface des électrodes et la stabilité du voltage. Ces résultats originaux démontrent que, malgré le consensus général sur la nécessité de réduire les dimensions des électrodes et les prédictions par modélisation de performances optimales pour des électrodes de quelques micromètres de large, des limites à la miniaturisation doivent être prises en compte lors de la conception et la fabrication des piles. Par ailleurs, ces observations présentent une confirmation expérimentale de l'utilisation avantageuse de structures de micro-électrodes interdigitées par rapport à une seule ligne par électrode.

De plus, l'impact de la géométrie des électrodes, de la méthode de collecte de courant et de la nature des matériaux composant les électrodes sur le fonctionnement des piles a également été étudié. La preuve a été faite dans cette thèse de la faisabilité de SC-μSOFCs avec électrodes coplanaires de géométries arbitraires et complexes. En outre, la forme n'affecte pas de manière significative la performance dans le cas d'électrodes de dimensions comparables. Les limitations de la performance des SC-μSOFCs avec électrodes coplanaires interdigitées dues au long parcours des électrons dans les électrodes et aux pertes ohmiques résultantes sont un fait connu, mais elles ont été quantifiées pour la première fois dans le cadre de cette thèse. La méthode conventionnelle de collecte de courant sur le segment reliant chacune des lignes constituant l'électrode entraîne une perte de 50% de la puissance électrique par rapport à une collecte sur toute la surface de l'électrode. Une anode plus conductrice et plus

riche en nickel n'a pas amélioré la collecte de courant à cause de l'instabilité du nickel dans un mélange combustible-air. Une collecte de courant efficace reste un défi important pour améliorer les performances des SC-μSOFCs avec électrodes coplanaires. Dans le but de déterminer l'influence des matériaux d'électrodes sur le fonctionnement des piles, différentes combinaisons de matériaux ont été testées. L'observation d'interactions chimiques entre des anodes et cathodes très proches démontre la nécessité d'un choix approprié des matériaux par rapport à la performance de la pile ainsi que des possibilités d'interactions chimiques.

Finalement, des considérations théoriques quant à la performance d'une pile ont mis en évidence plusieurs défis pour la modélisation des performances des SC-μSOFCs avec électrodes coplanaires. Ces défis incluent une modélisation exacte de la résistance ohmique lors du transport ionique et électronique, l'étude de la cinétique des réactions aux électrodes dans le mode de fonctionnement en chambre unique et l'effet de l'écoulement des gaz au voisinage d'électrodes très proches. Un modèle simplifié basé sur l'électrochimie permet néanmoins de donner une estimation de la performance des piles constituées d'une seule ligne par électrode et d'établir des critères de conception pour les SC-μSOFCs avec électrode coplanaires.

L'évaluation de l'efficacité des piles a confirmé l'utilisation potentielle des SC-μSOFCs avec électrodes coplanaires dans les applications de cogénération, de capteur et de récolte d'énergie à partir de rejets de gaz dans les systèmes d'échappements industriels et automobiles.

Les travaux menés dans le cadre de cette thèse ont démontré que l'écriture directe est une technique de microfabrication appropriée pour la fabrication de SC-μSOFCs avec électrodes coplanaires. L'utilisation d'encres viscoélastiques constitue une innovation pour la fabrication par écriture directe d'électrodes coplanaires empêchant l'étalement des encres newtoniennes généralement utilisées. Grâce à la flexibilité de la méthode d'écriture directe, une multitude de piles de différentes dimensions, compositions et géométries ont pu facilement et rapidement être réalisées. Plusieurs paramètres influençant les performances des SC-μSOFCs avec électrodes coplanaires ont ainsi été étudiés dans le but d'améliorer le fonctionnement de ces piles

et de rendre leur commercialisation possible pour les applications de développement durable.

Abstract

Single-chamber solid oxide fuel cells (SC-SOFCs) constitute an interesting approach to eliminate gas sealing issues and simplify cell designs of conventional SOFCs due to the use of a mixture of fuel and oxidant. Their working principle is based on the selectivity of the electrodes for either the fuel oxidation at the anode or the reduction of the oxidant at the cathode. Single-chamber operating conditions permit the development of new cell configurations such as coplanar electrode designs, where both anode and cathode are situated on the same side of an electrolyte substrate. Miniaturization of electrode width and the gap between adjacent anodes and cathodes was found essential to reduce the ohmic cell resistance and enable improved cell performance. However, the working principles of such SC-microSOFCs (SC-μSOFCs) with coplanar electrodes are not yet fully understood, partly because of the lack of suitable microfabrication techniques.

This thesis aims at evaluating the robot-controlled direct-write microfabrication technique for creating SC-μSOFCs with coplanar electrodes, and at characterizing the fabricated cells to advance the understanding of this fuel cell technology. Direct-write microfabrication consists of the pressure-driven extrusion of the electrode material in the form of inks through micronozzles and its robotically controlled deposition on the electrolyte substrate in the desired shape. Electrode inks were synthesized from conventional SOFC electrode materials by adapting inks used for screen printing to the direct-writing technique. Coplanar microscale electrode structures of different shapes and geometries were successfully fabricated. The Newtonian flow behavior of the inks, however, caused slight variations in electrode width and interelectrode gap. The development of viscoelastic, gel-like inks improved the shape retention of the deposited electrode structures and led to enhanced control of the electrode dimensions.

In the second part of this thesis, the fabricated cells with interdigitated electrodes were electrochemically characterized at 700°C in a methane-air mixture. The generation of open circuit voltages of ~0.8 V and maximum power densities of a few mW/cm^2 confirmed the feasibility of SC-μSOFCs with coplanar electrodes by direct-write microfabrication and their practicability for fuel cell applications in the mW-range.

Subsequently, the limits to the miniaturization of such micro fuel cells were systematically investigated using cells composed of one line per electrode. Below a critical electrode width, the establishment of a stable OCV and power output was impeded by the small active electrode surface area, which did not enable a stable oxygen partial pressure gradient between the closely-spaced microelectrodes. This miniaturization limit could be circumvented by increasing the number of electrode lines to form interdigitated electrode structures with maximized surface area and reduced ohmic resistance. These original results highlight that, despite the general consensus on the need for microscale electrode structures and model-based predictions of optimal cell performance for electrodes of several microns in width, miniaturization limits must be considered in cell design and fabrication. At the same time, these observations present an experimental confirmation of the advantages of using interdigitated microelectrode patterns as compared to a single line per electrode.

Furthermore, the effects of electrode shape, current collection method and electrode material on cell performance were characterized. A proof-of-concept of SC-μSOFCs with geometrically complex coplanar electrode patterns was provided. Additionally, for electrodes of similar dimensions, differences in electrode shape were found not to significantly affect the cell performance. Performance limitations of SC-μSOFCs with coplanar interdigitated electrodes due to long electronic conduction paths and resulting elevated ohmic resistance are known to the community, but were quantified for the first time in this thesis. A 50% loss in power was observed, when the current was collected, according to the state-of-the-art procedure, on the segment connecting the single lines of the respective electrode and not on the whole electrode surface. The use of a more conductive, nickel-rich anode did not improve current collection because of nickel instability in fuel-air mixtures. An efficient current collection method remains a critical challenge for improving the performance output of these fuel cells. Cells with different combinations of anode and cathode materials were characterized in order to investigate the effect of cell component materials on the cell functioning. The observation of chemical interaction between closely-spaced coplanar cathodes and anodes revealed the need for proper selection of cell component materials, both with respect to cell performance as well as possible interactions.

Finally, theoretical considerations of the cell performance led to the identification of several challenges for modeling the performance of SC-μSOFCs with coplanar electrodes. These challenges include an accurate modeling of the ohmic resistance to ionic and electronic conduction, details of electrode reaction kinetics under single-chamber operating conditions and the effects of gas transport in the vicinity of closely-spaced electrodes. However, a simplified electrochemistry-based model can be used as a tool for predicting the performance of cells composed of one line per electrode and establishing design guidelines for SC-μSOFCs with coplanar electrodes.

Evaluating the fuel utilization and efficiency of the tested cells emphasized the potential use of SC-μSOFCs for cogeneration, as sensors and in energy harvesting applications where waste gases from industrial or automotive exhaust gas streams can be transformed into electricity.

Direct-write microfabrication was shown to be a suitable method for creating SC-μSOFCs with coplanar electrodes. The use of viscoelastic inks constitutes an innovation for the direct-write microfabrication of coplanar electrodes with controlled dimensions by mitigating the ink spreading associated with the conventionally employed Newtonian inks. Due to the versatility and flexibility of direct-writing for creating electrodes of different shapes and materials, various cells of diverse dimensions, compositions and geometries could be easily and quickly synthesized. Different parameters affecting the performance of SC-μSOFCs with coplanar electrodes were characterized to gain more insight into the working principles of these fuel cells and to make their commercialization possible for applications as sustainable, low-pollution energy generating systems.

Condensé en français

Dans un contexte de développement de dispositifs électroniques de petites tailles avec des demandes énergétiques de plus en plus importantes, les piles à combustible sont considérées comme des candidats prometteurs pour améliorer la performance des batteries conventionnelles sous forme de systèmes hybrides ou même pour remplacer complètement ces dernières [1-3]. Les piles à combustible pourraient répondre aux besoins de densités énergétiques élevées, à la miniaturisation, à la réduction du poids, à la nécessité d'autonomie accrue et des temps de rechargement significativement réduits des dispositifs électroniques. De plus, grâce à une grande autonomie, elles seront intéressantes pour des applications dans les endroits peu accessibles où les changements de batterie s'effectuent difficilement.

Les piles à combustible à oxyde solide (l'abréviation du terme anglais « solid oxide fuel cell », SOFC, sera utilisée par la suite) fonctionnent à des températures élevées (300-1000°C) ce qui représente une contrainte quant à leur utilisation pour l'alimentation énergétique de dispositifs électroniques portables. En plus des efforts actuels visant à baisser davantage ces températures, l'utilisation du mode de fonctionnement de chambre unique « single-chamber solid oxide fuel cells » (SC-SOFCs) se révèle prometteuse pour l'implantation de telles piles dans les applications portables et de petite taille. Ayant été proposées pour la première fois en 1993 [4], les SC-SOFCs se différencient des SOFCs conventionnelles par l'utilisation d'un mélange gazeux de combustible et d'oxydant à la place de deux alimentations en gaz séparées. Le principe de fonctionnement des SC-SOFCs se base sur la sélectivité des électrodes pour les réactions d'oxydation du combustible à l'anode et de réduction de l'oxydant à la cathode. L'utilisation d'un mélange de gaz implique que la pile puisse être située dans une simple chambre de réacteur avec une seule entrée et une seule sortie pour les gaz. Les impératifs d'un scellement étanche sont ainsi éliminés, ceci constitue un grand avantage car le scellement représente un défi technique et coûteux dans les SOFCs conventionnelles qui nécessitent une étanchéité parfaite entre la chambre anodique où réagit le combustible, et la chambre cathodique où réagit l'oxydant. Les SC-SOFCs peuvent alors être construites de manière simple et compacte, facilitant leur

intégration dans un dispositif ainsi que leur miniaturisation. De plus, de nouvelles configurations de piles comme les SC-SOFCs avec électrodes coplanaires deviennent possibles. Celles-ci se caractérisent par une disposition côte-à-côte de l'anode et de la cathode sur le même côté de l'électrolyte agissant comme substrat. Dans le cas le plus simple, la pile est constituée d'une ligne d'anode et d'une ligne de cathode, situées parallèlement sur l'électrolyte. Pour maximiser la surface des électrodes, des structures interdigitées ont été proposées [5]. Le transfert des ions oxygène entre cathode et anode se fait par conduction surfacique dans la partie de l'électrolyte située entre les deux électrodes. Afin de réduire les pertes ohmiques liées à cette conduction, il faut réduire la distance inter-électrode et la largeur des électrodes [5-7]. Même si les techniques de lithographie permettent de créer des structures précises à l'échelle du micron, la fabrication de telles piles avec des micro-électrodes coplanaires s'avère un défi technique à cause des contraintes additionnelles liées à l'utilisation de matériaux céramiques multi-composants et la nécessité d'avoir une microstructure poreuse. Des techniques de microfabrication autre que la lithographie sont alors nécessaires. Le manque de techniques de fabrication adéquates limite l'étude de ce type de pile et explique le peu de publications disponibles.

L'objectif principal de cette thèse consiste en l'évaluation d'une technique de microfabrication par écriture directe pour la réalisation de « single-chamber micro solid oxide fuel cells » (SC-μSOFCs) avec électrodes coplanaires. Un outil de fabrication adapté permettra d'étudier différents paramètres influençant la performance des SC-μSOFCs afin de contribuer à l'avancement des connaissances sur les principes de fonctionnement de ces piles, peu connus jusqu'à présent.

La méthode de microfabrication par écriture directe « direct-write microfabrication » se caractérise par une grande variété de matériaux pouvant être mis en forme, ainsi que par la flexibilité pour créer des structures de géométries différentes. Cette technique est actuellement utilisée par un seul autre groupe de recherche sur les SC-SOFCs qui a débuté ses travaux en même temps que cette thèse [8]. La microfabrication par écriture directe consiste à extruder un matériau sous forme de suspension, encore appelée encre, à travers une micro-aiguille en appliquant une pression. Le filament d'encre extrudé est par la suite déposé sur la surface d'un

substrat dans la forme désirée en utilisant une plate-forme de micropositionnement à trois axes. Pour la fabrication de SC-μSOFCs avec électrodes coplanaires, des matériaux conventionnellement utilisés dans les SOFCs ont été employés [9]. L'anode se compose d'un mélange de NiO et d'oxyde de zirconium stabilisé par de l'oxyde d'yttrium « yttria-stabilized zirconia » (YSZ) tandis que la cathode est formée de $(La_{0.8}Sr_{0.2})_{0.98}MnO_3$ (LSM). Ces deux matériaux sont sous forme de poudre et sont mis en suspension en utilisant un solvant organique, un liant et un dispersant. La préparation de l'encre est basée sur les suspensions habituellement utilisées pour l'épandage d'électrodes planes [10]. Afin de pouvoir utiliser ces encres pour la mise en forme d'électrodes coplanaires par écriture directe, des ajustements ont été nécessaires par rapport à la viscosité. La viscosité de ces encres de comportement rhéologique newtonien a pu être adaptée pour permettre une extrusion et un dépôt homogènes grâce à un chargement en particules élevé. Cela est aussi favorable lors du frittage des piles afin d'obtenir la formation d'un réseau de particules bien liées entre elles.

L'ajustement des paramètres principaux du procédé d'écriture directe, la pression d'extrusion et la vitesse du système de positionnement, a été la prochaine étape pour la fabrication de structures d'électrodes. Le dépôt de simples lignes d'électrode à des combinaisons de pressions et de vitesses différentes et l'étude de la qualité des lignes déposées ont servi à établir une cartographie du procédé. Celle-ci a permis de déterminer un couple de pression d'extrusion et de vitesse de dépôt pour la fabrication de structures d'électrodes homogènes et continues sur des substrats d'électrolyte en YSZ.

Comme l'anode nécessite une température de frittage plus élevée que la cathode, l'anode est fabriquée et frittée avant la cathode. Par la suite, la cathode est déposée entre les lignes d'anode afin de former une structure d'électrodes interdigitées. Or, l'alignement de la cathode pour avoir des électrodes parfaitement parallèles se révèle difficile. C'est pour cela que, pour la suite de la fabrication des piles, l'anode et la cathode ont été déposées l'une après l'autre sans bouger le substrat d'électrolyte. La pile a été frittée à une température intermédiaire. La microstructure des piles après frittage a été caractérisée par microscopie électronique à balayage pour évaluer leur porosité et homogénéité microstructurale. Les dimensions des piles, comme la surface

des électrodes, la largeur des électrodes et la distance inter-électrode ont été déterminées à partir d'images optiques et en utilisant un logiciel de traitement d'images.

Après la fabrication, les piles ont été testées dans un dispositif de test électrochimique mis à disposition par le groupe de recherche du Prof. Meunier et du Dr. Napporn du département de génie physique de l'École Polytechnique. Le Dr. Napporn a développé ce dispositif pour tester des SC-SOFCs de configuration double-face avec anode et cathode situées sur les faces opposées de l'électrolyte. Il a donc été nécessaire de modifier le support des piles et les collecteurs de courant pour accueillir les piles unifaces à électrodes coplanaires. Les courants générés par ces piles de taille d'électrodes bien inférieure à celle des piles double-faces sont trop faibles pour être mesurés avec l'installation. Un système manuel a alors été mis en place pour tester les piles en faisant varier la valeur de la résistance d'une résistance à décade. Les valeurs respectives du voltage et du courant ont pu être lues à l'aide d'une centrale d'acquisition.

La température d'opération d'une pile à combustible est imposée par le matériau constituant l'électrolyte. Le transport des ions oxygène dans l'électrolyte étant un processus activé thermiquement, la conductivité de l'électrolyte dépend fortement de la température. Pour les électrolytes en YSZ, une conductivité de 1 S/m est obtenue à 700°C, une température souvent utilisée pour les piles à base d'YSZ [9] ainsi que pour l'intégralité des tests effectués dans le cadre de cette thèse. Méthane et air ont respectivement été choisis comme combustible et oxydant. Le méthane est le combustible le plus utilisé dans les SC-SOFCs, suivi du propane [11]. Le mélange de gaz est caractérisé par le rapport méthane sur oxygène, R_{mix}.

Pour les tests électrochimiques, la pile est située dans une chambre de réacteur à l'intérieur d'un tube cylindrique en quartz. Un autre tube de diamètre inférieur sert à amener le mélange de gaz à la pile. Dans le tube extérieur, la circulation d'azote crée un mouvement de gaz vers la sortie située à l'opposé de l'entrée de la chambre afin d'éviter toute stagnation de gaz. L'ensemble se trouve à l'intérieur d'un four qui est chauffé à 700°C. Le courant généré par les réactions électrochimiques aux électrodes est collecté par des grilles d'or séparément en contact avec l'anode et la cathode. Des fils d'or soudés aux grilles sortent du dispositif et sont reliés à la centrale d'acquisition. Les piles avec une seule ligne par anode et cathode sont fabriquées de sorte que les

deux lignes soient un peu décalées et qu'il y ait une partie libre sur chaque électrode permettant de placer la grille sans court-circuiter la pile. En ce qui concerne les électrodes interdigitées, les grilles sont fixées sur le segment reliant les différentes lignes constituant chaque électrode.

Les piles avec électrodes interdigitées ont donné des voltages en circuit ouvert (appelé par la suite OCV du terme anglais « open circuit voltage ») autour de 800 mV. A titre de comparaison, la valeur théorique de l'OCV se situe aux alentours de 1 V [9]. Les densités maximales de puissance et de courant étaient de 1,3 mW/cm^2 et 12 mA/cm^2 pour une pile avec des distances inter-électrodes de ~500 µm et une largeur moyenne d'électrode de ~140 µm, démontrant que les piles de petite taille d'électrodes (~0,22 cm^2 par électrode) peuvent générer des puissances de l'ordre du mW. Un test de vieillissement de 24 h a engendré des fluctuations de l'OCV à cause de cycles de réduction et d'oxydation du nickel. La perte de nickel dans l'anode a été constatée conformément à des études précédentes sur la stabilité d'anodes à base de nickel utilisées en chambre unique [12, 13]. Après le vieillissement de 24 h, la puissance maximale de la pile a diminué de 15%.

Ces premiers tests constituent la preuve de la faisabilité de SC-µSOFCs avec électrodes coplanaires par écriture directe. La technique a alors été employée pour la fabrication de piles avec électrodes de différentes tailles, compositions et configurations afin d'étudier le fonctionnement des SC-µSOFCs avec électrodes coplanaires.

Des études expérimentales ainsi que la modélisation des performances de SC-µSOFCs avec électrodes coplanaires ont montré que la réduction de la largeur des électrodes et de la distance entre anode et cathode permet de diminuer les pertes ohmiques et d'améliorer la puissance électrique des piles [5-7]. En revanche, des problèmes d'instabilité du voltage lors de test de piles de petite taille d'électrodes ont permis de découvrir l'existence de limites à la miniaturisation des électrodes dans le cadre de cette thèse. Pour des piles avec une seule ligne d'anode et de cathode, la largeur des électrodes joue un rôle important sur le fonctionnement de la pile. Une largeur critique a notamment été identifiée en-dessous de laquelle aucun OCV ne peut être établi. Un OCV a été observé pour les piles avec des électrodes légèrement

supérieures à la taille critique, mais d'importantes fluctuations du voltage ont engendré une puissance instable. En augmentant la largeur des électrodes par rapport à la taille critique, le voltage et la puissance deviennent stables. L'établissement de l'OCV est lié à une différence de pressions partielles entre anode et cathode. Les pressions partielles s'établissent à l'interface avec l'électrolyte. Pour une longueur d'électrode constante, la surface active est déterminée par la largeur des électrodes. Dans le cas d'électrodes fines, la surface catalytique active est réduite, ne permettant pas de générer une différence stable de pressions partielles. En augmentant la largeur des électrodes, la surface active est agrandie ce qui permet une stabilisation des pressions partielles et l'établissement d'un OCV. Par contre, l'augmentation de la largeur accroît le chemin de conduction ionique et les pertes ohmiques de la pile, induisant une diminution de sa puissance. Pour les piles avec des électrodes inférieures à la largeur critique, les limites à la miniaturisation peuvent être compensées en augmentant le nombre de lignes par électrode. Ces structures d'électrodes interdigitées permettent notamment d'augmenter la surface active comme dans le cas des électrodes plus larges des piles simples mais tout en maintenant une résistance ohmique faible.

Par ailleurs, la flexibilité de l'écriture directe pour la création de structures de toute forme a permis la fabrication de piles avec des électrodes de géométries arbitraires et complexes. Deux piles dont les électrodes constituent les lettres des mots « POLY » et « SOFC » ont été fabriquées. Dans les deux cas, la surface des électrodes, la largeur des électrodes et la distance inter-électrode sont respectivement d'environ 0,1 cm^2, 240 µm et 460 µm. Le test électrochimique de ces piles a démontré la viabilité de piles avec des électrodes de formes non-conventionnelles. De plus, les deux piles ont délivré une puissance maximale de 2,3 mW/cm^2 indépendamment de la forme des électrodes. En conclusion, pour les piles avec des électrodes de formes différentes, mais de dimensions (largeur et surface des électrodes, distance inter-électrode) semblables, la forme de l'électrode ne semble pas affecter la performance de la pile.

La collecte de courant s'effectue difficilement sur les piles avec des micro-électrodes interdigitées à cause de la petite taille et du risque de court-circuit. Par contre, en plaçant les collecteurs de courant juste sur le segment reliant chacune des lignes composant l'électrode, les électrons générés à l'interface avec l'électrolyte dans ces lignes doivent effectuer un long parcours jusqu'aux collecteurs, menant à une

augmentation de la résistance ohmique [13]. Afin de caractériser l'effet de la méthode de collecte de courant sur les pertes ohmiques de la pile, des piles avec une cathode plane et une anode sous forme de peigne sur les côtés opposés de l'électrolyte ont été fabriquées. La collecte de courant a été effectuée sur toute la surface de la cathode tandis que pour l'anode le courant a été collecté en appliquant les grilles d'or soit sur toute la surface ou juste sur le segment reliant les lignes du peigne. Cette approche a permis de montrer que la collecte sur le segment engendrait une augmentation de la résistance ohmique de 37% et une perte de 50% en puissance en comparaison avec la collecte sur toute la surface. Afin de compenser pour le chemin de conduction plus long et la résistance plus élevée, l'anode a été enrichie en nickel pour augmenter sa conductivité électronique. Cependant, l'instabilité du nickel dans les mélanges méthane-air à haute température [12, 13] n'a pas produit l'augmentation de la performance attendue. L'identification de méthodes de collecte de courant plus efficaces pour les SC-μSOFCs avec électrodes coplanaires reste un défi de taille.

Un noircissement de l'anode à proximité des cathodes en LSM a été observé pour toutes les piles après le frittage. Des analyses chimiques ont permis de mettre en évidence la présence de manganèse dans l'anode, probablement due à un mécanisme de diffusion du manganèse de la cathode vers l'anode. L'effet de cette interaction chimique sur les performances des piles n'est pas connu, mais la formation de nouvelles phases pourrait changer le comportement électrochimique de l'anode face aux réactions. Des études de spectroscopie d'impédance seraient nécessaires pour éclaircir davantage ces phénomènes et de mesurer les résistances spécifiques des électrodes. Par ailleurs, ces résultats démontrent la nécessité d'un choix de matériaux appropriés pour les électrodes coplanaires. L'utilisation de cathodes en $(La_{0.6}Sr_{0.4})_{0.995}(Fe_{0.8}Co_{0.2})O_3$ en combinaison avec les anodes en nickel évite les problèmes d'interaction chimique, mais l'activité catalytique de ce matériau pour le combustible semble réduire la performance de la pile. Les matériaux d'électrodes devraient donc être choisis afin d'empêcher toutes interactions chimiques et de garantir le bon fonctionnement de la pile.

Comme la performance des piles dépend des dimensions des électrodes, un contrôle très précis des dimensions est nécessaire lors de la fabrication. Avec les encres newtoniennes, les électrodes déposées ont tendance à s'étaler sur l'électrolyte

après dépôt rendant ce contrôle difficile. Des encres de comportement viscoélastique ont alors été élaborées. Ces encres se comportent comme un fluide sous l'application d'une contrainte et comme un solide en absence d'une sollicitation. Elles peuvent être facilement extrudées et maintiennent leur forme après le dépôt sans trop s'étaler. Des électrodes avec des sections transversales rectangulaires ainsi que des épaisseurs et largeurs de l'ordre du diamètre de l'aiguille d'extrusion (~100 μm) ont pu être réalisées. Malheureusement les piles ainsi fabriquées n'ont pas pu être testées à cause du décollement de l'anode du substrat d'électrolyte lors du frittage. La rupture de l'anode épaisse est probablement causée par la différence de coefficient d'expansion thermique entre le NiO de l'anode et le YSZ de l'électrolyte [9].

Un modèle simplifié basé sur l'électrochimie a été utilisé pour calculer la performance théorique des piles et comparer celle-ci avec les performances obtenues expérimentalement. Ce modèle permet le calcul du voltage de la pile en fonction du courant. Le voltage lors du fonctionnement de la pile est équivalent à la valeur de l'OCV moins les pertes liées à la résistance ohmique et à l'activation des réactions aux électrodes. L'OCV a été déterminé à partir du calcul de l'équilibre thermodynamique d'un mélange de méthane et d'air à 700°C. Les différences entre l'OCV théorique et l'OCV expérimental peuvent être attribuées aux réactions non désirées dans les piles réelles à cause de la sélectivité insuffisante des électrodes. Une approche simplifiée, basée sur la conduction des ions dans l'électrolyte entre les deux électrodes [7], a été utilisée pour le calcul des pertes ohmiques. La résistance ohmique liée aux transports des électrons dans les électrodes a été négligée. Pour les piles constituées d'une seule ligne par électrode, ayant une largeur moyenne entre 800 et 900 μm, cette approche a permis une bonne évaluation des pertes ohmiques. En revanche, dans le cas des piles avec des électrodes plus larges ou des piles avec des structures d'électrodes interdigitées, les résistances calculées sont plus faibles que les résistances réelles. Ceci indique la nécessité d'établir un modèle plus détaillé des pertes ohmiques en utilisant par exemple une méthode par éléments finis. L'utilisation d'une telle méthode permettra de représenter la conduction ionique dans l'électrolyte entre anode et cathode et d'intégrer la résistance ohmique liée aux transports des électrons. De plus, le ou les mécanismes de conduction ionique (purement surfacique ou combinaison surfacique/volumique) et l'influence de l'épaisseur de l'électrolyte seront à identifier.

Des expériences préliminaires ont d'ailleurs montré que l'épaisseur de l'électrolyte influence la performance des piles. Les pertes d'activation ont été calculées en utilisant l'équation de Butler-Volmer qui décrit la cinétique des réactions électrochimiques aux électrodes. La comparaison entre la performance obtenue expérimentalement et celle calculée a montré que le modèle utilisé permet une bonne estimation des performances des piles constituées d'une seule ligne par électrode. Pour ces piles, le modèle pourrait servir d'outil simple de prédiction de performances et d'évaluation de critères de conception. Cependant, un modèle plus complexe est nécessaire afin de calculer plus précisément les performances des SC-μSOFCs avec électrodes coplanaires de différentes formes et tailles. Ce modèle devra notamment prendre en compte l'écoulement des gaz et leur transport aux électrodes. La modélisation de l'écoulement des gaz s'avère complexe à cause de l'interaction des gaz entre des électrodes rapprochées, des changements locaux de température, de composition de gaz et de pression. De plus, le calcul des pertes d'activation nécessitera une connaissance plus approfondie des constantes de cinétique de réactions des matériaux d'électrodes dans les conditions de chambre unique.

L'évaluation de l'efficacité des piles testées (< 1%) a confirmé l'existence d'obstacles techniques à l'utilisation des SC-μSOFCs comme sources d'énergie de type batterie [14, 15]. Même si les SC-μSOFCs peuvent générer une puissance de l'ordre du mW nécessaire pour alimenter des dispositifs électroniques de petite taille, la faible utilisation du combustible et la faible efficacité impliquent plutôt une utilisation dans des domaines de la génération d'énergie à partir de rejets de gaz comme par exemple des gaz d'échappement [16]. Les SC-μSOFCs pourraient aussi être combinées avec des piles conventionnelles en agissant comme un convertisseur de combustible et en fournissant de la chaleur. Leur petite taille permettrait également une intégration avec des micro-dispositifs électromécaniques sur un même substrat. Des applications comme capteurs de température, de gaz ou de pression dans des environnements de mélanges gazeux à haute température sont aussi envisageables.

En résumé, il a été démontré que l'écriture directe est une technique adéquate pour la fabrication de SC-μSOFCs avec électrodes coplanaires. Le comportement

rhéologique de l'encre influençant l'uniformité et les dimensions des structures déposées, les encres viscoélastiques permettent une meilleure stabilité dimensionnelle des structures déposées. La fabrication de piles est néanmoins possible avec les encres newtoniennes basées sur l'épandage en ajustant de façon appropriée la viscosité de l'encre et les paramètres de déposition.

Avec la méthode de l'écriture directe, des piles avec des électrodes coplanaires de différentes configurations et tailles ont été fabriquées pour la caractérisation de différents paramètres influençant le comportement de ces piles. Entre autre, l'existence de limites à la miniaturisation, l'interaction chimique entre les matériaux d'électrodes et l'effet de la collecte de courant sur les performances des piles ont été identifiés. Ces résultats imposent de nouveaux critères sur la configuration des électrodes, le choix de matériaux et les conditions de test. Néanmoins, à cause de la multitude des paramètres (dimension des électrodes, sélectivité des matériaux, interaction entre les matériaux, paramètres de test, conception du dispositif de test, méthode de fabrication, morphologie des électrodes, etc.) influençant les performances et les différentes combinaisons possibles entre ces paramètres, le principe de fonctionnement des SC-μSOFCs avec électrodes coplanaires n'est pas encore entièrement compris. Afin d'approfondir les connaissances sur cette technologie de pile à combustible, les démarches suivantes sont proposées. Des analyses de la composition des gaz de sortie, des mesures de résistances de la pile à l'aide de spectroscopie d'impédance, des mesures de gradients de température par thermocouple seraient à envisager. La faible efficacité des piles est fortement liée à la sélectivité insuffisante des matériaux d'électrodes pour les réactions d'oxydation du combustible à l'anode et la réduction de l'oxygène à la cathode. Le développement de nouveaux matériaux sélectifs est nécessaire pour l'amélioration de la technologie des SC-μSOFCs. Finalement, le développement de modèles sur le transport ionique et électronique ainsi que sur l'écoulement des gaz entre des électrodes adjacentes et de petite taille permettrait de faciliter l'interprétation des phénomènes se déroulant dans les SC-μSOFCs avec électrodes coplanaires. Par la réalisation de ces démarches, le fonctionnement des SC-μSOFCs pourra être significativement amélioré ce qui pourra accélérer leur mise en œuvre dans des applications réelles.

Table of contents

List of tables

List of figures

List of symbols and abbreviations

Symbols

$A_{electrode}$	Electrode area (cm^2)
d	Interelectrode distance (μm, mm)
ΔG	Gibbs free energy (kJ/mol)
ΔG^0	Standard Gibbs free energy (kJ/mol)
ΔH	Enthalpy change (kJ/mol); enthalpy of combustion (kcal/mol)
E	Voltage (mV, V)
E^0	Standard reversible cell potential (mV, V)
E_{cell}	Cell voltage (mV, V)
E_L	Voltage losses due to gas cross leakage, side reactions, etc. (mV, V)
E_r	Nernst or reversible cell voltage (mV, V)
F	Faraday constant (96485 C/mol)
G'	Storage or elastic modulus (Pa)
G''	Loss or viscous modulus (Pa)
i	Current density (mA/cm^2)
i_0	Exchange current density (mA/cm^2)
$i_{0,c}^*$	Mean value of measured cathode exchange current densities (mA/cm^2)
I	Current (μA, mA, A)
I_t	Theoretical current for 100% electrochemical conversion of fuel (A)
k	Constant
K	Viscosity parameter
L	Overlapping electrode length (mm)
LFL(25°C)	Lower flammability limit at 25°C
LFL(T)	Lower flammability limit at a specific temperature
m'_F	Mass flow rate of fuel (g/s)
M	Molar mass (g/mol)
n	Number of electrons; shear-thinning exponent
n_{th}	Number of electrons being released by theoretical reactions
p	Gas partial pressure (atm)

p_{cond}	Ionic conduction path (µm, mm)
$p_{O2,anode}$	Oxygen partial pressure at anode (atm)
$p_{O2,cathode}$	Oxygen partial pressure at cathode (atm)
P	Power (density) (mW, mW/cm^2)
r	Number of electrons transferred in the rds
R	Ideal gas constant (8.31451 J/(mol·K))
R_{mix}	Ratio of methane to oxygen
$R_{mix,LFL}$	Mixing ratio corresponding to the lower flammability limit
$R_{mix,UFL}$	Mixing ratio corresponding to the upper flammability limit
R_{ohm}	Ohmic cell resistance (Ω)
t	Time (s)
t_{el}	Electrolyte thickness (µm, mm)
T	Temperature (°C, K)
UFL(25°C)	Upper flammability limit at 25°C
UFL(T)	Upper flammability limit at a specific temperature
w	Electrode width (µm, mm)
w_{av}	Average electrode width (µm, mm)
$w_{critical}$	Critical electrode width (µm)
$w_{effective}$	Useful or effective electrode width (µm)
w_{nozzle}	Inner diameter of extrusion micronozzle (µm)
x	Scaling exponent; portion of electrode width
y	Mechanical property of colloidal, gel-like ink

Greek symbols

α	Charge transfer coefficient
α_1, α_2	Charge transfer coefficient for anodic and cathodic electrode reaction
β	Symmetry factor
ε_{cell}	Cell efficiency
ε_f	Current or faradaic efficiency
ε_{FU}	Fuel utilization
ε_p	Potential efficiency

ε_s	System efficiency
ε_{th}	Theoretical or thermodynamic efficiency
ϕ	Particle loading; weight fraction of electrode powders; colloid volume fraction of gel-like ink
ϕ_{gel}	Colloid volume fraction at gel point
γ	Number of electrons transferred in the steps prior to the rds
$\dot{\gamma}$	Shear rate (s^{-1})
η^*	Complex viscosity (Pa·s)
η_{act}	Activation polarization (mV, V)
η_{conc}	Concentration polarization (mV, V)
ν'	Number of times the rds occurs
σ	Standard deviation
σ_{ionic}	Ionic conductivity (S/m)
τ	Shear stress (Pa)
τ_y	Shear yield stress (Pa)

Abbreviations

AFC	Alkaline fuel cell
BET	Brunauer, Emmett, Teller
BSCF	Strontium and iron doped barium cobaltite
CHP	Combined heat and power
CTE	Coefficient of thermal expansion
DMFC	Direct-methanol fuel cell
EDX	Energy-dispersive X-ray
FEM	Finite element method
GDC	Gadolinium doped ceria
LFL	Lower flammability limit
LSCF	Strontium and iron doped lanthanum cobaltite
LSGM	Strontium and magnesium doped lanthanum gallate
LSM	Strontium doped lanthanum manganite
MCFC	Molten carbonate fuel cell

MEMS	Microelectromechanical system
μSOFC	Micro solid oxide fuel cell
OCV	Open circuit voltage
PAA	Polyacrylic acid
PAFC	Phosphoric acid fuel cell
PEI	Polyethyleneimine
PEM	Proton exchange membrane
PEMFC	Proton exchange membrane fuel cell
PVB	Poly(vinyl butyral-co-vinyl alcohol-co-vinyl acetate)
rds	Rate determining step
sccm	Standard cubic centimeters per minute (cm^3/min)
SC-SOFC	Single-chamber solid oxide fuel cell
SC-μSOFC	Single-chamber micro solid oxide fuel cell
SDC	Samarium doped ceria
SEM	Scanning electron microscopy
SOFC	Solid oxide fuel cell
SSC	Strontium doped samarium cobaltite
TPB	Triple phase boundary
UFL	Upper flammability limit
vol	Volume
wt	weight
YSZ	Yttria-stabilized zirconia

Subscripts

a	Anode
c	Cathode
calc	Calculated
F	Fuel
in	Inlet
m	Measured
max	Maximum
out	Outlet

Introduction and aim of the thesis

I. Background

"I believe that water will one day be employed as fuel, that hydrogen and oxygen which constitute it, used singly or together, will furnish an inexhaustible source of heat and light, of an intensity of which coal is not capable."

–Jules Verne, The Mysterious Island, 1874.

During an era of full industrial development relying on the utilization of coal as the principal fuel, Jules Verne already stated this visionary idea of a future based on efficient, renewable energy sources such as hydrogen fuel from water. Although fossil fuels have long been our principal source of energy, their limitations to satisfy the increasing energy demand worldwide cannot be denied. Our resources of fossil fuels will one day be completely exhausted or be too difficult to extract. Price fluctuations, unstable markets and dependence on import and export impose reliability issues on the accessibility of fossil fuels. Additionally, the pollution resulting from the exploitation and use of fossil fuels raises environmental concerns.

Thus, there is a need for alternative, environmentally friendly and renewable energy sources. In addition to solar, wind and hydro energy, fuel cells are being considered for renewable and clean energy production and are one of the most attractive energy conversion systems due to their elevated efficiency and low pollution. Similarly to a combustion engine, a chemical fuel such as hydrogen is used as energy source. However, like in batteries, the chemical energy is converted directly into electrical energy, leading to significantly higher efficiencies than those of combustion engines.

Fuel cells are a key technology for clean and efficient generation of electrical power with applications ranging from power plants in the MW and kW size range, to the automotive industry, transportation, housing and finally to portable power applications like laptop computers, mobile phones and small-scale devices (e.g., sensors) down to the μW range. Although batteries are still our primary energy source for powering portable, multifunctional and wireless electronics, the need for enhanced power, longer operation time and quick recharging is growing with the development of new electronic

devices. Batteries might not be able to keep pace with the increasing energy demands [1]. However, micro fuel cells are becoming attractive candidates for supplying power to small-scale and mobile devices [2, 3].

The use of solid oxide fuel cells (SOFCs) as battery replacements or rechargers might seem questionable at first sight due to the elevated operating temperatures (300-1000°C). However, the concept of single-chamber operation opens new doors to thermally self-sustainable, miniaturized fuel cells [15]. In single-chamber SOFCs (SC-SOFCs), a mixture of fuel and oxidant is allowed to flow over the cell located in a single gas chamber or reactor [4]. In contrast to conventional dual-chamber operation, where the fuel and oxidant are supplied separately to the electrodes, the use of a gas mixture eliminates the need for complex and expensive gas-tight sealing and gas manifolding. Cells can thus be developed in very simple and compact designs, allowing easy cell stack fabrication and packaging of the final device. Within the current efforts of downsizing fuel cells for small- and microscale applications, SC-SOFCs are thus ideally suited for miniaturization.

II. Problem definition

Single-chamber operation allows the development of new cell designs such as SC-SOFCs with coplanar electrodes located on the same side of the electrolyte [5]. These cells consist of a single pair of parallel anode and cathode lines (one line per electrode) or interdigitated electrode patterns (comblike electrodes composed of multiple lines) in order to maximize the electrode area. A schematic representation of such a cell with coplanar interdigitated electrodes is shown in Fig. I1.

The transport of oxygen ions from cathode to anode occurs via surface ionic conduction in the electrolyte part bridging the gap between the adjacent electrodes [5]. In order to reduce the ohmic resistance for the ionic conduction and increase the cell performance, the conduction path, composed of the interelectrode distance and electrode width (Fig. I2), needs to be reduced [5-7, 17]. Theoretical considerations and performance modeling predict optimal performance for electrode width and interdistance on the order of a few microns [7, 18]. Experimental work on single coplanar anode and cathode lines confirmed the reduction of the ohmic resistance and increase in the cell power output by decreasing electrode width and gap size [5, 6, 17].

The interdigitated electrode design permits the combination of closely-spaced microscale electrodes for reduced ohmic cell resistance while maximizing the electrode area [5].

However, the fabrication of SC-microSOFCs (SC-μSOFCs) with coplanar microelectrodes faces several challenges in addition to their small size. The electrodes are generally composed of complex ceramic materials such as NiO-YSZ (yttria-stabilized zirconia) for the anode and strontium doped lanthanum manganite (LSM) for the cathode. A porous electrode microstructure (25-40 vol% [19]) is required to enable gas transport to the reaction sites at the electrode-electrolyte interface and to increase the active surface area.

Although standard microfabrication techniques such as lithography-based techniques feature the required resolution to create electrode patterns at the microscale, it is difficult to fabricate porous electrode structures of different complex ceramic materials on the same side of an electrolyte substrate. Therefore, conventional ceramic processing techniques are more convenient, as they enable the creation of electrode patterns from colloidal suspensions of the respective electrode material and permit microstructural control during a subsequent sintering step [9].

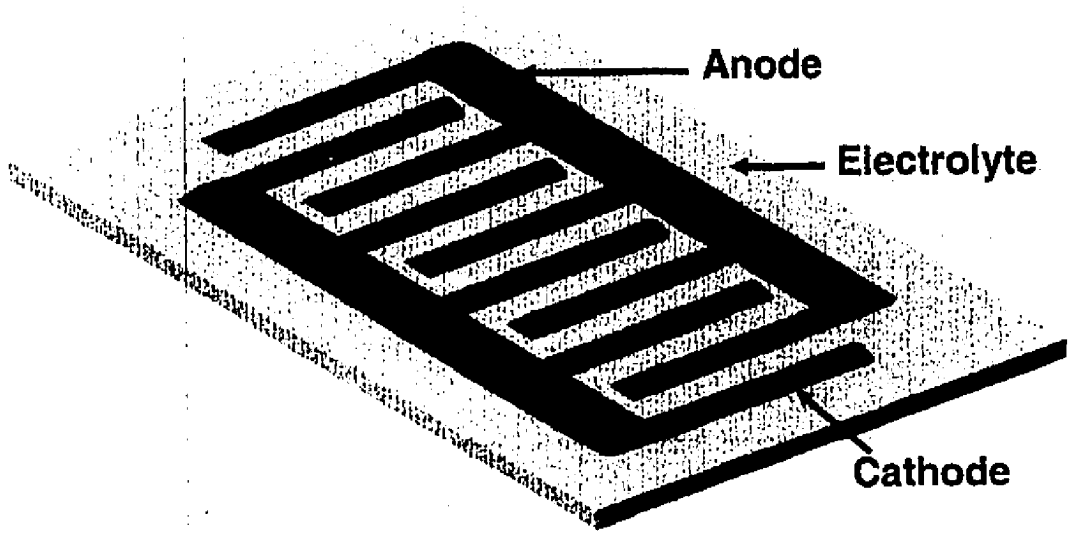

Figure I1: Schematic representation of SC-SOFC with coplanar interdigitated electrodes.

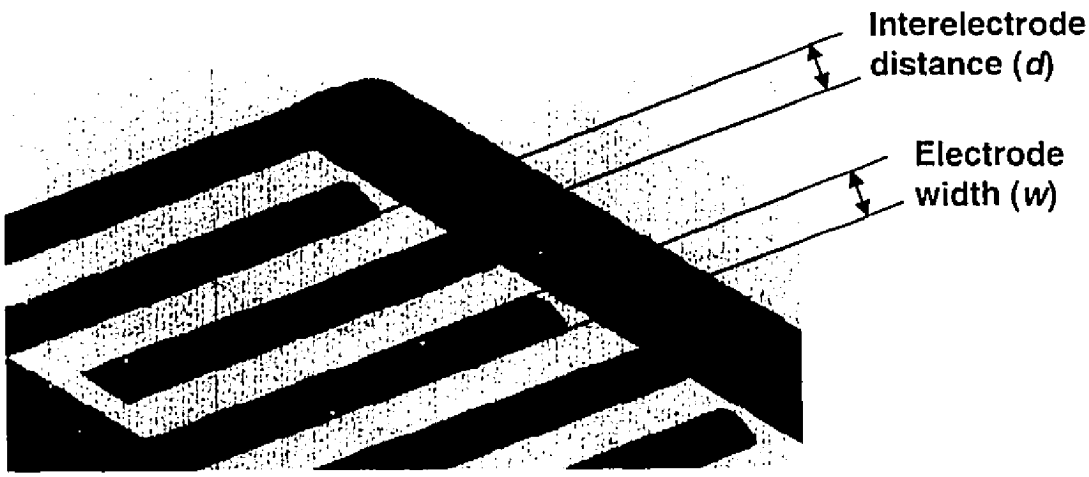

Figure I2: Schematic illustration of interelectrode distance and electrode width.

SC-SOFCs with coplanar anode and cathode were thus fabricated by screen printing [6, 13] or by smearing electrode suspensions on the electrolyte with a brush [5]. A major drawback of these techniques is the requirement for masks and brushes, imposing limits on electrode miniaturization and the fabrication of interdigitated microelectrode patterns. For instance, the minimum electrode width and interelectrode distance for a cell with a single electrode pair fabricated by screen printing were 0.5 and 0.2 mm, respectively [6]. Micromolding in capillaries [13] and microfluidic lithography [20] have been proposed for the fabrication of interdigitated microelectrode patterns. However, these techniques also rely on the use of molds, and the flexibility for easily creating different electrode designs and dimensions is limited by fabricating different molds each time. Additionally, reproducibility issues when filling the microchannels of the molds were stated [13].

The lack of suitable microfabrication techniques not only limits the feasibility of SC-μSOFCs with coplanar electrodes, but also the possibility to perform comprehensive investigations of their working principles and to assess the parameters influencing the cell performance. Only a few studies on SC-SOFCs with coplanar electrodes can be found in the literature, mainly providing general feasibility studies and focusing on operating parameters such as gas mixing ratio [6, 13, 21], flow rate [21], orientation of the electrodes with respect to the gas flow direction [6, 21] and the effect of electrolyte roughness [17]. However, despite the general consensus on the necessity to decrease

electrode width and interelectrode gap, the optimal electrode sizes or the existence of possible miniaturization limits are not known. No comprehensive studies on the effect of electrode and electrolyte material on cell performance or possible interaction between adjacent anodes and cathodes have been conducted yet. The exact mechanism of the oxygen ion conduction and the possibility of gas intermixing between closely-spaced electrodes need to be further clarified.

Thus there is a need to find suitable microfabrication tools for the easy and flexible fabrication of SC-μSOFCs with coplanar electrodes in different patterns (i.e., single electrode pairs or interdigitated designs) and for enabling further investigations of the working principles and the parameters affecting the cell performance. In this project, a robot-controlled direct-writing technique is used to fabricate SC-μSOFCs with coplanar electrodes. Direct-writing obviates the use of molds and permits fast, low-cost and versatile manufacturing. This technique is currently employed by only one other research group for the fabrication of SC-μSOFCs with coplanar microscale electrodes [8, 21]. With their first publication in 2006 [8], their research probably began in parallel with or a little before this thesis work.

III. Objectives

The overall goal of this work is to study the feasibility of SC-μSOFCs with coplanar microelectrodes and to advance the scientific understanding of their working principles. This dual goal implies the use of a suitable microfabrication technique and the investigation of different cell and testing parameters affecting the cell performance output. The first objective of this thesis (objective 1) is therefore to demonstrate the fabrication of closely-spaced, interdigitated coplanar microscale electrodes for SC-μSOFCs using a robot-controlled direct-write microfabrication method. Objective 2 consists in characterizing the electrochemical performance of the fabricated cells in order to confirm their feasibility by the direct-write fabrication approach and their suitability for fuel cell applications. The third objective (objective 3) is to investigate the effect of electrode size on cell performance and stability with respect to the ongoing efforts of miniaturizing SC-μSOFCs with coplanar electrodes. Benefiting from the versatility and flexibility of the direct-writing technique, objective 4 addresses the

feasibility of SC-μSOFCs with new electrode geometries. The influence of different parameters such as current collection method, electrode material and electrolyte thickness is characterized with respect to the cell performance (objective 5). Finally, a simplified electrochemistry-based modeling approach is used to calculate the theoretical cell performance with regard to cell performance prediction and establishing cell design guidelines (objective 6).

IV. Methodology

With respect to objective 1, anodes and cathodes were fabricated by a robot-controlled direct-write microfabrication technique, which consists of the pressure-driven extrusion of an ink or suspension of the respective electrode material through a micronozzle and its robot-controlled deposition in the desired shape on an electrolyte substrate. Anodes and cathodes were fabricated from conventional SOFC electrode materials, that is, NiO-YSZ and LSM, respectively. The electrolyte material was YSZ. In the first approach, inks were prepared based on conventional ceramic powder processing recipes used, e.g., for screen printing. As the control of electrode width and interelectrode spacing is crucial for the performance of SC-μSOFCs with coplanar electrodes, the preparation and use of viscoelastic, gel-like inks was also addressed. Viscoelastic inks were reported for the direct-write microfabrication of three-dimensional structures with elevated shape retention after deposition [22, 23]. In addition to ink composition and rheology, the influence of the process parameters (e.g., extrusion pressure and deposition speed) on the quality of the deposited electrode structures was investigated. The microstructure and dimensions of the fabricated electrodes were analyzed by scanning electron microscopy (SEM) and optical microscopy, respectively. The values reported for interelectrode distance, electrode width, electrode length and electrode area were measured after sintering.

In order to assess the feasibility of SC-μSOFCs with coplanar electrodes by direct-writing (objective 2), the electrochemical performance of the cells was characterized in a fuel-air mixture at 700°C using a single-chamber testing setup. Methane was used as the fuel whereas synthetic air composed of nitrogen and oxygen in a ratio of 4:1 was employed as the oxidant. The methane-to-oxygen ratio, R_{mix}, of the used fuel-air mixtures corresponds to the ratio of methane flow rate to oxygen flow rate.

The flow rates are given in standard cubic centimeters per minute (sccm). For the majority of the tests performed throughout this work, the electrodes were positioned perpendicular to the flow direction of the incoming gas mixture with the cathode being exposed first to the reactant gases, based on previous studies on the effect of electrode position as to the gas flow [6]. The measured cell power and current were normalized with respect to the average of the projected surface area of anode and cathode on the electrolyte. In the case of cells with multiple lines per electrode, the electrode surface area also included the connecting segment in addition to the single electrode lines.

For the realization of objective 3, cells with one pair of electrodes of different widths, cells with varying numbers of electrode pairs, but similar electrode dimensions, and cell stacks were fabricated using the direct-writing technique and were electrochemically tested. Similarly, cells with coplanar electrodes of arbitrary, geometrically complex shapes were fabricated, followed by electrochemical characterization and comparison of their cell performance (objective 4).

The use of a suitable dual-face cell design enabled the investigation of the effect of current collection method in cells with comblike electrodes (objective 5) without creating complex current collector configurations and causing electrical short circuits between the closely-spaced electrodes. Electrodes of different composition and electrical conductivity were investigated to improve current collection and cell performance. With the direct-writing technique allowing the use of different materials by simply changing the ink, electrodes were fabricated from other materials in addition to NiO-YSZ and LSM (objective 5). Cell performance was compared to determine suitable material combinations for improved power output. Additionally, interaction between closely-spaced adjacent anodes and cathodes was studied using material characterization techniques such as energy-dispersive X-ray analysis (EDX). In order to explore the effect of electrolyte thickness on cell power output (objective 5), interdigitated electrode patterns of similar dimensions were fabricated on electrolyte substrates of different thickness by direct-writing. The different cells were electrochemically tested under identical testing conditions and their performance was compared.

Finally, objective 6 was realized by using a simplified electrochemistry model, which included the calculation of the open circuit voltage (OCV), the ohmic resistance

and the activation polarization in order to obtain the cell voltage as a function of cell current. The calculated performance was compared to the experimentally measured performance of selected cells of this work.

V. Scope

A comprehensive review of the state of the art of solid oxide fuel cells, single-chamber fuel cell technology and direct-write microfabrication is presented in Chapter 1. The scientific approach and the coherence between the research objectives and the publications resulting from the thesis work are described in Chapter 2. Chapters 3 to 7 have either been published [24-26] or been submitted for publication in peer reviewed scientific journals. Chapter 3 presents the direct-write microfabrication and electrochemical characterization of SC-μSOFCs with coplanar electrodes. Chapter 4 discusses miniaturization limits for SC-μSOFCs with coplanar electrodes, and Chapter 5 shows the feasibility of SC-μSOFCs with coplanar electrodes of nonconventional shapes. The effect of current collection method on cell performance is studied in Chapter 6, followed by electrode material investigations in Chapter 7. The direct-write microfabrication of SC-μSOFCs with coplanar electrodes using viscoelastic, gel-like electrode inks is summarized in Chapter 8, together with unpublished results on the effect of electrolyte thickness and material on cell performance as well as the cell performance calculations. In Chapter 9, SC-μSOFCs with coplanar electrodes and strengths and weaknesses of the employed fabrication technique are discussed. Finally, the conclusion of this work is presented in Chapter 10.

Chapter 1 Review of the literature

1.1 General aspects of fuel cells

Fuel cells are electrochemical devices that convert chemical energy of a fuel and an oxidant directly into electrical energy [27-29]. A fuel cell is generally composed of an electrolyte and two electrodes, the anode and the cathode. Fuel is fed to the anode and oxidized, whereas the oxidant is reduced at the cathode. The electrolyte assumes the transfer of charged species between the two electrodes. Electrons are released by the electrochemical oxidation of the fuel and travel through an external circuit to do electrical work. While electrochemical batteries store the reactants inside in the form of the cell components and electric energy production ceases with the consumption of the reactants, reactants are fed to fuel cells from an external source, and the fuel cell electrodes are inert catalysts of the electrochemical reactions. In a fuel cell, a continuous supply of fuel and oxidant enables continuous generation of electrical power. Unlike heat engines, the efficiency of fuel cells is not limited by the Carnot cycle, as the chemical energy of the fuel is directly converted into electrical energy without any intermediate conversion steps to thermal energy. Fuel-to-electricity conversion efficiencies range from 40 to 60% and can be further improved by using the by-product heat in cogeneration systems (combined heat and power, CHP) [9, 28].

The working principle of a fuel cell was first demonstrated by Sir William Grove in 1839 [30]. His experiments were based on the idea that, if water can be split into hydrogen and oxygen using an electrical current, it should also be possible to reverse the reaction and produce electricity by combining hydrogen and oxygen to form water. His first fuel cell consisted of two platinum stripes with one end of each electrode being immersed in a liquid acid electrolyte solution and the other end being exposed to hydrogen and oxygen, respectively. By combining several of those cells in series, the generated current was used to electrolyze water [31].

By now, six major types of fuel cells have been developed: alkaline (AFC), phosphoric acid (PAFC), proton exchange membrane (PEMFC), molten carbonate fuel cells (MCFC) and SOFCs. The direct-methanol fuel cell (DMFC) is based on the polymer electrolyte membrane fuel cell, with the difference that liquid methanol is used

as a fuel. The two main distinguishing features between the different types of fuel cells are the nature of the electrolyte material and the operating temperature. Table 1.1 gives an overview of the existing fuel cell types and their different kinds of applications [27-29].

Table 1.1: Comparison of the different types of fuel cells [27-29].

Type	Electrolyte	Mobile ion	Operating temperature (°C)	Applications
Alkaline (AFC)	35 - 50% KOH	OH^-	50 - 200	Space applications
Phosphoric acid (PAFC)	H_3PO_4	H^+	160 - 220	Distributed power generation, CHP*, transportation, military
Proton exchange membrane (PEMFC)	Polymer membrane	H^+	50 - 100	Portable applications, transportation, stationary CHP*
Direct-methanol (DMFC)	Polymer membrane	H^+	70 - 90	Portable applications, transportation
Molten carbonate (MCFC)	Molten carbonate salt (Li_2CO_3/Na_2CO_3)	CO_3^{2-}	600 - 700	Distributed power generation, CHP*
Solid oxide (SOFC)	Solid oxide ion-conducting ceramic	O^{2-}	300 - 1000	Portable applications, transportation, distributed power generation, CHP*

* Combined heat and power generation

1.2 Solid oxide fuel cells

Solid oxide fuel cells were first developed by Baur and Preis in 1937 [32]. SOFCs are an all-solid-state electrochemical device and a high-temperature fuel cell technology. The use of a solid oxide electrolyte avoids material corrosion and liquid electrolyte handling problems, and also allows for flexible and compact designs. High operating temperatures (300 to 1000°C) are necessary in order to activate the ion conductivity of the electrolyte. While AFC, PAFC and PEMFC require almost 100% pure hydrogen fuel to avoid poisoning of the electrode catalysts and to guarantee proper functioning, the high operating temperatures of SOFCs enable the direct use of high energy density hydrocarbon fuels, resulting in a multifuel capability of these fuel cells. If hydrocarbon fuels are used in low-temperature fuel cells, prior processing in an external reforming system is necessary to generate hydrogen. In SOFCs, internal reforming (conversion of hydrocarbon to hydrogen at the anode) or direct electrochemical oxidation of the hydrocarbon fuel [33-35] eliminate the need for an external reforming system and therefore reduce system volume, complexity and costs, while increasing the system efficiency. Additionally, the elevated operating temperatures increase the reaction kinetics for the electrochemical reactions at the electrodes and avoid the need for expensive metal catalysts, like platinum used in PEMFCs. The higher reaction kinetics are especially beneficial for the rather sluggish oxygen reduction reaction at the cathode, which generally is a major source of voltage losses. Also, high-quality by-product heat is generated that can be used for cogeneration and combined SOFC/gas turbine power plants [9].

On the other hand, high operation temperatures impose the use of temperature-resistant materials that involve complex and costly processing techniques [9, 36]. Thermal stresses can evolve from heating-cooling cycles during start-up, operation and shut-down due to differences in the thermal expansion coefficients between cell components, resulting in rapid performance degradation and low long-term stability. Research on SOFCs focuses on reducing the operating temperatures by using very thin electrolyte layers and optimizing electrode design and composition. In addition to reduced thermomechanical stresses, low- or intermediate-temperature SOFC systems

(500-800°C) require less complex materials and simpler fabrication methods, lowering fabrication costs and opening the way to commercialization [27, 36].

Possible applications of SOFCs range from powering portable devices to small power systems (e.g., residential power or automobile auxiliary power units, up to 5 kW), distributed generation power plants (100-500 kW) and combined heat and power [37]. Integrating SOFCs with gas turbines allows construction of highly efficient MW-scale hybrid systems with efficiencies of up to 70%. Residual fuel and heat from the fuel cell can be used in the gas turbine.

1.2.1 Working principle

As shown in Fig. 1.1, SOFCs are composed of three primary components: the electrolyte and two electrodes, i.e., the anode and the cathode. The electrodes are preferably porous so that the reaction gases can pass through to the electrode-electrolyte interface, where the electrochemical reactions take place. The dense electrolyte, together with gas-tight high-temperature sealing, separates the cell into two gas compartments, in each of which one electrode is located. The electrolyte is generally an oxygen ion conductor, but SOFCs with proton-conducting electrolytes are also possible [38].

The operating principle is described here with hydrogen as the fuel and oxygen as the oxidant, the most common fuel-oxidant gases used in fuel cells [9]. The fuel is fed to the anode and is oxidized at the triple phase boundaries (TPB), formed by the electronic conducting, the ionic conducting and the gas phase. H_2 and oxygen ions react to form water and electrons:

$$H_2 + O^{2-} \rightarrow H_2O + 2\,e^- \qquad (1.1)$$

Via an external circuit the electrons travel to the cathode, where the oxygen is electrochemically reduced:

$$\tfrac{1}{2}\,O_2 + 2\,e^- \rightarrow O^{2-} \qquad (1.2)$$

Summing up reactions (1.1) and (1.2) leads to the overall reaction:

$$H_2 + \tfrac{1}{2}\,O_2 \rightarrow H_2O \qquad (1.3)$$

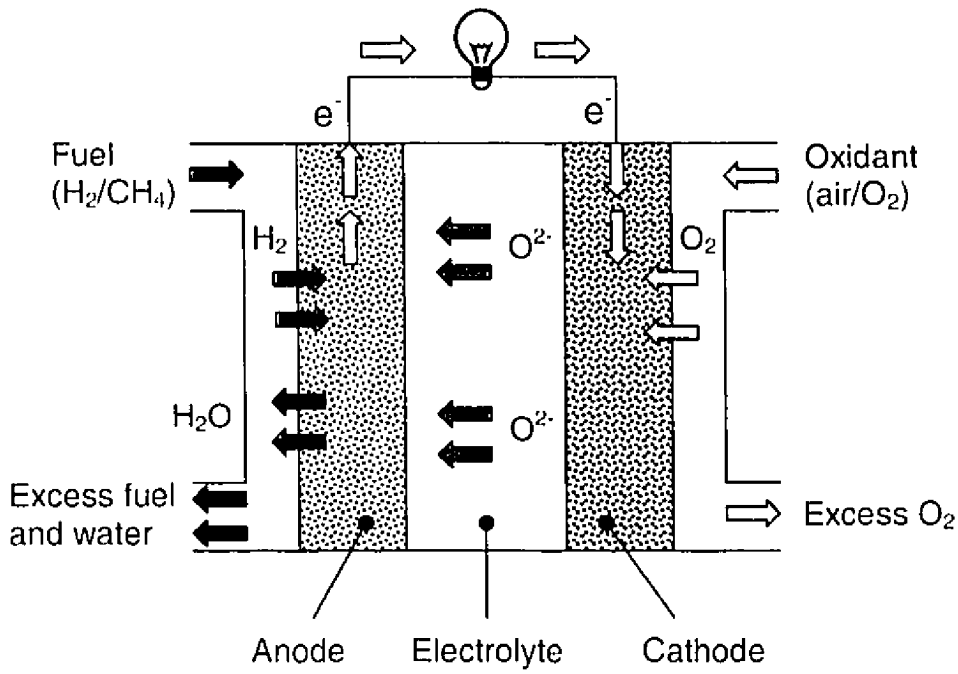

Figure 1.1: Schematic representation of the working principle of a solid oxide fuel cell.

SOFCs, like other fuel cells, are not Carnot-limited. The chemical free energy, available for useful (electrical) work, of the reactant gases (Gibbs free energy, ΔG) is directly converted into electrical energy, as given by equation (1.4), with E_r the Nernst or reversible cell voltage, n the number of electrons taking part in the reaction per mole of reactant and F the Faraday constant (96485 C/mol) [9].

$$E_r = -\frac{\Delta G}{nF} \tag{1.4}$$

The cell voltage can also be calculated by the Nernst equation:

$$E_r = E^0 + \frac{RT}{2F} \ln\left(\frac{p_{H_2} p_{O_2}^{1/2}}{p_{H_2O}}\right) \tag{1.5}$$

with R the ideal gas constant (R = 8.314 J/(mol·K)), T the temperature in K, F the Faraday constant, E^0 the standard reversible cell potential and p the gas partial pressure. At 600°C with ΔG^0 = -199.6 kJ/mol and the product H_2O in vapor form, the maximum possible cell potential or standard reversible cell potential, E^0, amounts to

1.04 V for one single cell [28]. By assembling several cells in series in the form of a stack, higher voltages can be generated.

The driving force for the migration of the oxygen ions from cathode to anode through the electrolyte results from the oxygen chemical potential or oxygen partial pressure gradient between anode (10^{-15}-10^{-30} atm) and cathode (0.21 atm) [39]. Therefore the Nernst equation can also be written as

$$E_r = \frac{RT}{nF} \ln\left(\frac{p_{O2,cathode}}{p_{O2,anode}}\right) \tag{1.6}$$

with p_{O2} indicating the oxygen partial pressure at cathode and anode, respectively [9].

In real SOFC systems, the measured or operating cell voltage, E_{cell}, is generally lower than the maximum thermodynamically possible value. Under open circuit conditions, this loss in voltage, E_L, is due to gas leaks through the electrolyte in the case of poor sealing or cracks in the electrolyte, to electric current flow through the electrolyte or to side reactions at equilibrium [19]. Additionally, when current, I, is drawn from the cell under closed circuit conditions, the cell voltage decreases and finally reaches 0 V at the limiting current. Ohmic losses, R_{ohm}, as well as cathodic and anodic overpotentials (i.e., difference between ideal and real cell voltage), η_{conc} and η_{act}, are the reason for the voltage drop. Ohmic polarization or resistance losses result from the ohmic resistance to ionic and electronic flow in the cell and is the sum of the contributions from electrolyte, electrodes, current collectors, interconnects that combine single cells in a fuel cell stack, wire materials, etc. Cathodic and anodic overpotentials are attributed to both activation polarization and concentration losses. Activation polarization describes kinetic losses which are due to slow reaction rates of the electrochemical charge-transfer reactions at the electrodes. In most hydrogen/oxygen fuel cells, slow oxygen reduction at the cathode is mainly responsible for the activation overpotential. The weak hydrogen bonds can be easily broken during electrochemical oxidation over a wide range of anode catalysts, and reaction rates are rather high. Concentration losses are caused by mass diffusion limitations and low mass diffusion rates of reactants flowing to the TPBs through the electrodes and reaction products moving away. At high current densities, mass diffusion overpotentials become important as more and more reaction products are formed, which cannot be removed sufficiently

quickly, blocking the way for fresh reactant gases. The real cell voltage can thus be expressed as:

$$E_{cell} = E_r - E_L - I \cdot \Sigma R_{ohm} - \eta_{act} - \eta_{conc} \quad (1.7)$$

Fig. 1.2 shows a typical polarization curve of a fuel cell, that is, cell potential as a function of current.

The power of an operating cell is the product of current and cell voltage. It reaches its peak value at intermediate voltages. High cell efficiency and elevated power densities are achieved for low overpotentials, that is, when (i) the electrolyte is dense and the single cell is correctly sealed, (ii) the electrolyte shows high ionic conductivity and is a bad electronic conductor at the operating temperature, (iii) the electrochemical reaction rates at the electrodes are elevated, (iv) the electrodes are highly electronically conductive, and (v) the mass diffusion of reactant gases and reaction products to/from the electrolyte is fast. The efficiency ε of a single cell can be calculated by [9, 27, 28]:

$$\varepsilon_{cell} = \varepsilon_{th}\varepsilon_p\varepsilon_f\varepsilon_S \quad (1.8)$$

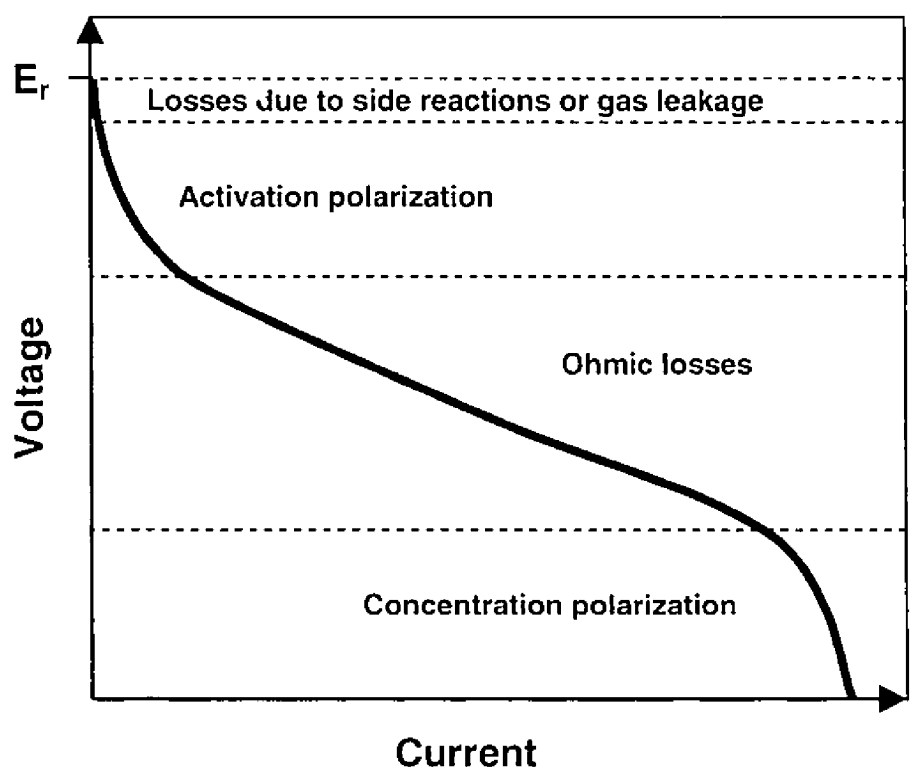

Figure 1.2: Typical polarization curve of a fuel cell.

The theoretical or thermodynamic efficiency ε_{th} is given by:

$$\varepsilon_{th} = \frac{\Delta G}{\Delta H} \tag{1.9}$$

where ΔG is the Gibbs free energy converted into electrical energy and ΔH the reaction enthalpy. ε_p describes the potential efficiency:

$$\varepsilon_p = \frac{E_{cell}}{E_r} \tag{1.10}$$

The current or faradaic efficiency ε_i corresponds to the losses that occur due to parasitic side reactions and is expressed by:

$$\varepsilon_f = \frac{n}{n_{th}} \tag{1.11}$$

where n is the number of electrons actually taking part in the reactions and n_{th} the number of electrons being released by the theoretically occurring reactions. The fuel utilization efficiency is commonly represented by the current efficiency [9]. The system efficiency ε_S takes fuel pretreatment, system cooling and reprocessing of reaction products into account.

1.2.2 Materials

SOFC electrode and electrolyte materials have to fulfill several requirements [9]. The electrolyte must exhibit elevated ionic conductivity while at the same time being an electronic insulator in order to avoid internal short circuiting of the cell. It must maintain its high ionic and low electronic conductivity over a wide range of oxygen partial pressures and gas atmospheres. In conventional dual-chamber operation, the electrolyte also has to be fully dense and gas-tight in order to completely separate the fuel and air compartments of the cell. The electrodes must be electronically conductive for the transport of electrons, and ionic conductivity is desired in order to extend the TPBs from the electrode-electrolyte interface into the electrode volume [40]. Furthermore, the electrodes have to enable the transport of the reactant gases and reaction products to and from the TPBs and therefore should exhibit a porous microstructure (25-40 vol% porosity [19]). Additionally, the electrodes must be catalytically active materials to catalyze the respective electrochemical reactions. They must also show a thermal expansion coefficient close to the one of the electrolyte to

ensure thermomechanical compatibility. Proper adhesion of the electrode on the electrolyte is important, as a weak electrode-electrolyte interface reduces the contact area. An optimized interface yields improved long-term mechanical stability as well as reduced degradation during thermal cycling. Finally, the electrolyte, anode and cathode must be chemically compatible and show sufficient mechanical strength. The anode needs to exhibit chemical stability under reducing atmospheres, whereas the cathode must be stable under oxidizing conditions, and the electrolyte under both reducing and oxidizing atmospheres.

1.2.2.1 Electrolyte

The conventional electrolyte material is YSZ, which shows good mechanical properties and chemical resistance for use in SOFCs [19]. Doping with Y_2O_3 stabilizes the cubic fluorite crystal structure of ZrO_2 from room temperature to the melting point, thus avoiding undesired phase transitions during cell operation. Doping also increases the oxygen vacancy concentration and thus the ionic conductivity of the YSZ electrolyte. The ionic conductivity becomes activated at elevated temperatures. At 700°C, the ionic conductivity of YSZ is 1 S/m [19]. However, chemical compatibility issues were observed between YSZ electrolytes and LSM-based cathodes [9, 41-43]. During sintering, YSZ was found to chemically react with LSM cathodes, and insulating phases such as $La_7Zr_2O_7$ are formed, inducing high cathode overpotentials and affecting the conductivity of the electrolyte.

Decreasing the electrolyte thickness permits the reduction of SOFC operating temperatures. Additionally, the temperatures can be decreased by improving the electrolyte composition (e.g., bilayer electrolytes [44] or surface modified materials [45]) or using different materials with higher ionic conductivity than YSZ at temperatures below 800°C [41, 46]. Doped ceria [47] and lanthanum compounds [48, 49] are promising alternative electrolyte materials. Ceria-based oxides are excellent ionic conductors for the intermediate temperature range (500-800°C). However, the main disadvantage of doped ceria electrolytes is their electronic conductivity under reducing atmospheres (low oxygen partial pressures), which can lead to internal short-circuiting and lower the OCV. Using a bilayer electrolyte of ceria (cathode-side) and YSZ (anode-side) can protect the ceria against exposure to the reducing atmosphere at the anode

side and avoid interaction between YSZ and LSM cathodes. Strontium and magnesium doped lanthanum gallates, $La_{1-x}Sr_xGa_{1-y}Mg_yO_3$ (LSGM), show high ionic conductivity and are stable over a wide range of oxygen partial pressures, as well as in reducing, oxidizing and CO_2 atmospheres [49]. However, these materials are difficult to fabricate and can interact with the anode [41]. Bi_2O_3-based electrolytes show the highest conductivities among the different possible SOFC electrolyte materials, but they are also electronically conductive and stability issues remain to be solved [19, 41]. Perovskite-type oxides based on strontium and barium cerate or zirconate-based oxides are proposed as proton-conducting electrolytes [38, 50].

1.2.2.2 Anode

The state-of-the-art anode material consists of a porous Ni-ceramic composite, also called a cermet [9]. Nickel is available at low cost, is a good catalyst for hydrogen oxidation and reforming of hydrocarbons, and exhibits good chemical stability under reducing environments at high temperatures. The addition of YSZ allows matching of its thermal expansion coefficient to that of the YSZ electrolyte [51]. The YSZ forms a skeleton-like structure for dispersing the Ni particles and inhibits excessive Ni coarsening at high temperature. While the metallic nickel is electronically conductive, the YSZ adds ionic conductivity to the electrode, and thus enhances the triple phase boundaries for the electrochemical reactions [52]. Generally, anodes are fabricated from NiO, which is reduced to metallic nickel when the cell is put into operation for the first time. Using NiO as starting material allows processing under air atmosphere and reduces cell fabrication costs. Additionally, the reduction of NiO to Ni increases the porosity of the anode for better gas diffusion to and from the reaction sites at the Ni/YSZ/gas interface. A porosity of approximately 40% is recommended for SOFC anodes [53].

However, Ni-based anodes show poor redox stability and low tolerance to sulfur [54]. Nickel is additionally active for hydrocarbon cracking, and when using hydrocarbon fuels, carbon is easily deposited on the nickel catalyst [55, 56]. Cu-based anodes with CeO_2 have therefore been proposed as suitable anode materials for SOFCs operated on hydrocarbon fuels, as copper shows low activity for hydrocarbon cracking [40, 54, 57]. However, Cu is a purely electronically conducting current collector with almost no

electrochemical activity, so that CeO_2 is added as the catalytically active phase. Another drawback of Co is its low melting temperature (1083°C compared to 1453°C for nickel [58]), which limits cell component processing and cell operating temperatures. Therefore, Cu-Ni alloys are also considered as anode materials. Fluorites [54], perovskite-type materials [59, 60], Fe-doped $CaTiO_3$ and ruthenium [61] are other possible anode materials.

1.2.2.3 Cathode

The cathode should be composed of mixed conductive materials with elevated activity for the oxygen reduction reaction. As most metals would be oxidized under the oxygen-rich atmosphere at the cathode side, electronically or mixed conductive metal oxides and composites of electronic and ionic conducting phases are good candidates. Perovskite type oxides (ABO_3) with high electronic conductivity are conventionally used as SOFC cathodes. The A-cations generally are rare earth or alkaline earth elements such as lanthanum, strontium or calcium, whereas transition metals (e.g., Cr, Mn, Fe, Co) occupy the B-sites for electronic conductivity. LSM, $La_{0.8}Sr_{0.2}MnO_{3-\delta}$, is the most common perovskite cathode material. LSM exhibits intrinsic electronic conductivity, which can be enhanced by the addition of divalent dopants such as Sr on the A-site of the lanthanum manganite, leading to the transformation of Mn^{3+} to Mn^{4+}.

As the low reaction kinetics of the oxygen reduction reaction are a key reason for elevated cathode overpotentials and high activation losses in SOFCs, cathode catalyst improvement constitutes a major field of research in SOFC technology. The cathode polarization resistance can be decreased by increasing electronic and ionic conductivity of the cathode material and by maintaining chemical and thermal expansion compatibility with the electrolyte. Doping LSM with different B-cations and incorporation of electrolyte material in the cathode are promising possibilities to lower polarization losses [46, 62]. Composite cathodes of LSM and YSZ are used to increase the catalytic activity for the oxygen reduction. While LSM is an electronic conducting material, the addition of an ionic conducting electrolyte phase (e.g., YSZ) enhances the diffusion of oxygen ions within the cathode and enlarges the active area for the electrochemical reactions into the electrode volume. The addition of YSZ also reduces the mismatch of the thermal expansion coefficient between cathode and electrolyte. $La_{1-x}Sr_xCo_{1-y}Fe_yO_{3-\delta}$

(LSCF) [63], $La_{0.75}Sr_{0.25}CuO_{2.5-\delta}$ [64], $La_{0.6}Sr_{0.4}CoO_3$ [49], $Sm_{0.5}Sr_{0.5}CoO_3$ (SSC) [49] and $Ba_{0.5}Sr_{0.5}Co_{0.8}Fe_{0.2}O_{3-\delta}$ (BSCF) [65] exhibit higher conductivities and catalytic activities than LSM and are therefore good alternatives for intermediate temperature SOFCs. For SOFCs operating at temperatures of 500-600°C, yttria-stabilized bismuth oxide has been investigated [66].

1.2.2.4 Interconnect

In cell stacks, interconnects or bipolar separators are used to electrically connect the anode of one cell to the cathode of the neighbor cell and to separate fuel and oxidant gas streams of adjacent cells [9, 67]. Additionally, gas channels can be manufactured into the interconnect plates to allow for gas supply and manifolding to the electrodes in planar SOFCs. The material requirements for the interconnect include high electronic conductivity, chemical compatibility with the other cell components and elevated stability under both oxidizing and reducing conditions and at elevated temperatures. $LaCrO_3$ is one of the most common interconnect materials, but with the reduction of operating temperatures, metallic materials such as ferritic steels can also be used.

1.2.3 Cell designs and operating modes

SOFC single cells are composed of an electrolyte sandwiched between anode and cathode in a dual-face, three-layer assembly. This single cell configuration can be external- or self-supporting. External-supporting configurations use either interconnects or porous substrates as the structural support, whereas in the case of self-supporting cells, one cell component forms the supporting part so that electrolyte-, anode- or cathode-supported cells are possible. Electrolyte-supported cells consist of a thick, mechanically-strong electrolyte, which necessitates elevated operating temperatures to minimize ohmic polarization losses. For low or intermediate temperature operation, electrode-supported cells with thin electrolyte films are used to overcome the decrease in ionic conductivity and increase in internal resistance of the electrolyte.

SOFC single cells can be built in various designs, with the most common ones being the planar and tubular designs [9, 67]. Tubular cells are in general cathode-supported, whereas planar cells can be fabricated in all of the different supporting

configurations. Advantages of the tubular over the planar design include seal-free construction and higher thermomechanical strength, but because of long current pathways along the tubular electrodes, lower power outputs are obtained. Additionally, the fabrication is more complex and expensive compared to well-established, low-cost ceramic processing techniques (e.g., tape casting and screen printing) for planar electrodes [19]. A new design developed by Rolls-Royce combines the tubular with the planar geometry in a so called integrated planar SOFC which consists of segmented cells connected in series [68]. Finally, monolithic cell designs are formed of thin cell components in a corrugated structure [9].

SOFCs can be operated in three different modes. The most conventional operating mode is the dual-chamber mode where fuel and oxidant are supplied separately to the respective electrodes. In the single-chamber mode, the fuel cell consists of one gas compartment, and a mixture of the two reactant gases is used. A new operation concept reported in the literature is the no-chamber or direct-flame SOFC (Fig. 1.3) [69-71]. The no-chamber cell is operated on a fuel-rich flame which not only constitutes the source of the fuel, but also enables thermally self-sustaining cells by providing the necessary heat for SOFC operation without using an external heating system. The anode is exposed to the fuel flame, whereas ambient air is used at the cathode (air-breathing cathode).

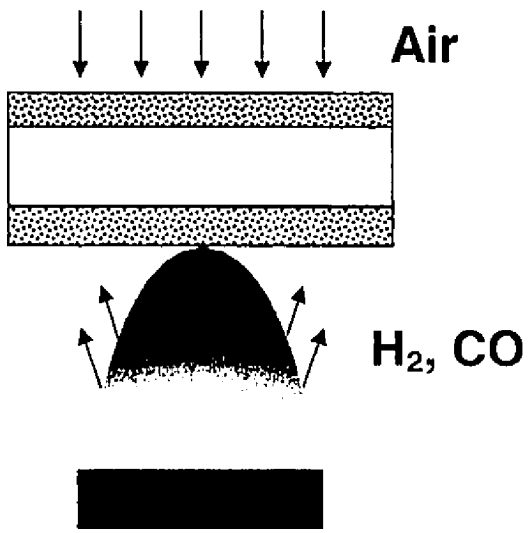

Figure 1.3: No-chamber or direct-flame SOFC.

1.2.4 Micro-SOFCs

The growing market of portable, multifunctional and wireless consumer electronics (e.g., personal digital assistant, laptop computer, cellular phone and battery rechargers), microsystems (e.g., sensors and actuators) and military applications is facing an increased demand for high volumetric energy density and quickly rechargeable power sources. Secondary rechargeable batteries (e.g., nickel metal hydride and Li-ion) provide low cost power with relatively long operation times. However, electronic devices are becoming smaller and lighter while at the same time demanding increased power and longer operation time combined with uninterrupted power or quick recharging. Battery technology is believed not to be able to keep pace with the growing demand for power [1], whereas fuel cells are being considered for powering future mobile devices [2, 3]. Micro fuel cells could meet the requirements of more reliable portable power, higher energy densities, small volume, lightweight packaging and rapid refueling due to miniaturization of fuel cell stacks and the use of small, easily replaceable, high concentration fuel cartridges. The intrinsic higher price of future, complex electronic devices could buffer the costs of the micro fuel cell power source as compared to the price of conventional batteries [72].

In Ref. [1], the use of a fuel cell was compared to battery systems with recharging components. The fuel cell system considerably reduced weight and volume of the power generating device and therefore led to an increased system energy density. A hybrid system where the fuel cell continuously recharges a battery could increase the run time and efficiency during peak power demands and lead to 6-times higher energy densities. The complete replacement of the battery by the fuel cell was found to engender up to a 12-fold improvement. However, from a safety point of view with the battery being a sealed system, fuel cells should allow ambient-temperature and air-breathing operation, and storage of hydrogen fuel also remains a critical issue. Additionally, despite the possibility of down-scaling fuel cell systems, the need for peripheral components such as gas storage and supply, water removal and control systems might lead to higher costs and system complexity.

Although SOFCs necessitate elevated operating temperatures accompanied by thermal insulation issues and heat management, they are becoming very promising as micro power generating devices for sensors, actuators, microelectromechanical

systems (MEMS) and microscale portable systems [73-75]. SOFCs show elevated fuel flexibility and enable the direct use of high energy density hydrocarbon fuels being converted inside the system. The possibility of internal reforming leads to reduced system complexity compared to additional external reforming systems, and simplifies downsizing and cell stacking. The waste heat can be used to preheat the incoming gases and increase the conversion efficiency. Decreasing the electrolyte thickness allows a decrease of the operating temperature, and self-sustaining systems for simplified thermal management and rapid start-ups are being developed. Micro-SOFCs (μSOFCs) are most commonly built in tubular and planar designs, which can be easily scaled down by conventional ceramic processing technologies and new microfabrication techniques such as direct-writing [76]. Tubular fuel cells with a small diameter show an increased effective electrode area per unit volume and therefore a reduced stack volume and increased power density. Additionally, tubular systems are tolerant to rapid temperature changes and enable rapid start-ups [77, 78]. Single-chamber SOFCs are also well suited for miniaturization because of their compact design and absence of any high-temperature gas-tight sealing requirements [11].

In addition to down-sizing macroscale SOFCs, miniaturization can be achieved by integration with MEMS technology and silicon microfabrication techniques such as thin-film deposition, photolithographic patterning and etching [7, 79-84]. These techniques allow fine feature resolution, high repeatability, batch fabrication and integrated process sequences. Miniaturization is achieved by creating thin-film cell components as well as effective scaling of fuel delivery, gas manifold and cell stack components for applications as miniature and microscale energy conversion systems. Thin-film μSOFCs can be built on a thin silicon wafer to form highly integrated systems-on-a-chip consisting of a miniature fuel cell on a silicon chip with other electronic circuits [85, 86]. Planar stacks can be fabricated as multiple cells on one silicon wafer into which gas channels and feedholes are directly integrated by micromachining and microfabrication. Current collectors are formed by deposition of thin metal films on the electrodes. However, thin-film cell components can exhibit intrinsic residual stresses, which have to be controlled to ensure long-term stability. Modeling and evaluation of design criteria are employed to enhance the thermomechanical stability over a wide temperature range and reduce heat losses in μSOFCs [73, 85, 87].

Ref. [7] defines μSOFCs as SOFCs on silicon substrates with lateral dimensions in the millimeter or sub-millimeter range. Single-chamber μSOFCs with coplanar electrodes and dual-chamber micro cells with thin electrolyte membranes are presented as the principal μSOFC designs on silicon substrates. Microscale electrode dimensions are required to reduce the ohmic cell resistance in single-chamber μSOFCs with coplanar electrodes, whereas the use of thin-film electrolytes permits reduced ohmic resistance for low and intermediate temperature operation in the case of dual-chamber μSOFCs. The thin-film electrolyte used in dual-chamber μSOFCs can either be a free-standing membrane (covering an opening in the supporting silicon substrate) or be supported by a porous electrode. Current constriction at the TPBs imposes a lower limit of 300 nm for the electrolyte thickness below which the ohmic resistance can not be significantly further reduced [7].

1.2.5 Hydrocarbon reforming in SOFCs

The high operating temperatures of SOFCs allow direct internal reforming of hydrocarbon fuels at the anode without the need for external reforming systems. In the endothermic steam reforming process, hydrocarbons (e.g., methane) are converted with steam to hydrogen and carbon monoxide [88].

$$CH_4 + H_2O \rightarrow CO + 3\,H_2 \qquad (\Delta H_{298K} = 206\ \text{kJ/mol}) \qquad (1.12)$$

CO reacts with steam to form H_2 and CO_2 according to the water-gas shift reaction:

$$CO + H_2O \rightarrow H_2 + CO_2 \qquad (1.13)$$

The presence of steam at nickel-based anodes reduces carbon formation, but increases the need for complicated water management [89]. Additionally, the addition of water dilutes the fuel and can lead to a decrease of the OCV and enhance activation losses. The endothermic reforming reaction can also provoke large thermal gradients within the cell. Partial oxidation of hydrocarbons such as in SC-SOFCs can be employed in conventional SOFCs by supplying a fuel-air mixture to the anode and air to the cathode [90]. Although the addition of steam is avoided, relatively dilute hydrogen is produced for the electrochemical reactions.

Improved fuel conversion can be obtained by direct electrochemical oxidation of the hydrocarbon fuels. The use of dry fuel gas can simplify water management, and ceria-based anodes with Cu instead of Ni avoid carbon deposition [33-35]. The direct

electrochemical oxidation of the fuels can either be a complete or partial oxidation reaction, with the latter being less favorable because of lower fuel utilization and conversion. Direct electrochemical oxidation without reforming could be an alternative to hydrogen-based fuel cell technologies for transportation and distributed power applications where production and storage of hydrogen still are a technological challenge.

1.3 Single-chamber solid oxide fuel cells

Single-chamber solid oxide fuel cells can be defined as fuel cells with only one gas compartment operating in a non-equilibrium gas mixture of fuel and oxygen [91]. The term "single-chamber" was introduced in 1999 [92] by Hibino, one of the pioneers of the SC-SOFC technology, and is generally used. But "one-chamber" [93], "single-compartment" [94], "mixed-gas" [95-97], "mixed-fuels" [98] "mixed-reactant" [99-101], "compact mixed-reactant" [102] and "separator free" [103] fuel cells as well as "SOFCs with reaction-selective electrodes" [104] can also be found in the literature.

In conventional dual-chamber SOFCs, gas-tight sealing in combination with a dense electrolyte separates the cell into two compartments so that the oxidant is fed to the cathode and the fuel to the anode through separate gas supplies without any intermixing of the two reactant gases (Fig. 1.4a). The difference in oxygen partial pressure between the two separate electrode compartments leads to the build-up of an OCV. For the generation of electrical power, the electrodes have to show high catalytic activity for the specific redox-reaction, that is, the anode for the oxidation of the fuel and the cathode for the reduction of the oxidant. In SC-SOFCs, the cell is located in a single gas chamber and a mixture of fuel and oxidant flows over the cell (Fig. 1.4b). The working principle of SC-SOFCs is therefore based on the selectivity of the electrodes for the respective reactions. The anode must be selective and electrochemically active for oxidizing the fuel and inert to the oxidant, whereas the cathode needs to exhibit catalytic activity for the reduction of oxygen and inertness to the fuel. Thus, the difference in catalytic activity and selectivity of the electrodes for the fuel reactions is at the origin of the generation of the OCV and electricity in SC-SOFCs [11].

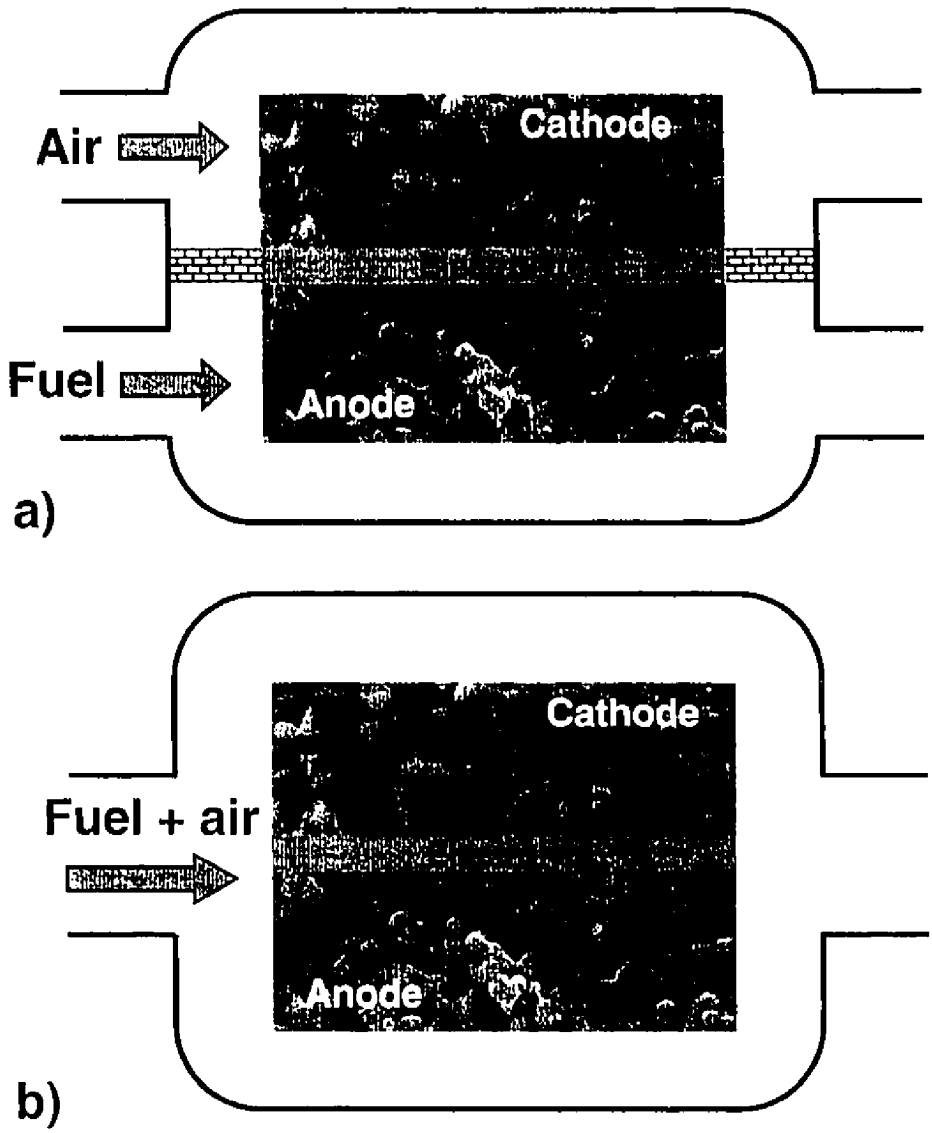

Figure 1.4: Schematics of a) dual-chamber and b) single-chamber SOFC.

Table 1.2 summarizes advantages and challenges of SC-SOFCs. A major drawback of SC-SOFCs is the insufficient selectivity of current electrode materials, resulting in low fuel utilization and cell efficiency [15]. Therefore, one of the main challenges of SC-SOFC technology consists in finding highly selective materials for the next generation of SC-SOFCs with improved efficiencies for practical implementation. Another drawback of SC-SOFCs is the risk of explosion related to working with fuel-air gas mixtures at elevated temperatures.

Table 1.2: Advantages and challenges of SC-SOFCs.

Advantages	Challenges
• Sealing-free structure • Less complex gas manifolding • Increased thermomechanical stability • More compact and simplified designs • Easier stack assembly • Great potential for miniaturization • No need for gas-tight electrolyte • Exothermic reactions to sustain cell temperature • New cell designs • Easier fabrication	• Highly selective and catalytically active materials necessary • Low efficiency due to parasitic, non-electrochemical reactions • Lower fuel utilization than in dual-chamber SOFCs • Risk of explosion for fuel-air mixtures at high temperatures

Despite those challenges, solid oxide fuel cells operated in the single-chamber mode exhibit several advantages over conventional SOFCs. In dual-chamber SOFCs, gas-tight, high-temperature and mechanically resistant sealing is essential to separate the cell into leakproof anode and cathode compartments. Glass or ceramic materials are generally used for cell sealing because of elevated rigidity and gas tightness. However, degradation over time and thermal stresses resulting from thermal cycling often lead to the formation of cracks. Sealing by mechanical compression with mica increases thermomechanical strength but results in higher leakage rates. Gas separation and sealing thus have a severe impact on the mechanical and thermal shock resistance of SOFCs and their long-term stability. Bulky cell designs limit miniaturization and stack build-up, and severe constraints exist on fabrication technique and material choice, and significantly contribute to elevated fabrication costs.

Due to the use of a gas mixture, one key advantage of SC-SOFCs consists in the elimination of the gas-tight sealing. Additionally, since the cell is located in one gas compartment, less complex gas manifolding and flow field structures are necessary for reactant supply. The resulting simplified, compact, sealing-free cell structure shows improved resistance to thermal and mechanical stresses. SC-SOFC fabrication is much

simpler, and reduced fabrication costs can be expected. Due to the use of a gas mixture, novel geometries such as fully porous and single-face SC-SOFCs with coplanar electrodes become possible that could not work in conventional, dual-chamber SOFCs.

Moreover, the exothermic fuel oxidation reactions on the SC-SOFC anode cause a rise of the effective cell temperature by up to 200°C [10, 105, 106], allowing lower operation temperatures and rapid start-ups. This heat release can lead to higher power densities in SC-SOFCs than in dual-chamber SOFCs at nominally lower furnace temperatures. Additionally, the released heat enables thermally self-sustaining cells [15]. The overheating can be further enhanced by the use of platinum current collectors due to the catalytic activity of platinum for methane [10]. Studies on the cell overheating detected local temperature gradients between the fuel inlet and outlet [107]. Controlling the overheating and measuring the real cell temperature are therefore recommended to control the system and its performance as well as thermal degradation.

The use of a hydrocarbon-air mixture additionally enables internal hydrocarbon reforming over the nickel-based anode catalyst without addition of steam, as carbon deposition can be controlled by adjusting the oxygen content in the fuel-air mixture [11].

Stack assembly and cell packaging are simplified as no sealing and separated gas chambers, gas channels, valves, etc. have to be applied in SC-SOFCs. Significant reduction in mass and volume result, making SC-SOFCs very attractive for portable power applications. The simple design and enhanced thermomechanical stability allow rapid start-ups and shut-downs, as thermal mismatches between sealing material and cell components are eliminated. Miniaturization of cell designs to sizes in the milli- and micrometer range benefits from the reduced number of gas flow channels and the elimination of the gas-tight sealing. Planar cell designs allow for the use of silicon-based microfabrication techniques for the creation of microscale SC-SOFCs.

1.3.1 Working principle

Methane-air mixtures are the principal fuel-oxidant gas mixtures used in SC-SOFCs and are used here to describe the working principle of these fuel cells. However, operation with other fuels such as propane [108-110], higher hydrocarbons

[108, 111] or even liquid fuels [112] has also been reported. The gas mixture is characterized by the fuel-to-oxygen ratio, R_{mix}.

The working principle of SC-SOFCs is based on the difference in catalytic activity and selectivity of the electrode materials for the fuel reaction [11]. In the single-chamber operating mode, two types of catalytic reactions are occurring: (i) the heterogeneous catalysis of the fuel (partial oxidation) at the anode (1.14-1.15), and (ii) the selective electro-catalysis of fuel oxidation at the anode (1.1 and 1.16) and oxygen reduction at the cathode (1.2).

$$CH_4 + \tfrac{1}{2} O_2 \rightarrow CO + 2 H_2 \quad (1.14)$$

$$CH_4 + O_2 \rightarrow CO + H_2 + H_2O \quad (1.15)$$

$$CO + O^{2-} \rightarrow CO_2 + 2 e^- \quad (1.16)$$

Nickel-based catalysts were identified to exhibit activity for promoting the partial oxidation of methane within methane-oxygen gas mixtures [113, 114], but temperatures below 1000°C are necessary in order to avoid nickel volatilization and metal loss [115]. Due to the activity of nickel for methane cracking in oxygen-lean gas mixtures [113], different anode materials such as Ru-Ni-cermets [116], ruthenium oxide catalysts [113, 117, 118] and Ni-free anodes (e.g., $(La_{0.75}Sr_{0.25})(Cr_{0.5}Mn_{0.5})O_3$ [119]) are also considered for methane partial oxidation at SC-SOFC operating temperatures.

The working principle of SC-SOFCs was first described by van Gool [120], who attributed the possibility of power generation in fuel-air mixtures to the difference in selectivity of the electrodes for the fuel reactions. Fig. 1.5 shows a schematic representation of the operating principle of SC-SOFCs. On the anode catalyst, internal reforming of the hydrocarbon occurs via selective catalytic partial oxidation (1.14-1.15). A syngas consisting of hydrogen and carbon monoxide is formed, which reacts electrochemically with oxygen ions at the anode TPBs (1.1 and 1.16). Additional syngas can be generated by reforming reactions of unused methane reacting with water vapor (1.12) and carbon dioxide (1.17).

$$CH_4 + CO_2 \rightarrow 2 CO + 2 H_2 \quad (1.17)$$

The water-gas shift reaction (1.13) converts CO and steam into H2 and CO2. The H2 is more easily electrochemically oxidized than CO. The cathode is inactive towards the fuel and promotes the electrochemical reduction of oxygen (1.2).

The selective partial oxidation of the fuel and the selective electrochemical reactions at the anode and the cathode create a difference in oxygen concentration between the two electrodes. The partial fuel oxidation and depletion of incoming oxygen lead to a drop of the oxygen partial pressure at the anode and create a reducing environment, whereas a high oxygen partial pressure, depending on R_{mix}, is established at the cathode due to its inertness towards the fuel. This gradient in oxygen partial pressure is the driving force for the cell operation and is at the origin of the open circuit voltage according to the Nernst equation (1.6). In closed-circuit conditions, the electrochemical reactions lead to a net flow of current through the electrolyte and the external circuit.

Exhaust gas analysis and half-cell measurements are a suitable means to experimentally demonstrate the SC-SOFC operating principle. Hibino et al. [4, 121, 122] specifically used a two-chamber setup where anode and cathode were examined against a Pt reference electrode. The catalytic activity of the anode for the partial oxidation of methane was confirmed by the consumption of methane and formation of syngas, whereas the cathode showed limited and low activity for the methane reaction. It was found that the oxygen partial pressure as well as the anode and cathode potentials depend on the catalytic activity of the electrodes for the partial oxidation of methane. Increased activity of the anode and limited activity of the cathode for this reaction led to an increased OCV [121].

Theoretical considerations by Riess [123] also confirmed that the OCV depends on the difference in selectivity of the electrode materials for the specific reactions. For ideally selective electrodes, the OCV of SC-SOFCs should be the same as in a conventional dual-chamber SOFC. However, OCVs lower than the theoretical cell voltage are generated in real SC-SOFC systems due to the insufficient selectivity of current electrode materials. The cathode is not totally inert to the fuel, and at the anode direct, non-electrochemical fuel oxidation (1.18-1.20) is promoted due to operation at elevated temperatures. These parasitic reactions are of purely chemical nature and do not contribute to the generation of electrical power but only to the generation of heat, and should therefore be impeded to achieve higher power outputs and cell efficiencies [97].

$$CH_4 + 2\ O_2 \rightarrow CO_2 + 2\ H_2O \qquad (1.18)$$

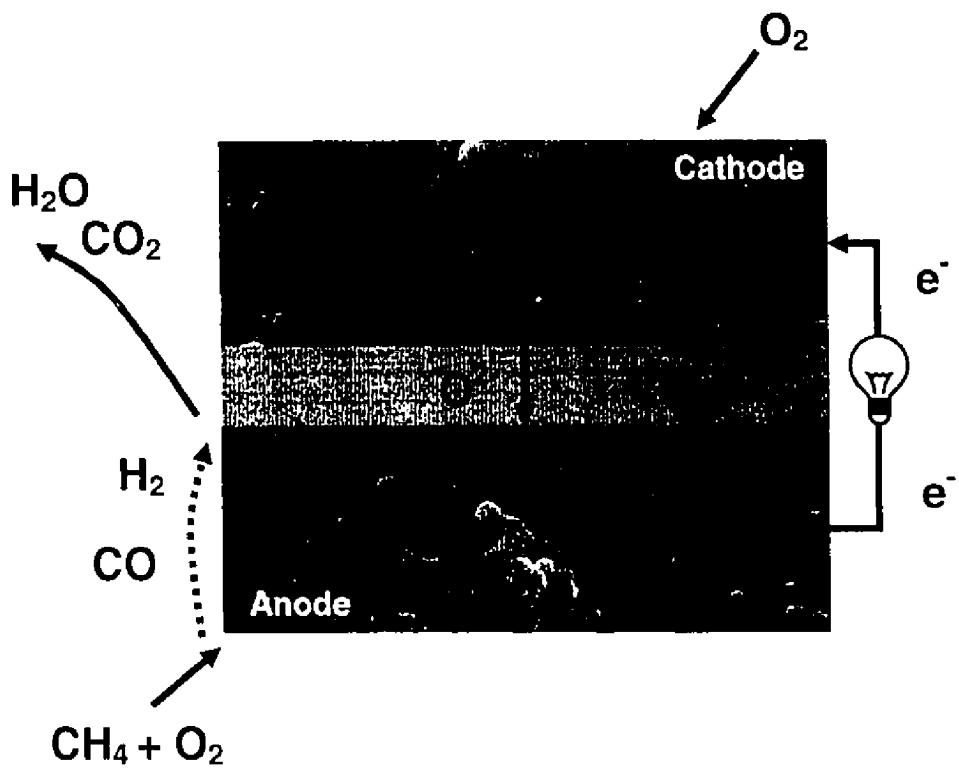

Figure 1.5: Schematic representation of the single-chamber working principle.

$$CH_4 + O_2 \rightarrow CO_2 + 2\ H_2 \quad (1.19)$$

$$CH_4 + 3/2\ O_2 \rightarrow CO + 2\ H_2O \quad (1.20)$$

Additionally, the syngas formed by the partial fuel oxidation can also be chemically oxidized according to reactions (1.3) and (1.21), and is lost for the electrochemical, electricity generating reactions.

$$CO + ½\ O_2 \rightarrow CO_2 \quad (1.21)$$

Other problems during cell operation are associated with carbon deposition on the anode catalyst surface according to the Boudouard reaction (for $T < 700°C$) (1.22) and methane cracking (for $T > 500°C$) (1.23) [39].

$$2\ CO \rightarrow C + CO_2 \quad (1.22)$$

$$CH_4 \rightarrow C + 2\ H_2 \quad (1.23)$$

Carbon deposition has a negative impact on the performance and long-term stability of the system, and $R_{mix} \leq 2$ is generally recommended in order to avoid carbon formation [39, 118]. A lower limit of the mixing ratio is imposed by the gas mixture becoming

explosive [39]. For very low R_{mix} (< 0.5), complete fuel oxidation is favored and the amounts of formed H_2 and CO are too low to allow power generation [39].

1.3.2 Flammability and explosion limits of methane-air mixtures

As mixtures of methane and air at elevated temperatures are used in SC-SOFCs, it is useful to know the explosion and flammability limits of such mixtures. The concentration of a combustible gas in air (or pure oxygen) determines whether there is a danger of combustion. With decreasing fuel concentration, the gas mixture becomes poor in combustible gas and reaches its lower flammability limit (LFL). At this point, the mixture contains too little fuel to sustain combustion. The upper flammability limit (UFL) is reached with increasing fuel concentration. At this point, the mixture is too rich in fuel and too poor in oxygen to enable combustion. The LFL and UFL for methane in air at 25°C and 1 atm are 5 and 15 vol% respectively [124, 125]. For methane concentrations between the LFL and UFL, the mixture is flammable and explosive.

Zabetakis established the following equations to obtain the flammability limits as a function of temperature [124, 125]:

$$LFL(\mathrm{T}) = LFL(25\ \mathrm{C}) - \frac{0.75}{\Delta H}(T - 25\ \mathrm{C}) \tag{1.24}$$

$$UFL(\mathrm{T}) = UFL(25\ \mathrm{C}) + \frac{0.75}{\Delta H}(T - 25\ \mathrm{C}) \tag{1.25}$$

where LFL(T) and UFL(T) are the lower and upper flammability limit at a specific temperature, LFL(25°C) and UFL(25°C) the lower and upper flammability limit at 25°C, ΔH the enthalpy of combustion in kcal/mol (at 25°C) and T the temperature in °C. With LFL(25°C) = 5, UFL(25°C) = 15 and $\Delta H_{25\,\mathrm{C}}(CH_4)$ = 191.8 kcal/mol [124], LFL(T) and UFL(T) were calculated for methane in air and are plotted as a function of temperature in Fig. 1.6.

The methane-air mixture used in SC-SOFCs is characterized by the ratio of methane to oxygen, R_{mix}, which can be expressed as a mole, volumetric or flow rate ratio [11-13, 15].

$$R_{mix} = \frac{CH_4}{O_2} \tag{1.26}$$

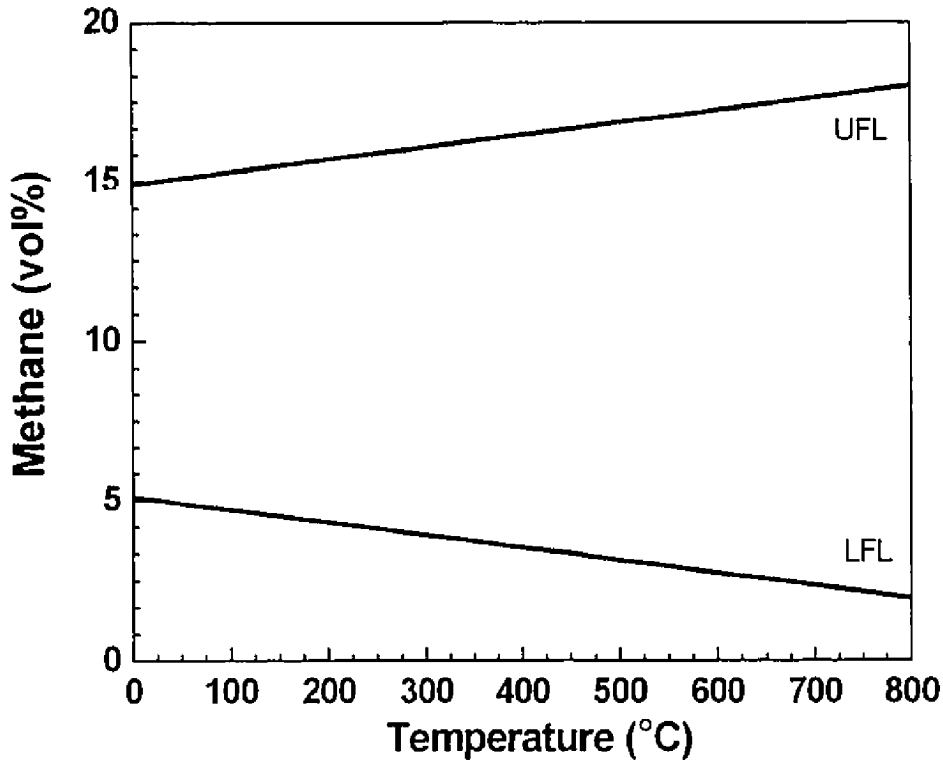

Figure 1.6: Lower and upper flammability limits of methane in air at 1 atm as a function of temperature.

The critical R_{mix} corresponding to the lower ($R_{mix,LFL}$) and upper ($R_{mix,UFL}$) flammability limit at a certain temperature can be calculated from *LFL*(T) and *UFL*(T). *LFL*(T) and *UFL*(T) correspond to the methane concentration in air. Thus, 100-*LFL*(T) or 100-*UFL*(T) gives the concentration of air. For synthetic air composed of oxygen and nitrogen in a ratio 20:80 = 1:4, the oxygen concentration corresponds to 1/5 of the air concentration. Thus, $R_{mix,LFL}$ and $R_{mix,UFL}$ can be expressed as:

$$R_{mix,LFL}(T) = \frac{CH_4}{O_2} = \frac{LFL(T)}{(100 - LFL(T))/5} \tag{1.27}$$

$$R_{mix,UFL}(T) = \frac{CH_4}{O_2} = \frac{UFL(T)}{(100 - UFL(T))/5} \tag{1.28}$$

$R_{mix,LFL}$ and $R_{mix,UFL}$ are plotted as a function of temperature in Fig. 1.7. The region between the two straight lines represents the zone of flammability and R_{mix} within that zone should be avoided during testing. At 700°C, the explosive range corresponds to $0.12 \leq R_{mix} \leq 1.07$.

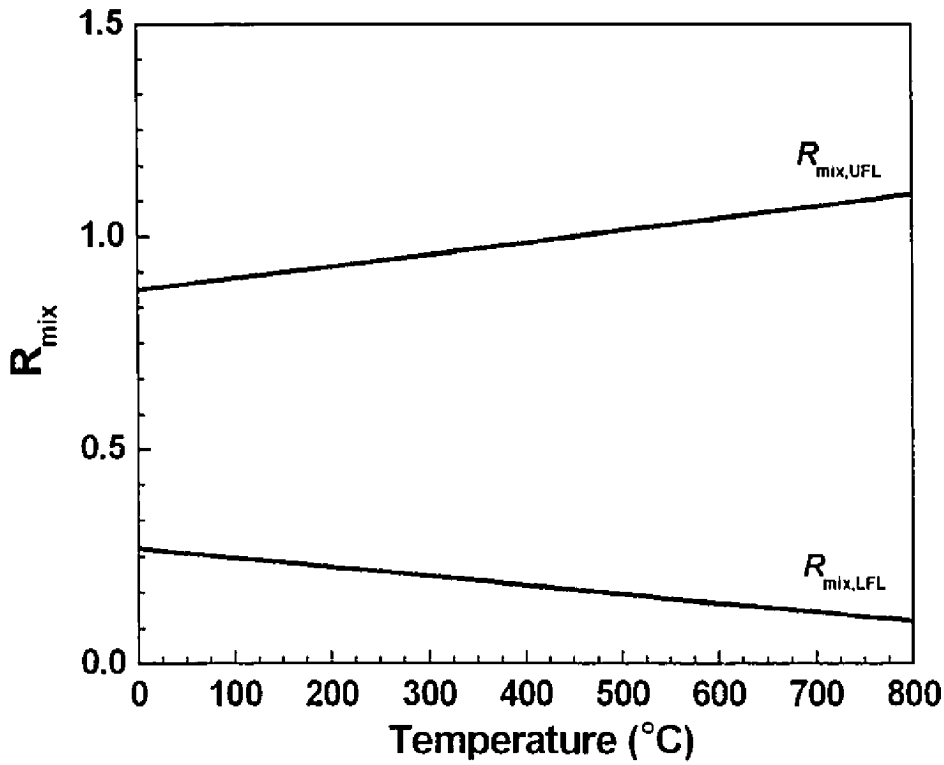

Figure 1.7: Critical methane-to-oxygen ratio R_{mix} as a function of temperature. The area between $R_{mix,LFL}$ and $R_{mix,UFL}$ represents the zone of flammability.

1.3.3 Applications

SC-SOFCs are expected to be used in applications where the simplicity of the seal-free cell design and possible rapid start-ups are more important than elevated efficiency. The compact and flexible designs enable the fabrication of a wide variety of geometries, sizes and shapes for different kinds of applications. Applications of SC-SOFCs might include rapid-start-up batteries for electric vehicles [106] and micropower applications in portable electronics [15, 126], sensors [127, 128] and actuators. Miniaturized SC-SOFCs (< 1 cm^2) are proposed for integration with MEMS, systems-on-a-chip designs and Si-based microelectronics [86, 129]. Due to the heat release during single-chamber operation, SC-SOFCs can be used for cogeneration or bottoming cycles [130]. Energy harvesting applications such as power generation from exhaust gases of heat engines in cars [131] or motorcycles [16, 132] are also envisaged, as the low efficiency of SC-SOFCs can be compensated by the generation of electrical power from waste gases. In addition to electrical energy, SC-SOFCs also

produce a synthesis gas of H_2 and CO, making the system interesting for cogeneration of electrical power and chemicals [133].

1.3.3.1 Microsystems and portable power applications

Due to the absence of gas-tight sealing, SC-SOFCs exhibit increased thermal shock resistance and enable rapid start-up, making them interesting for portable and small-scale power generation applications. To overcome the drawbacks of the elevated operating temperatures, however, thermal management and heat supply must be optimized. An approach of a thermally self-sustaining miniature SC-SOFC was proposed in Ref. [15]. Using the heat evolving from the partial oxidation of the fuel, the fuel cell temperature could be maintained at a sufficiently high level to allow power generation without an external heating source. This thermally self-sustaining SOFC was operated in the single-chamber mode with propane as fuel and exhibited high power densities (247 mW/cm^2 for a single cell and 275 mW/cm^2 for a two-cell stack) and rapid start-ups (less than 1 min). Cell start-up was initiated in a preheated furnace at 500°C. After removal of the cell and adequate thermal insulation, a cell temperature around 580°C could be maintained without an external heating system. The generated cell voltage and power output of a two-cell stack were sufficient to power a 1.5-V MP3 music player. However, the low efficiency (~1%) of SC-SOFCs imposes severe constraints on their practical implementation for portable power applications.

1.3.3.2 Energy harvesting applications

SC-SOFCs have been proposed to generate electrical power from automotive exhaust gases [16, 131, 132]. The high temperature of the exhaust gases provides sufficient heat for fuel cell operation, whereas different hydrocarbon fuels and oxygen are available in the exhaust gas stream. The cell can be simply put inside the exhaust pipe, as demonstrated by Hibino et al. [16, 132]. A twelve-cell SC-SOFC stack delivered OCVs of 5-8 V and a power output of 1 W in the exhaust gas of a motorcycle. Performance studies of a single cell under modeled exhaust gases identified optimal operating conditions for a cell temperature of 800°C or less and for a ratio of all present hydrocarbons to oxygen corresponding to the stoichiometric composition of the gas mixture for the partial oxidation of the hydrocarbons. These optimal conditions were

very similar to the ones of the real motorcycle exhaust. The energy generated from the engine exhaust gas streams could be used to supply auxiliary power units. This energy harvesting application could additionally be expanded to electricity generation from housing and industrial exhaust gases.

1.3.3.3 Sensor applications

The difference in catalytic activity between anode and cathode for the fuel and oxidant can also be used in sensor technology for the detection of fuel gas in gas streams, gas mixtures or air as well as for the control of the fuel concentration [127]. In a combined fuel cell-sensor system the fuel cell could deliver electrical power to adjust fuel fluctuations detected by the sensor part.

Hibino et al. presented a H_2-gas sensor operating in the single-chamber mode at a temperature of 30°C [128]. Cells were fabricated from a proton-conducting $Sn_{0.9}In_{0.1}P_2O_7$ electrolyte and Pt/C and C electrodes. Both planar cells with anode and cathode situated on opposite sides of the electrolyte and cells with coplanar electrodes on the same side of the electrolyte showed a change in their OCV when hydrogen was present in the oxygen gas.

To continuously provide low power to MEMS systems, capacitors or sensors in unsupervised, secluded applications, a closed-cycle microscale power generating device was proposed in Ref. [134]. By splitting water, a radiolytic source provides hydrogen and oxygen to an alkaline single-chamber micro fuel cell which in return produces an electrical power output and returns water to the radiolytic source. The whole power generating device could be integrated into a miniaturized package of about 1 cm^3 and deliver power in the mW range. This concept might also be applicable to SC-SOFCs.

1.3.4 Development of SC-SOFCs

The single-chamber concept started with the early work on nuclear fission where the possibility of radiolytic splitting water into hydrogen and oxygen followed by electrochemical recombination of the gas mixture to generate electricity was investigated [102]. The first single-chamber electrochemical device was conceived by Eyraud in 1961 in an attempt to increase the specific power of a fuel cell [135]. A cell

composed of a Ni anode, an alumina electrolyte and a Pd cathode delivered an OCV of 600 mV in a mixture of air and hydrogen.

In 1965, van Gool [120] further investigated the principle of using gas mixtures in fuel cells. He pointed out that single-chamber fuel cells work through heterogeneous catalysis of the fuel and that the catalysts must show high selectivity for the respective reactions. Based on surface-migration of ions, he also proposed a SC-fuel cell in the single-face configuration with coplanar electrodes.

In 1990, Dyer [136] fabricated a single-chamber fuel cell operating in a H_2-O_2 mixture at room temperature with voltages exceeding 1 V. His device consisted of thin films of a dense platinum electrode sputtered on a quartz substrate, a sputtered gas-permeable boehmite (γ-AlOOH) membrane and finally a porous, gas-permeable Pt electrode sputtered on top of the device (Fig. 1.8). The achieved power density was 1-5 mW/cm^2. Dyer suggested that this thin-film, light-weight device working in a gas mixture could simplify fuel cell designs and enable the low-cost fabrication of small systems.

Hibino and co-workers are the pioneers in implementing the single-chamber operating mode to solid oxide fuel cells. In 1993 [4], the first SC-SOFC operated in a methane-air mixture (R_{mix} = 2) showed an OCV of 350 mV and a maximum power output of 2.36 mW/cm^2 at 950°C. Ni-YSZ anode, YSZ electrolyte and Au cathode in an electrolyte-supported cell were used. In addition to electrical energy, the cell also produced a synthesis gas of H_2 and CO. By supplying the gas mixture to the two electrodes in separated compartments and analyzing the outlet gases, it was found that the establishment of an OCV was due to the catalytic activity of the anode for the partial oxidation of CH_4.

The cell performance of SC-SOFCs was gradually improved by employing different electrolyte materials ($SrCe_{0.95}Yb_{0.05}O_{3-\alpha}$ [137], $BaCe_{0.8}Y_{0.2}O_{3-\alpha}$ [122], $(CeO_2)_{0.9}(SmO_{1.5})_{0.1}$ [94]) and by doping YSZ electrolytes [138, 139] in combination with Pt anodes and Au cathodes, but the elevated overpotentials of these electrode materials [140] finally led to the use of conventional SOFC electrode materials. A Ni//YSZ//LSM cell enabled an OCV of ~0.8 V and a maximum power density of 121 mW/cm^2 at 950°C and R_{mix} = 1, whereas a Pt//YSZ//Au cell only delivered 0.5 V and 0.57 mW/cm^2 [92].

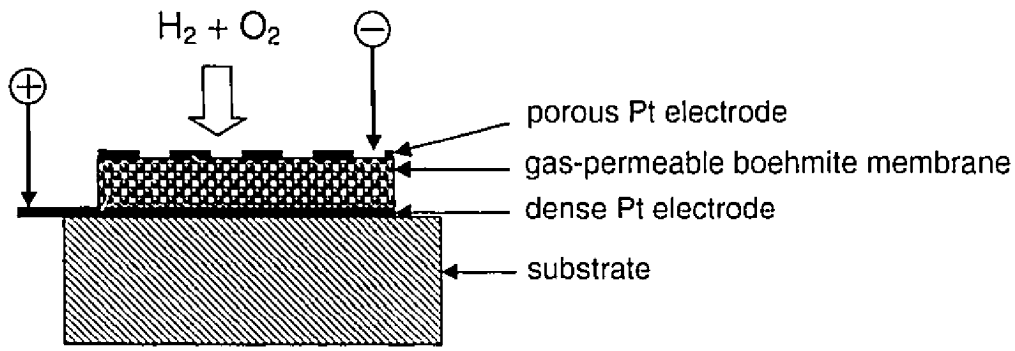

Figure 1.8: Schematics of Dyer's room-temperature single-chamber fuel cell.

The power output could be raised to 162 mW/cm^2 by doping Ni with GDC (gadolinium doped ceria) and LSM with MnO_2, enhancing the catalytic activity of the anode for the partial oxidation of methane and decreasing the activity of LSM for fuel reactions [121].

In addition to electrolyte-supported cells, SC-SOFCs were proposed in three additional cell designs: anode-supported cells, fully porous cells and single-face cells with coplanar electrodes (Fig. 1.9). Compared to electrolyte-supported cells, anode-supported systems are composed of a thick, mechanically supporting anode on which very thin electrolytes can be fabricated, enabling low ohmic cell resistance for low-temperature operation and elevated mechanical stability. Fully porous cells use a porous electrolyte which permits the passage of reactant gases for flow-through operation. In single-face cells, both anode and cathode are situated on the same side of the electrolyte.

1.3.5 Electrolyte-supported cells

With the confirmation of the feasibility of SC-SOFCs by reproducing the results of Hibino et al. [105, 141], the further development of electrolyte-supported SC-SOFCs focused on studying the effects of Ni-based anodes of different composition [111, 142, 143], reducing the catalytic activity of LSM for the fuel reactions by optimizing sintering conditions [109] and exploring new cathode (LSCF [144, 145], SSC [145]) and electrolyte (LSGM [108], $BaLaIn_2O_{5.5}$ [146]) materials.

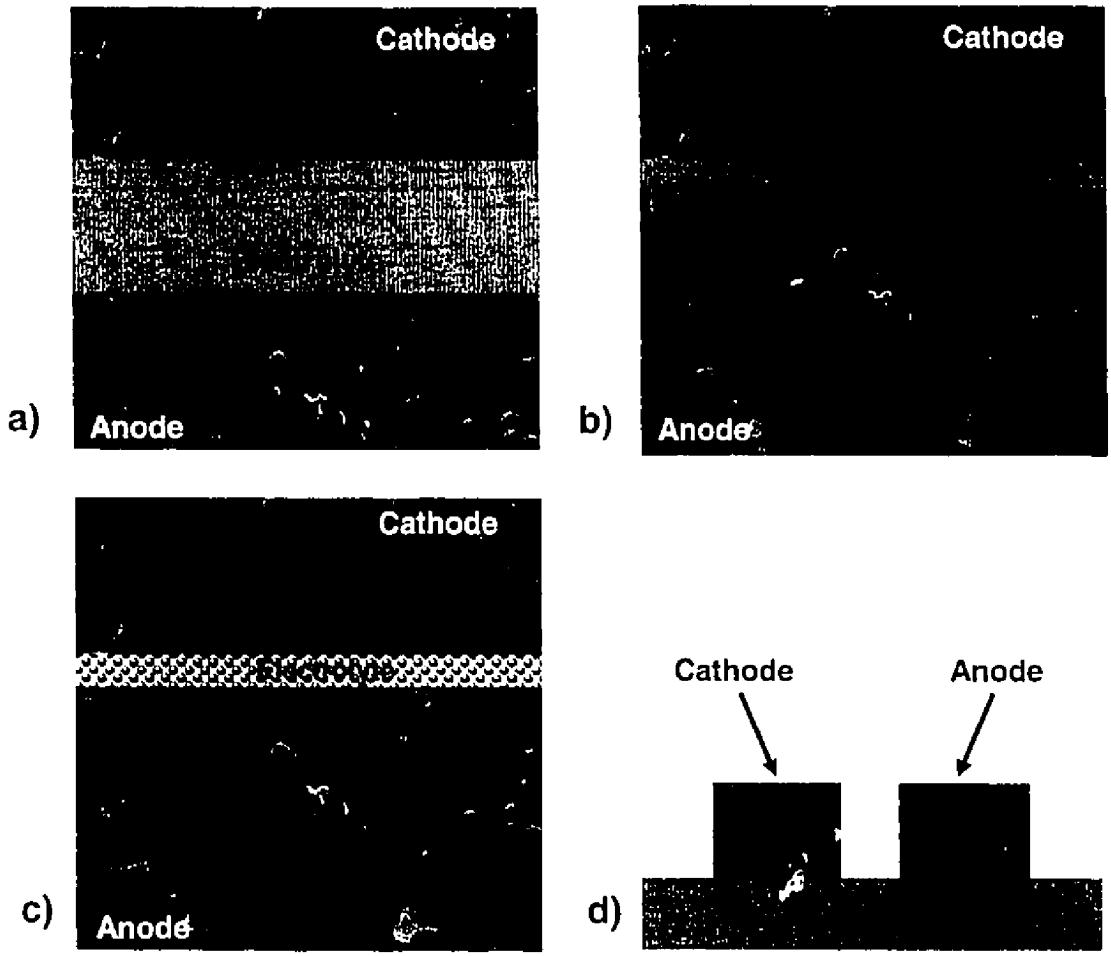

Figure 1.9: Schematics of the different SC-SOFC cell designs: a) electrolyte-supported cell, b) anode-supported cell, c) fully porous cell and d) single-face cell with coplanar electrodes.

The catalytic activity of platinum current collectors towards methane was reduced by embedding the collectors inside the electrodes during cell fabrication [141]. The necessity to carefully design the reaction chamber was discussed [93, 147], as a continuous flow of the reactant gases with reduced stagnation and limited gas mixing between anode and cathode were found to be beneficial for cell operation. Anode thickness was shown to affect the stability of the cell voltage due to oxidation-reduction cycles of nickel [148].

Attempts to reduce the cell operating temperatures below 950°C led to the use of hydrocarbons with higher reactivity than methane. The reactivity of methane was too

low to sustain its partial oxidation at temperatures below 600°C, and no power output could be obtained [111]. Higher hydrocarbons such as ethane, propane, liquefied petroleum gas and ethanol enabled the generation of an electrical power output at reduced operating temperatures, and the best performance was obtained with ethane as fuel in a temperature range between 400 and 700°C. Cell operation was also possible at furnace temperatures of 300-450°C in butane-air mixtures, due to the heat release from the exothermic oxidation reactions of the fuel [106].

The first demonstration of assembling and operating SC-SOFCs in stacks consisted in a serial connection of several single cells [104]. An OCV of 800 mV and a maximum current density of 55 mA/cm^2 were measured at 700°C in a methane-air mixture with a single cell, whereas 3 V in open circuit were obtained from the series connection. Au cathodes and Pt or Ni-CeO_2 anodes on a YSZ or barium-based electrolyte were used. A cell stack, composed of two Ni-SDC (samarium doped ceria) anodes on one side and two LSCF-SDC cathodes on the opposite side of a 0.5 mm thick SDC electrolyte, delivered open circuit voltages of 1.48 and 1.6 V at 500°C in a propane-air mixture (R_{mix} = 1/1.8) [149]. A 20 cell stack was estimated to deliver 15 V.

Direct comparison between the different studies reported in the literature is difficult due to differences in cell materials, cell size, testing parameters and testing setup. However, the highest power output for an electrolyte-supported SC-SOFC (644 mW/cm^2) was reported for a Ni-Pd-SDC//SDC//SSC cell tested in a methane-air mixture with R_{mix} = 1 at 550°C [143]. The lowest operating temperature demonstrated so far was 300°C at which the Ni-SDC//SDC//SSC cell delivered a maximum power density of 42 mW/cm^2 for isobutane, 38 mW/cm^2 for butane, 20 mW/cm^2 for propane, 17 mW/cm^2 for ethane and 0 mW/cm^2 for methane as fuel.

1.3.6 Anode-supported cells

Due to the insufficient selectivity of current electrode materials for the respective reactions and the resulting low cell efficiencies, research on anode-supported SC-SOFCs focused on the improvement of the cathode catalyst. Doping LSM with SDC induced a reduction of the catalytic activity of LSM for fuel reactions [150]. A performance increase was also observed when replacing LSM by LSCF [151]. BSCF was proposed as a new cathode material with elevated catalytic activity for the oxygen

reduction reaction for intermediate temperature operation (400-575°C) [65]. Compared to SSC and LSCF cathode materials, this material additionally exhibited the lowest activity for methane conversion [152]. For a cell with Ni-SDC anode, BSCF cathode and SDC electrolyte tested in a methane-air mixture with R_{mix} = 1.2 at 650°C, a maximum power density of 760 mW/cm^2 was obtained, corresponding to the highest power output for SC-SOFCs reported in the literature so far [152]. Additionally, this cell performance was comparable to the performance of a conventional dual-chamber SOFC.

On the anode side, aging experiments revealed reduction-oxidation cycles of the Ni-based electrodes and loss of metallic nickel due to nickel volatilization, leading to voltage fluctuations and anode degradation [12].

The heat generated from the partial oxidation of the hydrocarbon fuel at the anode was shown to be sufficient to sustain the temperature of a cell at 500-600°C without any external heating [15]. This thermally self-sustained system permitted rapid start-up from cold start to stable power output in less than 1 min and delivered peak power densities of 182 to 247 mW/cm^2.

The reduction of electrolyte thickness by changing from electrolyte-supported to anode-supported cells enabled cell operation at temperatures below 400°C [153]. With butane as fuel, cells could be operated at furnace temperatures down to 200°C as the heat release during fuel oxidation increased the real cell temperatures by up to 150°C. At such low operating temperatures, operation of cells on liquid fuels such as dimethyl ether and ethanol was possible [112].

1.3.7 Fully porous SC-SOFCs

The use of non-gas tight, porous electrolytes enables the cost-reduced, low-temperature fabrication of electrolytes using conventional processing techniques, e.g., screen printing of an electrolyte film on top of the anode substrate. Densification of the electrolyte at high sintering temperatures is no longer required. A minimum thickness of 10 µm should, however, be respected for porous electrolytes in order to physically separate the electrodes and avoid short circuits [101]. In addition to bulk ionic conduction, a porous electrolyte also exhibits surface ionic conduction, permitting a reduction of the ohmic resistance [120]. The use of a porous electrolyte can also increase the number of TPBs and lead to improved cell performance [154].

Two types of SC-SOFCs with porous electrolytes are possible, depending on the gas-flow configuration [123]. In the first type, the whole cell is located in the gas flow, creating a flow-by configuration. In a flow-through configuration, the reactant gases have to pass through the first electrode and the electrolyte in order to reach the opposite electrode, enabling improved mass transport compared to flow-by configurations [102]. The operation of a fully porous SC-SOFC in the flow-through configuration was demonstrated for the first time for a Ni-GDC//GDC//SSC cell operated at a methane-to-oxygen ratio of R_{mix} = 1 and at 733°C, delivering 10 mW/cm^2 [91]. The cathode was exposed first to the incoming gases, which had to pass through cathode and electrolyte to reach the anode. A fully porous SC-SOFC operated in the flow-by regime with Ni-YSZ anode, LSCF cathode and porous YSZ electrolyte exhibited a maximum power density of 660 mW/cm^2 at 600°C in a methane-air mixture with a current efficiency of approximately 4-8% [154]. Gas flow rates were found to significantly affect cell performance for both configurations. Notably, high flow rates were beneficial in order to avoid the flowing back of reaction products [91] and the diffusion of reaction products through the porous electrolyte between the electrodes [154].

1.3.8 SC-SOFCs with coplanar electrodes

In SC-SOFCs with coplanar electrodes, both anode and cathode are situated on the same side of the electrolyte. The gap between adjacent electrodes is bridged by the electrolyte, which provides an ion conduction path from one catalyst to another. This type of SC-SOFC is also called a surface-conduction SC-SOFC [155]. The basic design of SC-SOFCs with coplanar electrodes consists of a side-by-side electrode pattern of parallel electrode lines [99] or electrode strips [101]. Anode and cathode strips can also be arranged in an alternating fashion on the same side of the electrolyte to form coplanar electrode arrays [156] or interdigitated, comblike electrode patterns [5, 7] to increase the effective electrode area.

The advantage of the single-face configuration over the dual-face configuration is the possibility to use a thick, mechanically strong electrolyte substrate. The dual-face designs require very thin electrolytes to reduce ohmic resistance and losses, but those thin films are not only fragile but also involve elevated fabrication costs. In the case of

cells with coplanar electrodes, the ohmic resistance is determined by the gap size between adjacent anodes and cathodes and can therefore be decreased by decreasing the interelectrode distance while maintaining a thick electrolyte substrate. The result is a higher mechanical and thermomechanical stability of the cell and enhanced integration compatibility for packaging and stack assembly. Additionally, the single-face configuration enables easy serial and parallel connection of multiple single cells on the same electrolyte substrate.

1.3.8.1 Development of SC-SOFCs with coplanar electrodes

The concept of fuel cells with coplanar electrodes was introduced in 1965 by van Gool based on the idea of ion transport via surface migration between electrode catalysts on the same side of a solid electrolyte [120]. An interdigitated electrode structure was also proposed. A gap size of 1 µm was suggested for the generation of 1 V in a surface-migration cell, making the use of gas mixtures necessary. Van Gool pointed out that challenges for this type of fuel cell included suitable fabrication techniques, highly selective electrode materials, elevated surface conductivity of the electrolyte and explosion risks of gas mixtures.

Based on the surface-migration principle, Louis et al. [99] patented solid electrolyte fuel cells with closely-spaced, rectangular electrodes on the same side of the electrolyte for room temperature operation in separated fuel-air gas streams or gas mixtures. Single cells consisted of one anode and cathode arranged side-by-side on an alumina electrolyte. $SrRuO_3$ was used for the cathode, and Pt for the anode. Although photolithography was suggested as suitable fabrication technique to fabricate cells with small interelectrode gaps for improved cell performance, the cell components were fabricated by painting the electrolyte slurry on top of a substrate and painting electrode slurries with interelectrode gaps of 0.3 to 0.4 mm on the electrolyte. Operation of a single cell at room temperature in a hydrogen-air mixture gave an OCV of 0.67 V and a maximum power of 0.32 $\mu W/cm^2$.

The feasibility of SC-SOFCs with coplanar electrodes was experimentally proven by Hibino et al. in 1995 [157]. Later patented [103], the side-by-side design was proposed for the simplification of solid oxide fuel cell systems. The first SC-SOFC with coplanar electrodes consisted of one Pd and one Au electrode line arranged parallel on

a $BaCe_{0.8}Gd_{0.2}O_{3-\alpha}$ electrolyte. An OCV of 700 mV and a maximum current of 24 mA were generated at 950°C in a methane-oxygen mixture (R_{mix} = 2) [157].

1.3.8.2 Performance considerations

The working principle of SC-SOFCs with coplanar electrodes is schematically shown in Fig. 1.10 and is similar to that of dual-face SC-SOFCs (see Section 1.3.1). H_2 and CO are formed at the anode by the partial oxidation of the fuel and are electrochemically reduced at the anode-electrolyte interface by reaction with oxygen ions coming from the cathode. The transport of oxygen ions mainly occurs at the electrolyte surface and strongly depends on the electrolyte surface morphology [5]. In the case of a $BaCe_{0.8}Gd_{0.2}O_{3-\alpha}$ electrolyte, a smoothly polished surface enabled a surface ionic conductivity similar to its bulk conductivity and led to a smaller ohmic resistance and better cell performance, as compared to cells composed of electrolytes with roughened surface [5]. Similarly, reduction of the ohmic cell resistance and increase in peak power density by reducing the electrolyte surface roughness were found for an SDC electrolyte [17]. A decrease in surface roughness from 1.6 μm to 0.06 μm led to an increase in power density from 68 to 90 mW/cm^2 for a fixed gap size of 1 mm and operation in ethane-air mixtures at 600°C.

In addition to the electrolyte surface morphology, the electrode feature sizes, that is, electrode width and interelectrode gap, affect the ohmic cell resistance. In a theoretical study on single-face SC-SOFCs based on electrode and electrolyte resistance considerations [7], maximum performance was calculated for very small electrode widths and gap sizes on the order of only a few microns to minimize the ohmic resistance. Comparison of different interelectrode distances (10, 20, 40 and 80 μm) by using the finite element method (FEM) also identified maximum cell performance for the smallest studied gap size [18, 158]. The first experimental confirmation of the size effect was provided in Ref. [157] for a cell with parallel Pd and Au electrode lines on a $BaCe_{0.8}Gd_{0.2}O_{3-\alpha}$ electrolyte. Reducing the interelectrode distance from 5 to 0.5 mm led to an increase in the maximum current from 8 mA to 24 mA at 950°C in a methane-oxygen mixture (R_{mix} = 2). The OCV was found to be independent of the variation of the interelectrode gap [8, 21], which principally affected the ohmic resistance of the electrolyte [17].

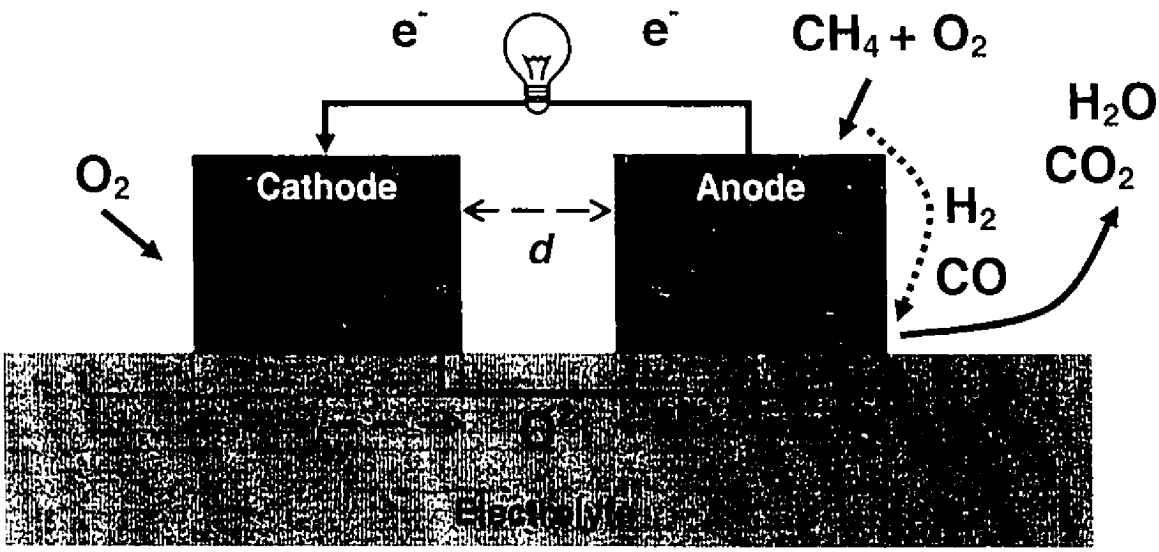

Figure 1.10: Schematics of the operating principle of SC-SOFCs with coplanar electrodes; *d* is the interelectrode spacing and *w* denotes the electrode width.

Similarly, for a cell with coplanar electrodes of Ni-SDC and SSC on an SDC electrolyte tested at 600°C in a C_2H_6-air mixture, a reduction of the gap size from 3 to 0.5 mm (electrode width fixed at 0.5 mm) caused an increase in peak power density from 38 to 193 mW/cm^2, whereas the power density increased from 90 to 130 mW/cm^2 when the electrode width was decreased from 1 mm to 0.5 mm (gap fixed at 1 mm) [17]. Compared to a dual-face cell with an electrolyte thickness equal to the interelectrode gap of the single-face SC-SOFC, the latter exhibited a higher ohmic resistance and lower cell performance. This difference was due to a longer ion conduction path (which corresponds to $2w + d$, with w the electrode width and d the interelectrode distance) in the single-face cell, where the electrode widths have to be taken into account in addition to the electrode distance [17, 159]. By decreasing the electrode widths to match the ionic path, similar performance between dual- and single-face SC-SOFCs could be obtained [17].

However, there seem to be certain limits on how far the miniaturization of the electrode feature sizes can actually be useful. Despite an increase in power output by reducing the electrode width, larger electrodes were found to be more stable during aging [6]. Nickel loss and destabilization affected the whole surface of small electrodes, whereas larger electrodes were only partially degraded. Also, for the smallest cell

reported so far, with two parallel electrodes spaced only 5 μm apart, very poor performance was obtained [160]. The low operating temperature of 400°C and the used electrode materials (Pt and Au) might also contribute to the low voltage output.

Furthermore, the use of closely-spaced electrodes can create problems during fuel cell operation. Reactant gases and reaction products from one electrode can easily migrate to the opposite electrode and destabilize the oxygen partial pressure and therefore the OCV and overall cell performance. This undesired gas-phase transport was observed in Ref. [15] for anode-supported SC-SOFC stacks, where the rapid transport of partial oxidation products from the anode to the cathode of the adjacent cell led to a near-zero OCV. It was suggested that such intermixing and diffusion of reaction gases and products also reduces performance in SC-SOFCs with coplanar electrodes. A partition between anodes and cathodes located on the same side of the electrolyte was proposed to avoid the intermixing and prevent voltage drops [161]. Turbulent flow and gas intermixing between closely-spaced microelectrodes were considered to be at the origin of very low OCVs of only 350 mV [20] and a low power output [162] for coplanar microelectrode arrays. However, in a study with interdigitated microelectrodes with gaps of 14 μm, OCVs over 0.7 V were measured, indicating that diffusion of H_2 and CO from anode to cathode did not affect the cell voltage [13]. According to Ref. [79], a laminar flow field is required for optimal functioning of SC-SOFCs with coplanar electrodes, and very closely-spaced electrodes (< 50 μm) could induce turbulent gas flow leading to low cell performance. Also, there is a minimal gap size of approximately 1 μm [120]. For this interelectrode distance and a potential difference of 1 V between anode and cathode, the electrical field would be 10^6 V/m, which is very close to the electric field leading to disruptive discharge or electrical breakdown ($3x10^6$ V/m in air).

As previously observed for electrolyte-supported cells [148], anode thickness was found to affect the voltage stability of SC-SOFCs with coplanar electrodes [6]. The use of a 300 μm-thick Ni-rich anode layer (80 wt% NiO) on top of a 20 μm thick contact layer consisting of 55 wt% NiO and 45 wt% YSZ enabled a stable open circuit voltage close to 1 V without any major fluctuations during 80 hours of testing, whereas thinner anode layers caused significant voltage fluctuations. Nickel loss due to nickel

volatilization reduced the stability of nickel-based anodes in methane-air mixtures [12], but thick anodes were less subject to degradation, and cell stability could be increased.

Electrode size also plays a role for the operation of SC-SOFCs with coplanar electrodes of the same material [155]. For both electrodes made of platinum, a difference in catalytic activity could be created by using a different size for the anode and cathode. The larger electrode generally worked as the cathode. However, only a few distinct gas compositions allowed the generation of a voltage difference, and the measured OCVs were below 500 mV.

In his work on SC-SOFCs, Riess [101] argues that SC-SOFCs with coplanar electrodes do not function well because of long residence times of the gas mixture over the electrodes in the gas chamber and inhomogeneous current density distribution in the strip electrodes. The latter point can be combined with experimental observations, where Ni-anodes were found to turn white in the anode parts closest to the interelectrode gap, due to microstructural changes resulting from enhanced nickel loss [6, 13]. It was suggested that not the whole electrode surface area participated equally in the electrochemical reactions because of a longer conduction path of the remote electrode regions and increased ohmic cell resistance. The region of an electrode close to the next adjacent counter electrode is therefore believed to be principally involved in the energy generating reactions.

To date, only few publications are available on SC-SOFCs with coplanar electrodes. Most of them are feasibility or proof-of-concept studies and deal with fabrication techniques and effects of testing parameters, cell geometry and electrode size. However, as to what is really happening on and between the electrodes, almost no analyses have been conducted yet. The small size of the electrodes yields very low conversion rates of the reactant gases, making it difficult to detect differences between input and output gases by mass spectroscopy in order to identify occurring reactions. Also, there is little understanding of the actual conduction path of the oxygen ions in the electrolyte. In one study, the difference in catalytic activity between anode and cathode for ethane-air mixtures was investigated using mass spectroscopy [17]. Additionally, impedance analysis of the ohmic cell resistance due to different electrolyte materials and electrode gaps was performed. However, the studies were applied to rather big electrodes (1 mm gap and width) as compared to microscale electrode structures. Due

to the lack of fundamental studies, models, and appropriate characterization and fabrication techniques, the actual working principles of SC-SOFCs with coplanar electrodes are not yet fully understood.

1.3.8.3 Testing conditions

Among the different testing conditions, the effect of gas flow direction, gas composition and operating temperature on cell performance has mainly been studied. For cells with two parallel electrode lines being exposed to various gas flow directions, the highest OCV was obtained for parallel gas flow [21]. Oxygen consumption at the anode and reaction gas intermixing caused the lowest OCV for perpendicular gas flow with the anode being placed ahead in the gas stream. Slightly different results were obtained in Ref. [6]. Lowest performance was confirmed for a cell position with the anode being exposed first to the gas mixture. Enhanced oxygen consumption at the anode and an oxygen-lean gas mixture reaching the cathode caused a low OCV and hence performance. Oxygen-rich mixtures with $R_{mix} \approx 1$ could compensate for the partial reaction of oxygen at the anode and the composition change of the gas mixture, but positioning the cathode first in the incoming gas stream led to the highest power output. For a fuel cell stack composed of several pairs of anode and cathode lines, highest performance was achieved for parallel positioning, which least affected the gas composition. Using FEM modeling, perpendicular gas flow with the cathode being exposed first to the incoming gas mixture was confirmed to be most favorable for an increased power output [18, 158].

The optimum gas mixture composition differs between studies depending on cell component materials, chamber design, temperature and reaction gases. For instance, for coplanar Ni-YSZ and LSM-based electrodes on YSZ electrolytes, the maximum OCV was observed in the vicinity of $R_{mix} = 2$ with a significant voltage drop for $R_{mix} = 0.5$ at 800°C in methane-air mixtures [6]. Similar results were obtained for anode-supported cells [105].

For SC-SOFCs with coplanar electrodes composed of Ni-GDC-Pd anode and LSM-YSZ cathode on a YSZ electrolyte, testing at 850°C in a methane-air mixture revealed an increase of the OCV with increasing R_{mix} [163]. Low OCVs (< 0.4 V) were obtained at $R_{mix} = 1$, whereas OCVs > 500 mV could only be measured for higher R_{mix},

with a maximum at R_{mix} = 5. For single electrode lines [8] and microelectrode arrays [20], R_{mix} = 3.75 was necessary for operation in methane-air mixtures at 900°C. However, such high R_{mix} values are unsuitable for cell operation, as they favor carbon formation and restrain performance [39]. For methane-air mixtures containing 3% H_2O at 900°C, a range of R_{mix} from 2.78 to 6.67 was confirmed to lead to superior cell performance, whereas the stoichiometric ratio (R_{mix} = 2) for the partial oxidation of methane led to the highest OCV for dry reaction gas [21]. The explanation of the high R_{mix} in the wet gas mixture was based on the occurrence of methane steam reforming.

In the case of interdigitated microelectrodes, fuel-rich gas mixtures were found to improve the cell performance output, whereas oxygen-rich mixtures lowered the OCV by transporting more oxygen to the very thin anode (2-3 μm) than it could convert [13].

The use of other fuels than methane was studied for operation at lower temperatures of 500-600°C [17]. Among the different electrolyte materials studied, SDC showed a lower ohmic resistance and led to a higher power output than YSZ or LSGM electrolytes in combination with a Ni-SDC and a SSC cathode. Similar cell performance was measured for ethane, propane and butane as fuel, whereas the low catalytic activity of the anode for methane partial oxidation at the reduced operating temperatures caused very poor performance in methane-air mixtures. The addition of PdO to the anode was found to enhance the catalytic activity of the anode for the hydrocarbon partial oxidation.

1.3.8.4 Microfabrication techniques

The use of closely-spaced small-scale electrodes points out the great potential of SC-SOFCs with coplanar electrodes for miniaturization and their potential application as small- and microscale power sources. However, it also imposes challenges on the fabrication of such small electrode dimensions. Standard photolithography based microfabrication techniques enable the precise creation of microscale patterns, but the difficulty lies in creating such patterns out of multicomponent ceramic materials and creating electrodes with a porous microstructure. Thus, there is a need to find suitable, alternative techniques with high versatility to fabricate electrode patterns of precise dimensions at the microscale, to fabricate different electrode geometries, to precisely deposit the electrodes on an exact position on the electrolyte substrate, to allow

elevated deposition and fabrication rates, and finally to manufacture porous electrodes from ceramic materials.

Although thin-film deposition techniques and photolithography-based microfabrication are suggested in the literature, the fabrication and the testing of complete cells are still lacking. Thin-film technologies (e.g., spin-on techniques, plasma spraying, chemical vapor deposition, laser deposition, sputtering, evaporation and wet spray) are proposed to fabricate coplanar thin-film microelectrodes with interdigitated, comblike or differently shaped electrodes [129]. The electrodes can either be formed by deposition of the electrode material in the desired shape or by filling trenches in the electrolyte or substrate with electrode material. Standard photolithography and wet chemical etching were used to fabricate interdigitated lanthanum strontium cobalt oxide cathodes from sputtered thin films [164]. Despite spacings and electrode widths of 50 μm, the technique has not been expanded yet to the fabrication of interdigitated patterns of both anode and cathode. Also, the technique yielded very dense electrodes, decreasing the number of TPBs for the electrochemical reactions. Photoresist molding of coplanar microelectrode arrays on a radio-frequency sputtered GDC electrolyte resulted in interelectrode distances and electrode widths of 20 μm [156]. The smallest interelectrode gap for a functional single-face SC-SOFC with two parallel electrode lines (electrode width of 15 μm) reported so far was 5 μm and was achieved by thin-film deposition techniques and photolithographic patterning [160]. However, the electrodes were made of Pt and Au instead of conventional, cermet and/or ceramic-based SOFC materials. The cells could actually be tested, but showed very poor performance.

The first SC-SOFCs with coplanar electrodes were fabricated by manually smearing electrode inks with a brush on the electrolyte surface [157]. This technique has been used by Hibino et al. ever since, but cells with interelectrode gaps and electrode widths smaller than 0.5 mm were not fabricated. Screen printing with electrode masks yielded minimum gap sizes of 0.3 mm [13] and 0.2 mm [6, 98] with minimum electrode widths of 0.5 mm [6]. For further miniaturization and the creation of interdigitated microelectrode patterns, different microfabrication techniques are necessary, among which micromolding, microfluidic lithography and robotic direct-writing approaches are currently the principal fabrication methods reported in the literature.

A micro-patterning method based on polymer molds and vacuum-assisted infiltration enabled the fabrication of interdigitated electrodes with an interelectrode distance of 50 μm and a width of 100 μm [20]. In contrast to thin-film fabrication techniques, this microfluidic lithography approach integrated colloidal processing of ceramics and thus had the advantage of enabling a better control of the electrode microstructures in a subsequent sintering step. Microchannels in the mold were filled with electrode material (LSM for the cathode and Ni-SDC for the anode) and formed the microscale electrode structure on the YSZ electrolyte substrate.

A similar approach, called micromolding in capillaries, was employed to fabricate SC-SOFCs with interdigitated, 100 μm wide electrodes separated by gaps of only 14 μm [13]. However, the technique led to low reproducibility, and incomplete filling of the mold channels with electrode material resulted in only a few interdigitated electrode lines.

After the successful fabrication of dual-chamber SOFCs using a robot-controlled direct-writing technique [76], this method was also applied to the creation of SC-SOFCs with single and multiple pairs of coplanar electrodes [8, 21]. For average electrode widths of ~600 μm, interelectrode distances ranging from 255 to 783 μm were reported for single electrode pairs, whereas interdigitated electrode structures were fabricated with average gaps of approximately 300 μm.

1.3.8.5 SC-SOFCs with interdigitated coplanar electrode designs

The first SC-SOFC with coplanar microelectrode arrays was fabricated and tested by Kim et al. in 2005 [156]. The cell was composed of Ni-GDC anode and SSC cathode lines spaced apart by a 20 μm gap on a $Ce_{0.9}Gd_{0.1}O_{1.95}$ electrolyte. An OCV of 205 mV and a maximum power density of 67 mW/cm^2 were measured in a methane-air mixture at 500°C.

An OCV of only 350 mV was obtained for microarrays of Ni-SDC and LSM on YSZ (electrode gap of 50 μm) using methane as a fuel [20]. At 900°C and R_{mix} = 3.75, the maximum power density was ~75 mW/cm^2. The low OCV was attributed to turbulent flow and gas intermixing between the closely-spaced electrodes, as well as methane consumption in undesired reactions. Operation at lower temperatures in propane-air

mixtures with a SSC-SDC cathode did not yield any performance improvement [162]. In addition to gas intermixing between the interdigitated electrodes with gap sizes of 100 µm, phase decomposition of the cathode led to a power output of only 1.5 mW/cm^2 at 550°C.

OCVs over 800 mV were then achieved for combshaped Ni-SDC anodes and LSM cathodes on SDC and YSZ electrolytes [98]. OCV as well as power density were found to depend on the furnace temperature. While the OCV slightly decreased with increasing temperature from 550 to 700°C, the maximum power density increased, reaching 40 mW/cm^2 at 700°C and R_{mix} = 1.

A dependence of the OCV on the number of electrode pairs was observed for Ni-GDC-Pd anodes and LSM(-GDC) cathodes on a YSZ electrolyte [8, 21]. When the number of electrode pairs was increased from 1 to 8, the OCV decreased from 0.8 V to 0.4 V. The OCV drop was attributed to an increased system complexity, where the intermixing of reaction products was enhanced and the oxygen partial pressure at the cathode was reduced. In the case of cells with two electrode pairs, this performance loss could be overcome by decreasing the distance between the two pairs [21]. Increasing the pair-to-pair distance to 8 mm led to a recovery in cell performance and finally the same OCV and maximum power density as for a single pair of electrodes.

The feasibility of SC-SOFCs with interdigitated microelectrodes was also shown by comparing the performance of macro-, milli- and micro-SC-SOFCs [13]. Micro SC-SOFCs with interdigitated electrodes separated by gaps of only 14 µm were successfully operated in methane-air mixtures at 650°C, delivering a maximum power density of 17 mW/cm^2. Compared to macro and milli cells, the reduction of the interelectrode gap as well as the increased number of anode-cathode pairs connected in parallel in the interdigitated pattern of the micro cell maximized the usable cell surface area and enabled a ten-times higher power density.

1.3.8.6 Cell stacks

In his patent on SC-SOFCs in the single-face configuration [99], Louis et al. discussed the possibility of series connection of single cells on the same electrolyte substrate. Different connecting approaches were proposed such as electrically connecting adjacent electrodes of each cell pair, depositing electrodes on alternately

arranged stripes of electrolyte and interconnect, or bridging the gap between electrodes of one cell by an electrolyte layer and the gap between adjacent cells by overlaying interconnect material.

The possibility of series and parallel connection of two unit cells on the same electrolyte plate was experimentally demonstrated by Hibino et al. [5]. Series connection of two cells doubled the measured OCV, whereas parallel connection led to half the maximum current of a single cell. An electrode configuration composed of several electrode lines arranged in a comblike, interdigitated manner was proposed to maximize the electrode area and create closely-spaced electrodes [5, 17, 165]. A stack assembly of such electrode structures being connected in series and in parallel was patented in 1996 [166]. Another stack design consisted of a thin-film electrolyte applied on both sides of an alumina support, followed by deposition of alternating anode and cathode bars on top of the electrolyte [167].

In comparison to a single cell composed of one anode and cathode line, stacked cells of two and three sets of electrodes connected in parallel on the same electrolyte substrate led to an increase in cell performance [6]. A stack of two sets of electrodes doubled the power output as compared to the single cell, whereas the power could be doubled further by increasing the number of electrodes to three sets.

1.3.8.7 Summary of SC-SOFCs with coplanar electrodes

Tables 1.3 to 1.4 summarize fabrication technique, electrode gap size and width, cell component materials, operating parameters and performance of SC-SOFCs with coplanar electrodes reported in the literature.

Table 1.3: Summary of SC-SOFCs with one pair of coplanar electrodes.

Ref.	Year	Fabrication technique	Gap size d / Electrode width w (mm)	Electrolyte	Anode	Cathode	$T_{furnace}$ (°C)	Gas mixture	OCV (V)	P_{max} or I_{max} (for smallest d and w)
[99]	1981	Painted*	0.3-0.4/0.5	Alumina	Pt-Al_2O_3	$SrRuO_3$-Al_2O3	21	H_2-O_2-N_2	0.67	3 μA
[157]	1995	Smeared*	0.5-5	$BaCe_{0.8}Gd_{0.2}O_{3-\alpha}$	Pd	Au	950	CH_4-air R_{mix}=2	0.7	24 mA
[5]	1996	Smeared*	0.5-5/1-4	$BaCe_{0.8}Gd_{0.2}O_{3-\alpha}$	Pd	Au	950	CH_4-air R_{mix}=2	0.7	24 mA
[121]	2000	Smeared*	1-4/1	YSZ	Ni-GDC	LSM-MnO_2	950	CH_4-air R_{mix}=1	0.8	102 mW/cm^2
[159]	2000	Smeared*	0.5-3	YSZ-MnO_2	Ni-GDC	LSM-MnO_2	950	CH_4-air R_{mix}=1	0.8	143 mW/cm^2
[168]	2001	Smeared*	0.5	YSZ	Ni	LSM	950	CH_4-air	0.8	140 mW/cm^2
[17]	2002	Smeared*	0.5-3/0.5-1	SDC	Ni-SDC-PdO	SSC	600	C_4H_{10}-air R_{mix}=0.6	0.8	245 mW/cm^2
[17]	2002	Smeared*	1/1	YSZ	Ni-SDC	SSC	600	C_2H_6-air R_{mix}=1.1	0.97	20 mW/cm^2
[17]	2002	Smeared*	1/1	LSGM	Ni-SDC	SSC	600	C_2H_6-air R_{mix}=1.1	0.92	50 mW/cm^2

Ref.	Year	Fabrication technique	Gap size d / Electrode width w (mm)	Electrolyte	Anode	Cathode	$T_{furnace}$ (°C)	Gas mixture	OCV (V)	P_{max} or I_{max} (for smallest d and w)
[169]	2005	Screen printing	1/6	YSZ	Ni-YSZ	LSM	800	CH_4-air R_{mix}=1.5	0.6	1.2 mW/cm^2
[8. 163]	2006	Direct-writing	0.255-0.783/0.6	YSZ	Ni-GDC-Pd	LSM	900	CH_4-air R_{mix}=3.75	0.8	101 mW/cm^2
[21]	2007	Direct-writing	0.255-0.783/0.6	YSZ	Ni-GDC-Pd	LSM-GDC	900	CH_4-air + 3% H_2O R_{mix}=3.75	0.8	101 mW/cm^2
[6]	2007	Tape casting	0.2-1/0.5-4	YSZ	Ni-YSZ	LSM	800	CH_4-air R_{mix}=2	0.9	40 mW/cm^2
[13]	2007	Screen printing	1.2/0.5	GDC	Ni-GDC	SSC	600	CH_4-air R_{mix}=3.2	0.8	1.5 mW/cm^2
[160]	2007	Sputtering, lithography	0.005/0.015	YSZ	Pt	Au	400	CH_4-air R_{mix}=1	0.38	
[155]	2008	Smeared*	1-1.2/1	YSZ SDC	Pt	Pt LSM	600-1000	H_2-O_2	0-0.7	

*painted/smeared: electrode slurries or pastes were painted/smeared on the electrolyte.

Table 1.4: Summary of SC-SOFCs with coplanar interdigitated, comblike electrodes.

Ref.	Year	Fabrication technique	Gap size d / Electrode width w (mm)	Electrolyte	Anode	Cathode	$T_{furnace}$ (°C)	Gas mixture	OCV (V)	P_{max} (mW/cm^2)
[156]	2005	Photoresist molding	0.02/0.02	GDC	Ni-GDC	SSC	500	CH_4-air	0.2	67
[98]	2006	Screen printing	0.2-1	SDC	Ni-SDC	LSM	700	CH_4-air R_{mix}=1	0.8	40
[98]	2006	Screen printing	0.2-1	YSZ	Ni-SDC	LSM	700	CH_4-air R_{mix}=1	0.9	
[20]	2006	Microfluidic lithography	0.05/0.1	YSZ	Ni-SDC	LSM	900	CH_4-air R_{mix}=3.75	0.35	75
[8, 21]	2007	Direct-writing	0.3/0.6	YSZ	Ni-GDC-Pd	LSM-GDC	900	CH_4-air R_{mix}=3.75	0.43-0.65	12-15
[162]	2007	Microfluidic lithography	0.1/0.1	SDC	Ni-SDC	SSC-SDC	550	C_3H_8-air R_{mix}=0.7	0.67	1.5
[13]	2007	Screen printing	0.3/1.2	GDC	Ni-GDC	SSC	650	CH_4-air R_{mix}=1	0.72	1.5
[13]	2007	Micro-molding in capillaries	0.014/0.1	CGO	Ni-CGO	SSC	650	CH_4-air R_{mix}=2	0.7	17

1.4 Direct-write microfabrication

Direct-write assembly techniques allow fabrication of complex structures and geometries with high design flexibility. These techniques figure among freeform fabrication methods [170] and include ink-jet printing, micropen, hot-melt printing and robotic deposition (or robocasting) [171, 172]. In contrast to conventional microfabrication techniques such as lithography based methods, there is no need for masks or molds. Generally, a paste-like material (e.g., ink or suspension) composed of powder particles, solvents, binders, dispersants, precursors, etc., is deposited on a substrate either by droplet-based (e.g., hot-melt and ink-jet printing) or continuous (e.g., micropen writing and robotic deposition) methods [171].

The direct-writing technique used in this project consists of the robot-controlled deposition of a colloidal suspension on a substrate (see Fig. 1.11). The ink, which is contained in a syringe, is continuously extruded through a micronozzle by applying pressure and is deposited onto a substrate mounted on a mobile platform.

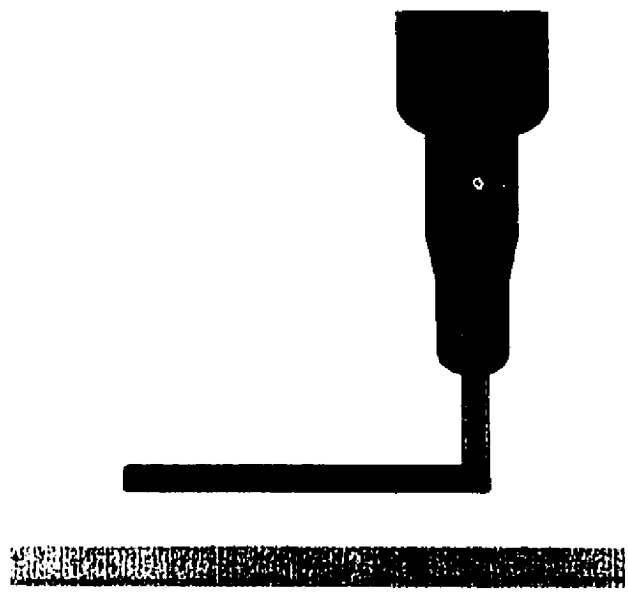

Figure 1.11: Schematic representation of direct-write deposition of a continuous ink filament on a substrate by pressure-driven extrusion through a micronozzle.

The term generally used in the literature for this fabrication technique is direct-writing [173] or direct-write assembly [171, 174], but robocasting [170], robo-dispensing [21] and extrusion freeforming [175] can also be found.

The technique can be applied to a wide range of materials that can be processed as inks [171, 176, 177]. Control of the rheological properties of the ink is essential for a successful deposition. Possible layer-by-layer deposition and the use of extrusion micronozzles make direct-writing an interesting technique for the fabrication of three-dimensional and microscale structures [178, 179]. As an example, ceramic micro-fibers and lattices [175], 3D microfluidic networks [23], microscale piezoelectric arrays [180] and photonic crystals [181] were fabricated by direct-writing. The direct-writing method also enables the fabrication of electrode structures for fuel cell applications [182]. After the successful fabrication of dual-chamber μSOFCs [76, 183], the technique was also applied to the creation of SC-μSOFCs with coplanar micro-patterned electrodes [8, 21].

Chapter 2 Scientific approach and coherence of articles

2.1 Scientific approach and organization of research work

This work was essentially of an experimental nature, as its principal aim was to study the feasibility of SC-μSOFCs with coplanar electrodes and to enlarge the knowledge of their operation principles and of the different parameters affecting the cell performance. Cells were to be fabricated by a direct-write microfabrication technique (objective 1). The electrochemical characterization of the fabricated cells should then confirm their feasibility (objective 2) and include investigation of the effects of electrode size (objective 3), electrode shape (objective 4), current collection method, electrode material and electrolyte thickness (objective 5) on cell performance. Finally, cell performance should be calculated using an electrochemistry model and be compared with the experimentally obtained performance (objective 6). The research was therefore organized in three main parts: a) the direct-write microfabrication of SC-μSOFCs with coplanar electrodes, b) the characterization of the fabricated cells and c) the performance calculations.

The first part of the project started with familiarization with the direct-writing apparatus and the fabrication of cells using electrode inks based on state-of-the-art ceramic colloidal suspensions. Electrodes were to be fabricated from conventional SOFC electrode materials. At the beginning, focusing only on one electrode permitted identification of the effects of the main process parameters such as deposition speed and extrusion pressure on the quality of the deposited electrode structures. Additionally, the electrode inks conventionally used for screen printing had to be adapted for the direct-writing technique. The anode was chosen for this preliminary work because its higher sintering temperature in comparison to the cathode material implied its fabrication prior to the cathode. Once ink properties and deposition technique were sufficiently mastered, microscale anode comb-structures were successfully fabricated. After sintering, the anode exhibited a porous microstructure and adhered well to the electrolyte substrate. The fabrication of the cathode was then tackled in order to create SC-μSOFCs with interdigitated electrodes. Based on the work on the anode, the cathode could be similarly synthesized. However, after sintering of the already

deposited anode, the cells had to be reinstalled on the direct-writing apparatus for the cathode deposition. Cell alignment for perfectly parallel anode and cathode patterns proved rather difficult. Therefore, the fabrication procedure was later simplified by employing cofabrication and cosintering of both electrodes.

After the successful fabrication of cells with coplanar electrode patterns, the electrochemical characterization followed as the second part of this project. A high-temperature testing setup had been previously designed by Dr. Napporn and Prof. Meunier from the Department of Engineering Physics at École Polytechnique for testing dual-face SC-SOFCs. With their research activities on SC-SOFCs having completely moved to the Hydro Québec Research Center in Varennes, their first testing setup at École Polytechnique was left to the entire disposition of this project. Although the testing setup had originally been designed for dual-face electrolyte- or anode-supported cells, it could also be employed for the characterization of single-face cells with coplanar electrodes after some modifications concerning cell holder and current collectors. Additionally, the current and power generated from the micro cells with coplanar electrodes were much lower than those of the larger dual-face cells and could not be measured with the original installation. Thus, a manual measuring system had to be added consisting of a decade resistor and a digital multimeter. The cells could be tested by varying the resistance on the decade resistor and reading the corresponding value of the cell current. The fabricated cells exhibited sufficiently high open circuit voltages to permit a power output and enable their electrochemical characterization.

Originally, the main objective of the project was to demonstrate the fabrication of structurally stable, closely-spaced interdigitated coplanar electrodes for SC-μSOFCs using the direct-writing technique. The fabrication of electrode structures with widths and interelectrode gaps of 100 μm down to 10 μm was targeted. Characterization of the fabricated cells should include microstructural analysis, electrode conductivity measurements and mechanical stability studies during thermal cycling. The electrochemical testing was not initially planned. Merely one year after the beginning of the project, the suitability of the direct-write microfabrication technique for creating SC-μSOFCs with interdigitated coplanar microscale electrodes was already demonstrated. The obtained electrode widths ranged between 100 and 400 μm, whereas cells with

interelectrode gaps down to ~50 μm were fabricated. Microstructural analysis confirmed a porous electrode microstructure with a percolating particle network after sintering.

The collaboration with Prof. Meunier's group enabled access to an electrochemical testing setup specifically designed for single-chamber SOFCs, and the scope of the project was then expanded to include the electrochemical testing of the fabricated cells. The electrochemical characterization showed that, before aiming to fabricate SC-SOFCs with coplanar electrodes down to only a few micrometers, the stable, repeatable operation of cells with electrodes at a size scale of a few hundred micrometers, as currently reported in the literature, had first to be ensured. Notably, the necessity to correctly understand the working principles of SC-μSOFCs with coplanar electrodes was judged more crucial for the advancement of this technology than proving the fabrication of cells with electrode sizes below 50 μm. The observation of a zero voltage for cells with single microelectrode pairs additionally raised questions on the miniaturization of the electrode size. New objectives were therefore defined with regard to further studying the working principles and functioning of SC-μSOFCs with coplanar electrodes. The direct-writing technique was to be employed as a suitable tool for creating electrode structures of different configurations, dimensions and materials. Still in concordance with the original objective of electrode miniaturization, the possible existence of size limits was to be studied. The experimental work following the newly defined objectives should also include the characterization of the effects of electrode shape, electrode material and current collection method on the cell performance. Additionally, a theoretical part was added in order to compare the measured cell performance with the performance calculated by using a simplified electrochemistry-based model.

Finally, a two-month visit within Prof. Lewis' Colloidal Assembly Group at the Department of Materials Science and Engineering at the University of Illinois at Urbana-Champaign permitted the development of new electrode inks for direct-writing. The group of Prof. Lewis is specialized in colloidal science as well as direct-write microfabrication. They develop viscoelastic, gel-like, polyelectrolyte-based inks for the direct-write assembly of three-dimensional structures with elevated shape retention.

2.2 Article presentation and coherence with research objectives

The work presented in this thesis was disseminated in the form of five peer reviewed papers in archival journals and two peer reviewed proceedings papers. Three of these papers focused on the direct-write microfabrication of SC-μSOFCs with coplanar electrodes, whereas four publications reported the results from cell characterization with the effects of electrode size, electrode shape, current collection method and electrode composition. These seven papers cover the objectives of fabrication (objective 1) and characterization (objectives 2-5) of SC-μSOFCs with coplanar electrodes as detailed in the following sections.

2.2.1 Direct-write microfabrication of SC-μSOFCs with coplanar electrodes: Chapter 3 and Appendix I and II

The first results on the direct-write microfabrication of SC-μSOFCs with coplanar interdigitated electrodes (objective 1) were presented at the *Materials Research Society Fall Meeting 2006* in Boston, MA, and were published in the form of the peer reviewed proceedings paper reproduced in Appendix I. The paper described preliminary investigations on:

- Electrode ink rheology and composition;
- Influence of process parameters on the quality of the deposited electrode structures;
- Microstructural analysis of the fabricated electrodes;
- Demonstration of the feasibility of SC-μSOFCs with coplanar interdigitated electrodes using the direct-writing technique.

With the successful electrochemical testing of the fabricated cells (objective 2), direct-write microfabrication was presented as a useful tool for the fabrication of SC-μSOFCs with coplanar electrodes (objective 1) in the *Journal of Micromechanics and Microengineering* (Chapter 3). The article entitled "Direct-write microfabrication of single-chamber micro solid oxide fuel cells" was published on November 28, 2007. This paper described the link between a microfabrication technique and its ability to create

novel microscale devices, corresponding exactly to the theme covered by the chosen journal. Specifically, the accomplishments of this paper are the following:

- Detailed process characterization including ink fabrication, ink rheology and ink deposition:
  - Ink composition recommendations with respect to particle loading, ink viscosity and electrode sintering;
  - Rheological characterization, revealing the Newtonian flow behavior of the electrode inks;
  - Establishing a process map for deposition of uniform electrodes using these inks in combination with the direct-writing technique.
- Detailed characterization of the final device:
  - Microstructural characterization of the sintered electrodes;
  - Characterization of the electrode feature sizes;
  - Detailed description of the electrochemical testing setup;
  - Electrochemical characterization involving 24 h aging test;
  - Demonstration of the feasibility of SC-μSOFCs with coplanar interdigitated electrodes delivering a power output in the mW range.

Finally, the use of viscoelastic, gel-like inks for the direct-write microfabrication of SC-μSOFCs with coplanar electrodes (summarized in Chapter 8 and described in detail in the proceedings paper in Appendix II) was presented at the *Materials Research Society Spring Meeting 2009* in San Francisco, CA, and the corresponding proceedings paper has been submitted on March 16, 2009. With respect to objective 1, concerning the suitability of the direct-writing technique for creating coplanar microelectrode patterns, the following results are discussed:

- Fabrication and rheological characterization of gel-like anode and cathode inks;
- Direct-write microfabrication of uniform electrode structures with increased shape retention after deposition as compared to the previously used Newtonian inks;

- Improved control over electrode width and interelectrode distance, and fabrication of electrodes with square cross-section;
- Difficulties in sintering thick NiO-YSZ anodes due the difference in thermal expansion coefficient with the YSZ electrolyte.

2.2.2 Characterization of SC-μSOFCs with coplanar electrodes: Chapters 4-7

With regard to objective 3, the study on miniaturization limitations of SC-μSOFCs with coplanar electrodes is the subject of the paper in Chapter 4. "Miniaturization limits for single-chamber micro solid oxide fuel cells with coplanar electrodes" was submitted to the *Journal of Power Sources* on March 9, 2009. This journal was chosen because it constitutes an important platform for publications on fuel cells and many references on SC-SOFCs can be found in this journal. The paper's main results are:

- The cell performance and stability of SC-μSOFCs with one pair of coplanar electrodes were found to be affected by the electrode width.
- A critical electrode width was identified below which no OCV and power output could be obtained for cells with one electrode pair due to an insufficient active electrode area.
- Cells with electrode widths close to the critical size exhibited voltage and power fluctuations.
- Stable performance was obtained for electrode widths above the critical size. But an upper limit for the useful electrode width exists, as not the whole electrode width seems to contribute to the electrochemical reactions due to an increased ohmic resistance with increased electrode width.
- The miniaturization limit could be compensated by increasing the number of electrode lines in the form of interdigitated electrode structures. The stability of the OCV improved with increasing number of electrode pairs.
- Building cell stacks did not overcome the voltage instability for cells with electrode widths below the critical size. However, the power output was increased for stacks composed of cells with interdigitated electrode patterns.

Benefiting from the versatility of the direct-writing technique, SC-μSOFCs with coplanar electrodes of nonconventional shape were fabricated and electrochemically

tested (objective 4). The corresponding paper entitled "Fabrication and testing of coplanar single-chamber micro solid oxide fuel cells with geometrically complex electrodes" (Chapter 5) was available online on November 17, 2007, and appeared in the printed version of the *Journal of Power Sources* in 2008. The principal contributions of this paper include:

- Demonstration of the versatility of the direct-writing technique;
- Proof of concept of SC-μSOFCs with coplanar electrodes of geometrically complex, arbitrary shape;
- Cells with coplanar electrodes of different shapes, but similar width, interdistance and area exhibited similar performance.

The paper "Experimental study of current collection in single-chamber micro solid oxide fuel cells with comblike electrodes" in Chapter 6 was published on August 1, 2008, in the *Journal of The Electrochemical Society*. As this journal is specialized in solid-state and electrochemical systems, many references on SC-SOFCs are published there, and it was considered suitable for this paper on current collection method. The study on current collection method was conducted with regard to objective 5, the investigation of different parameters affecting the cell performance. The principal results of this paper can be summarized as:

- A double-face cell configuration with a comblike anode and a planar cathode on opposite sides of the electrolyte substrate was used to study the effect of current collection method on the cell performance of SC-μSOFCs with comblike electrodes. While the current was collected on the whole cathode surface, current collection on the connecting segment of the anode comb-structure and on the whole anode surface area was compared. This cell and current collection configuration allowed circumventing the problems associated with applying current collectors on the whole electrode area of closely-spaced comblike anodes and cathodes in interdigitated patterns and short circuiting the cell.

- The current collection method affected the cell performance of SC-μSOFCs with comblike electrodes with regard to the ohmic cell resistance and the activation polarization.
- Current collection on the segment connecting the single anode lines led to a 50% loss in power as compared to collecting the current on the whole electrode surface.
- Increasing the electrical conductivity of the NiO-YSZ anode by increasing the content of nickel did not compensate for the power loss associated with the current collection method because of instability issues of the nickel-rich anodes in methane-air mixtures.

Finally, Chapter 7 presents a preliminary study on the effect of electrode material on the cell performance of SC-μSOFCs with coplanar electrodes (objective 5). The paper entitled "Single-chamber micro solid oxide fuel cells: Study of anode and cathode materials in coplanar electrode design" was submitted on March 12, 2009 to *Solid State Ionics* because of the journal's scope on reactions and interactions in solid materials. The paper describes the:

- Comparison between four different anode and cathode material combinations for SC-μSOFCs with coplanar electrodes;
- Higher power output for cells with NiO-YSZ anodes in comparison to NiO-GDC because of poor adhesion of the latter on the YSZ electrolyte;
- Better performance for cells with LSM-YSZ instead of LSCF cathodes, possibly due to a higher catalytic activity of LSCF for the fuel reactions at the cell operating temperature of 700°C;
- Blackening of anodes in vicinity of LSM-YSZ cathodes, probably caused by diffusion of manganese from the cathode into the anode. The impact of this chemical interaction on cell performance will necessitate further investigations.

2.3 Personal contribution

For all the articles presented in this work, the literature review, the experimental work including ink preparation and characterization, direct-write microfabrication,

electrode sintering, electrochemical testing and microstructural analysis, the analysis of the obtained results and the writing were performed by me. Dr. Napporn and Prof. Meunier from the Department of Engineering Physics are co-authors because of our close collaboration consisting in the use of their cell testing setup. At the beginning of the project, I additionally benefited from Dr. Napporn's expertise to acquire the necessary knowledge for ink preparation and manipulation of the testing setup. Dr. Napporn also helped with the analysis of the results from electrochemical testing and suggested the study on the current collection method in SC-μSOFCs with coplanar interdigitated electrodes using the double-face design. The EDX analysis for the paper in Chapter 7 was performed in collaboration with Philippe Beaulieu from the CM^2 at École Polytechnique. While Mr. Beaulieu operated the SEM and EDX equipment, I was nonetheless present during the measurements to direct the investigation.

Dr. Rao is a co-author of the *Materials Research Society Symposium Proceedings* paper on the direct-write microfabrication of coplanar electrodes using viscoelastic electrode inks, as the results described in this paper were obtained during a two-month visit at the laboratory of Prof. Lewis at the University of Illinois at Urbana-Champaign. Dr. Rao helped to familiarize me with the lab equipment and the gel-like ink fabrication method.

Chapter 3 Direct-write microfabrication of single-chamber micro solid oxide fuel cells

M. Kuhn, T. Napporn, M. Meunier, S. Vengallatore, D. Therriault, *Journal of Micromechanics and Microengineering*, vol. 18, p. 015005 (8 pp.), 2008.

3.1 Abstract

Single-chamber micro solid oxide fuel cells (SC-μSOFCs) are promising systems for portable power generation. Here we report the direct-write microfabrication and electrochemical testing of SC-μSOFCs in the single-face configuration, which consists of closely-spaced interdigitated electrodes on an electrolyte substrate. In direct-write microfabrication, powdered electrode materials are first synthesized into inks, which are subsequently extruded through a micronozzle onto an electrolyte plate mounted on a robot-controlled platform. The microfabricated structures are then sintered to remove the organic components of the inks and to obtain porous electrodes. Processing-structure relationships were obtained using systematic experimentation for the direct-write microfabrication of nickel oxide – yttria-stabilized zirconia (NiO-YSZ) anodes and lanthanum strontium manganite (LSM) cathodes on a YSZ electrolyte. Single-chamber μSOFCs were fabricated with interdigitated electrodes of a few hundred microns in size. When tested in a fuel-air mixture (methane-to-oxygen ratio R_{mix} = 2) at a furnace temperature of 700°C, the cells exhibited an open circuit voltage of 800 mV and a peak power density of ~1 mW/cm^2. Implications for the use of these devices for portable power generation are discussed.

3.2 Introduction

Miniaturized fuel cells are attractive candidates for portable power generation to enable the operation of electronic devices and microelectromechanical systems (MEMS). Compared with conventional electrochemical batteries, micro fuel cells are capable of higher energy densities and lower recharging times. Research in this

relatively new field currently focuses on two major categories of fuel cells, namely, polymer-based proton exchange membrane (PEM) fuel cells operating at low temperatures of 20-100°C [184], and ceramic-based solid oxide fuel cells (SOFCs) requiring significantly higher temperatures of 500-1000°C for efficient operation [9]. PEM fuel cells are restricted to operate only on hydrogen or methanol fuels, whereas SOFCs can operate on a wide range of hydrocarbon fuels with greater energy densities and without the need for expensive catalysts.

The first type of micro solid oxide fuel cells (μSOFCs) explored was a traditional dual-chamber design in which an electrolyte layer is sandwiched between porous anode and cathode layers [73]. The term dual-chamber refers to the operating mode wherein the two reactant gases – fuel (hydrogen or hydrocarbons) and oxidant (oxygen or air) – are fed to the anode and to the cathode, respectively, without any intermixing. Significant progress has been made in thin-film microfabrication of fuel cell components and in structural design of dual-chamber micro fuel cells [73, 87]. However, this experience has also highlighted several significant difficulties in the miniaturization of the dual-chamber design, including (i) developing high-temperature microfluidic sealing technologies to keep the two gas streams separated [185], (ii) controlling intrinsic residual stresses in vapor-phase-deposited thin films of electrodes and electrolytes, and (iii) ensuring thermomechanical stability and minimizing thermal losses in the design of the thin three-layer sandwich structure [73, 87].

The difficulties encountered with miniaturizing dual-chamber designs motivated us to explore an alternate concept of single-chamber micro SOFCs (SC-μSOFCs). In this operating mode, the fuel and air streams are pre-mixed, and the mixture is allowed to flow over both electrodes. The operation of the device relies upon selective reactions at the anode and cathode in terms of oxidation and reduction processes. The single-chamber concept dates back to the 1950s [186] and 1960s [135], but it was only recently that this operating mode has been investigated for SOFCs [105, 108]. Several configurations of single-chamber SOFCs have been proposed, including the traditional three-layer sandwich structure (with the electrolyte contained between the two electrodes) [15, 105, 108], a flow-through structure with a fully porous electrolyte and electrodes [154], and planar single-face configurations in which both electrodes are patterned on the same side of the electrolyte [5, 6, 8].

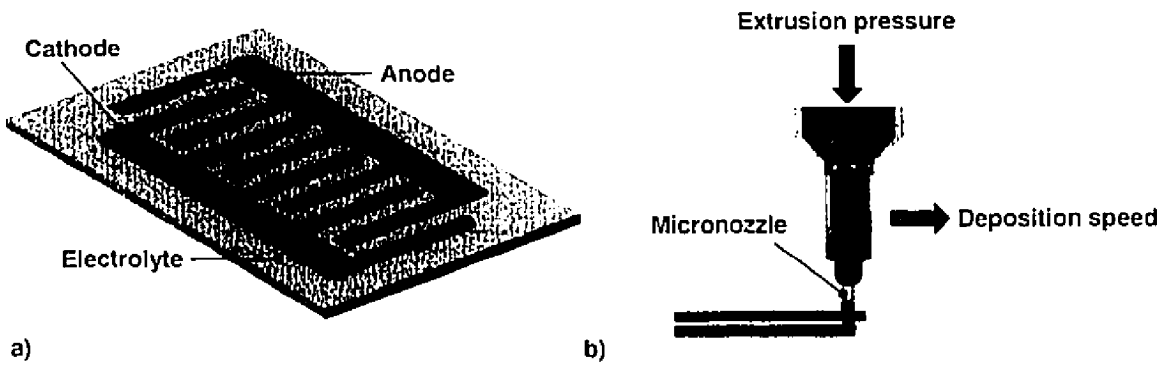

Figure 3.1: a) Schematic illustration of a single-chamber solid oxide fuel cell in single-face configuration with interdigitated electrodes. b) Schematic illustration of the robot-controlled direct-write microfabrication of electrode lines on an electrolyte plate. The quality of the deposited structures strongly depends on the two main process parameters, extrusion pressure and deposition speed.

Fig. 3.1a shows a schematic illustration of a planar SC-μSOFC in the single-face configuration, in which interdigitated patterns of the anode and cathode are fabricated on the same surface of a thick electrolyte plate. This configuration is particularly appealing for miniaturization because the use of pre-mixed air and fuel streams eliminates the need for gas-tight microfluidic sealing. In addition, a thick electrolyte can be used without any penalties on electrochemical performance, while ensuring mechanical strength and stability during operation at high temperatures. Finally, the planar configuration is suited for parallel or serial connection of multiple individual micro fuel cells on the same electrolyte substrate, as well as for integration with microsensors and microactuators used in MEMS technology.

Experimental work [5, 6, 8] on SC-μSOFCs in the single-face configuration and modeling [7] suggest that minimized ohmic resistance for surface ionic conduction and optimal electrochemical performance are achieved by reducing the interelectrode spacing between adjacent anode and cathode structures to the order of a few tens of micrometers. Additionally, porous electrodes are required to maximize the number of gas/electrode/electrolyte triple phase boundaries for the electrochemical reactions. However, these requirements, especially the synthesis of thick porous electrodes using multicomponent ceramics, are largely incompatible with traditional thin-film processing

and photolithography-based microfabrication. Hence, alternate methods of microfabrication, such as screen printing [98], soft lithography [20] and direct-write microfabrication [8, 187], are being explored for the synthesis of high-performance SC-μSOFCs.

In this paper, we present a detailed report of direct-write microfabrication, structural characterization and electrochemical testing of SC-μSOFCs. The essential principles and challenges of direct-write microfabrication, and the key process parameters associated with this method, are discussed in Section 3.3. Section 3.4 presents an experimentally determined process map for direct-write microfabrication of ceramic structures. Section 3.5 describes the synthesis and characterization of interdigitated microelectrodes on an electrolyte substrate using an optimal set of process parameters. Finally, the electrochemical testing of fabricated SC-μSOFCs in methane-air mixtures is presented in Section 3.6.

3.3 Principles of direct-write microfabrication

The direct-write microfabrication technique used here refers to the pressure-driven extrusion of an ink (or suspension) through a micronozzle and its robot-controlled deposition on a suitable substrate, as schematically illustrated in Fig. 3.1b. This technique enables rapid, repeatable and potentially low-cost manufacturing of complex shapes and patterns [171, 188]. The primary steps in the direct-write microfabrication of ceramic or metallic electrodes for single-chamber solid oxide fuel cells in single-face configuration are as follows. First, the electrode materials are obtained in the form of powders and processed to synthesize suspensions (or inks) of the desired viscosity. Next, the inks are deposited onto an electrolyte plate by means of pressure-driven extrusion through a micronozzle at room temperature. This plate is mounted on a robot-controlled mobile platform, which permits the deposition of electrodes of different two-dimensional shapes and sizes. After deposition, the electrode structure is sintered to remove the organic components of the inks and to obtain porous electrodes.

The direct-writing of SC-SOFCs involves numerous parameters such as the particle size and size distribution of the electrode powders, rheological properties of the inks, the extrusion parameters (micronozzle diameter, extrusion pressure), the deposition parameters (deposition speed) and the sintering time and temperature. An

optimal selection of these material and process parameters is essential in order to achieve continuous and uniform deposits of specified dimensions and with a homogeneous microstructure. Consider first the preparation of the ceramic inks. The rheological properties (specifically, viscosity and storage modulus) govern the flow of the ink through the nozzle during deposition and dictate the extent to which the extruded shape is retained after deposition [189]. In turn, the rheological properties of the inks are dominated by the particle loading, ϕ, (i.e., weight fraction of electrode powders). Previous studies [170] suggest that the particle loading must be chosen so as to (i) permit uniform flow of inks through the nozzle during extrusion, (ii) retain shape after deposition, (iii) minimize shrinkage and damage during drying and sintering, and (iv) obtain a homogeneous porous microstructure with a percolating interconnected particle network after high-temperature sintering. Consideration of these factors suggests an optimal range of $0.5 < \phi < 0.6$ [170]. Our preliminary experiments indicate that, for higher solid loadings, the suspension easily clogs the micronozzle during extrusion and exhibits poor flow characteristics. Conversely, for lower values of ϕ, the ink is easily extruded, but the deposit will not retain its shape and size after extrusion. Also, a non-percolating microstructure with poorly bonded particles can result after sintering.

Once the ink is prepared, the direct-write process parameters, namely, extrusion pressure and deposition speed, must be considered. Optimal deposition is achieved when the deposited structures are uniform, continuous, and exhibit an average width, w_{av}, that is comparable to the inner diameter of the extrusion micronozzle, w_{nozzle}. For a given deposition speed, the deposited structures are expected to be discontinuous for low extrusion pressures, but oversized ($w_{av} > w_{nozzle}$) for high pressures. Similar arguments hold for deposition under fixed extrusion pressure and varying deposition speeds. Hence, it is expected that there exist optimal ranges of direct-write process parameters over which uniform deposits of the desired size can be obtained. However, reliable quantitative estimates for these ranges have not been established yet. This motivated us to undertake a series of systematic experiments to identify the ranges of viscosities, extrusion pressures and deposition speeds that lead to optimal deposited structures.

3.4 Experimental details and process maps

3.4.1 Preparation of electrode suspensions

The electrode materials were obtained from NexTech Materials in the form of NiO-YSZ (8 mol% yttria) powder (a median particle size of 0.9 μm, specific surface area (BET-surface) of 2.071 m^2/g, weight ratio of NiO:YSZ of 60:40) and $(La_{0.8}Sr_{0.2})_{0.98}MnO_3$ powder (a median particle size of 0.6 μm and a specific surface area (BET-surface) of 4.2438 m^2/g). In addition, an anode powder with a weight ratio of NiO:YSZ = 55:45 was also prepared. Anode and cathode suspensions with different particle loadings between 36 wt% and 60 wt% were prepared by ball milling for 1 h with YSZ balls (5-10 mm in diameter) in a Spex Mixer/Mill (Spex 8000 M), using α-Terpineol as solvent, Triton as dispersant and polyvinyl butyral (PVB) as dispersant.

3.4.2 Rheological characterization

The viscosity and rheological behavior of ink suspensions are critical for their successful pressure-driven extrusion through a micronozzle [189]. The rheological characterization of anode suspensions with different particle loadings was performed at room temperature on a controlled stress oscillatory rheometer (Bohlin CVO 120) using a parallel plate geometry (the diameter of the upper plate was 25 mm). An amount of about 1 mL of the different suspensions was used for the measurements. The complex shear modulus (composed of the storage and the loss modulus, G' and G'') and the complex viscosity, η^*, were measured as a function of stress in an oscillatory shear stress amplitude sweep at a frequency of 10 Hz. A constant viscosity and shear modulus were observed for all suspensions over the applied shear stress range. Fig. 3.2 presents a comparative graph of the storage modulus and complex viscosity as functions of the shear stress amplitude for two different suspensions with particle loadings of $\phi = 0.36$ and $\phi = 0.6$. A significant increase of both storage modulus and viscosity with increasing particle loading is evident. Following the guidelines developed by Cesarano et al. [170], we focused on the inks with high particle loadings for the direct-write microfabrication of electrode structures.

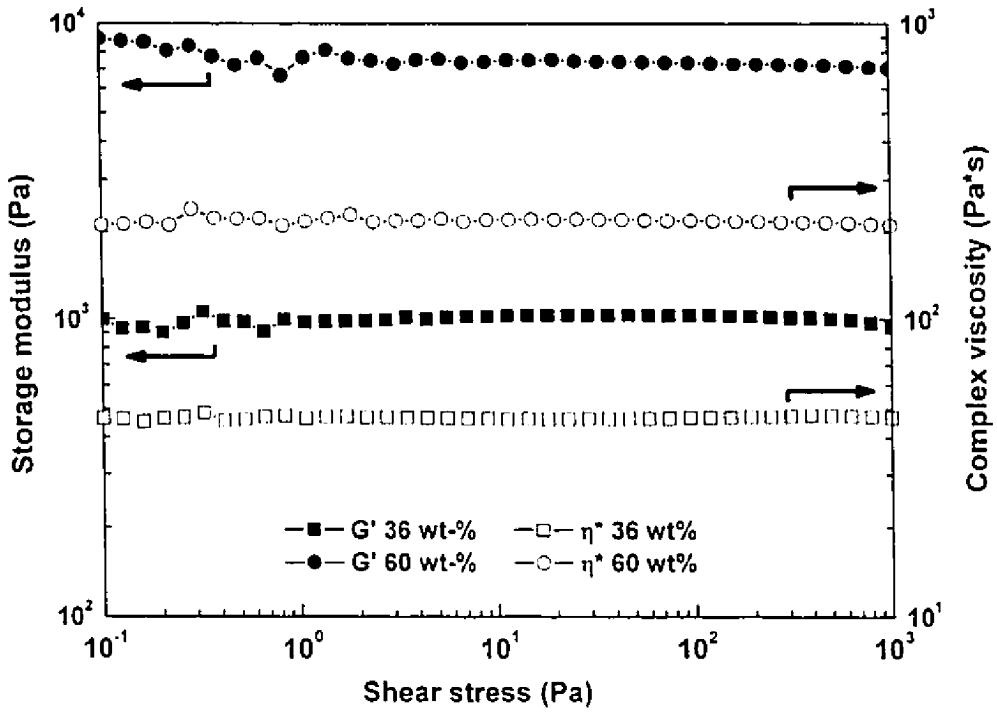

Figure 3.2: Rheological properties (storage modulus, G', and complex viscosity, η^*) of anode suspensions with two different particle loadings as a function of shear stress at a frequency of 10 Hz.

3.4.3 Direct-write process map

A photograph of the direct-writing system is shown in Fig. 3.3. The electrode suspensions were filled in syringes (volume = 3 cm^3, barrel diameter = 9.6 mm, EFD Inc.) and extruded through high precision stainless steel micronozzles (EFD Inc.) using a pressure regulator (Ultra™ 2400 series, EFD Inc.) combined with an air-powered micro-extrusion system (HP7x, EFD Inc.), which enabled a maximum pressure of 49 bar. Micronozzles with different inner diameters (100, 150 and 330 μm) were used. The combination of the micro-extrusion system with a robotic deposition apparatus (I & J 2200-4, I & J Fisnar Inc.) enabled the deposition of the extruded suspensions onto an yttria-stabilized zirconia (YSZ) plate (0.2 mm thick, Marketech International). The pattern for direct-writing was programmed using the software JR Points for dispensing (Version 4.85E, Janome Sewing Machine Co. Ltd.). An optical microscope was used for *in situ* observation of the extrusion and deposition process.

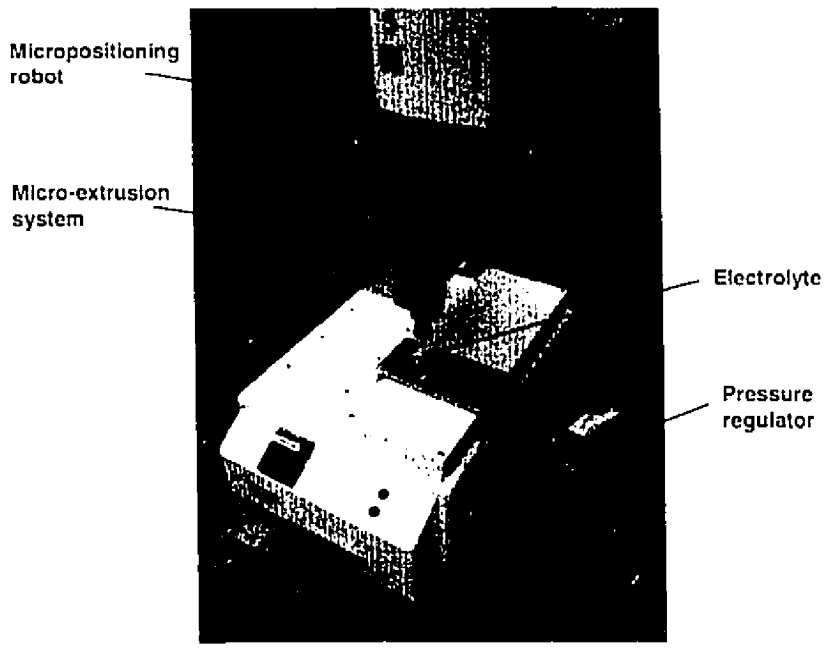

Figure 3.3: Picture of the direct-write microfabrication setup. The sample is mounted on a translation stage, and the micro-extrusion system on a robotic arm permits writing of arbitrary shapes.

Fig. 3.4 shows a representative process map that was obtained from the analysis of several straight electrode lines deposited under different combinations of extrusion pressure and deposition speed. All depositions were performed using a 60 wt% anode suspension extruded through a micronozzle with an inner diameter of 150 μm. Optical micrographs of the deposited anode lines were obtained with an Olympus SZX12 stereomicroscope and an Evolution™ VF color camera with 1.4 million pixel resolution. Straight lines of the anode suspension were deposited at five different speeds (0.1, 0.2, 0.3, 0.4 and 0.5 mm/s) and at pressures ranging from 5.6 to 11.2 bar. At low extrusion pressures and at elevated deposition speeds, the deposited lines are discontinuous. For high pressures and low speeds, the width of the deposited lines is significantly larger than the micronozzle diameter, resulting in broadened lines. Multiple optimal combinations of extrusion pressures and speeds can also be identified that lead to the deposition of narrow, continuous lines, and an optimal zone is shown on the process map.

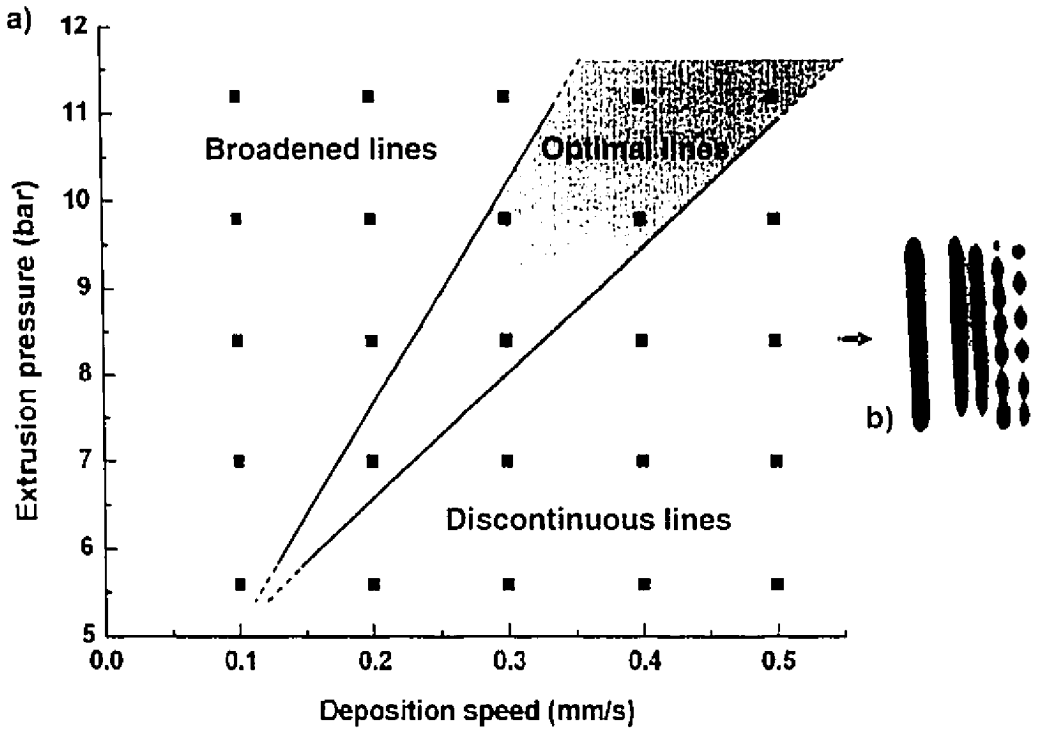

Figure 3.4: a) Representative process map for direct-write microfabrication of anode lines with axes corresponding to extrusion pressure and deposition speed. The 60 wt% anode suspension was extruded through a micronozzle with an inner nozzle diameter of 150 μm. Optimal deposits with uniform, continuous lines were obtained for pressure-speed combinations within the grey area. b) Optical micrograph corresponding to an extrusion pressure of 8.4 bar. From left to right, the single lines correspond to the deposition speed of 0.1, 0.2, 0.3, 0.4 and 0.5 mm/s, respectively.

Several practical considerations impact the selection of a few optimal combinations from this set. The structures of interest are only a few millimeters in length and, therefore, only a few minutes are required for deposition even at low deposition speeds in the range of 0.1 mm/s. However, the pressure corresponding to this speed is low and subject to fluctuations during deposition using our dispensing system. In contrast, at significantly higher velocities (> 0.6 mm/s), there is a reduced control in the deposition of short structures. Hence, speeds in the range of 0.2-0.5 mm/s, and the corresponding pressures in the range of 7-11 bar, were used for optimal deposition.

Importantly, the optimal process parameters identified in Fig. 3.4 pertain only to the microfabrication of uniform, continuous, narrow electrodes by direct-write microfabrication. The next step is to enquire whether such structures lead to optimal electrochemical performance, efficiency and reliability. As the first step toward the goal of formulating robust process-structure-performance-reliability correlations, the following section describes the microfabrication and testing of SC-μSOFCs.

3.5 Fabrication and structural characterization of SC-μSOFCs

After optimizing the direct-write process parameters to achieve uniform and continuous electrode structures, SC-μSOFCs in single-face configuration were fabricated. A deposition speed of 0.3 mm/s and an extrusion pressure of 8.4 bar, as identified from the optimal zone in Fig. 3.4, were used for the fabrication of both anode and cathode structures. The anode structures were deposited first on the YSZ plate using a 60 wt% anode suspension and then sintered at 1250°C for 3 h under ambient atmosphere in a chamber furnace. Subsequently, the cathode structures were deposited by extruding a suspension with a particle loading of 57 wt%, and the fuel cell device was sintered at 1100°C for 3 h.

Several micro solid oxide fuel cells were manufactured with interelectrode spacings ranging from 37 μm to 846 μm, and average electrode widths ranging from 125 μm to 316 μm. These values of interelectrode spacing and electrode width were obtained from optical imaging analysis (Image-Pro Plus 6.2, Media Cybernetics) and were confirmed by profilometry of the electrode structures. Fig. 3.5a shows a representative example of a SC-μSOFC with interdigitated pairs of five anode and five cathode lines. The average interelectrode spacing of this cell is 300 μm. The width of each electrode line was measured at 20 different locations, and the mean value and standard deviation are reported in Table 3.1. These values provide an indication of the stability of the direct-write process during microfabrication of the anode and cathode. The average anode and cathode width are 137 μm and 125 μm, respectively. A micronozzle with an inner nozzle diameter of 100 μm was used for the direct-write fabrication of this cell.

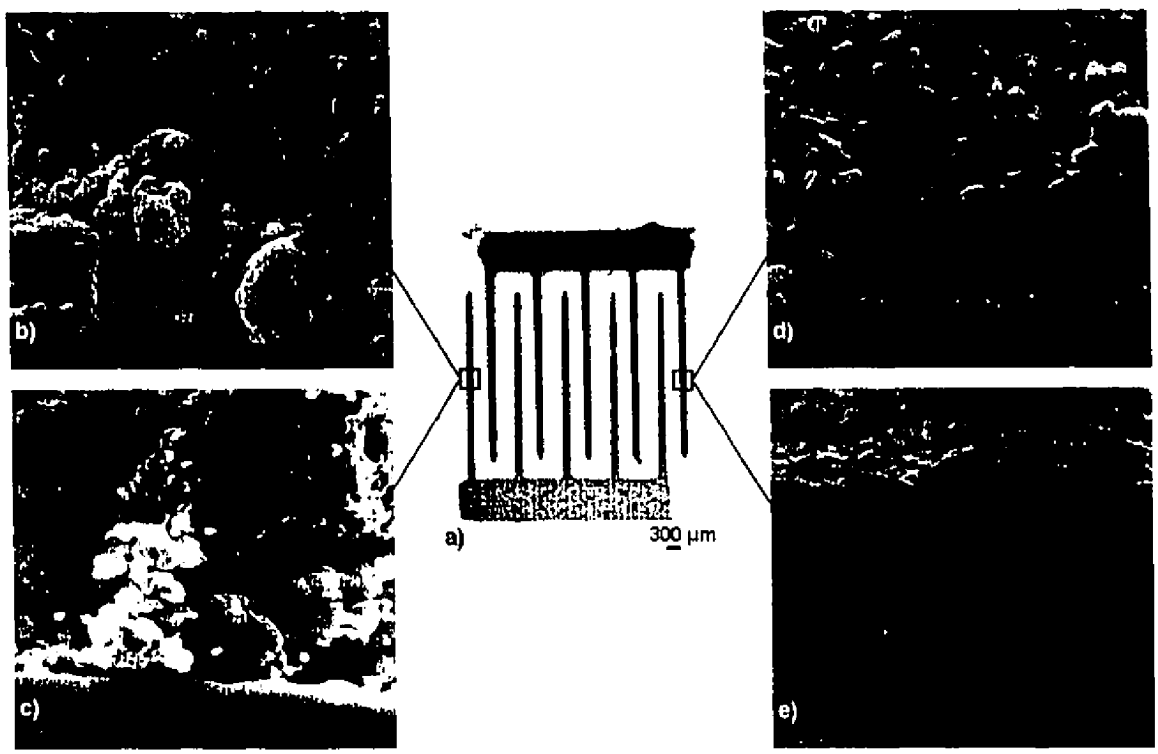

Figure 3.5: a) Optical micrograph of SC-µSOFC with interdigitated electrodes fabricated by the direct-write technique. SEM images of the anode microstructure in b) top and c) cross-sectional view. SEM microstructure characterization of the cathode in d) top and e) cross-sectional view.

The microstructure and thickness of the sintered electrodes were characterized using a Quanta FEG 200 (FEI Instruments) scanning electron microscope (SEM) with the software xT Microscope control and xT Docu (FEI Instruments). Fig. 3.5b-e show the SEM micrographs for both electrodes in plan and cross-sectional view, revealing a porous and homogeneous microstructure for anode and cathode. The thickness of the electrodes varies from 10 to 30 µm in different cells. At lower magnification, the cross-sectional images reveal that the electrode sidewalls are not vertical, but instead exhibit rounded edges. This lens-like shape is due to the spreading of the inks on the substrate after deposition. Optimizing the direct-write method and tailoring the rheological properties of the inks, to reduce the wetting of the substrate by the inks and to achieve thicker and uniform electrodes with reduced interelectrode spacings, remains an open question that will be addressed in our future efforts.

Table 3.1: Average electrode line width, w_{av}, and standard deviation, σ, for anode and cathode lines of the SC-μSOFC from Fig. 3.5a. The lines are numbered from the left to the right. All values are given in μm. One pixel in the image corresponds to 5.6 μm. A micronozzle with an inner nozzle diameter of 100 μm was used for the direct-write microfabrication of the electrode structures.

	line 1		line 2		line 3		line 4		line 5	
	w_{av}	σ	w_{av}	σ	w_{av}	σ	w_{av}	σ	w_{av}	σ
Anode	124	11	138	16	146	12	142	14	133	21
Cathode	130	9	125	7	133	7	122	9	117	7

3.6 Electrochemical testing

Electrochemical characterization of the fabricated SC-μSOFCs was performed using a high-temperature test station that is shown schematically in Fig. 3.6 and is described in detail in Ref. [10].

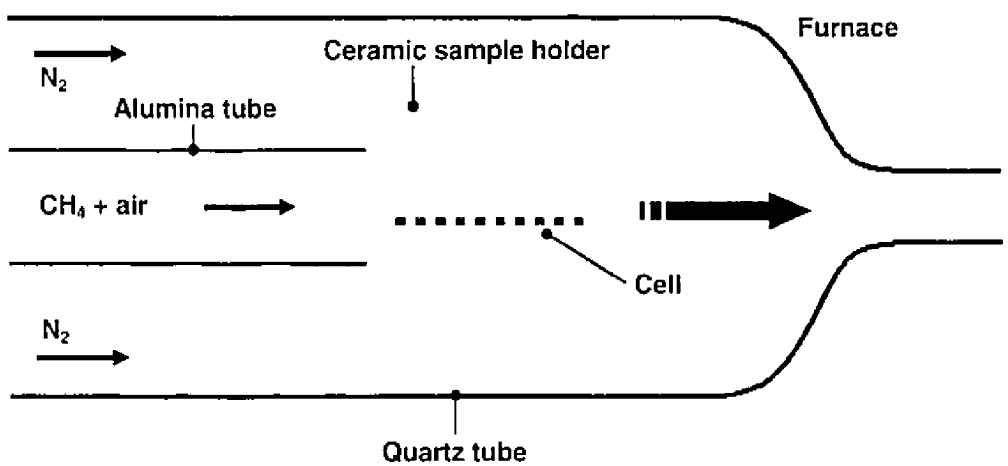

Figure 3.6: Schematic of the electrochemical testing setup. The cell is placed in a ceramic holder inside a quartz tube. The methane-air mixture is supplied to the cell through an inner alumina tube. Additional nitrogen is used as carrier gas and to avoid counter-diffusion.

The cell was located in a ceramic sample holder inside a quartz tube, and a methane-air mixture was allowed to flow over the cell at a total gas flow of 150 sccm. The characteristic value associated with the gas mixture is the methane-to-oxygen ratio, R_{mix}. The electrode lines were orientated perpendicular to the gas flow. Nitrogen was used as a carrier gas to prevent any counter-flow. Gold wire and grid (Alfa Aesar) fixed with gold paste (paste C5450 from Heraeus Inc.) served as current collector. The furnace temperature was set to 700°C, and the cell potential was recorded as a function of the electrical current drawn from the micro fuel cell.

Fig. 3.7 shows the results of a test using a micro fuel cell in which the average interelectrode distance was 517 μm, and the surface area per electrode was 0.22 cm^2.

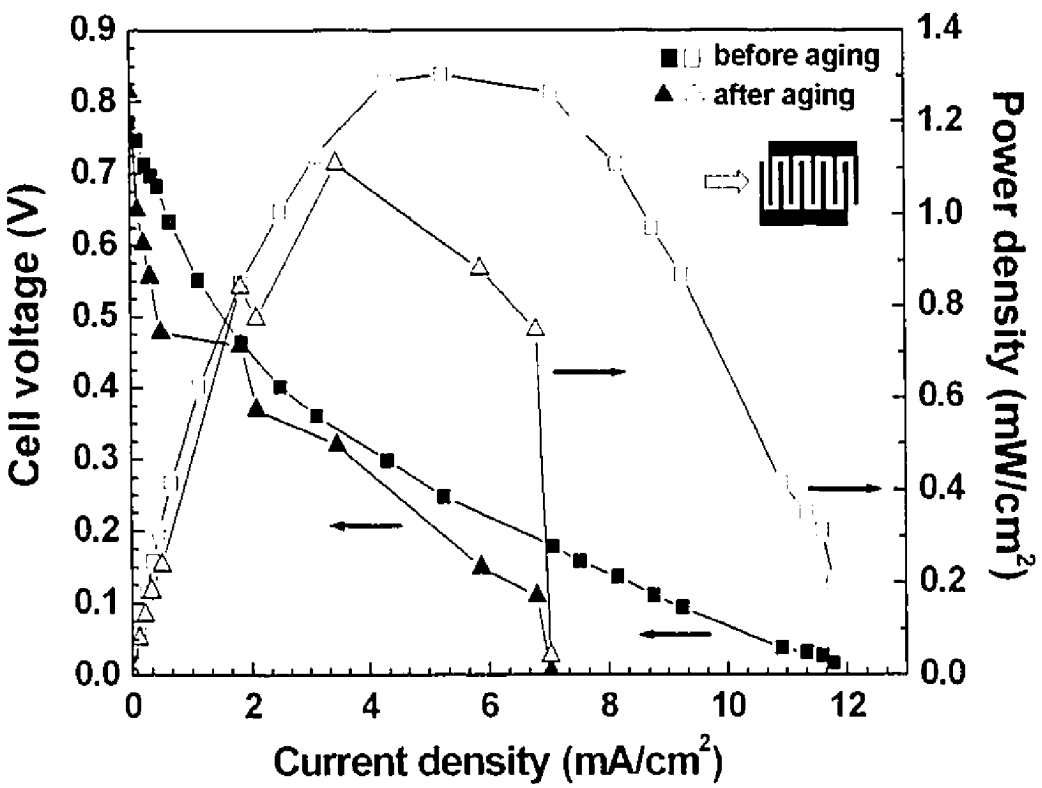

Figure 3.7: Polarization curve of SC-μSOFC with interdigitated electrodes (average interelectrode spacing of 517 μm) at 700°C, a total gas flow of 150 sccm and a methane-to-oxygen ratio R_{mix} = 2. The results before and after an aging period of 24 h are shown.

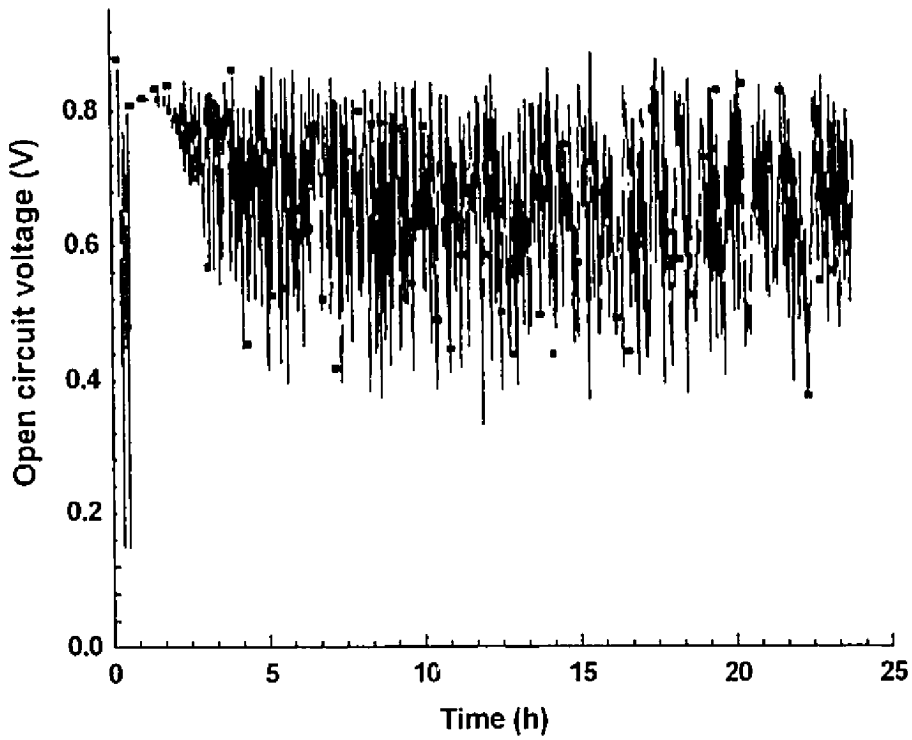

Figure 3.8: Open circuit voltage (OCV) as a function of time for aging of a direct-written SC-μSOFC at 700°C, R_{mix} = 2 and a total gas flow of 150 sccm. No current load was applied.

The anode had an average width and thickness of 320 μm and 27 μm, respectively, and the corresponding values for the cathode were 130 μm and 10 μm, respectively. The vertical axes of the graph correspond to the cell voltage and power density, and the horizontal axis is the current density. Both power and current were normalized by the electrode surface area of 0.22 cm^2. At R_{mix} = 2, an open circuit voltage (OCV) of ~800 mV was rapidly obtained. For comparison, the theoretical maximum OCV is 1.23 V. A maximum power density of 1.3 mW/cm^2 and a maximum current density of 12 mA/cm^2 were also measured (Fig. 3.7).

The cell was tested in open circuit conditions for 24 h in the methane-air mixture (R_{mix} = 2) at 700°C to characterize its long-term stability. The open circuit voltage was monitored as a function of time. It shows oscillations between 400 mV and 800 mV (Fig. 3.8). Jacques-Bedard et al. [12] have previously suggested oxidation-reduction cycles of the anodic nickel as a probable cause of these oscillations. After this aging test, the

cell was polarized again. Although there was no significant change in the OCV, a degradation of the performance was noted (Fig. 3.7). The peak power density dropped by 15% to 1.1 mW/cm^2, and the maximum current density decreased by 41% to about 7 mA/cm^2. As observed by Jacques-Bedard et al. [12], this performance decrease is due to the partial loss of nickel at the anode by transformation into volatile $Ni(OH)_2$.

The characterization of the anode microstructure after electrochemical testing indicated that the nickel oxide had been reduced to metallic nickel in the reducing atmosphere of the testing furnace. The flake-like structures in the SEM image shown in Fig. 3.9 were identified as nickel using energy-dispersive X-ray analysis.

At this stage, it is instructive to compare our results with those reported in the literature for the performance of single-chamber SOFCs. As compiled in a recent review by Yano et al. [11], values for the peak power density range from 1 mW/cm^2 to 100 mW/cm^2 at temperatures between 700 and 900°C. Unfortunately, a direct one-to-one comparison of results is not possible because of subtle, but critical, differences in the materials used for electrodes and electrolytes, differences in electrode architectures and dimensions, use of different test conditions (especially, ratio of fuel and air in the gas mixture, furnace temperature and the flow direction with respect to electrode geometry) and differences in the design of the setup used for electrochemical testing.

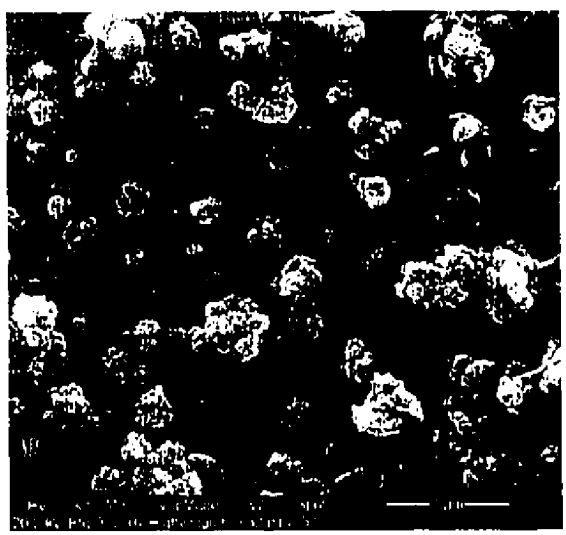

Figure 3.9: Scanning electron micrograph of the anode after electrochemical testing. The bright flake-like regions consist of metallic nickel.

As an illustrative example of the importance of such differences, we compare the OCV between different sets of SC-μSOFCs in the single-face configuration manufactured using direct-write microfabrication. Recently, Ahn et al. [8] tested such fuel cells with interdigitated electrodes in a methane-air mixture at 900°C, and reported OCV values of ~800 mV and 540 mV for cells with one pair and four pairs of electrodes, respectively. In contrast, in our fuel cells, a relatively high OCV of 800 mV is obtained at 700°C even in structures with five pairs of interdigitated electrodes. In addition, the OCV fluctuates periodically between 400 mV and 800 mV as a function of time in aging tests. Importantly, the electrolyte (YSZ) and cathode (LSM) are nominally identical in all these fuel cells. However, the anodes used by Ahn et al. [8] were a mixture of NiO, gadolinium-doped ceria and metallic Pd, whereas our fuel cells used a mixture of NiO and YSZ for the anode. Thus, taken together, these results highlight the importance of subtle material and geometric parameters in determining the performance of SC-μSOFCs.

3.7 Summary

A direct-write microfabrication method has been used for the manufacture of single-chamber micro solid oxide fuel cells with interdigitated electrodes. The method is simple in concept, but involves numerous process parameters. Process-structure correlations were obtained experimentally and catalogued in the form of process maps. Specifically, the effects of particle loading on viscosity, and the effects of extrusion pressure and deposition speed on the geometry and quality of the deposited structures were elucidated. Single-chamber μSOFCs were fabricated with NiO-YSZ anode and LSM cathode on a YSZ electrolyte. Scanning electron microscopy confirmed the formation of homogeneous, porous electrodes after sintering. The fabrication process is quick and stable. Electrochemical testing showed an OCV of ~800 mV at 700°C. An important conclusion is that a high OCV can be achieved even with multiple interdigitated electrodes.

This work provides a foundation for further exploration of single-chamber μSOFCs. Specifically, we intend to investigate the effects of testing conditions on electrochemical performance, and the synthesis and testing of cells with different electrode geometries and sizes. The long-term goal of these activities is to develop

detailed processing-structure-performance-reliability correlations for single-chamber μSOFCs developed by direct-write deposition. Such correlations will help in evaluating the benefits of this technology for portable power generation and for integration with microsystems employed in harsh high-temperature environments.

Chapter 4 Miniaturization limits for single-chamber micro solid oxide fuel cells with coplanar electrodes

M. Kuhn, T. W. Napporn, M. Meunier, S. Vengallatore, D. Therriault, *Journal of Power Sources*, submitted March 9, 2009.

4.1 Abstract

Single-chamber solid oxide fuel cells with coplanar microelectrodes were operated in methane-air mixtures (R_{mix} = 2) at 700°C. The performance of cells with one pair of NiO-YSZ (yttria-stabilized zirconia) anode and $(La_{0.8}Sr_{0.2})_{0.98}MnO_3$-YSZ cathode, arranged parallel on a YSZ electrolyte substrate, was found to be significantly dependent on the electrode width. For an interelectrode gap of ~250 μm, cells with average electrode widths exceeding ~850 μm could establish a stable open circuit voltage (OCV) of ~0.8 V, while those with widths less than ~550 μm could not establish any OCV. In the intermediate range, the cells exhibited significant fluctuations in voltage and power under our testing conditions. This behavior suggests that a lower limit to electrode dimensions exists for cells with single electrode pairs below which neither a stable difference in oxygen partial pressure, nor an OCV, can be established. Conversely, increasing the electrode width imposes a penalty in the form of an increase in the ohmic cell resistance. However, both size limits can be circumvented by employing multiple pairs of microscale electrodes in an interdigitated configuration.

4.2 Introduction

Single-chamber solid oxide fuel cells (SC-SOFCs) are operated in uniform mixtures of fuel and oxidant gases, whereas conventional dual-chamber SOFCs rely on the strict separation of the two reactant gases [4, 108]. In SC-SOFCs, the selectivity of the electrodes for catalyzing the reaction of the respective gas, that is, the anode for the fuel oxidation and the cathode for the oxidant reduction, enables the generation of an electrical power output. The use of a single gas chamber and reactant gas mixtures

eliminates the challenges of separate gas manifolding and high-temperature gas-tight sealing, which enables simple and compact designs for SC-SOFCs and makes these devices attractive for miniaturized portable power generation. Additionally, single-chamber operation permits the development of new cell designs such as fully porous cells [154] and single-face cells with coplanar electrodes located on the same side of the electrolyte [5, 6, 13, 17, 21, 24, 25, 157], neither of which is possible under dual-chamber conditions.

The single-face configuration was first mentioned by van Gool in 1965 [120] in connection with the possibility of surface ionic migration between adjacent coplanar electrodes in fuel cells. This idea was later adapted in a patent by Louis et al. in 1981 [99], but it was not until the early 1990s that the feasibility of SOFCs with coplanar electrodes operating in fuel-air mixtures was experimentally demonstrated by Hibino et al. [5, 157]. In conventional three-layer electrode-electrolyte-electrode designs, the thickness of the electrolyte determines the ohmic resistance to the conduction of oxygen ions from cathode to anode through the electrolyte, so that reducing the electrolyte thickness leads to a reduction of the ohmic losses. In the single-face design, the oxygen ions travel from one electrode to the other through the gap between the electrodes [5]. The ohmic resistance can thus be reduced by decreasing the interelectrode distance without the need for ultrathin electrolytes. Thick, mechanically strong electrolyte substrates can be employed, onto which multiple single cells can be fabricated and be connected in series or parallel [5, 6]. The conduction path and the ohmic resistance can further be decreased by reducing the electrode width [5, 6], as only a small part of the electrode closest to the gap and the opposite electrode appears to be active for the electrochemical reactions [6, 13].

Although it has repeatedly been shown that reducing interelectrode distance and electrode width leads to higher cell performance [5, 6, 17, 21, 157], no study has yet determined the ultimate limits on gap and width at which SC-microSOFCs (SC-μSOFCs) with coplanar electrodes can still be operated. Most SC-μSOFC studies report on cells consisting of one pair of parallel electrode lines with interelectrode gaps and electrode widths ranging from a few hundred micrometers to a few millimeters. Over this range, the highest power was obtained for the smallest of these cells, with interelectrode gaps and electrode widths of 0.5 mm and 1 mm [5, 17, 157], 0.255 mm

and ~0.6 mm [21], and 0.2 mm and 0.5 mm [6], respectively. There is a general consensus that further reduction to microscale dimensions could further improve performance. Results from modeling predicted optimal performance for interelectrode gaps of 10 μm and electrode widths of 20 μm [18], or 6 to 10 μm wide electrodes spaced 2 μm apart [7]. However, micrometer-sized gaps might induce intermixing of reactant gases and reaction products, which could limit the electrochemical performance of the cell [15, 21]. The low open circuit voltage (OCV) of 380 mV and the poor stability of a SC-μSOFC with an interelectrode gap of 5 μm and electrode widths of 15 μm [160] indicates that reduced electrode dimensions can degrade cell performance. To some extent, this degradation can be mitigated by employing multiple lines per electrode in an interdigitated configuration [13, 20, 24, 25]; for instance, cells containing interdigitated electrodes with electrode widths of 100 μm and spacings of 10 μm exhibited OCVs of 0.65 V and power densities of a few mW/cm^2 [13].

The aim of this study is to investigate the existence of a limit to the miniaturization of SC-μSOFCs with one pair of coplanar electrodes, and whether such a limit could be overcome by increasing the number of electrode lines in the form of interdigitated electrode patterns or by using cell stacks. Conventional SOFC materials, i.e., nickel oxide – yttria-stabilized zirconia (NiO-YSZ) for the anode, lanthanum strontium manganite (LSM)-YSZ for the cathode and YSZ for the electrolyte, were used to fabricate and test cells with one line per anode and cathode with average electrode widths ranging from 93 to 1380 μm, and with an interelectrode gap of ~250 μm. Subsequently, cells with one, two, three, four, five and ten electrode pairs in an interdigitated pattern with line widths of ~260 μm were tested to evaluate the effect of the number of electrode lines on cell performance. Finally, the performance of stacks composed of two to three cells, with either one pair or five electrode pairs per cell, was measured to assess the impact of stacking on cell performance.

4.3 Experimental

4.3.1 SC-μSOFC fabrication

The coplanar electrodes were fabricated using a robot-controlled direct-write microfabrication technique consisting of the pressure-driven extrusion of electrode inks

through micronozzles and their deposition onto the electrolyte substrate [21, 24-26, 187]. NiO-YSZ and LSM-YSZ were used for the anode and cathode, respectively. The characteristics of the electrode materials are listed in Table 4.1. The particle size and the specific surface area were provided by the supplier (NexTech Materials Ltd., Lewis Center, OH), and the powder density was obtained using a He-Pycnometer AccuPyc 1330 (Micromeritics Instrument Corporation, Norcross, GA). The NiO-YSZ mixture was prepared by mixing NiO and YSZ in a weight ratio of 55 wt% to 45 wt%, followed by ball milling for 8 hours in a Spex CertiPrep 8000M Mixer/Mill (Spex CertiPrep, Metuchen, NJ). For the ink fabrication, Triton (Alfa Aesar, Ward Hill, MA) was added to the respective electrode powder as a dispersant, and the two ingredients were ball milled for 10 min in the Spex Mixer/Mill with YSZ balls (0.5 and 1.0 mm in diameter) as milling media. A mixture of fully dissolved binder (Poly(vinyl butyral-co-vinyl alcohol-co-vinyl acetate), Sigma-Aldrich, St. Louis, MO) and organic solvent (Terpineol, Mallinckrodt Baker Inc., Phillipsburg, NJ) was then added for thorough mixing for 1 hour in the Spex Mixer/Mill. The solid loading of the different electrode inks ranged from 16 to 18 vol%.

Table 4.1: Characteristics of the powders used for the direct-write microfabrication of SC-μSOFCs with coplanar electrodes.

Material	Electrode	Nominal composition	Median particle size (μm)	Density (g/cm^3)	Specific surface area (BET) (m^2/g)
NiO	Anode	High purity green NiO	0.56	6.70	6.3
YSZ	Anode	92 mol% ZrO_2, 8 mol% Y_2O_3	0.25	5.99	6.1
LSM-YSZ	Cathode	70 vol% $(La_{0.8}Sr_{0.2})_{0.98}MnO_3$, 30 vol% $(ZrO_2)_{0.92}(Y_2O_3)_{0.08}$	0.56	6.19	9.7

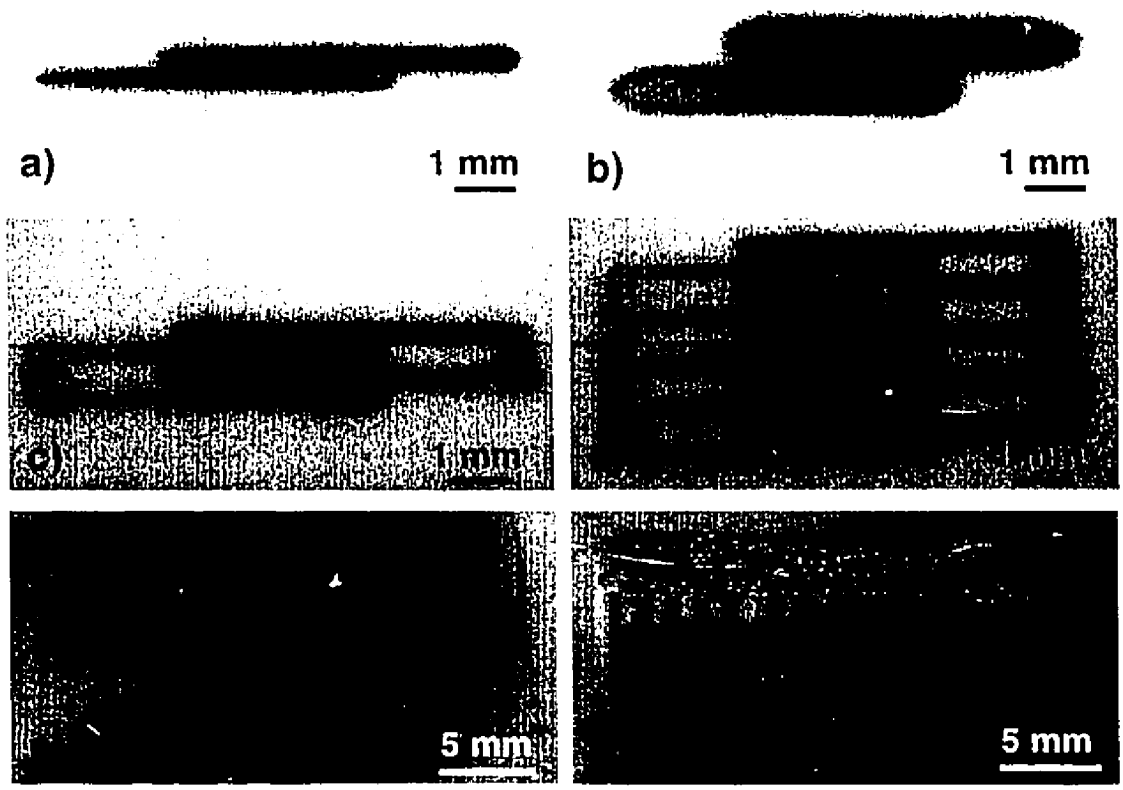

Figure 4.1: Optical micrographs of SC-μSOFCs with single electrode pair (average electrode width of a) 201 μm and b) 537 μm) and with c) two and d) five pairs of electrodes. Stack of three cells with e) one line per electrode and f) five lines per electrode.

The electrode inks were then extruded under air pressure (Ultra™ 2400 Series, EFD Inc., East Providence, RI) through stainless steel micronozzles (EFD Inc., East Providence, RI). A robotic direct-write deposition apparatus (I&J 2200-4, I&J Fisnar Inc., Fair Lawn, NJ) was used for their deposition onto the 0.2 mm thick YSZ (8 mol% Y_2O_3) electrolyte (Marketech International Inc., Port Townsend, WA). SC-μSOFCs with single electrode pairs as well as interdigitated electrode patterns composed of two, three, four, five and ten lines per electrode were fabricated (see Fig. 4.1a-d). The use of micronozzles of different diameters (inner nozzle diameter: 0.1-0.61 mm) were used to deposit single electrode pairs of different electrode width. The electrodes were cosintered under ambient atmosphere for 3 hours at 1200°C.

The electrode width and length, interelectrode distance and (projected) electrode surface area were measured from optical micrographs captured using an Olympus SZX12 stereomicroscope (Olympus Cooperation, Tokyo, Japan) and analyzed by using digital imaging software (Image-Pro Plus 6.2, Media Cybernetics Inc., Bethesda, MD). The electrode microstructure was characterized by scanning electron microscopy (ESEM, Quanta FEG 200, FEI Company, Hillsboro, OR). The electrode thickness was measured from SEM images of the cross-sectional view of the sliced electrodes and corresponds to the maximum thickness of the lens-like cross-sectional shape of the electrodes [25].

4.3.2 Electrochemical characterization

The SC-μSOFCs were characterized using a high-temperature testing setup [10, 24-26, 105]. A gas distribution plate was used based on the design described in Ref. [107], but modified to suit the needs of testing single-chamber fuel cells with coplanar electrodes. The cells were placed on a support plate inside the cell holder, and current collectors and gas distribution plate were installed over the coplanar electrodes (see Fig. 4.2a). The gas distribution plate with open design [107] contained holes to let the reaction gases pass through it and access the cell underneath (Fig. 4.2b). Posts were machined on the surface of the gas distribution plate facing the cells to enhance mixing of the gases flowing over the electrodes.

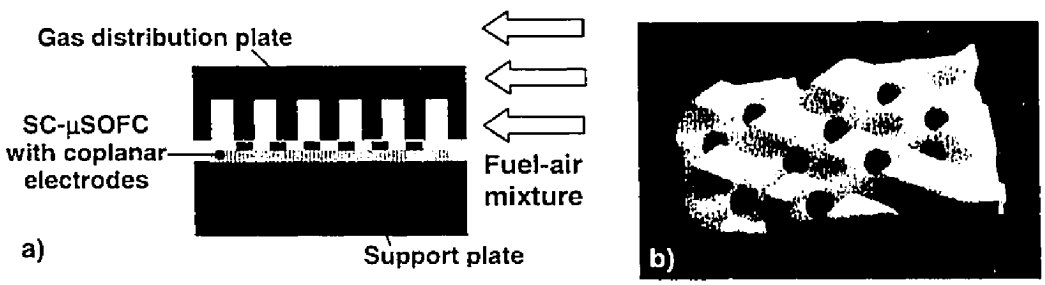

Figure 4.2: a) Schematic representation of the cell holder, where the SC-μSOFC with coplanar electrodes is placed between a support plate and a gas distribution plate. b) Photograph of the lower side of the gas distribution plate facing the cell. Holes are machined into the plate to let the reaction gases access the cell underneath, whereas the posts are to enhance mixing of the reactant gases flowing over the electrodes.

Table 4.2: Summary of electrode dimensions and cell performance for the fabricated SC-μSOFCs with one coplanar electrode pair.

Cell	Anode width (μm)	Cathode width (μm)	Average width (μm)	Inter-distance (μm)	Average electrode area (cm^2)	Anode thickness (μm)	Cathode thickness (μm)	OCV (V)	P_{max} (mW/cm^2)
1	107±6	80±19	93	153±11	0.00574	3.9	4.0	0	0
2	188±21	196±19	192	131±27	0.01199	7.7	8.5	0	0
3	174±14	211±24	192	144±21	0.01144	3.5	4.7	0	0
4	192±11	210±26	201	145±28	0.01268	8.1	7.0	0	0
5	180±23	250±50	215	257±34	0.01364	5.8	5.6	0	0
6	461±59	420±34	441	215±60	0.02753	6.7	10.7	0	0
7	450±18	468±37	459	186±58	0.02859	7.6	13.6	0	0
8	591±39	483±37	537	322±68	0.03374	12.8	13.9	0	0
9*	574±124	535±100	554	252±85	0.03338	23.0	22.8	0.898*	10.462*
10*	581±72	533±114	557	241±86	0.03272	18.5	23.3	0.878*	9.965*
11	745±126	949±161	847	305±129	0.05239	31.8	35.9	0.860	5.106
12	785±142	931±88	858	431±120	0.05219	34.3	48.3	0.865	4.886
13	772±157	968±187	870	400±166	0.05364	29.7	38.5	0.816	3.599
14	1248±147	1357±152	1303	267±148	0.08174	38.1	49.2	0.819	2.059
15	1200±151	1561±342	1380	274±145	0.08644	38.8	51.2	0.808	1.236

*OCV and P_{max} for cells 9 and 10 correspond to the maximum values for voltage and power obtained within the voltage and power fluctuations.

The cells were tested in the single-chamber mode at 700°C using a methane-air mixture with a methane-to-oxygen ratio R_{mix} = 2. Synthetic air, composed of nitrogen and oxygen in a ratio of 4 to 1, was used. The total flow rate of the gas mixture was 150 sccm. Additional nitrogen (with a flow rate of about 700 sccm) was used in the quartz tube around the cell holder to flush away the gases leaving the cell holder, and to prevent any counter gas diffusion. Before starting the electrochemical test and supplying oxygen into the system, the NiO anode was reduced in a methane-nitrogen mixture. The cells were positioned perpendicular to the direction of the gas flow, with the cathode being the first electrode to be exposed to the incoming gas mixture. This configuration has been identified to yield the highest power and OCV for SC-SOFCs with one single pair of coplanar electrodes [6]. Although SC-SOFC stacks have been reported to yield the highest power output for parallel gas flow [6], the perpendicular flow direction with cathode first was used throughout this study to permit direct comparison between single electrode pairs, interdigitated electrodes and cell stacks.

Gold wire (0.25 mm diameter, 99.9% (metals basis), Alfa Aesar, Ward Hill, MA) and mesh (82 mesh, woven from 0.06 mm diameter wire, 99.9% (metals basis), Alfa Aesar, Ward Hill, MA) were used for current collection. The gold grid was fixed with gold paste (C5450, Heraeus Holding GmbH, Hanau, Germany) over the electrode extremities in the case of the single electrode lines, and on the segment connecting multiple electrode lines. We have previously established that current collection on the whole electrode surface reduced activation and ohmic polarization and led to higher performance, compared to current collectors placed only over the connecting pads [26]. However, the small size of the interdigitated electrodes makes it difficult to apply gold grids over the whole anode and cathode, respectively, without causing internal short circuits. Therefore, and in order to eliminate effects due to variations in current collection method, the same current collection configuration was used for all cells. Fig. 4.1e-f show the cell and current collection configuration for stacks of three single cells.

The voltage was recorded using a data acquisition set (Agilent 34970A, Agilent Technologies, Santa Clara CA) in combination with the HP BenchLink Data Logger software (Agilent Technologies, Santa Clara CA). The voltage-current characteristics of the cell were obtained by varying the resistance on a decade resistor (Type 1432-M, General Radio Company, Cambridge, MA) and reading the voltage as well as the

current (197 Autoranging Microvolt DMM, Keithley Instruments Inc., Cleveland, OH) value. For all cells, the data for the plots of OCV against time were recorded immediately after the oxygen gas was turned on.

4.4 Results and discussion

4.4.1 Effect of electrode width on cell performance

In order to investigate the effect of electrode size on the performance of SC-μSOFCs with coplanar electrodes, cells with one line per anode and cathode of different electrode width and similar interelectrode gap were fabricated. Table 4.2 summarizes the geometrical characteristics, OCV and power output of these cells. The electrode width and interelectrode distance were obtained as the average of 20 equidistant measurements (pixel size of 7 μm) over the whole length of the electrode and of the interelectrode gap, respectively. The mean values with standard deviation given in Table 4.2 for anode and cathode widths, as well as interelectrode gap, therefore also take into account the tapered electrode edges (see Fig. 4.1b), and the variations in electrode width and interelectrode gap of one specific cell are due to a not perfectly rectangular electrode shape. The average interelectrode gap of all cells was ~250 μm, but the variations of the gap between the different cells are due to the limitations of the direct-writing technique using electrode inks with Newtonian flow behavior [21, 24, 25]. The reduced control of the electrode feature sizes also made it difficult to obtain cells with average electrode widths between 700 and 1000 μm, which is the reason for the uneven distribution of electrode widths reported in Table 4.2. The electrode length was ~0.6 cm for all cells. Cells 1 to 8 exhibited an average electrode thickness between 4 to 14 μm, whereas the other cells were ~35 μm thick as a result of the use of nozzles with different diameters during direct-write deposition. For reasons discussed later, these variations in electrode thickness are not a significant factor in this study.

Fig. 4.3a shows the OCV as a function of the average electrode width for the cells with a single electrode pair at 700°C, R_{mix} = 2 and a total gas flow rate of 150 sccm. Cells with average electrode widths exceeding ~850 μm delivered stable OCVs above 0.8 V. A slight increase of the OCV from 0.8 V to 0.86 V was also observed as the electrode width decreased from 1380 μm to 847 μm.

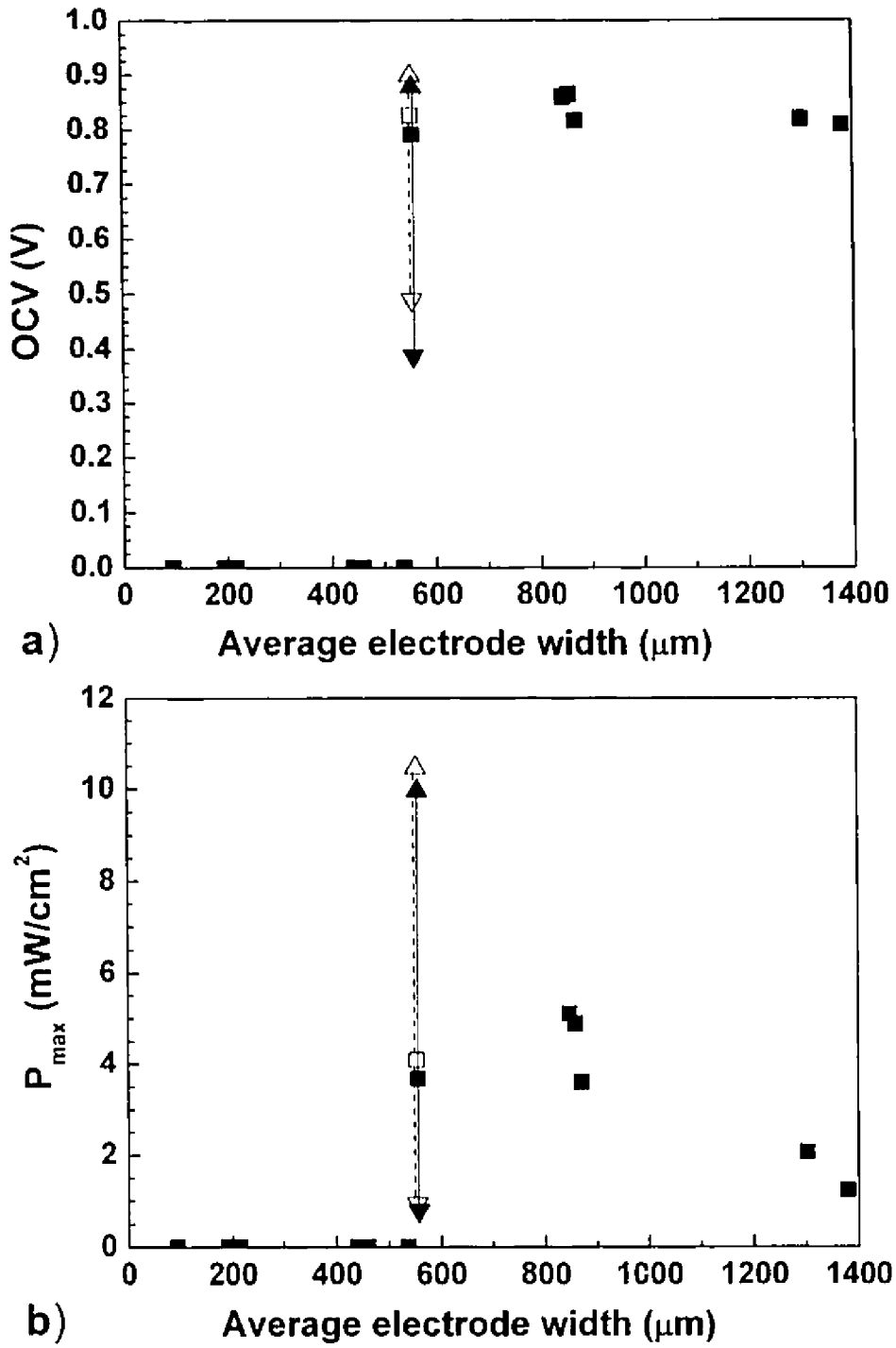

Figure 4.3: a) Open circuit voltage and b) maximum power density as a function of average electrode width for cells with a single electrode pair. The tests were performed at 700°C, R_{mix} = 2 and a total gas flow rate of 150 sccm. ▲Δ and ▼∇ correspond to the maximum and minimum value of the OCV and maximum power density obtained for the unstable cells with fluctuating voltage.

For cells with an average electrode width of ~550 μm, the OCV became unstable and exhibited significant fluctuations. Maximum, mean and minimum OCV are plotted in Fig. 4.3a for these cells to illustrate the voltage fluctuations, and the value in Table 4.2 corresponds to the maximum value measured during the OCV fluctuations. Finally, cells with electrode widths smaller than ~550 μm could not establish any significant OCV. Tests conducted at different gas flow rates (50 to 450 sccm), different R_{mix} values and different gas flow directions (parallel gas flow and perpendicular gas flow with anode first) led to the same result: a stable, non-zero OCV could not be established for these cells. A zero OCV was also obtained for cells with a single pair of electrodes with average electrode widths between 300 and 400 μm, composed of different electrode material combinations (NiO-YSZ or NiO-$Ce_{0.9}Gd_{0.1}O_{1.95}$ for the anode, and LSM-YSZ, LSM or $(La_{0.6}Sr_{0.4})_{0.995}(Fe_{0.8}Co_{0.2})O_3$ for the cathode) and tested under the same conditions.

Similarly, the power output was also significantly influenced by the electrode width (Fig. 4.3b). Due to a zero OCV, cells with small electrode widths below 550 μm did not yield any power output. For cells with electrode widths of ~550 μm, power fluctuations were observed; the maximum, mean and minimum values of the cell power output are given in Fig. 4.3b, and the maximum value is reported in Table 4.2. In the case of larger electrodes, a stable power could be measured. However, despite stable OCV and power, cells with the largest electrodes showed the lowest power among the cells with measurable power output. This behavior suggests that decreasing the electrode width leads to a decrease in the ionic conduction path and ohmic resistance [5, 6, 17], and a corresponding increase in the power. The increase in cell performance with decreasing electrode width is also shown in the voltage-current characteristics in Fig. 4.4. For the unstable cells, the maximum values of measured voltage and current were used to plot the corresponding curves. Decreasing the average electrode width from 1380 to 847 μm led to an increase of power by more than three times. Further reduction of the electrode width led to an additional increase in power, but the instability and voltage and current fluctuations during testing made stable and repeatable operation impossible (Fig. 4.4).

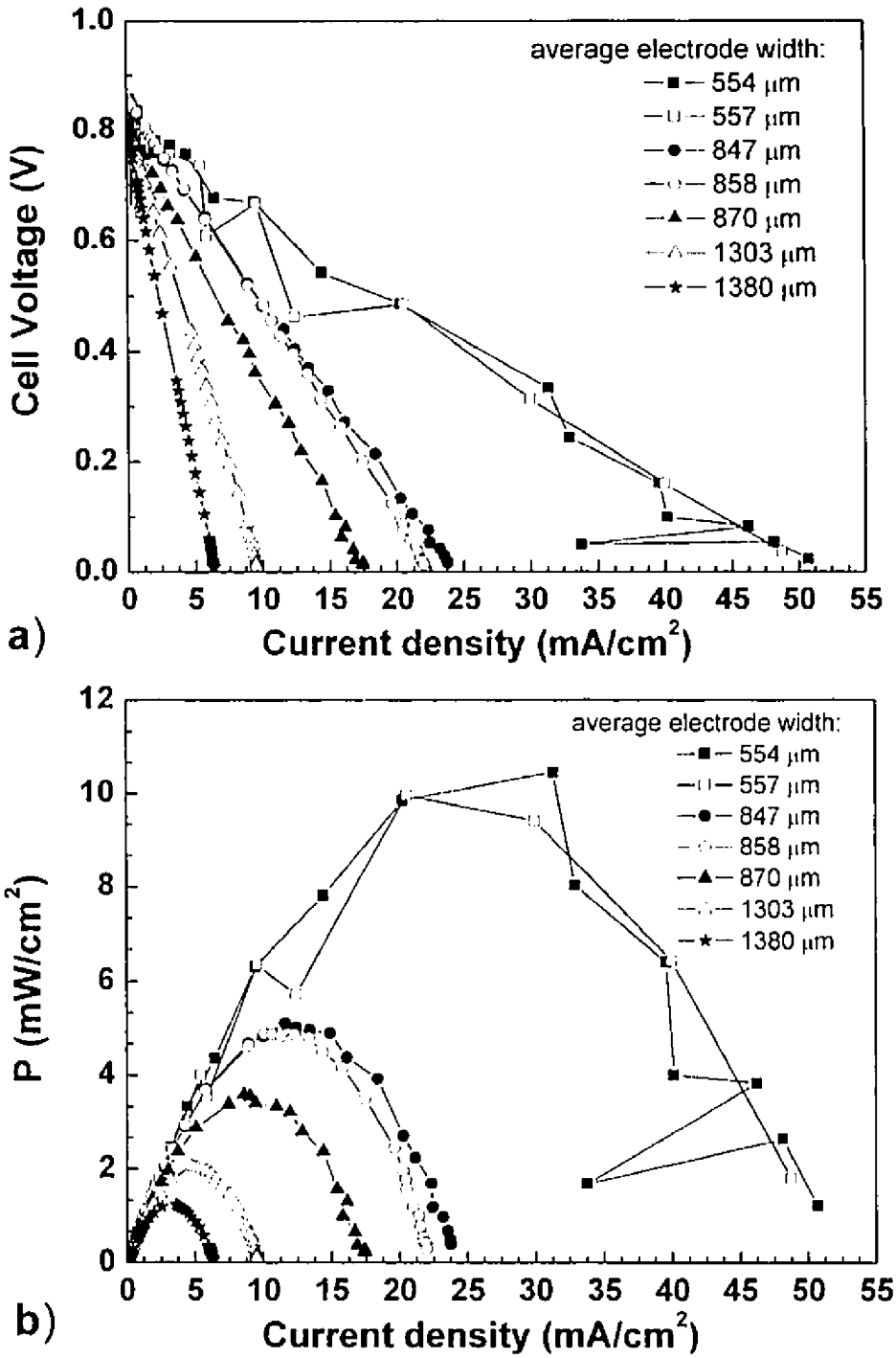

Figure 4.4: a) Cell voltage and b) power density against current density for cells with a single electrode pair delivering a non-zero OCV at 700°C, R_{mix} = 2 and a total gas flow of 150 sccm.

The aforementioned results suggest the existence of a critical electrode width, $w_{critical}$, around which voltage and current fluctuations are occurring, and below which stable operation is no longer possible. Three different regimes can thus be identified for cells with a single electrode pair: stable OCV (and cell power) for large electrodes ($w > w_{critical}$), fluctuating OCV (and cell power) for electrodes with widths near the critical value ($w \approx w_{critical}$) and zero OCV (and cell power) for small electrodes ($w < w_{critical}$). These observations can also be illustrated by plotting the OCV against time for selected cells from the three width groups (Fig. 4.5). While the small electrodes were not capable of establishing any OCV, the cells with critical electrode widths exhibited significant voltage fluctuations over a short time span, and cells with large electrodes exhibited stable voltages of ~0.8 V.

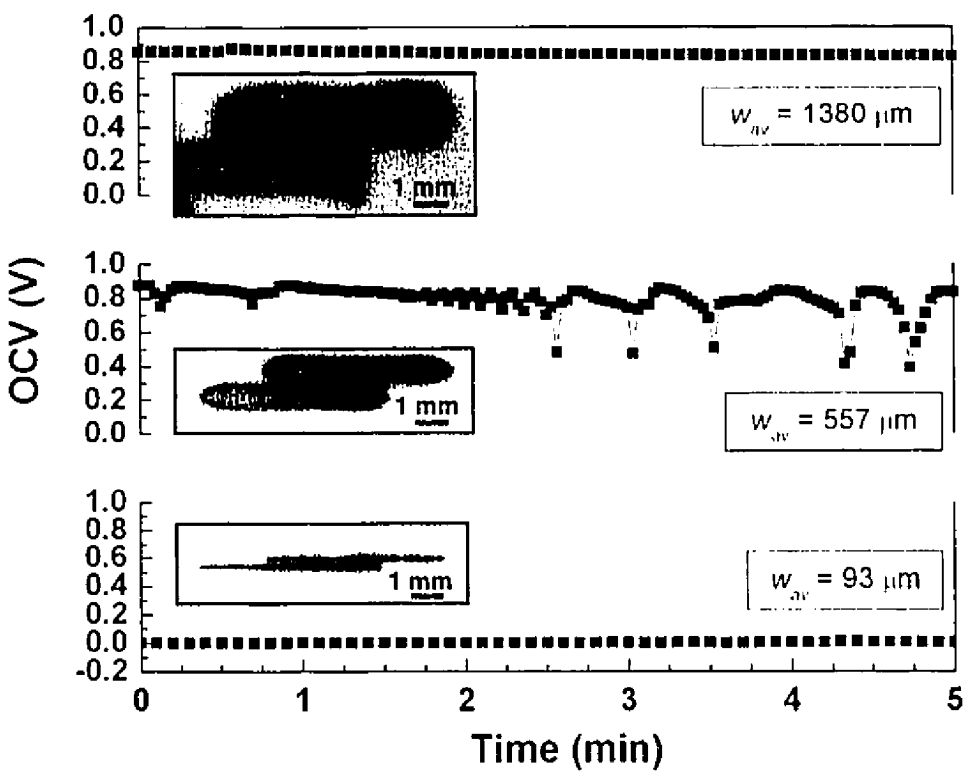

Figure 4.5: Representative time-dependent behavior of the OCV for cells with one electrode pair of different average electrode widths (93, 557 and 1380 μm) at 700°C, R_{mix} = 2 and a total gas flow of 150 sccm.

Voltage fluctuations have been reported to occur in the case of SOFCs operated under single-chamber conditions [12, 24, 26, 190]. Oxidation-reduction cycles of the nickel catalyst in methane-air mixtures were identified as a source of fluctuations of temperature, gas composition, product concentration and voltage. However, it is unlikely that those cycles should be at the origin of the voltage fluctuations observed in this study. The measured voltage fluctuations not only occur at a much shorter time scale (within seconds) as compared to the long-term (several hours to days) observations in the literature, but they should also be expected to occur for all cells with nickel-based anodes, independently of the electrode size. In particular, the larger electrodes with an increased content of nickel should be expected to undergo nickel oxidation-reduction cycles. As the latter do not exhibit any voltage fluctuations over the short time scale, other sources for the fluctuations, including electrode size effects, must be considered.

The OCV is established by a difference in oxygen partial pressure between anode and cathode, according to the Nernst equation:

$$OCV = \frac{RT}{nF} \ln \frac{p_{O_2,cathode}}{p_{O_2,anode}} \tag{4.1}$$

where R is the gas constant, T the temperature, F the Faraday constant, n the number of electrons and p_{O2} the partial pressure of oxygen at each electrode. In the case of SC-SOFCs, this difference in oxygen partial pressure is generated by the different catalytic activity and selectivity of the anode and cathode for the respective electrode reactions [122]. However, electrode selectivity is a known problem in SC-SOFCs [101]. The anode and cathode have been shown to be not completely selective for their respective reactions, leading to low voltage and power outputs, as well as low cell efficiencies [15].

The generation of the OCV depends on the oxygen partial pressure at the electrode-electrolyte interface, and thus the active surface area and the number of available triple phase boundaries. This area corresponds to the electrode area with a direct interface to the electrolyte. For electrodes of constant length, as in the case of the different cells tested in this study, the interfacial area is proportional to the electrode width. Therefore, the electrode width must be considered as a primary variable to correlate with the measured changes in the OCV. In contrast, the manufacturing-

induced variations in electrode thickness (ranging from 4 to 40 μm) are not a significant factor, because the effective thickness of the active interface is less than a micrometer [191]. Similarly, any effects due to intermixing of gases [15, 21] and impeded access of reactant gases to catalytic sites must be the same for all cells, because the interelectrode gaps are similar within the manufacturing tolerances. For these reasons, we believe that the observed changes in OCV correlate directly with electrode width for all the cells reported in this study.

Our results show that below a critical electrode width, stable cell operation is no longer possible for cells with single electrode pairs. This minimum size is expected to be a function of the testing conditions and cell materials used. In the case of Ni-YSZ anodes and LSM-YSZ cathodes on a YSZ electrolyte characterized under the testing conditions described earlier, the critical width was identified to be ~550 μm for an average interelectrode gap of ~250 μm. Below the critical width, the electrodes are too small to establish a sufficient gradient of oxygen partial pressure and promote the electrode reactions. An electrode width close to the critical size would enable high power outputs, but the small electrode surface areas and the amount of catalyst are still insufficient to maintain a constant difference in oxygen partial pressure and continuously sustain the reactions. Stable conditions can thus only be obtained for larger electrodes with an increased interfacial or active electrode area. A similar effect could probably be expected as a function of electrode length for a constant electrode width.

In addition to the miniaturization limit, there is also an upper limit of useful electrode width, $w_{effective}$. As shown in Fig. 4.4a, the cell resistance, represented by the slope of the *E-I* curve, increases with increasing electrode width while the cell performance decreases. Previous studies have shown that the anodic area active for electrochemical reactions is located closest to the interelectrode gap, and the rest of the anode did not contribute significantly to the cell performance due to an increased ionic conduction path and ohmic resistance [6, 13]. One indication of this was that the active anode region appeared white in color after testing due to an enhanced loss of nickel catalyst.

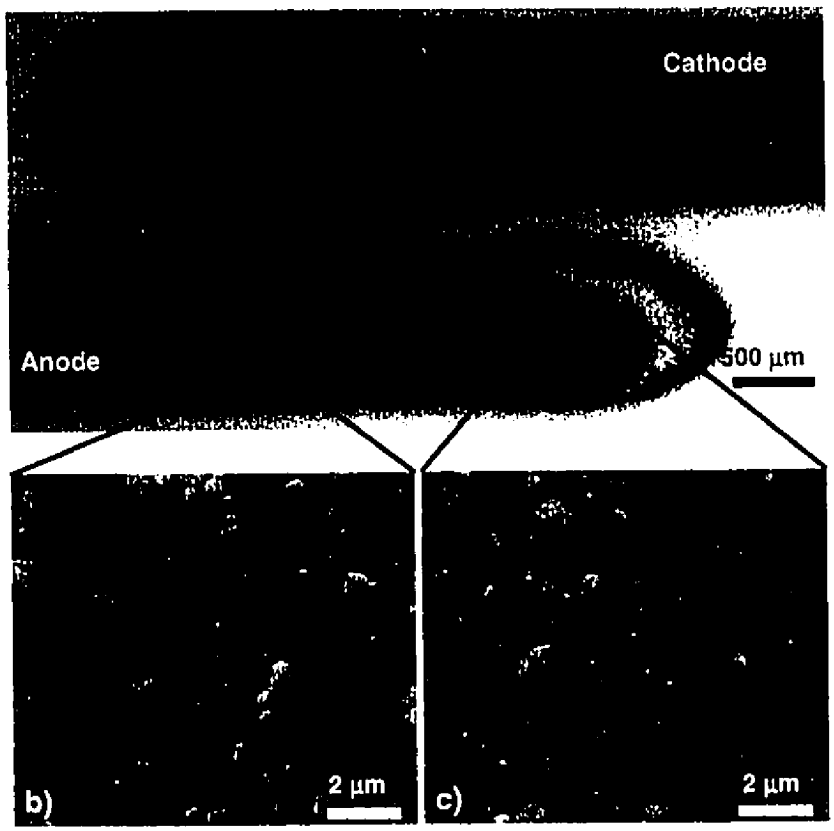

Figure 4.6: a) Optical micrograph of anode and cathode after testing (average electrode width: 858 µm). The anode exhibited a white color in the region closest to the cathode and at the tip. b) Representative SEM micrograph of tested anode in region away from interelectrode gap and c) in white region close to the gap.

In this study, such a white region close to the interelectrode gap and at the anode tip was observed only for cells with average electrode widths of 847 µm and larger (Fig. 4.6a). As reported in [13], SEM characterization confirmed the partial loss of nickel in this region (Fig. 4.6c), whereas metallic nickel was found on the remaining anode surface (Fig. 4.6b). The other cells exhibited an anode microstructure similar to the one in Fig. 4.6b after testing.

Fig. 4.7 provides a graphical summary of the effects of electrode width on the performance of SC-µSOFCs with one pair of coplanar electrodes. In this graph, the maximum cell power output is plotted against the average electrode width, w, and three performance regimes are identified. The first regime corresponds to a zero OCV and zero power output for cells with electrodes smaller than $w_{critical}$.

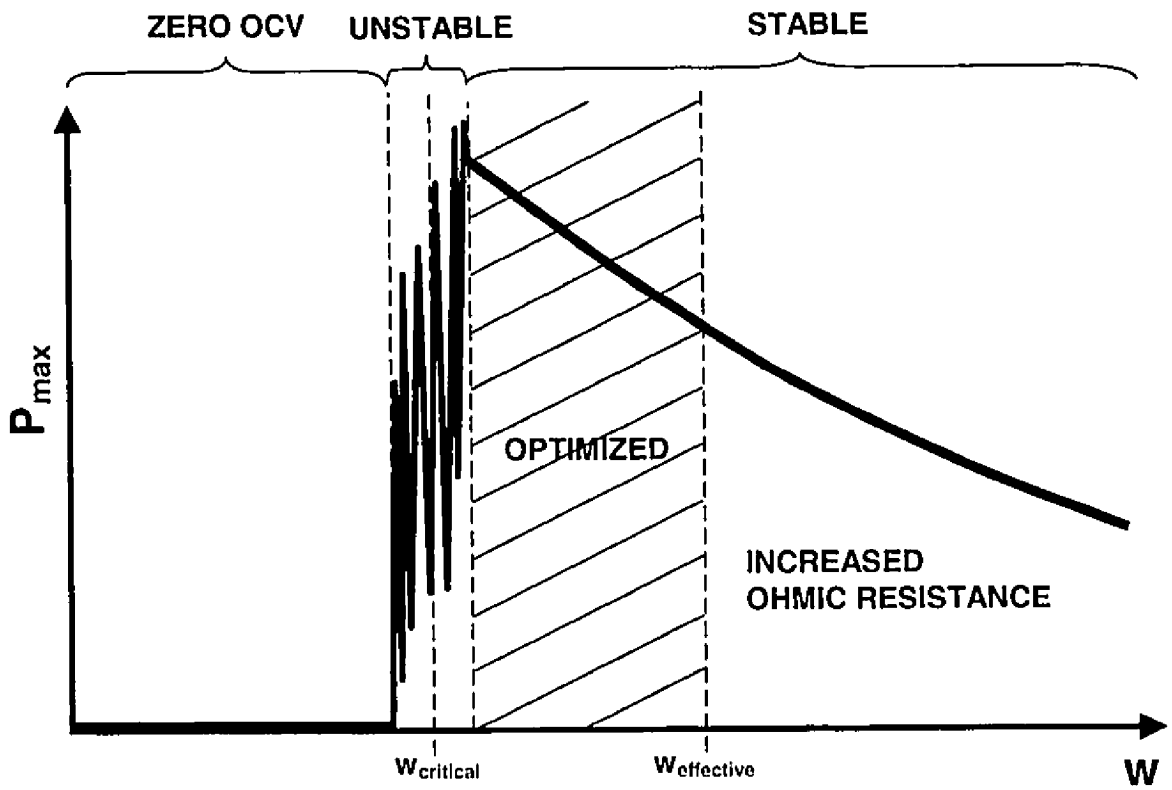

Figure 4.7: Schematic representation of design criteria for SC-μSOFCs with one coplanar electrode pair.

The unstable regime is characterized by voltage and power fluctuations for cells with electrodes of a width near $w_{critical}$. Stable power is obtained for cells with $w > w_{critical}$, but the increase in ohmic resistance with increasing electrode width ($w > w_{effective}$) continuously reduces the cell power output. Optimized performance can be obtained for electrode widths within the range $w_{critical} < w < w_{effective}$, which, under our testing conditions, was located between ~550 and 850 μm.

4.4.2 Effect of number of electrode lines

Numerous studies of successful operation of SC-SOFCs with multiple pairs of microelectrodes have been reported in the literature [13, 20, 21, 24, 25]. Therefore, it is of interest to enquire whether such structures are also subjected to the size limits found for cells with a single electrode pair. Cells with one, two, three, four, five and ten pairs of electrodes with widths of ~260 μm, thicknesses of ~17 μm and interelectrode gaps of

~114 μm were fabricated and tested. As previously shown, the cell with one line per electrode did not yield any OCV (Fig. 4.8a). However, a non-zero OCV could be obtained as the number of electrode lines increased. A cell with two lines per electrode enabled an OCV of ~0.2 V, which then decreased gradually to zero after about 10 minutes. A further increase of the OCV was measured for a cell with three electrode pairs. The voltage showed periodic fluctuations between 0.4 and 0.6 V. Higher OCVs of ~0.8 V could then be obtained by further increasing the number of electrode lines (Fig. 4.8b). While cells with four lines per electrode still exhibited significant voltage drops and fluctuations, the amplitude of fluctuations decreased for cells with five and ten electrode pairs. These observations confirm that higher and more stable OCVs can be obtained for SC-μSOFCs with multiple pairs of coplanar interdigitated microelectrodes, thereby relaxing the size limits imposed on a single pair of microelectrodes and enabling the use of closely-spaced microelectrodes for reduced ohmic cell resistance.

The OCV stability was shown to improve with an increasing number of electrode lines and thus an increasing interfacial or active electrode area, while an electrode thickness of ~17 μm was maintained between the different cells. These results thus corroborate the above postulated dependence of the OCV on the electrode width and the interfacial area and show that the OCV stability issues should not be attributed to an effect of electrode thickness. While one pair of electrodes smaller than the critical width is not capable of establishing a stable OCV, increasing the number of electrode lines to form an interdigitated electrode pattern increases the surface area and amount of catalyst available for the electrode reactions. An increased number of active reaction sites or triple phase boundaries permits the creation of a stable difference in oxygen partial pressure between anode and cathode and thus increases the voltage stability of the cell.

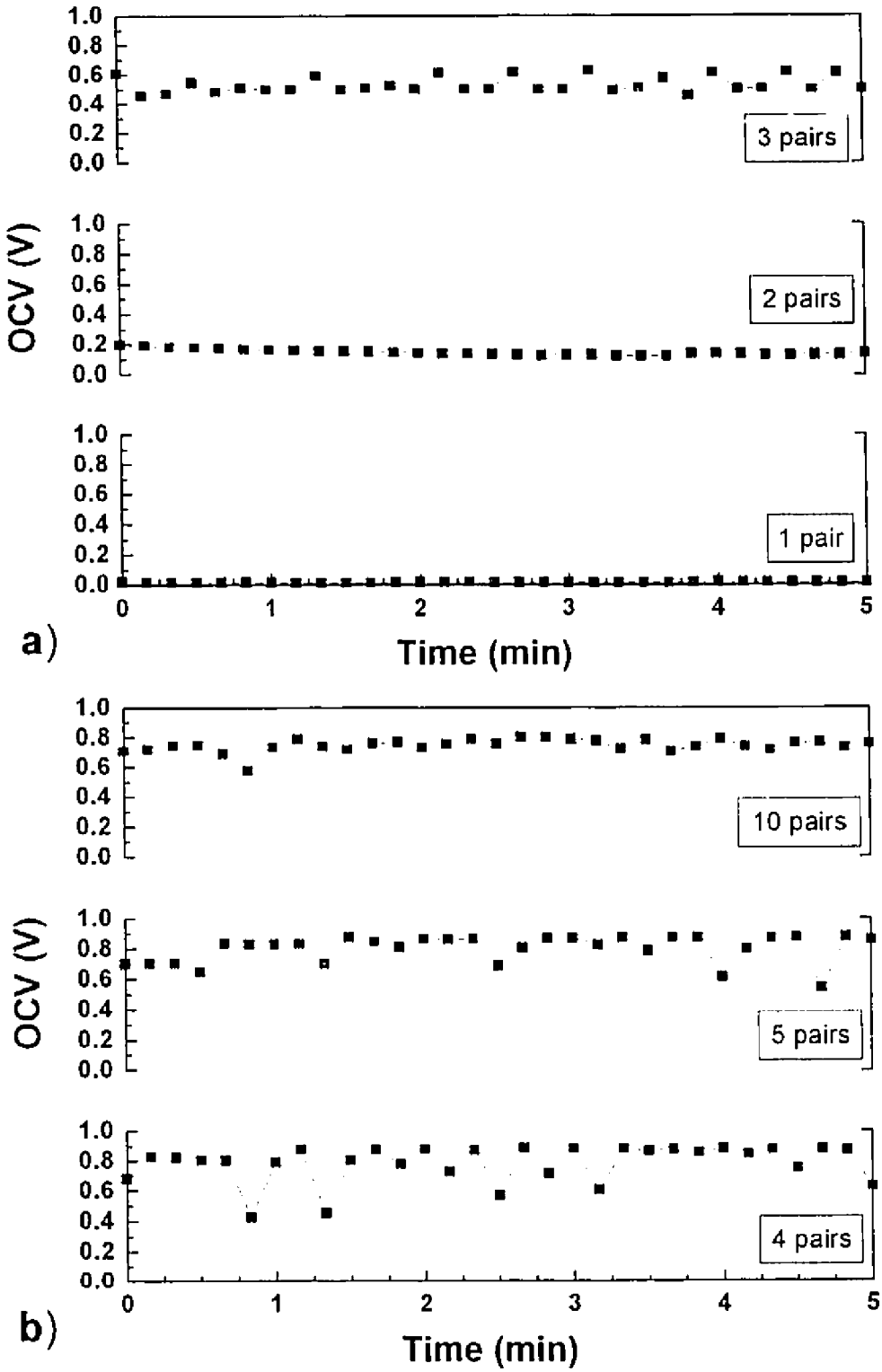

Figure 4.8: Representative time-dependent behavior of the OCV for cells with a) one, two, three and b) four, five and ten pairs of interdigitated electrodes. The OCV was measured at 700°C, R_{mix} = 2 and a total gas flow of 150 sccm.

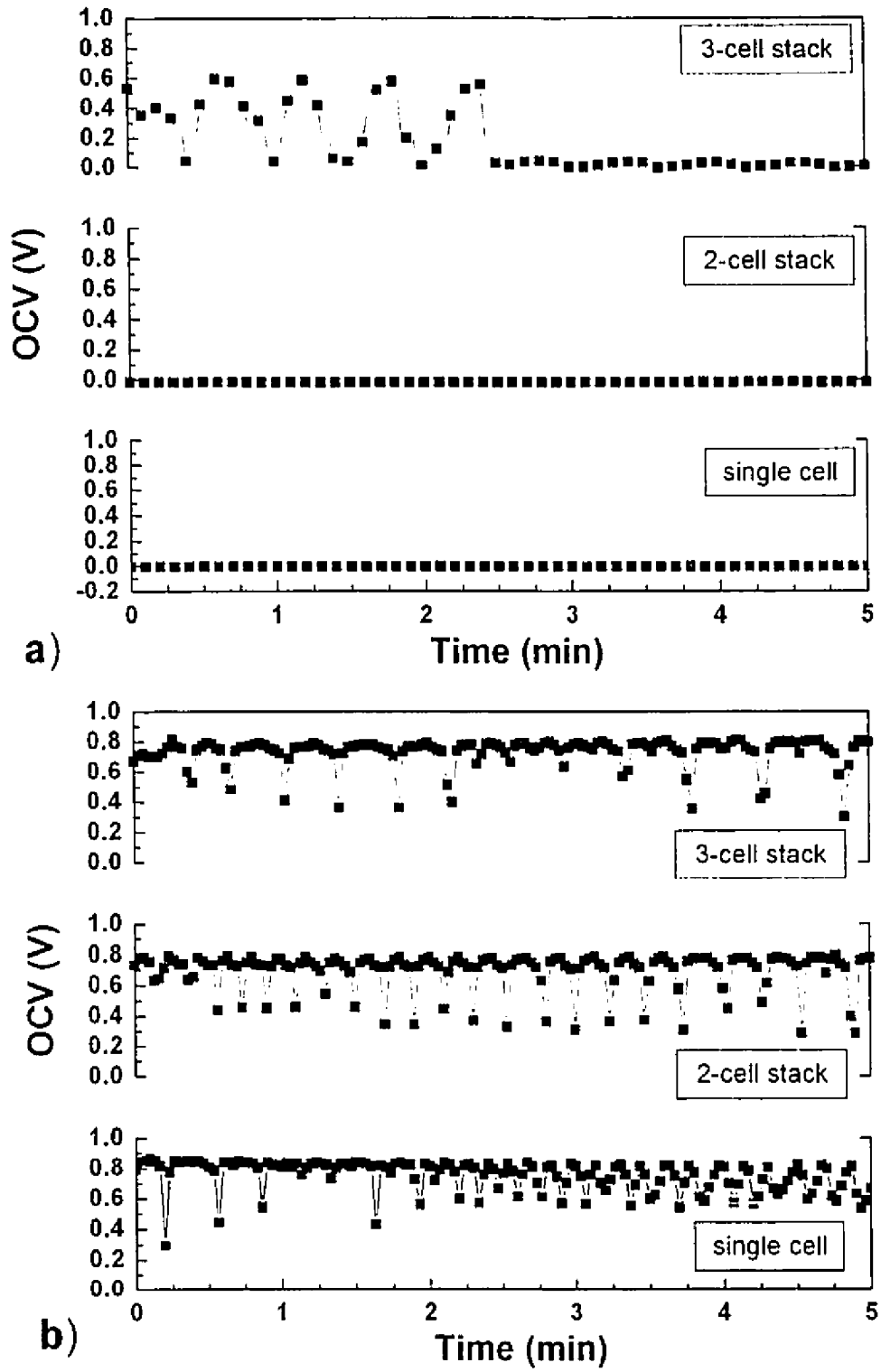

Figure 4.9: Representative time-dependent behavior of the OCV for cells with a) one and b) five electrode pairs as a single cell and assembled in a two-cell and three-cell stack. The OCV was measured at 700°C, R_{mix} = 2 and a total gas flow of 150 sccm.

4.4.3 Cell stacks

Cells with either one pair or five electrode pairs were assembled in a two- and three-cell stack (Fig. 4.1e-f) and their performance output was compared with the corresponding single cells. The average electrode width, thickness and interelectrode distance were ~400 µm, 13 µm and 290 µm, respectively. Fig. 4.9a-b show the OCV as a function of time for the different stack configurations. The zero OCV of the cell with one electrode pair and an electrode width smaller than the critical size could not be compensated by adding a second cell (Fig. 4.9a). Nevertheless, the three-cell stack enabled the temporary establishment of an OCV. In contrast to an increased number of electrode lines and an increased surface area in the case of interdigitated electrodes, stacks of cells with one line per electrode did not eliminate the problem of establishing a stable difference of oxygen partial pressure between two closely-spaced small electrodes.

When a cell with interdigitated electrodes of five lines per anode and cathode was used, an OCV with continuous fluctuations between 0.5 and 0.8 V (Fig. 4.9b) was established. For the two- and three-cell stack, the frequency of fluctuations diminished but the amplitude increased such that the OCV varied between 0.8 V and 0.2 V. Combining cells with five lines per electrode in a stack did thus not eliminate voltage fluctuations and instability of the single cells. Therefore no significant improvement of the voltage stability could be obtained from the stack configuration. Nonetheless, the cells with five lines per electrode delivered a sufficiently high OCV so that a power output could be measured for the single cell and the stack assembly, as summarized in Table 4.3. Notably, the power of a two- and three-cell stack increased by factors of 2.6 and 4.3, respectively, in comparison with the single cell.

Table 4.3: Performance of cell stacks with 5 lines per electrode.

Cell	OCV (V)	P_{max} (mW)
Single cell	0.833	0.178
2-cell stack	0.789	0.461
3-cell stack	0.801	0.760

4.5 Conclusions

Single-chamber solid oxide fuel cells with coplanar electrodes are well suited for miniaturization because of their compact and flexible design. Moreover, the ohmic resistance can be significantly reduced, and the performance output enhanced, by decreasing electrode width and interelectrode gap, thus reducing the ionic transport path. However, gas intermixing between very closely-spaced microelectrodes can degrade cell performance [15, 21]. In this study, a second scale effect was uncovered in the form of a minimum electrode width below which cells with one electrode pair could not be successfully operated. For a NiO-YSZ anode and LSM-YSZ cathode with an average interelectrode gap of ~250 μm on a YSZ electrolyte substrate, the critical electrode width was identified to be ~550 μm in a methane-air mixture (R_{mix} = 2) at 700°C. Cells with electrodes smaller than that size did not yield any voltage output. For electrodes with widths near the critical size, stable operation was not possible due to fluctuations in voltage and power. Only cells with larger electrodes enabled a stable voltage and power output. However, increasing the electrode width incurs a penalty on performance due to an increase in the ohmic loss. The design criteria for SC-μSOFCs with one pair of coplanar electrodes of a certain width, w, can thus be summarized as:

$w < w_{critical}$: no OCV (4.2)

$w \approx w_{critical}$: OCV and power fluctuations (4.3)

$w > w_{critical}$: stable OCV and power output (4.4)

$w > w_{effective}$: increased ohmic resistance (4.5)

$w_{critical} < w < w_{effective}$: optimized performance (4.6)

In this study, the optimal electrode width was estimated to be between 550 and 847 μm.

Electrodes with widths below the critical size can nonetheless be employed in interdigitated electrode structures. By increasing the number of electrode lines per anode and cathode, the active electrode area is increased, enabling a stable cell voltage despite the small width of the single electrode lines. This result highlights a significant benefit of using interdigitated architectures over single pairs of electrodes for SC-μSOFCs. Conversely, the use of single cells in stacks did not lead to any significant improvement in voltage stability.

Chapter 5 Fabrication and testing of coplanar single-chamber micro solid oxide fuel cells with geometrically complex electrodes

M. Kuhn, T. Napporn, M. Meunier, D. Therriault, S. Vengallatore, *Journal of Power Sources*, vol. 177, pp. 148-153, 2008.

5.1 Abstract

Coplanar single-chamber micro solid oxide fuel cells (SC-μSOFCs) with curvilinear microelectrode configurations of arbitrarily complex two-dimensional geometry were fabricated by a direct-write microfabrication technique using conventional fuel cell materials. The electrochemical performance of two SC-μSOFCs with different electrode shapes, but comparable electrode and interelectrode dimensions, was characterized in a methane-air mixture at 700°C. Both cells exhibited stable open circuit voltage and peak power density of 0.9 V and 2.3 mW/cm^2, respectively, indicating that electrode shape did not have a significant influence on the performance of these fuel cells.

5.2 Introduction

The increasing demand for miniaturized power generators with high energy density, reliable operation and fast regeneration is motivated by the rapid proliferation of consumer electronics and the steady commercialization of a wide variety of microelectromechanical systems (MEMS). The development of efficient energy systems beyond conventional battery technology is required to meet this demand [1]. Miniaturized solid oxide fuel cells (SOFCs) are one of the many concepts currently under development for portable power generation in such small-scale portable applications. SOFCs are attractive because the elevated operating temperatures (300-750°C) enable the efficient use of hydrocarbon fuels with high energy densities [35].

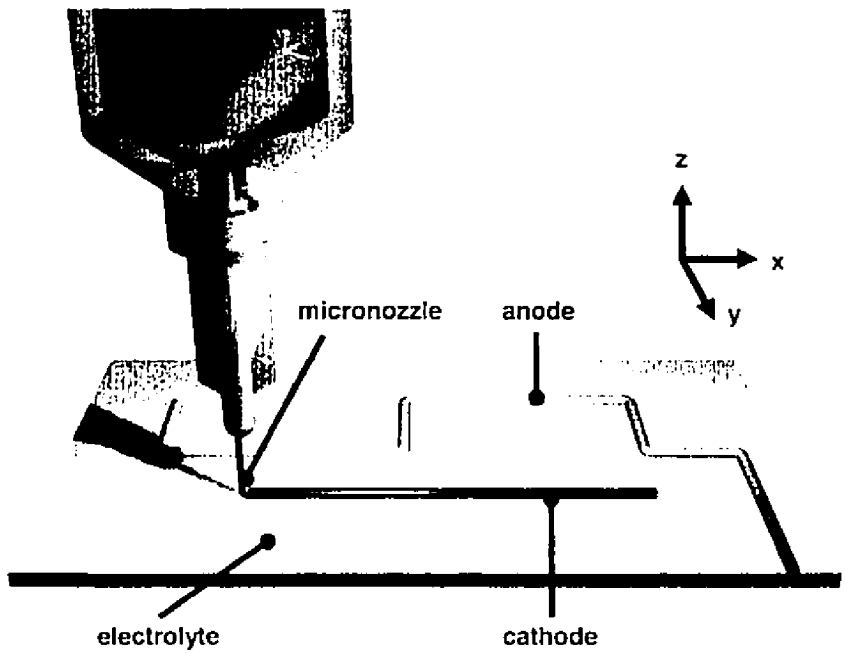

Figure 5.1: Schematic illustration of direct-write microfabrication. The direct-write technique consists of the pressure-driven extrusion of a paste-like material or suspension through fine micronozzles. The desired pattern is generated by the robot-controlled deposition of the extruded continuous filaments on a substrate.

Single-chamber solid oxide fuel cells (SC-SOFCs) are well suited for miniaturization and integration with MEMS [3]. Conventional dual-chamber fuel cells require high-temperature gas-tight sealing to keep the fuel (hydrocarbon) and oxidant (air) isolated at all times. In contrast, SC-SOFCs operate on mixtures of fuel and air [4, 10, 15], thereby removing the necessity of high-temperature sealing and complex gas manifolding. SC-SOFCs can be operated in several designs including a coplanar single-face configuration in which both electrodes, i.e., anode and cathode, are situated on the same side of a planar electrolyte [5, 6, 13, 20, 21, 24, 98]. This configuration enables the use of thick electrolytes for better thermomechanical stability and reliability during high-temperature operation. Furthermore, multiple SC-SOFCs can easily be connected in parallel and/or series to meet the power demand of portable devices [5].

Coplanar single-chamber SOFCs in the single-face configuration are a relatively recent development and correlations between processing, structure, properties,

performance and reliability are only now emerging. The studies reported in the literature have focused on fuel cells in which the anodes and cathodes are either a pair of parallel straight lines [5, 6, 13], or interdigitated structures with multiple pairs of parallel lines [13, 20, 21, 24, 98]. In addition to the effects of reactant gas composition and gas flow direction [6, 21], it has been established that the interelectrode width has a significant effect on power generation. The ohmic resistance for ionic conduction through the electrolyte is determined by the distance between adjacent electrodes and, hence, reducing interelectrode spacings has been demonstrated to improve fuel cell performance [5-7, 21, 158].

Robot-controlled direct-write microfabrication techniques are emerging as a simple and convenient method for fabricating SC-μSOFCs in the single-face configuration [21, 24]. Direct-writing allows the rapid fabrication of complex microscale structures and geometries using a wide variety of materials without the need for expensive photomasks [171]. The essential concepts in this approach are to prepare suspensions (or inks) using powders of electrode materials, and then to extrude the suspensions through a micronozzle onto the electrolyte substrate in the desired pattern, as illustrated in Fig. 5.1.

The single-face configuration is compatible with the design of closely-spaced electrodes in a variety of geometries. However, many critical issues associated with the use of complex curvilinear shapes for electrodes in SC-μSOFCs remain unexplored. These include the manufacturing limitations of microfabricating geometrically complex electrodes and the effects of electrode shape on fuel cell performance. The latter has implications for fuel cell modeling and optimized structural design. For these reasons, it is important to understand the relationships between microfabrication processes, electrode shape and structure, and the power and voltage generated by the fuel cell. As a first step towards that goal, this paper presents experimental results on direct-write microfabrication and electrochemical testing of coplanar SC-μSOFCs with electrodes of curvilinear two-dimensional geometry.

5.3 Experimental details

Conventional SOFC materials were used for anode, cathode and electrolyte in this study. For the anode, NiO powder (lot number: GRD-5, median particle size:

0.56 μm, density: 6.7 g/cm^3, surface area: 6.3 m^2/g) was mixed with YSZ powder (zirconia stabilized with 8 mol% yttria, lot number: 1606, median particle size: 0.25 μm, density: 5.99 g/cm^3, surface area: 6.1 m^2/g) in a ratio of 55 wt% NiO and 45 wt% YSZ. The powder mixture was thoroughly ball-milled using a Spex Mixer/Mill for 12 h. The cathode material was $(La_{0.8}Sr_{0.2})_{0.90}MnO_3$ (LSM) powder with a median particle size of 0.63 μm, density of 6.4 g/cm^3 and surface area of 4.24 m^2/g (lot number: 155-66). All powders were purchased from NexTech Materials. 0.2 mm thick YSZ plates (Marketech) were used as the electrolyte.

The electrode suspensions must be prepared so as to permit uniform flow of the suspensions through the micronozzle during deposition, and to ensure that the deposited structure retains its shape after extrusion. In turn, these characteristics are governed by the particle loading and the rheological properties of the suspension. Based on guidelines developed in a previous study [24], electrode suspensions with a particle loading of 16 vol% (equivalent to 56 wt%) were prepared by colloidal processing of the anode and cathode powders. A mixture of powder, solvent (Terpineol, J.T.Baker), dispersant (Triton X-100, Alfa Aesar) and binder (Poly(vinyl butyral-co-vinyl alcohol-co-vinyl acetate), Sigma-Aldrich) was ball-milled in the Spex Mixer/Mill for 1 h. The electrode suspensions were poured in a syringe barrel (3 cm^3, EFD Inc.) and then extruded under constant pressure through high precision stainless steel micronozzles (EFD Inc., inner nozzle diameter: 150 μm).

The direct-write technique used for the fabrication of the SC-μSOFCs in the single-face configuration has been described extensively, along with process-structure correlations, in a recent publication [24]. The essential details are as follows. A robotic deposition apparatus (I & J 2200-4, I & J Fisnar Inc.) was used for direct-write microfabrication of the desired electrode geometry on the YSZ plate. With respect to the coordinates shown in Fig. 5.1, the electrolyte substrate was mounted on a mobile, robot-controlled stage that could move in the x-direction, whereas the micronozzle was able to move in y- and z-direction. The distance between the nozzle and substrate was on the order of the nozzle diameter. An extrusion pressure of ~870 kPa for the anode and ~700 kPa for the cathode was applied while the robot velocity was fixed at 0.3 mm/s for a total electrode deposition time of less than 4 min. The anode structure

was deposited first and sintered at 1250°C for 3 h under ambient atmosphere. Subsequently, the cathode was deposited and the structure was sintered at 1100°C for 3 h to complete the fabrication of the SC-μSOFC.

Preliminary depositions were performed to confirm that electrodes of different designs (including wave-like, triangular and spiral geometries) could be obtained using direct-writing. Subsequently, two different illustrative designs of SC-μSOFCs were fabricated using the same feedstock materials for electrodes and electrolyte. The electrodes of these fuel cells contained a combination of curvilinear electrodes to spell "SOFC" and "POLY", respectively (Fig. 5.2). The electrode dimensions and average interelectrode spacings were designed to be constant, so that a comparison of the performance of these devices can isolate the effects of electrode shape from size.

The electrode dimensions and interelectrode distances were measured from optical micrographs obtained using an Olympus SZX12 stereomicroscope and by using image processing software (Image-Pro Plus 6.2). Twenty measurements were performed to determine each electrode width and interelectrode distance. The anodes constitute the letters of the words "SOFC" and "POLY", and the cathodes are the adjacent straight line segments.

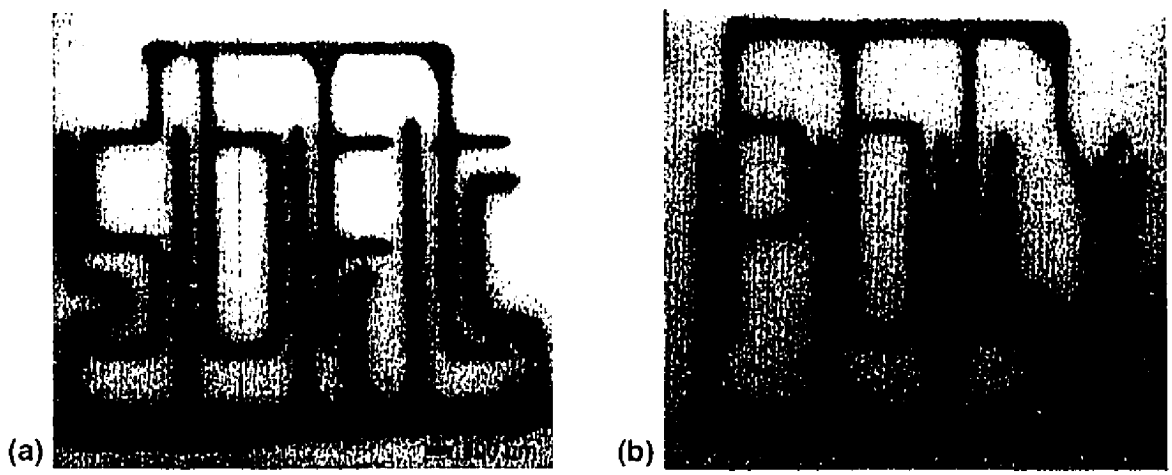

Figure 5.2: Optical micrographs of single-chamber micro solid oxide fuel cells in single-face configuration with curvilinear electrode geometries. These images were taken after sintering (and before electrochemical testing).

The interelectrode distance is a measure of the spacing between adjacent electrodes and was measured perpendicular to the orientation of the cathode segments. This choice enables a close comparison with SC-μSOFCs with interdigitated comblike electrodes [24]. The electrode surface areas listed in Table 5.1 include the connecting lines, on which the gold current collectors were placed during electrochemical testing. The measurement resolution (i.e., pixel size) was ~8 μm at the magnification used. A scanning electron microscope (SEM, Quanta FEG 200, FEI Instruments) was used to investigate the microstructure of the electrodes after sintering. The grain size and the electrode porosity were evaluated through SEM image analysis.

The electrochemical performance of the fabricated SC-μSOFCs was tested using a high-temperature testing setup that has been described previously [10, 105]. The fuel cells were operated in methane-air mixtures that are characterized by the methane-to-oxygen ratio, R_{mix}. A methane-air mixture with a total flow rate of 150 sccm and a ratio $R_{mix} = 2$ was used in testing.

Table 5.1: Electrode dimensions and interelectrode spacings of the SC-μSOFCs.

		"SOFC" geometry		"POLY" geometry	
		Anode	Cathode	Anode	Cathode
Electrode surface (cm^2)	Mean	0.129	0.115	0.107	0.111
Electrode width (μm)	Minimum	200	202	176	221
	Mean	251	263	229	242
	Maximum	283	400	265	346
	σ	19	36	15	14
Interelectrode distance (μm)	Minimum	158		176	
	Mean	434		487	
	Maximum	1525		1557	
	σ	392		448	
Length of overlapping electrode segments (mm)	Mean	4.4		4.0	

Additional nitrogen (with a flow rate of about 700 sccm) was used as a shielding gas to facilitate gas transport over the fuel cells. The furnace temperature was set to 700°C. Gold wire and grid (Alfa Aesar) served as current collectors. A gold grid was placed over the connecting lines (that is, the horizontal electrode segments that connect all the anode lines and all the cathode lines on each fuel cell). Subsequently, a gold wire was attached to the grids to facilitate electrical measurements. The NiO anode was reduced to nickel in a methane/nitrogen mixture before introducing oxygen into the furnace. The temperature of 700°C indicated throughout this paper refers to the preset furnace temperature. The actual cell temperature was measured to be between 720 and 740°C using the procedure described by Napporn et al. [10].

5.4 Results and discussion

The two electrode geometries are shown in Fig. 5.2a and 5.2b. In these micrographs, anode and cathode appear in green and black, respectively. Thus, the anodes spell the letters "SOFC" and "POLY", while the cathode was composed of closely-spaced linear segments between the letters. Table 5.1 summarizes the minimum, mean, maximum and standard deviation (σ) of the electrode width for each fuel cell. Also listed are the dimensions of the interelectrode area in terms of the average interelectrode distance and the length of the overlapping electrode segments. The variations in electrode widths (5% variation in mean values, and standard deviations that are ~10% of mean values) are an indication of the manufacturing tolerance associated with direct-write microfabrication. Details on the source of these variations are discussed in a recent paper [24], which investigated the relationships between process parameters (especially, ink viscosity, extrusion pressure and stage velocity) and the dimensions and continuity of deposited electrodes.

Fig. 5.3 shows representative scanning electron microscope images of the microstructure of the sintered anode and cathode. The anode exhibited an average grain size of less than 1 μm (Fig. 5.3a). The porosity was heterogeneous due to the presence of small pores with an average size of less than 1 μm and the presence of several larger pores. In comparison, the microstructure of the cathode was more homogeneous, with pore sizes ranging from 0.5 to 2 μm (Fig. 5.3b). The cross-sectional shape of a typical anode and cathode is shown in Fig. 5.3c and 5.3d, respectively.

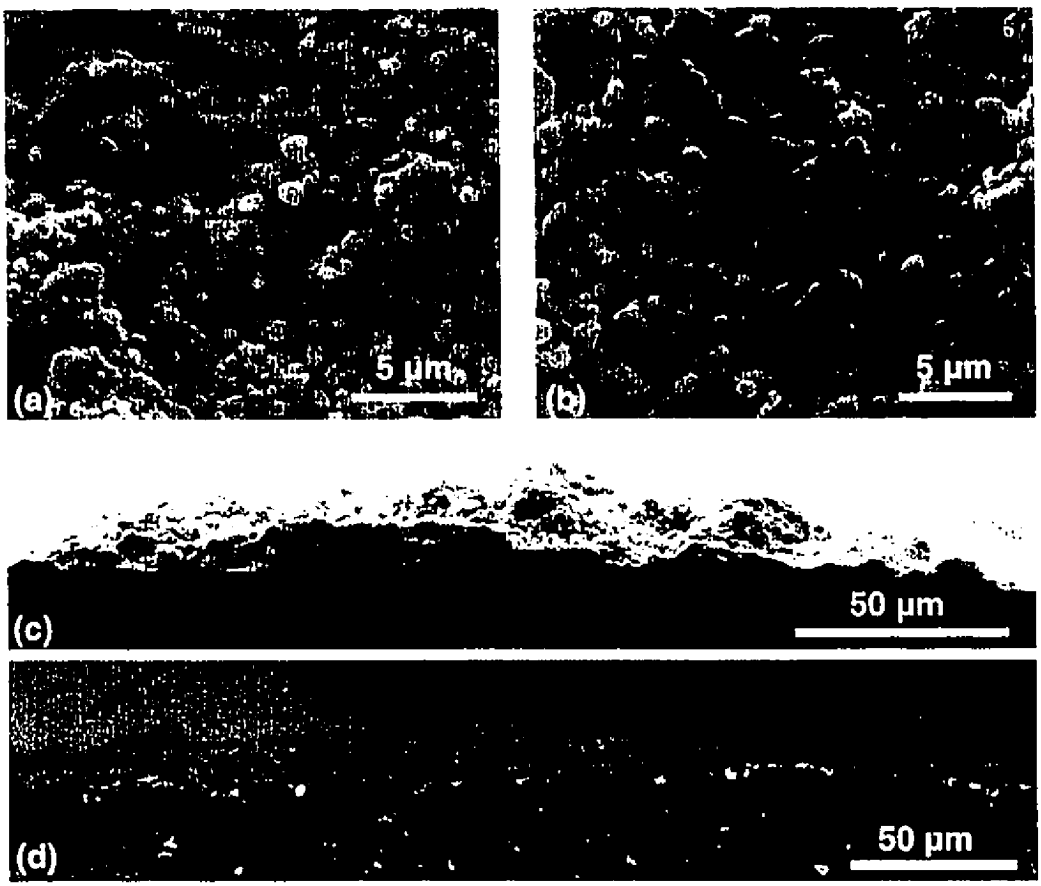

Figure 5.3: Scanning electron micrographs of the sintered electrodes showing plan views of a) anode and b) cathode, and cross-sectional views of c) anode and d) cathode.

The sidewalls of the electrodes formed a lens-like shape due to the spreading of the electrode suspension on the YSZ substrate during direct-write microfabrication. The maximum electrode thickness ranged between 12 and 20 µm. Notably, no differences were found between the microstructures of the electrodes in the two different fuel cells.

Electrochemical testing of the SC-µSOFCs was performed at 700°C in a methane-air mixture (R_{mix} = 2) and at a total gas flow of 150 sccm. The gas flow direction was from left to right with respect to the micrographs in Fig. 5.2a and 5.2b. The time responses of the open circuit voltage (OCV) following exposure to the gas mixture are shown in Fig. 5.4a and 5.4b. At time t = 0 s, the methane/nitrogen mixture is introduced into the chamber and this leads to the establishment of a transient open circuit voltage of ~0.6 V before oxygen is introduced into the chamber.

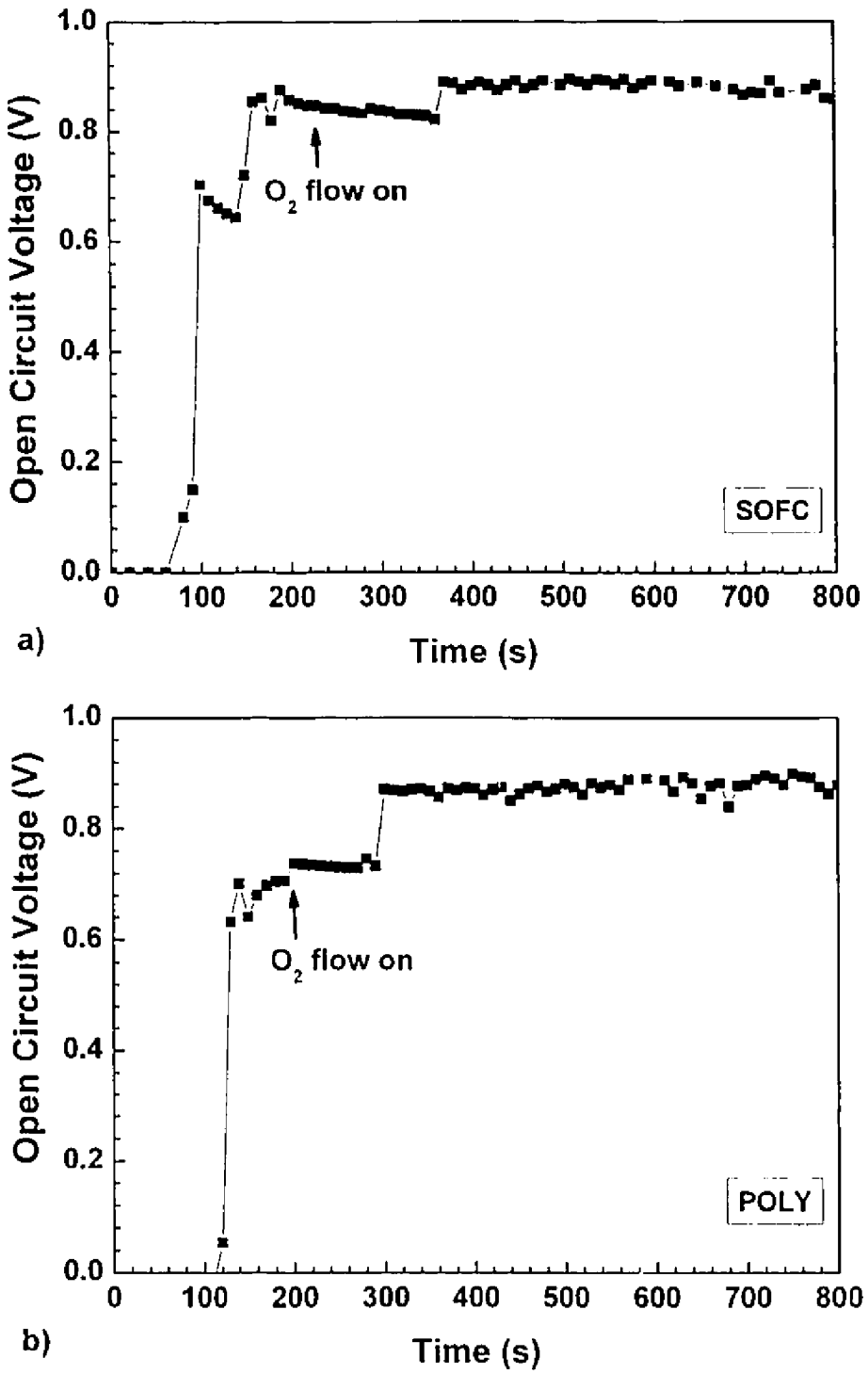

Figure 5.4: Open circuit voltage as a function of time for a) "SOFC" and b) "POLY" electrode geometry during fuel cell operation in a methane-air mixture (methane-to-oxygen ratio R_{mix} = 2) at 700°C and a gas flow rate of 150 sccm. The methane/nitrogen mixture was allowed to flow over the cell at t = 0 s.

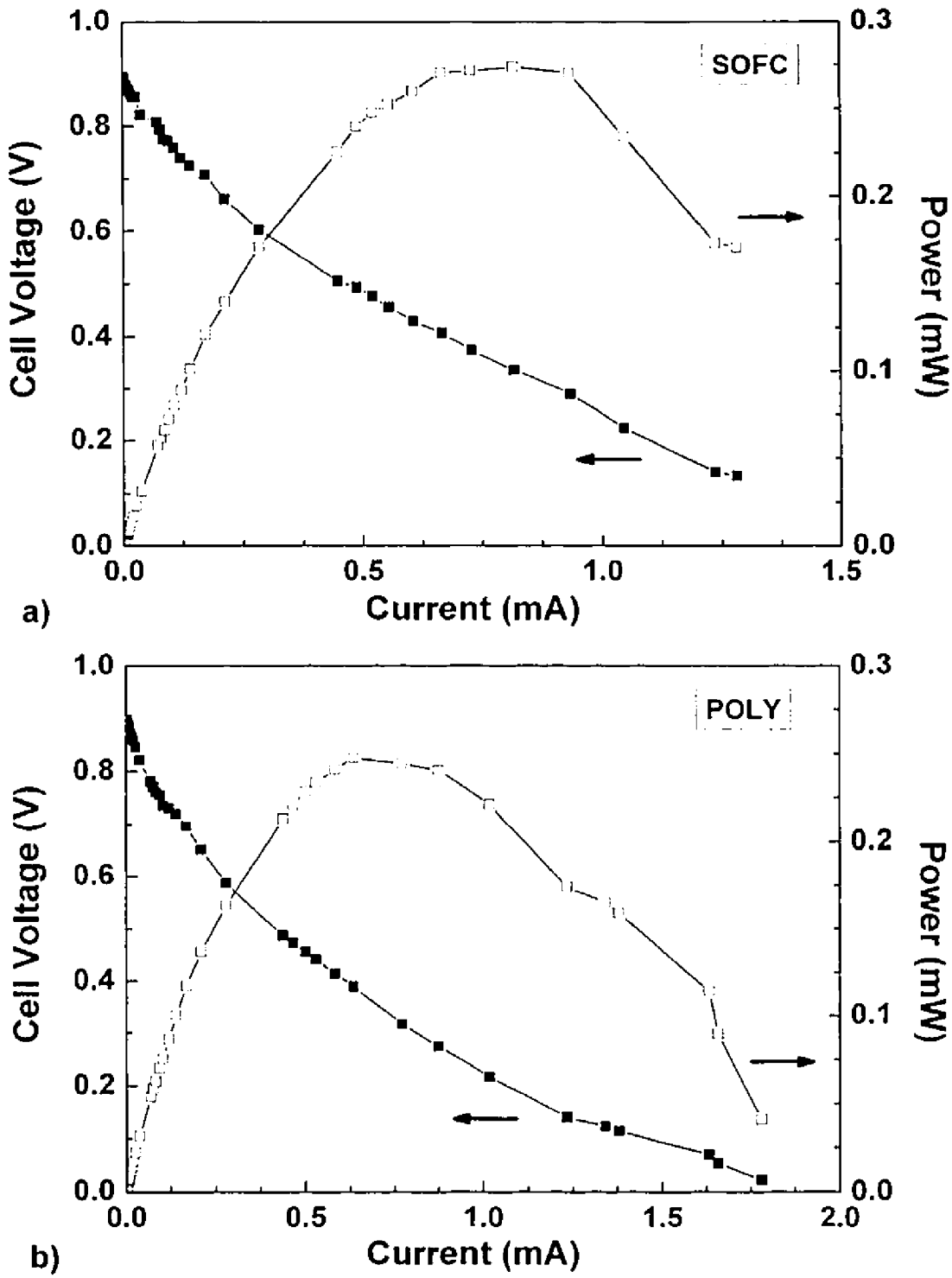

Figure 5.5: Voltage-current characteristics of the a) "SOFC" and b) "POLY" geometry. Both tests were performed in a methane-air mixture with R_{mix} = 2 and a total gas flow of 150 sccm at 700°C.

Now, once oxygen is added to the gas mixture, the OCV increases further to ~0.9 V, and remains stable at this value for both fuel cells. There are no significant differences in the responses of the two fuel cells, and it is concluded that electrode shape does not affect the open circuit voltage.

The recent experimental studies of Morel et al. [192] provide valuable insight into the mechanisms responsible for the time response of the OCV. In that study, the reduction processes of NiO anodes of SC-SOFCs were studied by analyzing the outlet gas compositions in real time using a quadrupole mass spectrometer. The dominant reaction under a CH_4 flow at 700°C was the reduction of NiO, leading to the formation of CO and H_2 gases, along with a smaller amount of CO_2.

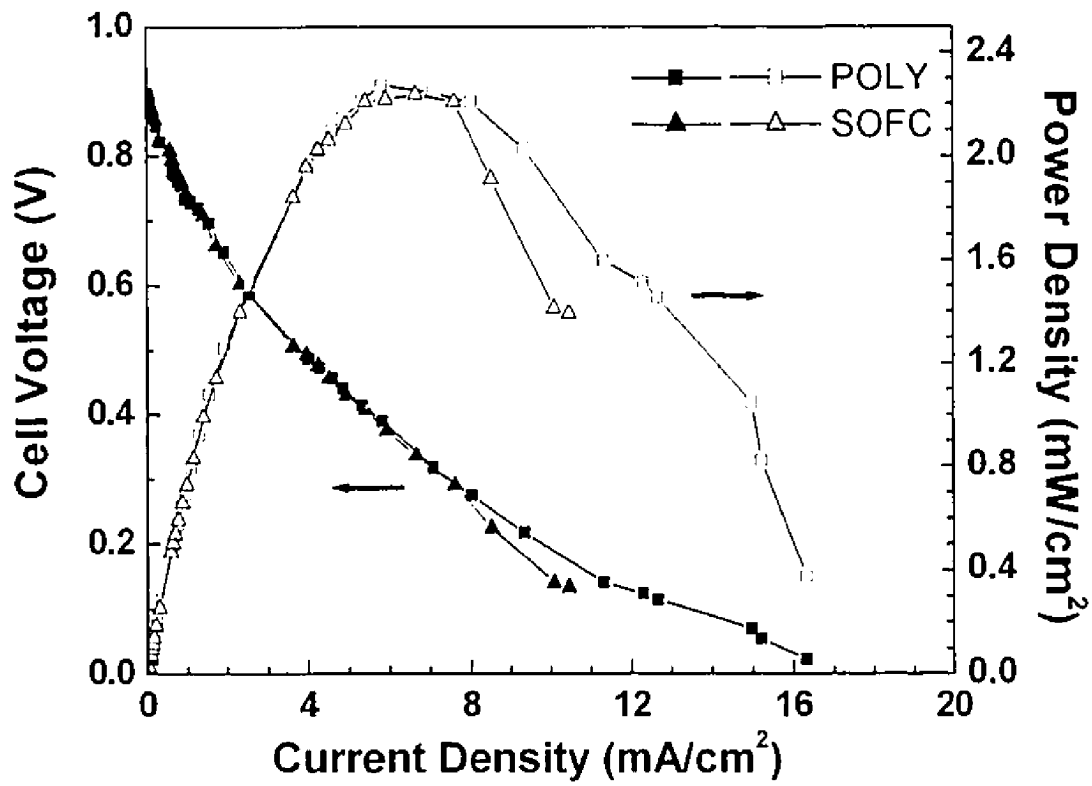

Figure 5.6: Comparison of the electrochemical performance of the "SOFC" and "POLY" geometry in a methane-air mixture with R_{mix} = 2 and a total gas flow of 150 sccm at 700°C. Voltage (closed symbols) and power density (open symbols) are plotted as functions of current density. The average electrode surface area is the normalization parameter.

The presence of the syngas at the anode/electrolyte interface creates a transient open circuit voltage even without the addition of oxygen. In addition, the cracking of methane is accompanied by carbon deposition on the electrodes. The introduction of oxygen leads to decarburization, followed by a further increase of the OCV to the stable value of 0.9 V.

Fig. 5.5 shows the voltage-current characteristics for the two SC-μSOFCs at 700°C in a methane-air mixture with R_{mix} = 2. The maximum power generated is 0.27 mW and 0.25 mW for the "SOFC" and "POLY" designs, respectively. However, since the electrode sizes are not identical in both cells, a normalized comparison is necessary to evaluate the effects of shape on performance.

The measured power can be scaled using either the average area of one electrode or the total area of the fuel cell [13], as normalizing parameters. Here, the former choice is adopted since it can lead to a close comparison with the performance of conventional SOFCs. That is, the performance of trilayered dual-chamber fuel cells is typically normalized with respect to the electrode areas, since these represent the electron generating surfaces. The thickness of the electrolyte, which is a measure of the ionic resistance, is not typically considered in normalizing the performance of such fuel cells. Similarly, in SC-μSOFCs with interdigitated electrodes, the average electrode area represents the electron generating surfaces, and the interelectrode area (which is a measure of ionic resistance) is ignored in normalization.

Fig. 5.6 shows the voltage and power density as functions of current density normalized with respect to the average electrode area. Both fuel cells exhibit a peak power density of 2.3 mW/cm^2, and this comparison suggests that in-plane electrode shape has no significant effect on electrochemical performance of these SC-μSOFCs. Therefore, there is no significant benefit in designing SC-μSOFCs with geometrically complex electrodes. However, additional testing of such fuel cells under different conditions (particularly the direction of gas flow with respect to electrode geometry) and using different fuel cell materials is necessary to confirm these preliminary results.

5.5 Conclusions

This paper is the first report of direct-write microfabrication and electrochemical testing of single-chamber micro solid oxide fuel cells with geometrically complex

electrodes. Two different SC-μSOFC designs were tested under identical conditions of gas composition, flow direction and furnace temperature. Both fuel cells exhibited identical open circuit voltage and peak power density of 0.9 V and 2.3 mW/cm^2, respectively, at 700°C. These results demonstrate the versatility of the direct-write microfabrication method for manufacturing SC-μSOFCs, and suggest that electrode shape does not have a significant impact on the performance of coplanar SC-μSOFCs.

Chapter 6 Experimental study of current collection in single-chamber micro solid oxide fuel cells with comblike electrodes

M. Kuhn, T. W. Napporn, M. Meunier, D. Therriault, *Journal of The Electrochemical Society*, vol. 155, pp. B994-B1000, 2008.

6.1 Abstract

The effect of current collection on the performance of single-chamber micro solid oxide fuel cells (SC-μSOFCs) with coplanar interdigitated, comblike electrodes was studied. Conventionally employed current collection on the electrode segment linking together the single lines of the electrode comb was compared to applying gold mesh current collectors on the whole electrode surface. A simplified design was used with a comblike Ni-YSZ (yttria-stabilized zirconia) anode on one side of the YSZ electrolyte and a square, planar cathode made of $(La_{0.8}Sr_{0.2})_{0.98}MnO_3$-YSZ and $(La_{0.8}Sr_{0.2})_{0.98}MnO_3$ on the opposite side. The cells were tested in methane-air mixtures at 700°C. Current collection on the whole anode surface led to a reduction in ohmic cell resistance for the conduction and collection of generated electrons, and 50% more power could be extracted from the cell. A nickel-rich anode with 80 wt% Ni content was investigated to enhance electron transport and conduction, but Ni instability in fuel-air mixtures prevented a performance increase. Additionally, the Ni-richer anode was more affected by aging. Collecting the current from the whole electrode surface area using suitable current collector designs will contribute to increasing the performance output of SC-μSOFCs with comblike electrodes in the interdigitated configuration.

6.2 Introduction

Single-chamber solid oxide fuel cells (SC-SOFCs) are gaining widespread interest in the fuel cell community because of their simplified design and their potential for portable and small-scale power generation applications. SC-SOFCs are operated in

mixtures of fuel and oxidant in a single gas chamber [4], thereby eliminating the need for high-temperature gas-tight sealing and complex gas manifolding. These features enable compact designs for fuel cells and offer the possibility of simplified stack assembly and low-cost fabrication. SC-SOFCs can be fabricated and operated in either the dual-face configuration, which consists of a three-layer structure with an electrolyte sandwiched between the electrodes, or the single-face configuration, which is composed of closely-spaced anodes and cathodes on the same surface of a planar electrolyte.

The earliest references to the concept of single-face SC-SOFCs are a report by van Gool in 1965 [120], and a patent issued to Louis et al. [99] in 1981 for a solid electrolyte fuel cell device with coplanar electrodes located on the same side of the electrolyte. The first SC-SOFC in the single-face configuration consisting of two parallel electrode lines was successfully operated by Hibino et al. in 1996 [5]. Since then, several aspects of the design, manufacture and testing of SC-SOFCs have been investigated. Experimental studies have addressed the effects of several variables including different electrolyte and electrode materials [17, 121], fuel gas composition [6, 13, 17, 21], position of the fuel cells in the gas stream [6, 21], various fabrication methods [13, 20, 21, 24, 98, 164], interelectrode distance [6, 17, 98, 159], and electrode shape and geometry [21, 25] on the performance of SC-SOFCs. Theoretical and numerical models have been developed to predict the performance of SC-SOFCs as functions of electrode shape, geometry and size [7, 18].

Although the aforementioned studies have greatly advanced our understanding of single-face SC-SOFCs, many important aspects of the operation, performance and reliability of these fuel cells still remain to be investigated. In this paper, we address one such open problem that relates to the method of current collection during the operation of small-scale SC-SOFCs (SC-μSOFCs). This problem is peculiar to SC-μSOFCs in the single-face configuration because of the constraints imposed by the electrode architecture. Typically, the closely-spaced anode and cathode are shaped as comblike structures arranged in an interdigitated manner, with electrode widths and interelectrode spacings ranging from tens of micrometers to several hundred micrometers or a few millimeters. This compact design maximizes the electrode area and allows simple series connection of various electrode lines on an electrolyte

substrate. However, the small size of electrodes poses significant challenges for efficient current collection.

In dual-face SC-μSOFCs with planar, square electrodes, the current collectors (typically metallic meshes) cover the whole electrode surface area, which reduces the current pathway and effective ohmic resistance for electron transport. The single-face configuration with comblike microelectrodes does not permit this current collection design because it is difficult to place a comblike metal mesh over an anode and cathode, respectively, without touching the other electrode and causing electrical short circuits. Therefore, the state-of-the-art practice is to connect each set of electrode lines to a common contact pad (also called the connecting line), and to place the metallic meshes on each contact pad corresponding to the anode and cathode [13, 21, 24, 98]. Thus, current is collected only on a small fraction of the electrode area, and the electrons generated in the interdigitated electrode segments must migrate a significant distance (on the order of millimeters) along the electrode to reach the current collectors. These considerations suggest that this method of current collection can degrade the performance of SC-μSOFCs [13], but the extent of the degradation has not been quantified.

A different approach to current collection using integrated (or embedded) current collectors was suggested recently by Buergler et al. [141]. In this approach, the current collector is embedded inside the electrodes during electrode fabrication and sintered together with the electrodes. Gold cannot be used as the current collector because the high temperatures (> 850°C) used for sintering of the electrodes cause material diffusion and melting. Platinum is not a good choice either because the catalytic effects of this material contribute to overheating of the fuel cell during operation in methane-air mixtures [10]. Embedding the platinum inside the electrodes does not reduce its catalytic activity because the material is still in contact with the reaction gases diffusing through the porous electrodes towards the triple phase boundaries. However, for anodes based on cermets of nickel and yttria-stabilized zirconia (YSZ), a simple strategy is to increase the electronic conductivity of the electrode by a corresponding increase in the content of nickel. The implications of this strategy for the performance and stability of SC-μSOFCs have not been systematically investigated.

Table 6.1: Characteristics of the powders used for fabrication of SC-μSOFCs.

	Electrode	Nominal composition	Median particle size (μm)	Density (g/cm^3)	Specific surface area (Brunauer, Emmett and Teller) (m^2/g)
NiO	Anode	High purity green NiO	0.56	6.70	6.30
YSZ	Anode	92 mol% ZrO_2, 8 mol% Y_2O_3	0.25	5.99	6.10
LSM	Cathode	$(La_{0.8}Sr_{0.2})_{0.98}MnO_3$	0.63	6.40	4.24
LSM-YSZ	Cathode	70 vol% $(La_{0.8}Sr_{0.2})_{0.98}MnO_3$, 30 vol% $(ZrO_2)_{0.92}(Y_2O_3)_{0.08}$	0.56	6.19	4.80

This paper presents detailed experimental studies to quantify the effects of both factors, namely, the use of conventional metallic meshes as current collectors and the use of nickel-rich anodes, on the performance of SC-μSOFCs in the single-face configuration. The underlying approach is based on the fabrication and electrochemical testing of SC-μSOFCs using conventional fuel cell materials (nickel, YSZ and lanthanum strontium manganite (LSM)). Due to the difficulty associated with positioning metallic current collectors on top of, or inside, the microfabricated electrodes, a much simpler approach was adopted to investigate the effects of current collection method on fuel cell performance. A dual-face cell configuration was used wherein one electrode (the cathode, in this study) and its current collection were maintained constant. Thus, the planar cathode covered the entire surface of the YSZ electrolyte, and was subsequently covered completely with a suitable gold mesh current collector. In contrast, two different current collection configurations (covering only the connecting line and covering the whole surface, respectively) for the comblike anode were studied. A comparison of the electrochemical performance of these different fuel cells under identical test conditions can isolate the effects of current collection method on fuel cell

performance. Subsequently, the use of nickel-rich anodes for enhanced current collection was considered, with particular attention to the effects of aging and long-term stability of these electrodes. The details of these studies are presented in the following sections.

6.3 Experimental

Table 6.1 summarizes the characteristics of the NiO, YSZ, LSM and LSM-YSZ powders used for the fabrication of the electrodes for SC-μSOFCs. The powder density was measured using a He-Pycnometer AccuPyc 1330 (Micromeritics). The data for the particle size and specific surface area were provided by the supplier (NexTech). The electrolyte consisted of 0.2 mm thick YSZ (8 mol% Y_2O_3) plates purchased from Marketech International. For the anode, two powder mixtures were prepared by mixing NiO and YSZ in different weight ratios in a Spex mixer/mill (Spex CertiPrep 8000M, ATS Scientific Inc.). The first mixture contained 55 wt% NiO and 45 wt% YSZ (NiO:YSZ = 55:45), and the second mixture was enriched in nickel and contained 80 wt% NiO and 20 wt% YSZ (NiO:YSZ = 80:20).

Electrode suspensions were prepared by mixing electrode powders with 2 wt% Triton as a dispersant for 10 min in the Spex mixer/mill with YSZ balls (0.5 and 1.0 mm in diameter) as milling media. Poly(vinyl butyral-co-vinyl alcohol-co-vinyl acetate) (Sigma-Aldrich) was used as a binder and was fully dissolved in Terpineol (J.T. Baker). The binder-solvent mixture was then added to the powder for thorough mixing for 1 h in the Spex mixer/mill. The solid loading of the different electrode suspensions ranged from 16 to 19 vol%.

The YSZ plates were cut into small squares of approximately 1 cm^2, onto which the anode and cathode suspensions were deposited. Comblike anodes were fabricated by using a robot-controlled direct-write microfabrication technique in which the anode suspensions were extruded under air pressure (Ultra™ 2400 Series, EFD Inc.) through stainless steel micronozzles (EFD Inc.) and robotically deposited (I&J 2200-4, I&J Fisnar Inc.) onto the YSZ plates in the desired pattern [24, 25]. Nine anode lines per cell were deposited, as shown in Fig. 6.1a. The anodes were composed of either 55 wt% NiO (Ni55) or 80 wt% NiO (Ni80). No nickel-rich, conductive contact layer on top [6] was used. The relatively small current and power density measured in this study can be

attributed to this simple anode layer composition. The cathodes were fabricated via screen printing using stainless steel masks and were deposited onto the opposite side of the electrolyte to form a dual-face cell configuration. A catalytic layer of LSM-YSZ was first deposited. Then, after drying, a conductive layer of pure LSM was printed on top of the previous layer. Sintering of the anode and cathode was performed under ambient atmosphere for 3 h at 1250 and 1200°C, respectively. Table 6.2 catalogues the principal characteristics of the different SC-μSOFCs fabricated in this study.

The width of the anode lines and the areas of the electrode surface and connecting lines were measured from optical micrographs captured using a stereomicroscope (Olympus SZX12) and analyzed by using digital imaging software (Image-Pro Plus 6.2). The electrode microstructure was investigated using scanning electron microscopy (ESEM, Quanta FEG 200, FEI Instruments). The electrode thickness was obtained from SEM images of the cross-sectional view.

A high-temperature testing setup [10, 24, 105] was used for the electrochemical characterization of the fabricated SC-μSOFCs. The furnace temperature was set to 700°C. The cells were operated in the single-chamber mode using methane-air mixtures with different methane-to-oxygen ratios, R_{mix}. The total flow rate of the gas mixture was fixed at 150 sccm. All cells were positioned in the testing setup with the anode facing down (Fig. 6.1b) and with the gas flow perpendicular to the anode lines. Additional nitrogen (with a flow rate of about 700 sccm) was used as a shielding gas to rapidly flush away the incoming gas passed through the cell holder, and also to avoid any counter gas diffusion. Gold wire (0.25 mm diameter, 99.9% (metals basis), Alfa Aesar) and mesh (82 mesh, woven from 0.06 mm diameter wire, 99.9% (metals basis), Alfa Aesar) were used for current collection. To evaluate the effect of electrode surface area used for current collection on the measured current and power, the gold mesh was placed either only over the anode connecting lines (Ni55cl and Ni80cl) or over the whole anode surface (Ni55w and Ni80w) (see Table 6.2). In the case of the cathodes, a gold mesh covering the whole cathode surface was used. Before the electrochemical test, the NiO anode was reduced to metallic nickel in a methane/nitrogen mixture before supplying oxygen into the system.

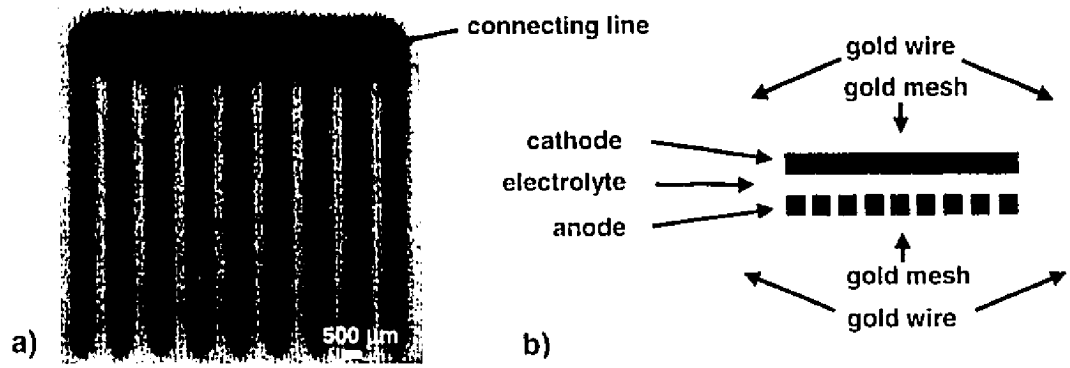

Figure 6.1: a) Micrograph of comblike anode after sintering. b) Schematics of SC-µSOFC in dual-face configuration.

6.4 Results

Electrode geometry and microstructure.—Table 6.2 catalogues the principal characteristics of the different SC-µSOFCs fabricated in this study. The connecting line area of the comblike anodes ranged from 23 to 29% of the total anode surface area. The width of the single anode lines in the comblike structure was 550 ± 90 µm. The thickness of the cathode and anode were 32 ± 6 µm and 25 ± 10 µm, respectively. The variation in anode thickness and width is due to the deposition repeatability associated with the direct-write microfabrication technique.

Table 6.2: Main characteristics of the SC-µSOFCs fabricated.

Cell	Anode composition NiO:YSZ	Current collection configuration	Anode surface area (cm^2)	Connecting line area (cm^2)
Ni55cl	55:45	Connecting line	0.439	0.100 (23%)
Ni55w	55:45	Whole surface	0.423	0.102 (24%)
Ni80cl	80:20	Connecting line	0.389	0.104 (27%)
Ni80w	80:20	Whole surface	0.409	0.117 (29%)

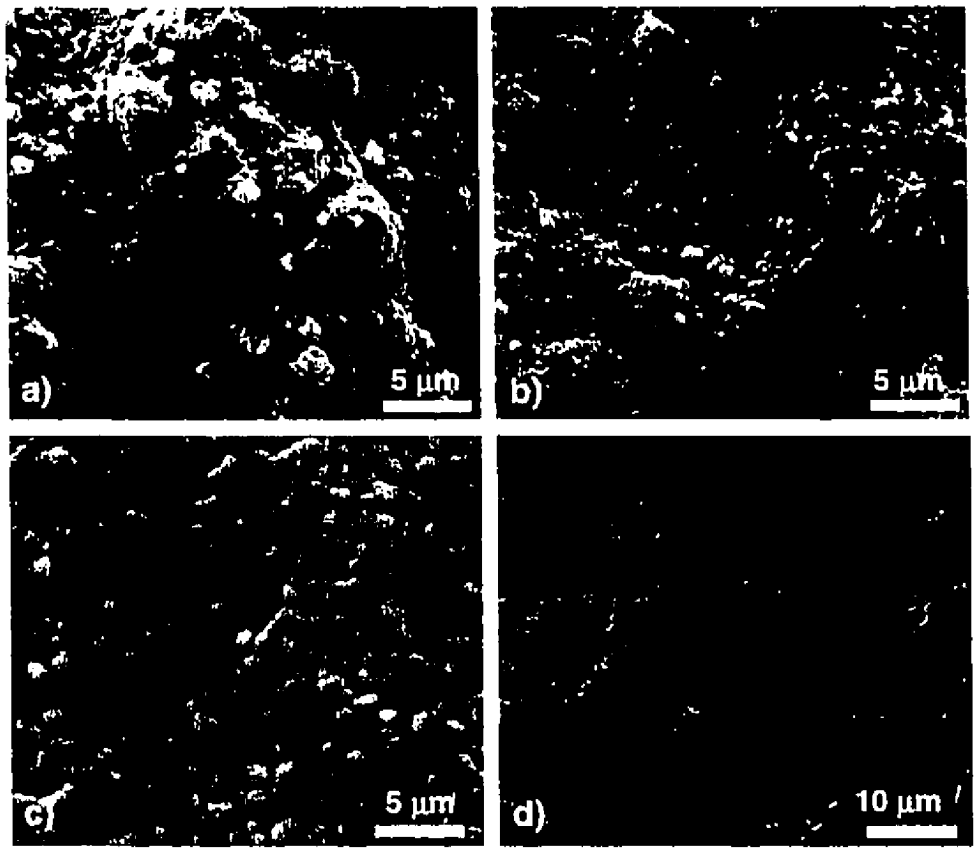

Figure 6.2: Anode microstructure of a) Ni55 cell and b) Ni80 cell after sintering. Cathode microstructure: c) top view, d) cross-sectional view.

Fig. 6.2 shows scanning electron micrographs of the electrodes after sintering. Uniform porous microstructures for the anodes (with the two different nickel contents) and the cathode were observed. In addition, the LSM-YSZ catalytic layer on the YSZ electrolyte can be discerned in the cross-sectional image (Fig. 6.2d). This layer had a distinctly finer microstructure in comparison with the coarser and thicker LSM layer on top.

Effect of current collection on cell performance.—Fig. 6.3 shows the polarization curves for two fuel cells with identical cathode and anode materials. These tests were performed at 700°C with R_{mix} = 2 and a total gas flow of 150 sccm. The current collector was either placed over the entire anode surface (Ni55w) or only the connecting line (Ni55cl).

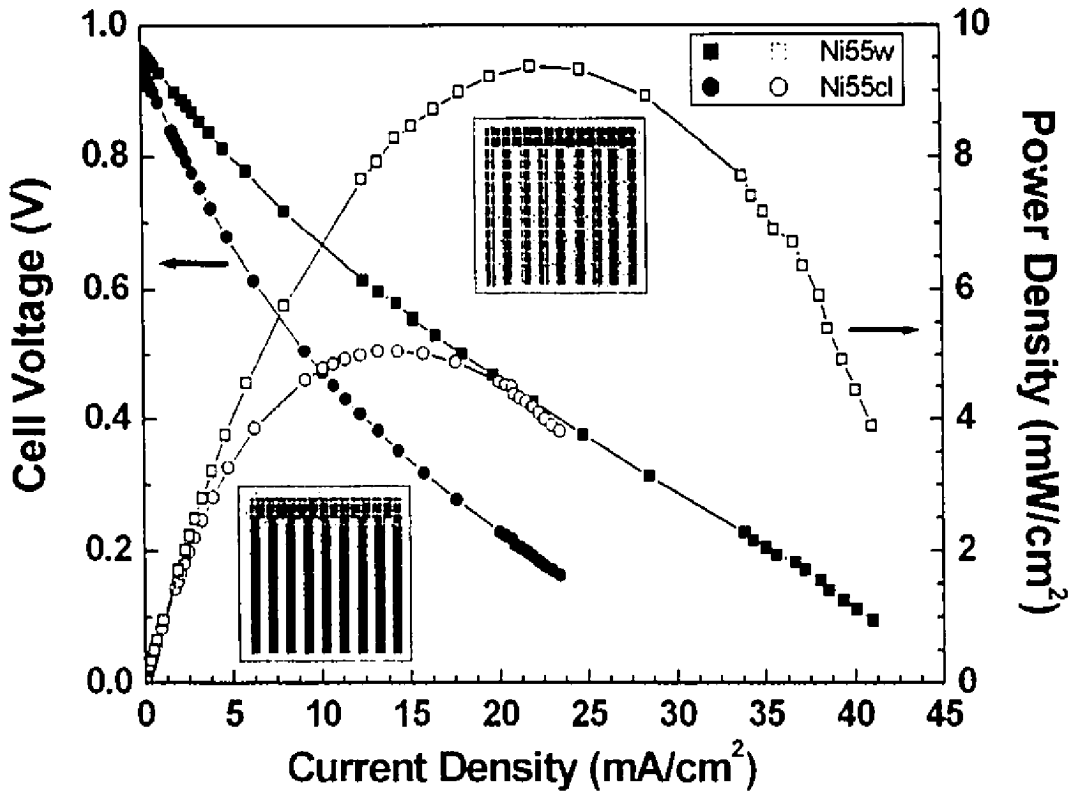

Figure 6.3: Cell voltage (closed symbols) and power density (open symbols) as a function of current density for current collection on the whole anode surface and on the connecting line at 700°C and R_{mix} = 2 (cell Ni55).

The measured open circuit voltage (OCV) exceeded 0.9 V for both current collection configurations. In contrast, the discharge properties were significantly degraded by collecting current only on the connecting line. The cell Ni55cl exhibited a decrease of 57 and 54% in the maximum current and peak power density, respectively, in comparison with the cell Ni55w. Table 6.3 summarizes measured OCV, peak current and power density.

Performance of nickel-rich anodes.—As an alternative for enhanced current collection, the use of a more conductive, nickel-rich anode was investigated. Higher nickel content in the anode was expected to enhance the conduction of electrons in the anode lines towards the gold grid placed on the connecting line.

Table 6.3: Summary of the OCV, maximum current and peak power density from the electrochemical tests of the different cells.

Cell	OCV (V)	i_{max} (mA/cm^2)	P_{max} (mW/cm^2)
Ni55cl	0.939	23.42	5.06
Ni55w	0.961	41.02	9.37
Ni80cl	0.932	9.56	1.64
Ni80w	0.940	22.19	4.89

Fig. 6.4 shows the polarization curves for two SC-μSOFCs with different nickel content. In both cases, the current collectors were placed on the connecting line, and the tests were performed at R_{mix} = 2. Both cells exhibited identical OCVs of over 0.9 V, but the use of a nickel-rich anode (cell Ni80cl) resulted in a decrease of current density (~40%) and a decrease in peak power density (~32%), in comparison to cell Ni55cl. Fig. 6.5 shows scanning electron micrographs of these anodes after testing. Both anodes exhibited an increase in porosity after testing, but compared with cell Ni55cl (Fig. 6.5a), the extent of this increase was significantly greater in the nickel-rich anode (Fig. 6.5b). The difference between current collection on the whole surface and the connecting line was also observed for anodes with 80 wt% of nickel (Table 6.3), confirming the previous result for different anode composition.

Effect of gas composition on OCV.—The effect of the methane-to-oxygen ratio R_{mix} was investigated by exposing the cells to various gas compositions and monitoring the cell performance. Four different cells were studied corresponding to the two different anode compositions and two different current collector configurations: Ni55cl, Ni55w, Ni80cl and Ni80w. Each test was performed by first exposing the cells to R_{mix} = 2, followed by decreasing the methane content ($1 \leq R_{mix} < 2$), and then exposing to fuel-rich mixtures ($2 < R_{mix} \leq 3$). Fig. 6.6 shows the OCV as a function of R_{mix} and indicates that for all cells, independently from anode composition and current collection, the highest OCVs were recorded over a range of gas mixtures with $1.6 < R_{mix} < 2.2$. The OCV dropped for lean mixtures with low methane-to-oxygen ratios.

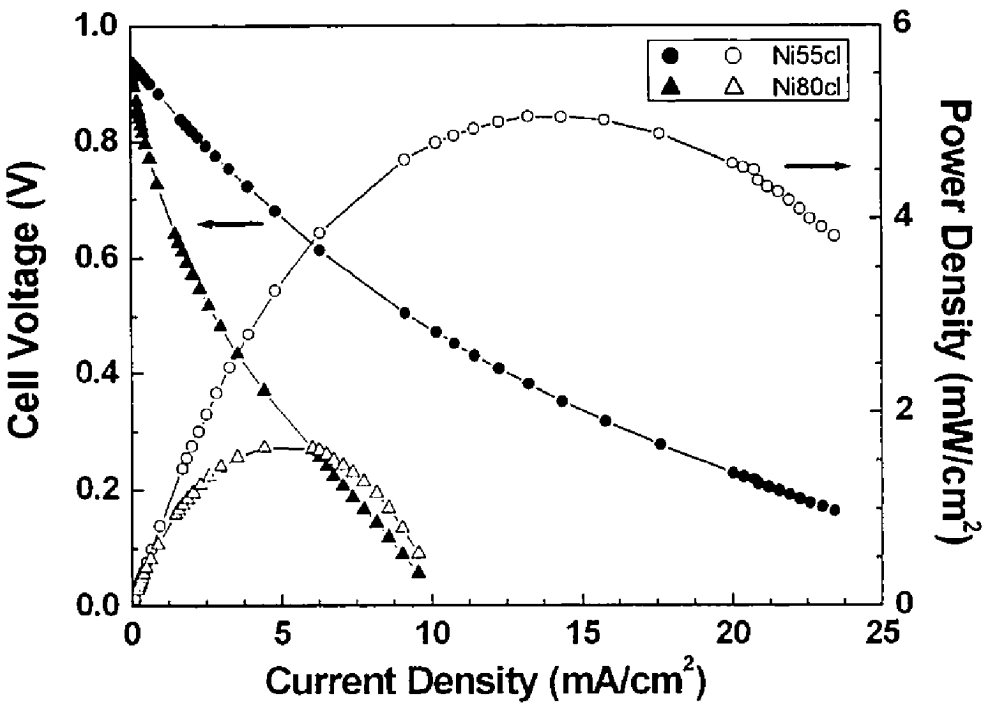

Figure 6.4: Cell voltage (closed symbols) and power density (open symbols) as a function of current density for cells Ni55cl and Ni80cl at 700°C and R_{mix} = 2.

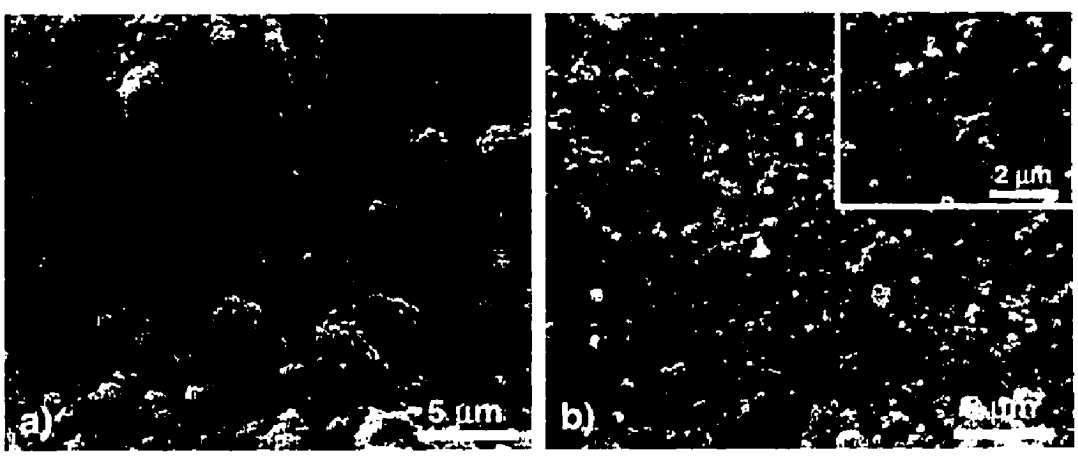

Figure 6.5: Anode microstructure of a) Ni55 cell and b) Ni80 cell after electrochemical testing under same conditions.

Effect of gas composition on current and power.—Fig. 6.7 shows the effect of R_{mix} on the current density and power density for the cells with the two different nickel concentrations in the anodes. In both cases, the current collectors were placed on the connecting lines. Each test was performed by first exposing the cells to R_{mix} = 2, followed by decreasing the methane content ($1 < R_{mix} < 2$), and then exposing to fuel-rich mixtures ($2 < R_{mix} < 3$). After changing R_{mix}, the OCV was allowed to stabilize for a few minutes (2 to 5 min) before discharge. Both cells Ni55cl and Ni80cl exhibited a decrease in performance when R_{mix} was changed from 2.0 to 1.2. However, the behavior of the two cells was different for subsequent increases of the methane-to-oxygen ratio. Specifically, fuel-rich mixtures with $R_{mix} > 2$ led to a continued loss of performance for Ni55cl, but resulted in a considerable recovery and enhancement of performance in the cell with higher nickel content (Ni80cl).

Effect of aging.—The effects of aging on cell performance were studied for three different aging operations: after discharges at different R_{mix} (aging I) (after about 2 h of operation), after aging for 18 h at open circuit (aging II), and after aging for 2 h at 50% of I_{max} (aging III). Fig. 6.8 shows the results for tests performed at 700°C for cell Ni55cl, and indicates that discharges performed after each aging step led to a decrease in cell performance. Thus, the maximum current and peak power decreased continuously with operating and aging time. These observations were consistent for all tested cells and were also reported for SC-μSOFCs in the single-face configuration [24].

The long-term stability of the cells Ni55cl and Ni80cl is shown as evolution of cell voltage with time (Fig. 6.9) for aging II and III. During aging at open circuit, the average voltage of cell Ni55cl remained constant at ~0.95 V over the entire 18 h testing time, and the OCV exhibited small oscillations of 1-2 mV in magnitude. Similar oscillations were observed during aging at 50% of I_{max}, but the mean value of the cell voltage monotonically changed with time such that the cell voltage had decreased by 20 mV at the end of the 2.5 h test. In the case of the nickel-rich anodes (cell Ni80cl), the mean value of the cell voltage was lower compared to the Ni55cl cell, and the magnitude of the oscillations was significantly larger (0.1 to 0.25 V) during both aging tests.

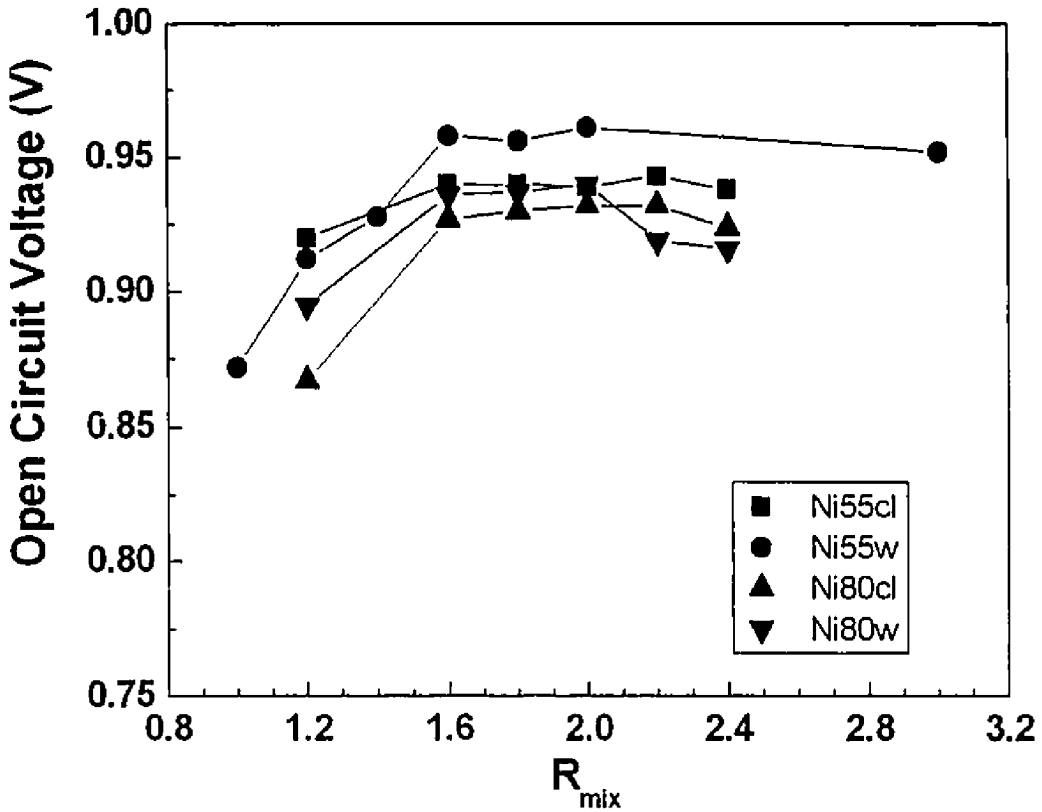

Figure 6.6: OCV as a function of R_{mix} for the four tested cells at 700°C.

6.5 Discussion

The results presented in the previous section provide insight on the effects of two primary factors associated with current collection in SC-μSOFCs in the single-face configuration. The first factor is the current collection configuration and the second is the use of nickel-rich anodes to promote electronic conduction. The effects of the current collectors can be interpreted in a straightforward manner, but enriching the nickel content in the anodes can lead to more subtle effects governed by reaction kinetics. These effects are considered sequentially for the OCV and discharge properties in the discussion that follows. Finally, suitable alternatives for improved current collection are discussed.

Magnitude and stability of the OCV.—The results shown in Fig. 6.3, 6.4, and 6.6-6.9 highlight that the OCV attained a consistently high value exceeding 0.9 V regardless of the details of current collection configuration and anode composition. The value of

the OCV was not sensitive to the fuel-to-oxygen ratio in the gas mixture for values in the vicinity of the stoichiometric composition for the partial oxidation of methane (R_{mix} = 2), but decreased for lean mixtures with R_{mix} = 1.2 or fuel-rich mixtures.

These results can be interpreted using the well-known Nernst equation, which relates the OCV to the partial pressure of oxygen at the electrodes such that

$$OCV = \frac{RT}{nF} \ln \frac{p_{O2,cathode}}{p_{O2,anode}} \quad (6.1)$$

Here, R is the gas constant, T is the temperature, F is the Faraday constant, n is the number of electrons and p_{O2} denotes the partial pressure of oxygen at the electrodes. According to this equation, the establishment of the OCV depends on the difference in partial pressure of O_2 between anode and cathode. The experimental results suggest that even small microfabricated electrodes can establish sufficient gradients in oxygen partial pressure to establish large OCVs.

Our observations of peak OCV values at R_{mix} ~ 2 are consistent with previous studies of small-scale SC-SOFCs with thin-film electrodes including Ni-YSZ//YSZ//LSM cells [12], Pt//YSZ//Au cells [140] and Pd-$Ce_{0.8}Sm_{0.2}O_{1.9}$-Ni//$Ce_{0.8}Sm_{0.2}O_{1.9}$//$Sm_{0.5}Sr_{0.5}CoO_3$ cells [143] in the dual-face configuration, as well as Pd//$BaCe_{0.8}Gd_{0.2}O_{3-\alpha}$//Au cells [157], NiO-$Ce_{0.9}Gd_{0.1}O_{1.95}$//$Ce_{0.9}Gd_{0.1}O_{1.95}$// $Sm_{0.5}Sr_{0.5}CoO_{3-\delta}$ cells [13] and Ni-YSZ//YSZ//LSM cells [6] in the single-face configuration. This ratio corresponds to the stoichiometric composition of the gas mixture for the partial oxidation of methane according to the following reaction:

$$CH_4 + \tfrac{1}{2}\, O_2 \rightarrow 2\, H_2 + CO \quad (6.2)$$

This reaction is expected to occur on the anode catalyst followed by the complete electro-oxidation of the syngas (H_2 + CO). However, for low values of R_{mix}, the oxygen-rich mixture can enhance the nonelectrochemical combustion of methane [12], thereby reducing the oxygen partial pressure differential between the electrodes and hence reducing the OCV. Similarly, fuel-rich mixtures will decrease the oxygen partial pressure at the cathode and therefore the cell voltage.

In contrast to the uniformly high value of the OCV for different current collection schemes and anode composition, the stability of the OCV during aging tests showed considerable differences for the two different anode compositions tested in this study.

The nickel-rich anodes were susceptible to voltage fluctuations of 0.1 to 0.25 V, which was an order of magnitude larger than the fluctuations observed in the NiO:YSZ = 55:45 composition. Ni-anodes are known to undergo oxidation-reduction cycles, which are accompanied by temperature, voltage, reactant and product concentration fluctuations [190]. These oxidation-reduction cycles, combined with the loss of nickel in the form of volatile $Ni(OH)_2$, led to the degradation of the nickel cermet anodes during electrochemical testing [6, 12, 24]. The nickel-rich anodes were more sensitive to the microstructural changes and less stable, leading to important voltage fluctuations and higher porosity after testing. Moreover, nickel-rich anodes are more affected by carbon deposition because pure Ni materials are not selective towards the oxidation of methane. The instability of Ni anodes is additionally problematic for microscale SOFCs because the small surface and thin microelectrodes are more affected by nickel volatilization and loss compared to larger electrodes. Despite its high catalytic activity, nickel therefore might not be the anode material of choice to guarantee long-term stability in single-chamber operation, especially for cells at the microscale.

Current and power.—The current density and power density were significantly affected by current collection configuration, anode composition, gas mixture ratio and aging properties of the fuel cells. Placing the current collectors only on the connecting lines (Ni55cl) yielded a considerably smaller current and power output in comparison with the cell in which the entire anode area was covered with the metallic mesh (Ni55w). Collecting the current over only 23% of the anode area resulted in a decrease of ~50% in the maximum current density and peak power density. Indeed, cell Ni55w exhibited a smaller slope in the linear region of the voltage-current characteristics, indicating a lower ohmic resistance (~46 Ω) than cell Ni55cl (~63 Ω). This difference can only be due to the differences in current collection geometries because all other factors (including material composition, gas mixture ratio and testing configuration) were identical for both cells. The increased ohmic resistance is attributed to the migration of electrons along the nickel-based anodes to the gold current collectors placed on the connecting lines. Current collection on the whole surface enables the direct flow of electrons into the external electrical circuit with shorter current pathways and leads to higher performance.

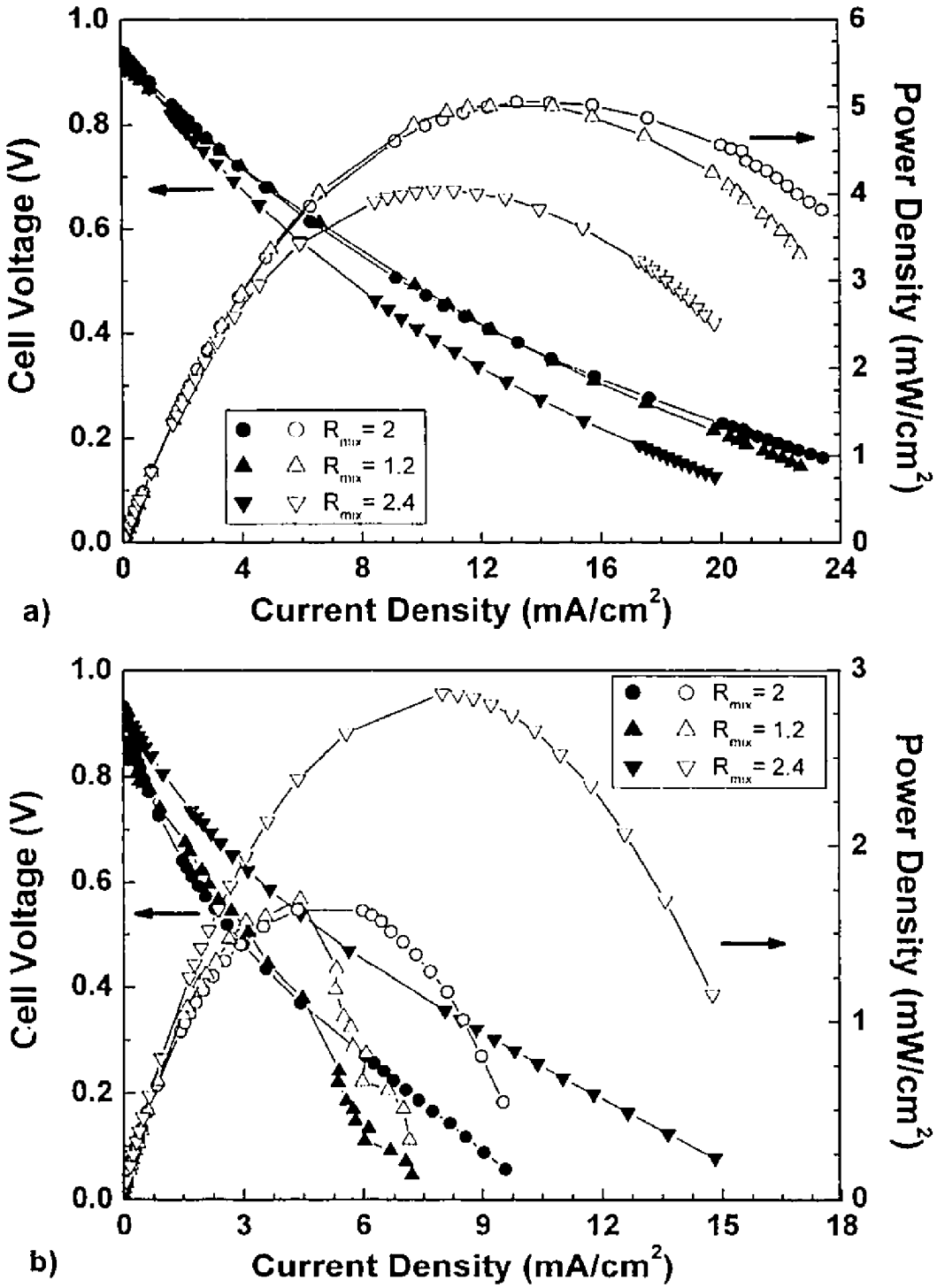

Figure 6.7: Cell voltage (closed symbols) and power density (open symbols) as a function of current density for different R_{mix} at 700°C. The cells, a) cell Ni55cl and b) Ni80cl, were first exposed to R_{mix} = 2, followed by R_{mix} = 1.2 and then R_{mix} = 2.4.

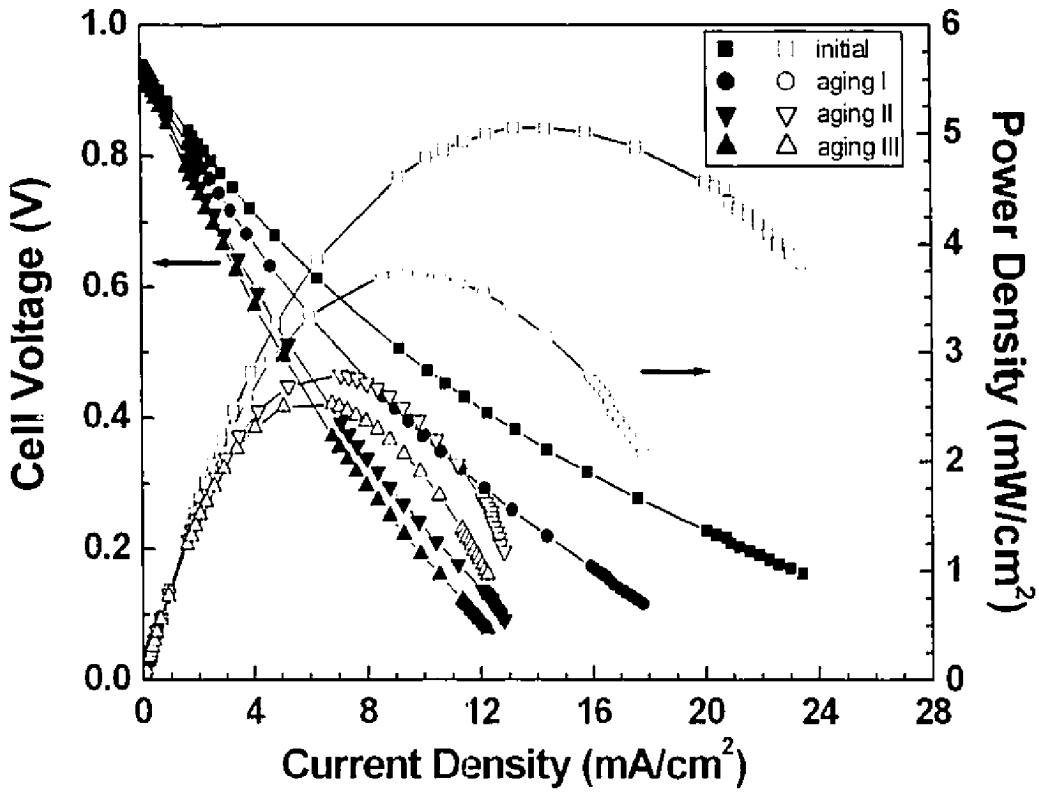

Figure 6.8: Voltage-current characteristics with performance decrease after aging I, II, and III, compared to initial performance, at 700°C and $R_{mix} = 2$ (cell Ni55cl).

Additionally, the current collection method seems to affect the electrode polarization resistance. The electrode polarization was smaller for the cells tested using current collection on the whole electrode surface compared to the current collection configuration on the connecting line only. Effective current collection might improve the electrode reaction itself and lead to a reduction in electrode overpotentials in addition to the ohmic resistance. Impedance analysis could clarify these observations in future work. These results quantify the critical importance of current collection methods in SC-μSOFCs operated in the single-face configuration.

The electrochemical tests performed at different methane-to-oxygen ratios and after aging illustrate the sensitivity of SC-μSOFCs to operating conditions and time. Tests at $R_{mix} = 2$ showed that the performance significantly degraded due to aging (Fig. 6.8). In addition, the use of lean gas mixtures ($R_{mix} < 2$) led to a degradation of performance in comparison to tests at the stoichiometric ratio (Fig. 6.7).

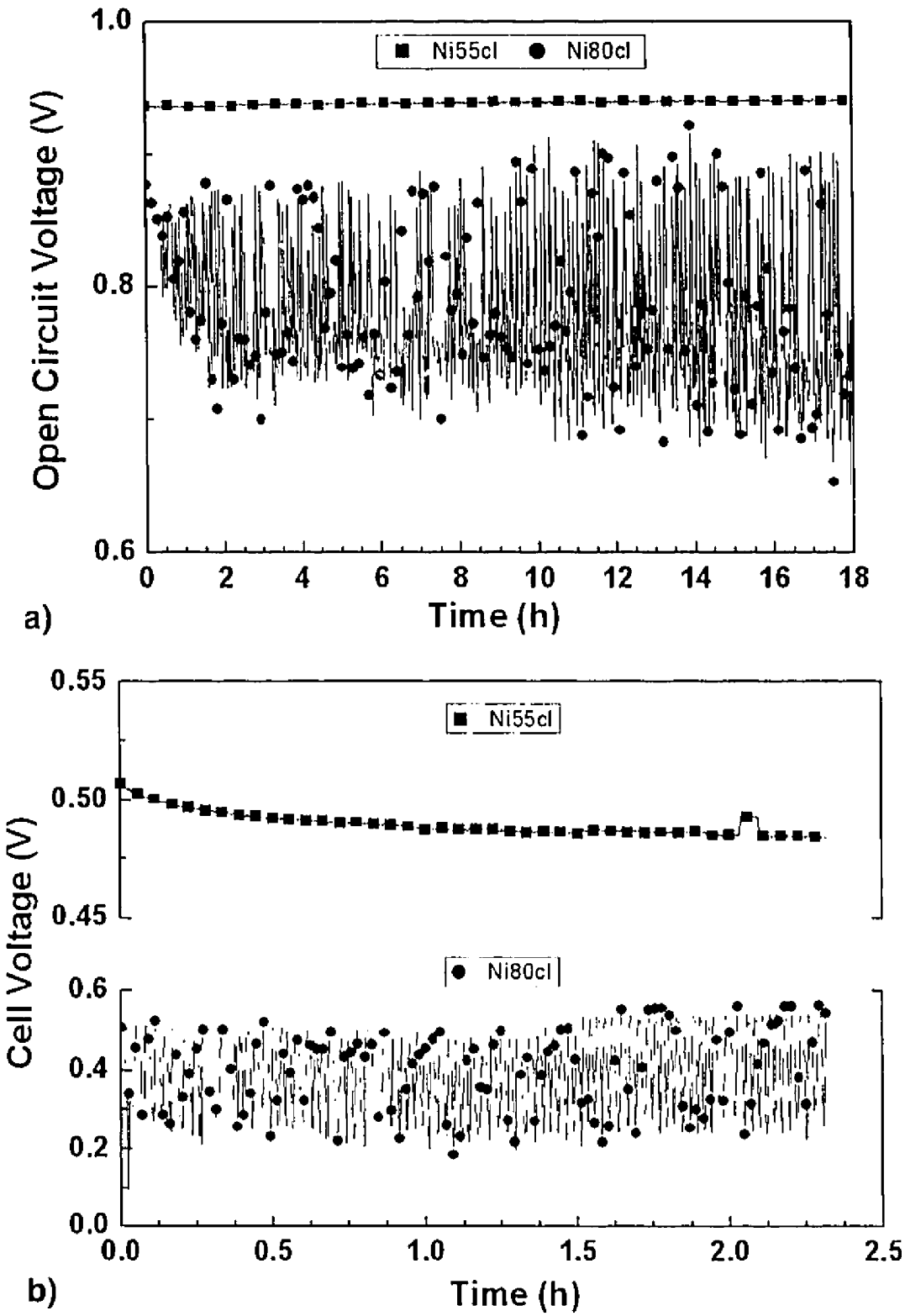

Figure 6.9: Voltage as a function of time for cells Ni55cl and Ni80cl during a) aging at $I = 0$ mA and b) at $I = 50\%$ of I_{max} (700°C, $R_{mix} = 2$).

This loss of performance was not recovered for cell Ni55cl even after R_{mix} was increased to higher values. In contrast, the performance recovered and increased beyond the value at R_{mix} = 2 for the cell with the nickel-rich anode. These results highlight the impact of reaction kinetics in dictating the response of the fuel cell to changes in the gas ratio during operation. When the cell is introduced in the furnace, the NiO is first reduced to nickel in a methane/nitrogen atmosphere before any oxygen is introduced into the test chamber. Any subsequent changes in the gas ratio can influence the details of the oxidation-reduction cycles of the anode during operation. Specifically, the anode can be expected to experience enhanced oxidation and reduction for oxygen-rich (R_{mix} < 2) and methane-rich (R_{mix} > 2) mixtures, respectively. After the electrochemical testing, the nickel-rich anode exhibited a significant increase in porosity due to the enhanced loss of nickel, as observed in Fig. 6.5b. This increased sensitivity to oxidation-reduction cycles and nickel volatilization suggests that the nickel-rich cell responded faster to changes in gas composition during testing than the Ni55 cell. The performance increase of cell Ni80cl after increasing R_{mix} might be attributed to a fast reduction of the NiO which was previously formed in the oxygen-rich atmosphere. Thus, nickel catalyst sites were rapidly available again under fuel-rich operating conditions. Additionally, from a catalysis point of view, the increasing porosity in the nickel-rich anode might lead to more dispersed nickel catalyst sites, facilitating gas transport and access to the reaction sites. In-situ microstructural investigations might be helpful to further elucidate the observed phenomena.

At R_{mix} = 2, the superior performance of Ni55 over the nickel-rich cell Ni80 points out the insufficient selectivity of nickel for partial oxidation of methane [89]. An increased nickel content enhances complete methane oxidation and other undesired reactions (such as methane cracking), leading to lower amounts of hydrogen and carbon monoxide available for the electricity generating electrochemical reactions, and therefore a lower power output.

Current collection.—The results presented show that the current collection configuration is critical for the power output of SC-μSOFCs with comblike electrodes. Using a more conductive nickel-rich anode as a simple alternative to complex gold meshes did not overcome the performance loss associated with the current collection

configuration, but led to a further decrease in power output. Therefore, different methods must be developed to enhance current collection and improve performance output of SC-μSOFCs with interdigitated electrodes.

Possible strategies to enable current collection on the whole anode and cathode surface without short-circuiting the system could include painting gold paste over the single lines towards a gold mesh placed over the connecting line. For small electrodes a gold pattern could be sputtered onto the lines using a suitable mask, or direct-write deposition techniques could be used. But, the current collector layer should not clog the electrode pores for gas diffusion. Or, based on Ref. [141], integrated or embedded current collectors could be used with the appropriate choice of the wire material. Platinum and gold should be avoided because of its catalytic activity and because of the elevated sintering temperatures, respectively. Nickel could be a suitable solution; however, it is easily oxidized during sintering.

Due to low fuel utilization, SC-μSOFCs are primarily considered for energy generation at low efficiency (20-30%) and energy harvesting applications [16, 131]. Hence, because of the difficulty of collecting current on the whole electrode surface of interdigitated electrodes, the performance loss due to current collection should be considered during system design. Proper material choice and optimization of electrode geometries and sizes (especially interelectrode spacing) should compensate for the increased ohmic resistance and enable sufficient energy generation for the selected application.

6.6 Conclusions

Single-chamber micro solid oxide fuel cells in the single-face configuration with coplanar, interdigitated electrodes are being developed for small-scale power generating applications and integration with microelectromechanical systems technology. This paper studied two different approaches to current collection during the operation of such fuel cells. A dual-face configuration with a planar square cathode (LSM-YSZ and LSM) on one side and a comblike anode (Ni-YSZ) on the opposite side of the YSZ electrolyte was chosen. This design enabled a simple approach to characterize the influence of the area of the comblike electrode used for current collection without applying complicated gold grid structures and risking system short

circuits. The method commonly used in the interdigitated electrode design consists of applying metallic meshes only on the connecting line to collect the current. This current collection configuration has no deleterious effect on the OCV, but leads to a considerable reduction in current and power (~50% drop) as compared to the performance obtained when the current was collected on the whole anode surface.

The second current collection approach investigated in this study was to enrich the metal content in the anode. The nickel-rich anodes exhibited large oscillations (~0.1 to 0.25 V) in the OCV due to enhanced oxidation-reduction cycles of Ni-NiO during operation in the fuel-oxygen mixtures. The same reaction is also responsible for the sensitivity of SC-μSOFCs with nickel-based anodes to changes in the methane-oxygen ratio during operation, and also to the duration of fuel cell use. Thus, such electrodes are not optimal for applications, for example in energy recovery from exhaust streams [16], in which the gaseous atmosphere is expected to change during operation. These results highlight the critical importance of developing efficient and stable methods for current collection and stable electrode materials.

Chapter 7 Single-chamber micro solid oxide fuel cells: Study of anode and cathode materials in coplanar electrode design

M. Kuhn, T. W. Napporn, M. Meunier, D. Therriault, *Solid State Ionics*, submitted March 12, 2009.

7.1 Abstract

The effects of electrode and electrolyte materials used in single-chamber micro solid oxide fuel cells (SC-μSOFCs) with coplanar electrodes on the cell performance have been little investigated so far. In this study, different combinations of conventional SOFC materials such as NiO-YSZ (ZrO_2 doped with 8 mol% Y_2O_3) and NiO-GDC ($Ce_{0.9}Gd_{0.1}O_{1.95}$) anodes as well as $(La_{0.8}Sr_{0.2})_{0.98}MnO_3$ (LSM) -YSZ and $(La_{0.6}Sr_{0.4})_{0.995}(Fe_{0.8}Co_{0.2})O_3$ (LSCF) cathodes in the form of coplanar interdigitated electrode patterns on YSZ electrolytes were compared at 700°C in methane-air mixtures with a methane-to-oxygen ratio R_{mix} = 2. The best cell performance was obtained for coplanar NiO-YSZ anodes combined with LSM-YSZ cathodes, whereas the NiO-GDC//YSZ//LSCF cell delivered the lowest power output. Chemical interaction between LSM-YSZ cathodes and adjacent anodes during sintering was identified to cause blackening of the anode parts in close vicinity to the cathode, and manganese was detected in the anode, probably through diffusion from the LSM cathode into the anode. In addition to cell performance, the proper choice of electrode materials for coplanar electrodes appears to be important because of the possible chemical interactions between the closely-spaced electrodes.

7.2 Introduction

Single-chamber solid oxide fuel cells (SC-SOFCs) are operated using mixtures of fuel and air, which eliminates the necessity for gas sealing and complex gas manifolding required for the conventional dual-chamber operation [4, 108]. The

difference in catalytic activity and the selectivity of anode and cathode materials for the specific electrode reactions generate a gradient of oxygen partial pressure between the electrodes and permit the establishment of an open circuit voltage (OCV). Because the separation between fuel and oxidant is no longer required, single-chamber operating conditions offer the possibility of fabricating cell designs with coplanar anodes and cathodes situated on the same side of the electrolyte [5]. The working principle of these cells underlies the surface ionic migration of oxygen ions between adjacent electrodes through the electrolyte, as identified by van Gool [120]. The ohmic cell resistance is determined by the interelectrode distance and the electrode width, both accounting for the oxygen ion conduction path [5, 6]. The simplest design of SC-SOFCs with coplanar electrodes consists of one set of closely-spaced anode and cathode lines arranged parallel to each other on the electrolyte. This electrode configuration is generally used for investigations on the effect of testing parameters such as gas mixing ratio [6, 13, 21], gas flow rate [21], orientation of the electrodes with respect to the gas flow direction [6, 21], as well as the effect of interelectrode distance and electrode width [5, 6, 17, 21] on cell performance. Cells can also be constructed with interdigitated or comblike patterns of several coplanar anode and cathode lines in order to maximize the available active electrode area and increase the cell power output [5, 13]. In addition, interdigitated closely-spaced microscale electrodes permit the reduction of the ohmic cell resistance [7]. Many studies on SC-microSOFCs (SC-μSOFCs) with coplanar interdigitated electrodes focused on finding suitable microfabrication techniques [13, 20, 21, 24, 25].

Table 7.1 shows an overview of the electrode and electrolyte materials used in studies on SC-SOFCs with coplanar electrodes found in the literature. Cells were primarily constructed from the most conventional SOFC materials, that is, Ni-YSZ (ZrO_2 doped with 8 mol% Y_2O_3) anodes and $(La_{0.8}Sr_{0.2})_{0.98}MnO_3$ (LSM) based cathodes on YSZ electrolytes [6, 24, 25, 169]. Ni-GDC ($Ce_{0.9}Gd_{0.1}O_{1.95}$) anodes have also been employed in combination with YSZ electrolytes and LSM cathodes in several studies [8, 21, 121, 159]. Additionally, anodes composed of nickel catalyst mixed with samarium doped ceria, samarium strontium cobalt oxide based cathodes and samarium doped ceria electrolytes for low-temperature operation are gaining increasing interest [17, 162]. However, the effect of the materials used for the different cell components on the

performance of SC-SOFCs with coplanar electrodes has only been addressed in Ref. [17, 98], where different electrolyte materials were compared with regard to the influence of ionic conductivity on cell resistance and performance. Hibino et al. also discussed the addition of different metal oxides to the anode in order to increase its catalytic activity for the fuel reactions and increase the peak power density [17]. But there are no comparative studies on the choice of anode, cathode and electrolyte material combinations in regard of the cell performance. Moreover, direct comparison between the references in the literature is difficult due to the use of different materials in addition to the different testing conditions and cell dimensions (e.g. number of electrode lines and electrode size). The possibility of chemical interactions between closely-spaced coplanar anodes and cathodes has also not been investigated yet.

The goal of this study is to create a basis for cataloguing the effects of electrode and electrolyte materials used in SC-SOFCs with coplanar electrodes on cell performance. For the direct comparison between cells of different composition, the electrolyte material was fixed and different anode and cathode material combinations were characterized, where only one electrode material was different between each cell. The interdigitated electrode design was chosen for this study because of its advantages over using single electrode pairs [5, 13, 193]. Additionally, the electrochemical performance of the cells was investigated under identical testing conditions.

7.3 Experimental

The electrode powders (NexTech Materials Ltd., Lewis Center, OH) used for the fabrication of SC-μSOFCs with coplanar interdigitated electrodes of different composition are listed in Table 7.2. For the anode, NiO and YSZ as well as NiO and GDC powder were mixed in a weight ratio of 55 to 45 and 60 to 40, respectively. The powder mixtures were ball milled in a Spex CertiPrep 8000M Mixer/Mill (Spex CertiPrep, Metuchen, NJ) with YSZ balls (0.5 and 1.0 mm in diameter) for 8 h. Electrode suspensions were fabricated by adding Triton (Alfa Aesar, Ward Hill, MA) as a dispersant, Poly(vinyl butyral-co-vinyl alcohol-co-vinyl acetate) (Sigma-Aldrich, St. Louis, MO) as a binder and Terpineol (Mallinckrodt Baker Inc., Phillipsburg, NJ) as a solvent to the electrode powders. The mixtures were ball milled for 1 h in the Spex

Mixer/Mill to obtain homogeneous electrode suspensions with a solid loading of ~58 wt%.

The detailed procedure for direct-write microfabrication of SC-μSOFCs with coplanar electrodes was described in our previous work [24]. The electrode suspensions were extruded through stainless steel micronozzles (EFD Inc., East Providence, RI) with an inner nozzle diameter of 0.2 mm using an air-powered fluid dispenser (Ultra™ 2400 Series, EFD Inc., East Providence, RI). Cells composed of coplanar interdigitated electrodes with five lines per anode and cathode were fabricated for each anode-cathode material combination by robot controlled deposition (I&J 2200-4, I&J Fisnar Inc., Fair Lawn, NJ) of the extruded suspensions on 0.2 mm thick YSZ electrolyte substrates (Marketech International Inc., Port Townsend, WA). The electrodes were cosintered at 1200°C for 3 h under ambient atmosphere.

Table 7.1: Summary of anode, cathode and electrolyte material combinations used for SC-SOFCs with coplanar electrodes reported in the literature.

Anode	Electrolyte	Cathode	Reference
Pd	$BaCe_{0.8}Gd_{0.2}O_{3-\delta}$	Au	[5]
Pt	YSZ	Au	[160]
Ni-YSZ	YSZ	LSM	[6, 24, 25, 169]
Ni-$Ce_{0.8}Gd_{0.2}O_{1.9}$	YSZ(-MnO_2)	LSM-MnO_2	[121, 159]
Ni-$Ce_{0.8}Gd_{0.2}O_{1.9}$-Pd	YSZ	LSM(-$Ce_{0.8}Gd_{0.2}O_{1.9}$)	[8, 21]
Ni-$Ce_{0.8}Sm_{0.2}O_2$	YSZ $Ce_{0.8}Sm_{0.2}O_2$	LSM	[20, 98]
Ni-$Ce_{0.8}Sm_{0.2}O_2$	$Ce_{0.8}Sm_{0.2}O_2$	$Sm_{0.5}Sr_{0.5}CoO_3$- $Ce_{0.8}Sm_{0.2}O_2$	[162]
Ni-$Ce_{0.8}Sm_{0.2}O_{1.9}$	YSZ $Ce_{0.8}Sm_{0.2}O_{1.9}$ $La_{0.9}Sr_{0.1}Ga_{0.8}Mg_{0.2}O_3$	$Sm_{0.5}Sr_{0.5}CoO_3$	[17]
Ni-$Ce_{0.9}Gd_{0.1}O_{1.95}$	$Ce_{0.9}Gd_{0.1}O_{1.95}$	$Sm_{0.5}Sr_{0.5}CoO_{3-\delta}$	[13]

Table 7.2: Characteristics of the powders used for the direct-write microfabrication of SC-μSOFCs with coplanar electrodes.

Material	Electrode	Nominal composition	Median particle size (μm)	Specific surface area (Brunauer, Emmett, Teller) (m^2/g)
NiO	Anode	High purity green NiO	0.56	6.3
YSZ	Anode	92 mol% ZrO_2, 8 mol% Y_2O_3	0.25	6.1
GDC	Anode	$Ce_{0.9}Gd_{0.1}O_{1.95}$	0.41	6.8
LSCF	Cathode	$(La_{0.6}Sr_{0.4})_{0.995}(Fe_{0.8}Co_{0.2})O_3$	0.49	7.6
LSM-YSZ	Cathode	70 vol% $(La_{0.8}Sr_{0.2})_{0.98}MnO_3$, 30 vol% $(ZrO_2)_{0.92}$ $(Y_2O_3)_{0.08}$	0.56	9.7

A SZX12 Olympus stereomicroscope (Olympus Cooperation, Tokyo, Japan) was used to take optical micrographs of the sintered cells, from which the electrode dimensions such as interelectrode distance, electrode width and (projected) electrode surface area were determined employing digital image software (Image-Pro Plus 6.2, Media Cybernetics Inc., Bethesda, MD). Interelectrode distance and electrode width were obtained as average values from equidistant measurements over the entire gap and electrode length, respectively. The electrode microstructures were investigated by scanning electron microscopy (ESEM, Quanta FEG 200, FEI Company, Hillsboro, OR). The thickness of the sintered electrode lines was determined from cross-sectional SEM images. Energy-dispersive X-ray (EDX) measurements were carried out on the sintered electrodes using a SEM (JSM-840A, JEOL-USA Inc., Peabody, MA) equipped with an EDX detector (INCAx-sight, Oxford Instruments, Oxfordshire, UK). Local EDX spectra, line scans and chemical map analyses over cathode, electrolyte and anode were performed.

The cells were electrochemically tested in a methane-air gas mixture using the high-temperature testing setup as described in Ref. [10, 24] with a slightly modified

sample holder [107]. The flow plate with open design [107] was placed over the cell and current collector meshes to firmly hold both in place and facilitate a uniform distribution of the gas mixture over the cell. The gas mixture was supplied with a methane-to-oxygen ratio of R_{mix} = 2 and a total gas flow rate of 150 sccm CH_4 and synthetic air (composed of nitrogen and oxygen in a ratio 80:20). Additional nitrogen gas at a flow rate of about 700 sccm was used as blanket gas [10]. The furnace temperature was set to 700°C. For current collection, gold mesh (82 mesh, woven from 0.06 mm diameter wire, 99.9% (metals basis), Alfa Aesar, Ward Hill, MA) was fixed with gold paste (C5450, Heraeus Holding GmbH, Hanau, Germany) over the electrode segment connecting the single lines of each electrode [26]. The mesh was welded to gold wires (0.25 mm diameter, 99.9% (metals basis), Alfa Aesar, Ward Hill, MA) which exited the testing chamber towards the data acquisition set. The cells were placed in the cell holder such that the electrode lines were orientated perpendicular to the incoming gas mixture flow direction, and such that the cathode was the first electrode to be exposed to the reactant gases [6]. A data acquisition set (Agilent 34970A, Agilent Technologies, Santa Clara CA) in combination with the HP BenchLink Data Logger software (Agilent Technologies, Santa Clara CA) was used to record the cell voltage. The voltage-current characteristics were obtained by varying the resistance on a decade resistor (Type 1432-M, General Radio Company, Cambridge, MA) and using a digital multimeter (197 Autoranging Microvolt DMM, Keithley Instruments Inc., Cleveland, OH).

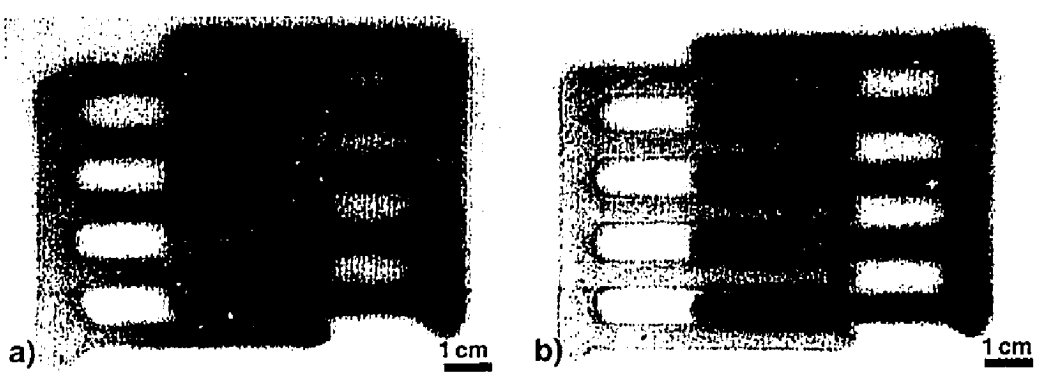

Figure 7.1: Optical micrograph of cell a) NiO-YSZ//YSZ//LSM-YSZ and b) NiO-YSZ//YSZ//LSCF after sintering.

7.4 Results

For the fabrication and comparison of SC-μSOFCs with coplanar interdigitated electrodes of different composition, YSZ as electrolyte, NiO-YSZ and NiO-GDC as anode and LSM-YSZ as cathode material were selected because they are conventionally used (see Table 7.1). The second cathode material was $(La_{0.6}Sr_{0.4})_{0.995}(Fe_{0.8}Co_{0.2})O_3$ (LSCF), which was shown to exhibit high oxide ion conductivity and good activity for the oxygen reduction reaction [144]. Four different combinations of those electrode materials on the YSZ electrolyte were fabricated by the direct-writing technique. Fig. 7.1 shows two representative optical micrographs of the fabricated SC-μSOFCs with coplanar interdigitated electrodes. Each electrode was composed of five lines linked together by a connecting pad over which the current collector mesh was placed. The average interelectrode distance, electrode width and electrode thickness were ~300 μm, ~380 μm and ~14 μm, respectively. From the optical micrograph in Fig. 7.1a, a black coloration of the NiO-YSZ anode can be observed in contrast to the same anode material in Fig. 7.1b, indicating possible chemical interaction between coplanar cathode and anode during sintering. Notably, the YSZ electrolyte around the LSM-YSZ cathode and the NiO-YSZ anode in close vicinity to the cathode appeared blackened after sintering (Fig. 7.1a), whereas the electrolyte and the anode close to the LSCF cathode did not undergo such a color change (Fig. 7.1b). The NiO-YSZ anode next to the LSCF cathode showed the same light green color over its whole surface. The staining of the anode was also observed in the case of the NiO-GDC//YSZ//LSM-YSZ cell.

Fig. 7.2a shows the *E-I* characteristics of the four tested cells. The cell composed of a NiO-YSZ anode and LSM-YSZ cathode gave the highest open circuit voltage (OCV) of 0.727 V, whereas the lowest OCV of 0.64 V was obtained for the NiO-GDC//YSZ//LSM-YSZ cell. Both cells with LSCF cathode delivered an OCV of ~0.68 V regardless of the anode material. All *E-I* curves exhibited a similar slope except for the NiO-GDC//YSZ//LSCF cell, for which a much steeper slope indicated higher cell resistance. Similarly to the highest obtained OCV, the combination of NiO-YSZ anode and LSM-YSZ cathode also enabled the highest power output of 0.7 mW/cm^2, whereas the lowest peak power density of 0.252 mW/cm^2 was measured for the NiO-

GDC//YSZ//LSCF cell (Fig. 7.2b). Fig. 7.2b also shows that the cells composed of NiO-YSZ anodes enabled a higher power output than the cells with anodes composed of NiO-GDC. Similarly, the cells with a LSM-YSZ cathode delivered a higher power density as compared to the cells with a LSCF cathode. Thus, the combination of the NiO-YSZ anode and LSM-YSZ cathode enabled the best cell performance for a SC-μSOFC with coplanar interdigitated electrodes among the tested electrode material combinations.

7.5 Discussion

LSCF has previously been investigated as a cathode material in electrolyte- and anode-supported SC-SOFCs because of its high activity for the oxygen reduction reaction, high oxygen conductivity and low interfacial resistance with the electrolyte [144, 145, 151]. However, one major drawback of LSCF cathodes is their catalytic activity for the oxidation of hydrocarbons such as propane [65, 194] and methane [195-197]. The activity of LSCF for methane oxidation was shown to be close to the activity of Ni-based catalysts at temperatures between 450 and 600°C [195]. Additionally, LSCF was found to become active for this reaction at temperatures above 400°C and to exhibit higher activity than LSM-based cathodes [196]. Adding SDC to a LSCF cathode reduced the catalytic activity of LSCF for propane oxidation [194]. As our tests were performed with pure LSCF cathodes at 700°C, the lower performance of the cells with LSCF cathode might be attributed to the catalytic activity of LSCF for methane conversion at this temperature. LSM-based cathodes are also known to catalyze fuel oxidation reactions when sintered at 1100°C [198]. However, sinter temperatures of 1200°C as used in our study lead to denser microstructures and the catalytic activity exhibited towards the oxidation of methane can be almost neglected [198].

The lower performance of NiO-GDC anodes as compared to NiO-YSZ anodes can be explained by the weak interface between the NiO-GDC anode and the YSZ electrolyte (Fig. 7.3). The NiO-GDC anode partially detached from the YSZ substrate (Fig. 7.3a), whereas the NiO-YSZ anode bonded well to the electrolyte (Fig. 7.3b). The NiO-GDC anode was also found to have detached in places from the YSZ electrolyte after testing in Ref. [121]. The use of NiO-GDC anodes in SC-SOFCs with coplanar electrodes might be more appropriate in combination with GDC electrolytes [13].

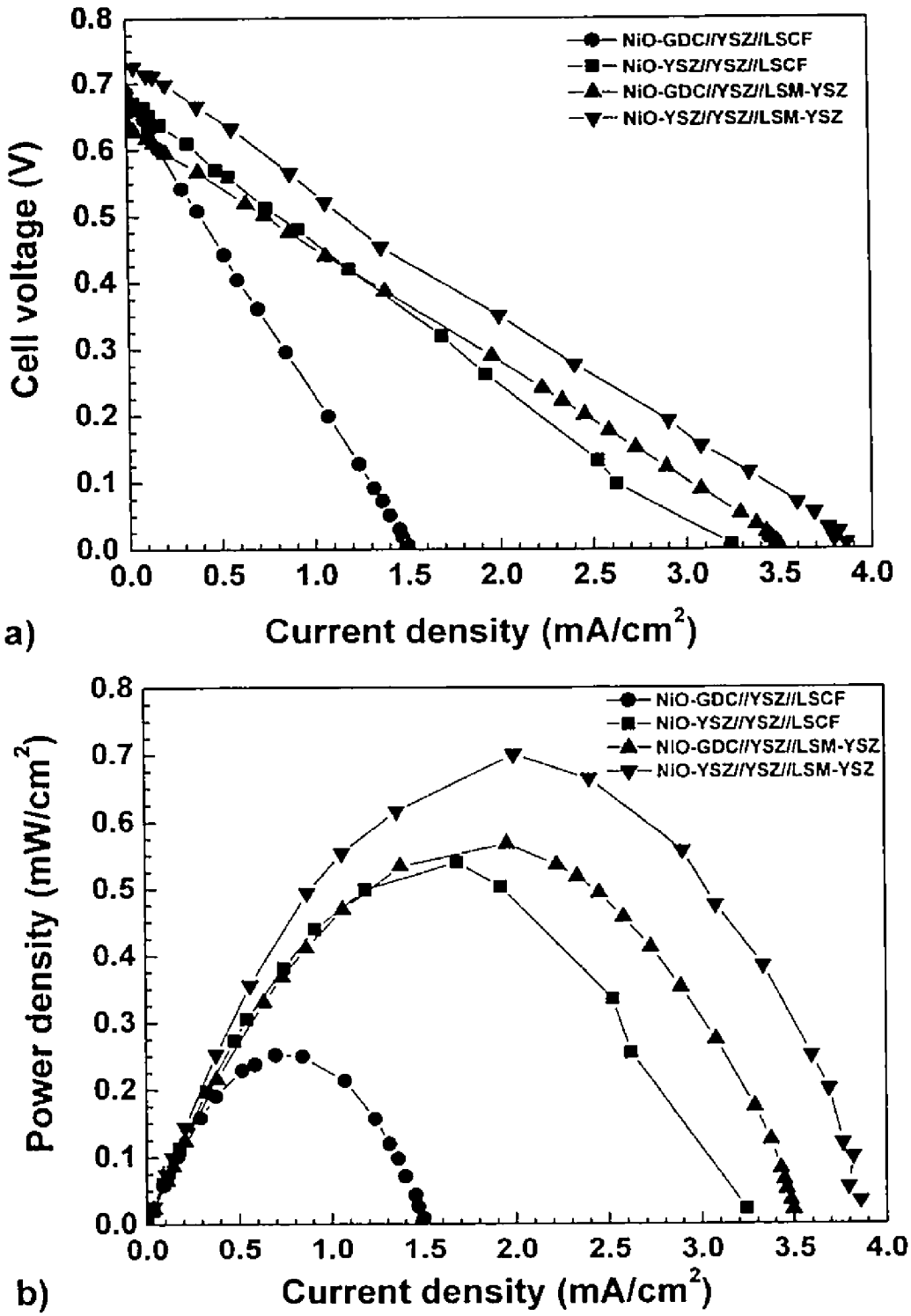

Figure 7.2: a) Voltage and b) power density as a function of current density for the different cells tested at R_{mix} = 2, a total gas flow rate of 150 sccm and at 700°C.

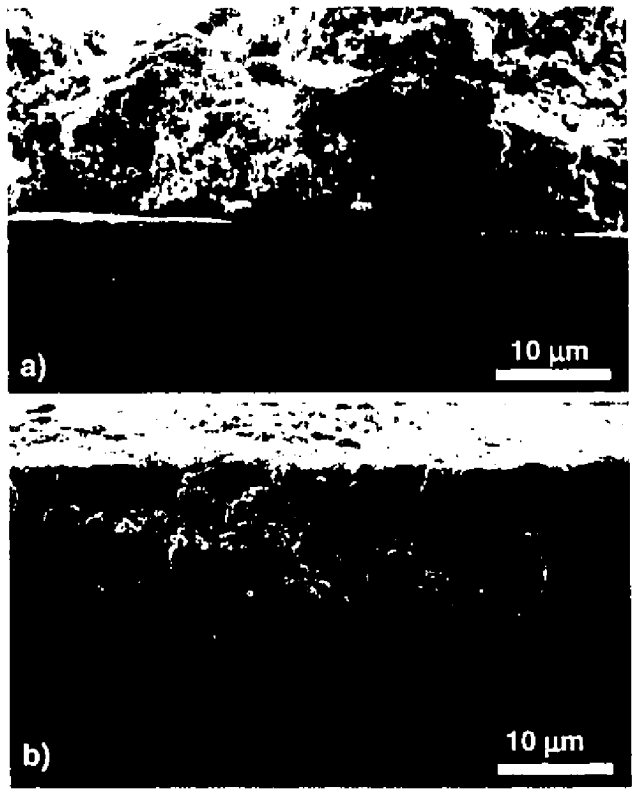

Figure 7.3: SEM micrograph of a) NiO-GDC and b) NiO-YSZ anode cross-section on top of the YSZ electrolyte after sintering.

Interaction of LSM cathodes with YSZ electrolytes is a known problem in the literature. Diffusion of manganese through the migration of oxygen vacancies [199] from the LSM cathode into the YSZ electrolyte occurs during sintering of the two materials [42, 43, 199]. At the cathode-electrolyte interface, secondary phases such as $La_2Zr_2O_7$ or $SrZrO_3$ crystals are formed, leading to destabilization and decomposition of LSM, an increase of the electrode overpotential, structural changes in the YSZ, reduced ionic conductivity and increased electronic conductivity of the electrolyte. In this study the interaction between LSM cathodes and YSZ electrolytes was also observed for SOFCs with coplanar electrodes and seemed to have additionally affected the adjacent anode. EDX analysis was therefore performed on NiO-YSZ anodes in close vicinity to LSCF and LSM-based cathodes, and the respective EDX spectra are shown in Fig. 7.4. In addition to the peaks of Ni, O, Y and Zr present in both NiO-YSZ anodes, a peak for manganese was found in the anode of the NiO-YSZ//YSZ//LSM-YSZ cell (Fig. 7.4a). The peaks for Au are due to gold sputtering of the samples for SEM characterization.

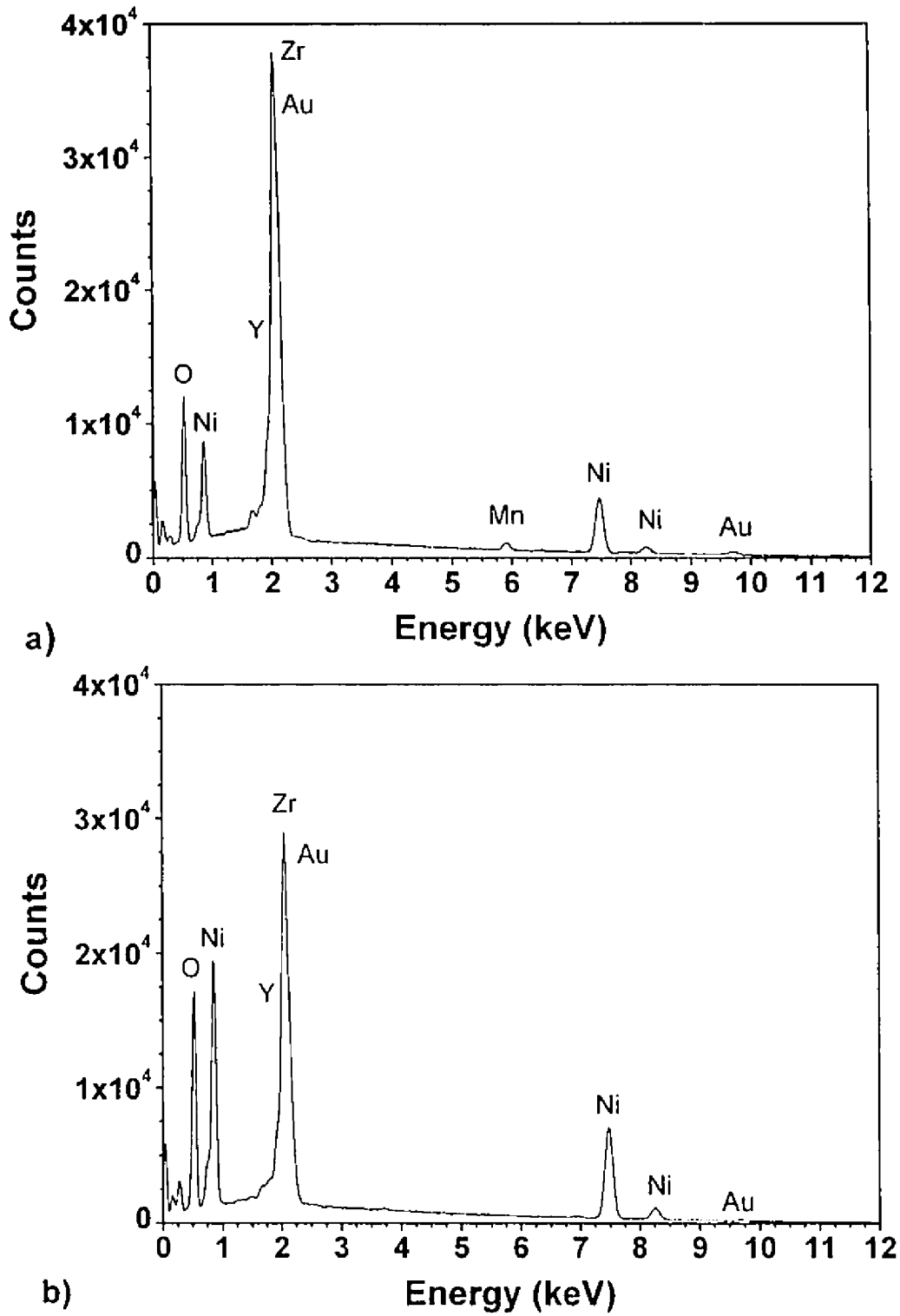

Figure 7.4: EDX spectra of NiO-YSZ anodes in close vicinity of a) LSM-YSZ and b) LSCF cathodes after sintering.

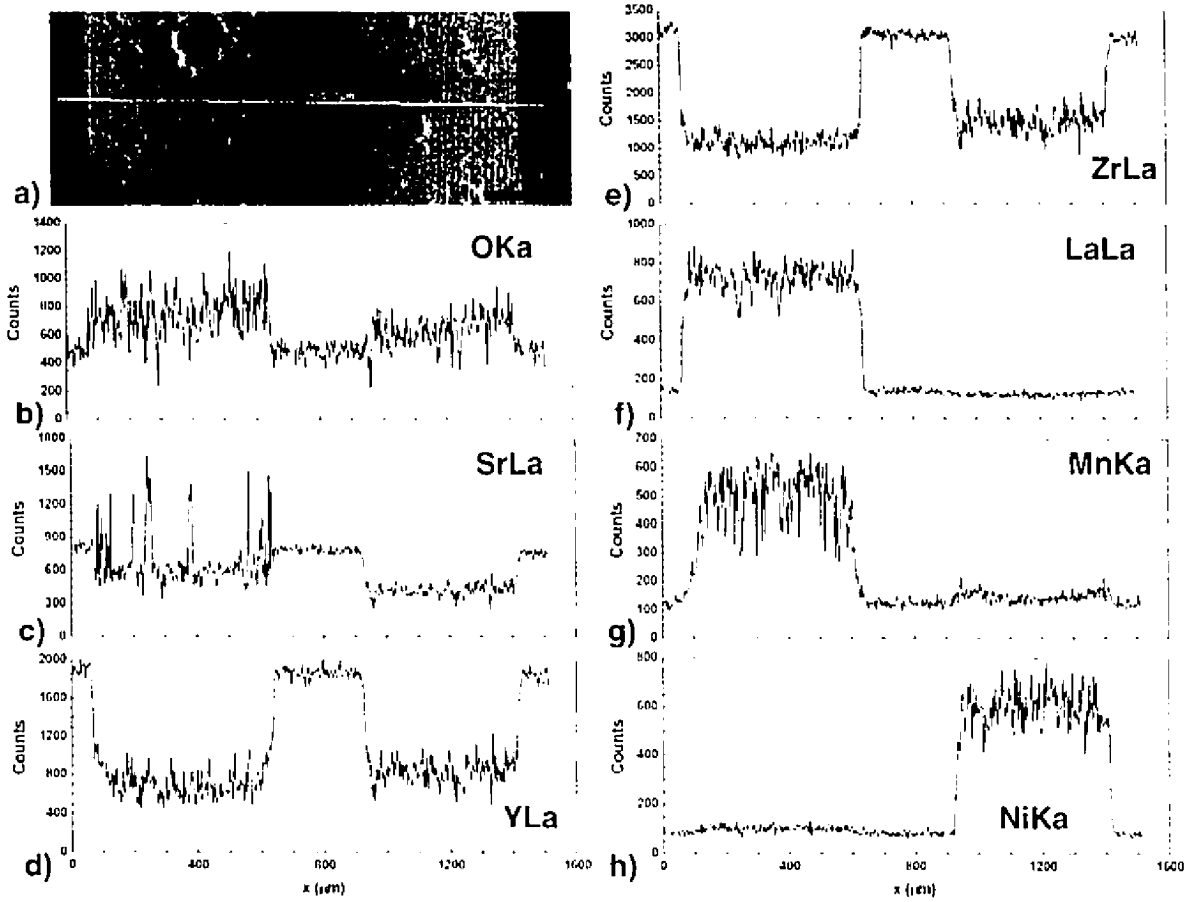

Figure 7.5: a) SEM micrograph of the section analyzed by EDX showing cathode (left electrode line), electrolyte and anode (right electrode line) of the NiO-YSZ//YSZ//LSM-YSZ cell; b)-h) Line scan chemical analysis performed over the three cell components.

In order to further investigate the possible interaction between cathode and anode, chemical analysis was performed along a line scan across LSM-YSZ cathode, YSZ electrolyte and NiO-YSZ anode (Fig. 7.5) as well as on a whole surface section of the three cell components (Fig. 7.6). The composition of the electrolyte substrate was the richest in Y and Zr whereas O was distributed over all three cell components with the highest intensity in the cathode. La and Ni were found only in the cathode and anode, respectively. The cathode contained the highest amounts of Sr and Mn. Nonetheless, Sr was also present in the electrolyte, probably due to the formation of $SrZrO_3$ [42]. Mn was visible in both the electrolyte and the anode.

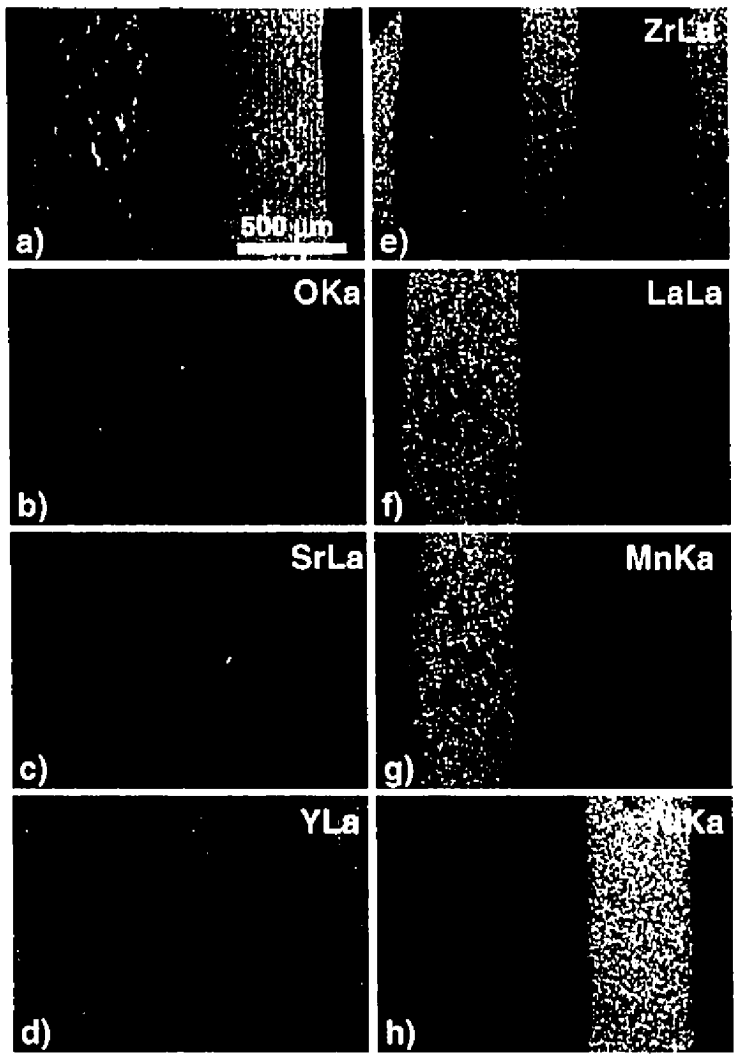

Figure 7.6: a) SEM micrograph of EDX analyzed section showing cathode (left electrode line), electrolyte and anode (right electrode line) of the NiO-YSZ//YSZ//LSM-YSZ cell. b)-h) Chemical map analysis of O, Sr, Y, Zr, La, Mn, Ni in cathode, anode and electrolyte.

The color change of the anode parts in close vicinity to the LSM-YSZ cathode during sintering can be attributed to the presence of manganese in the anode, which probably resulted from the diffusion of manganese from the LSM-based cathode into the closely-spaced anode. The sintering temperature of 1200°C used in this study was sufficiently high to enable the diffusion of manganese [43]. However, sintering LSM-based cathodes at this temperature permits significant reduction of their catalytic

activity for fuel reactions [198]. It might thus be necessary to find a compromise for the sintering temperature in order to impede the chemical interaction and at the same time limit the catalytic activity of the LSM-based cathode. The impact of manganese on anode overpotential and cell performance is, however, not known, and further investigations including impedance spectroscopy will be necessary.

7.6 Conclusions

The effect of anode and cathode materials on the cell performance of single-chamber micro solid oxide fuel cells with coplanar interdigitated microelectrodes was investigated in order to identify suitable electrode and electrolyte material combinations. Electrodes were fabricated from two different conventional anode and two different conventional cathode materials on YSZ electrolytes. For comparison reasons, the composition of only one electrode was changed between each cell. The conventional anode-cathode material couple composed of NiO-YSZ and LSM-YSZ enabled the highest power output of the studied cells at 700° C in a methane-air mixture. However, interaction between anode and cathode was observed through the blackening of the anode in vicinity of a LSM-YSZ cathode. EDX analysis confirmed the presence of manganese in the anode, probably caused by a diffusion mechanism from the LSM-based cathode into the anode during sintering. The manganese might lead to chemical destabilization of the anode, increased electrode resistance and modification of its catalytic activity. Further studies will be necessary to investigate the effect of anode and cathode interaction on the cell performance. LSCF cathodes were found not to chemically interact with the adjacent anode. However, the catalytic activity of LSCF for fuel reactions might have limited the cell performance. GDC-based anodes did not bond well to the YSZ electrolyte. These results constitute a preliminary study for identifying suitable electrode and electrolyte material combinations with regards to chemical interactions and reliable cell operation and performance of SC-μSOFCs with coplanar electrodes.

Chapter 8 Additional results

8.1 Direct-write microfabrication of SC-μSOFCs with coplanar electrodes using viscoelastic electrode inks

Direct-writing has been demonstrated as a promising technique for the fabrication of SC-μSOFCs with coplanar interdigitated electrodes in Ref. [8, 21] as well as in the previous chapters of this thesis. In addition to the process parameters, the design of the electrode inks is a key factor for the fabrication of uniform, continuous electrode structures. The inks used in this thesis and in Ref. [8, 21] were adapted from colloidal suspensions employed in conventional ceramic processing such as screen printing. These inks exhibit a Newtonian flow behavior and a low viscosity which cause spreading of the deposited ink on the substrate and reduce the shape retention of the electrode structures. Although tailoring of ink viscosity and process parameters counterbalances the spreading and permits the fabrication of homogenous electrodes, the ink spreading cannot be completely eliminated, resulting in reduced precision of the final electrode dimensions. It is therefore difficult to predict and adjust the electrode dimensions during cell fabrication. Additionally, thin, lens-like shaped electrodes with non-uniform cross-sectional thickness are obtained due to the ink spreading.

The Colloidal Assembly Group at the University of Illinois at Urbana-Champaign, under the direction of Prof. J. A. Lewis, has developed various ink designs for the direct-write microfabrication of materials and structures, among which colloidal gel-like inks were developed for the creation of three-dimensional architectures [22, 23, 171, 176, 178]. These inks are fabricated from a well dispersed particle suspension with elevated solid loadings. By adding polyelectrolytes or salts or by adjusting the pH, a fluid-to-gel transition is induced. The concentrated colloidal gels show a viscoelastic behavior suitable for the direct-writing process: a constant elevated shear modulus, G', in the linear viscoelastic regime is necessary to maintain shape after deposition (low shear stress), whereas shear-thinning flow (decreasing G') at higher shear stress after the yield point is desired during deposition. The mechanical properties of the colloidal gels can be tailored by adjusting the strength of the interparticle attractions at a constant colloid volume fraction, Φ, according to the scaling relationship:

$$y = k\left(\frac{\Phi}{\Phi_{gel}} - 1\right)^{x} \tag{8.1}$$

where y represents the mechanical property of interest (e.g., G' or the shear yield stress, τ_y), Φ_{gel} is the colloid volume fraction at the gel point, k a constant and x the scaling exponent [171]. With Φ being proportional to the interparticle bond density and Φ_{gel} scaling inversely with the interparticle bond strength, G' and τ_y can be increased by decreasing Φ_{gel} at a constant Φ. A decrease of Φ_{gel} is achieved by changing the pH, by inducing gelation using electrolyte salts or by causing flocculation through the addition of polyelectrolytes [22].

Colloidal gels are composed of a percolating network of attractive particles able to transmit stress above Φ_{gel}. G' is constant until their yield point, corresponding to τ_y, is attained. After this point, G' decreases due to the attrition of interparticle bonds in the gel, resulting in shear-thinning flow during direct-writing:

$$\tau = \tau_y + K\dot{\gamma}^{n} \tag{8.2}$$

where τ is the shear stress, n the shear-thinning exponent, K the viscosity parameter and $\dot{\gamma}$ the shear rate [171].

Colloidal viscoelastic gel-based inks were developed for the fabrication of SC-μSOFCs with coplanar electrodes for improved shape retention. Concentrated suspensions (between 30 and 40 vol%) were fabricated by dispersing and stabilizing the electrode powders, NiO-YSZ for the anode and LSM-YSZ for the cathode, in a mixture of deionized water and a cationic polyelectrolyte, polyethyleneimine (PEI). PEI is a highly branched polyamine with primary, secondary and tertiary amine groups in a ratio of 1:2:1 (Fig. 8.1a). It effectively neutralizes anionic colloidal charge in neutral and acid media. A fluid-to-gel transition was induced by the addition of polyacrylic acid (PAA). PAA is an anionic polyelectrolyte with a linear polymer chain containing one ionizable carboxylic acid group (COOH) per monomer unit (see Fig. 8.1b).

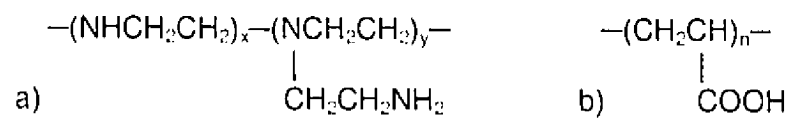

Figure 8.1: Molecular formula of a) PEI and b) PAA [200].

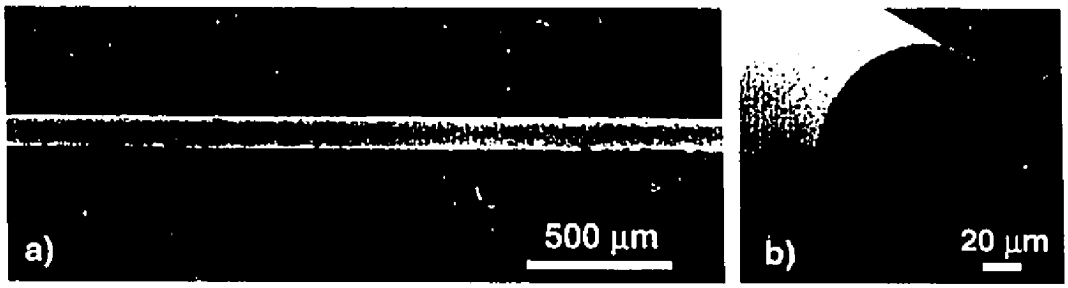

Figure 8.2: SEM image of a sintered NiO-YSZ electrode line fabricated from viscoelastic, gel-like inks using the direct-writing technique: a) top view, b) cross-sectional view.

By varying the ratio of positive NH_x^+ to negative COO^- ionizable groups and therefore varying the strength of the gel, the rheological properties of the ink can be tailored for the direct-write microfabrication process [23, 174].

The rheological properties were characterized in a controlled-stress viscometry mode and in oscillatory stress sweep measurements. The viscoelastic flow behavior of the fabricated gel-based inks enabled smooth flow during extrusion and elevated shape retention after deposition of the electrode structures on the YSZ substrate. Anode and cathode half cells as well as complete SC-µSOFCs with coplanar electrodes were deposited. The viscoelastic inks showed reduced spreading after deposition, and the enhanced shape retention enabled the fabrication of uniform, continuous electrode lines with improved control of the electrode feature sizes (Fig. 8.2a). The electrode cross-sections had a nearly circular shape when using circular extrusion micronozzles (Fig. 8.2b). Thickness and width of the sintered electrodes were close to the diameter of the extrusion nozzle, and the electrodes exhibited a porous, homogenous microstructure. The use of square capillaries as extrusion micronozzles additionally led to the fabrication of electrodes with square cross-section of constant thickness, which could be beneficial for stable long-term cell operation [6]. However, the fabricated cells could not be electrochemically tested because of anode delamination during sintering. The increased thickness of the electrodes (80 to 150 µm compared to 4 to 30 µm of previously fabricated cells using Newtonian inks) might cause mechanical stresses during sintering due to the thermal expansion coefficient mismatch between anode and electrolyte [9].

These results were presented at the *Materials Research Society Spring Meeting 2009* (April 15, 2009, San Francisco, CA), and a proceedings paper has been submitted to the *Materials Research Society Symposium Proceedings*. This paper is reproduced in the Appendix II, where the experimental procedure and the obtained results are described in detail.

8.2 Effect of electrolyte thickness and material on cell performance

The ohmic resistance of a fuel cell to the transport of ions from one electrode to another depends on the length of the conduction path separating the two electrodes in addition to the ionic conductivity of the materials. In a conventional three-layer cell where the electrolyte is sandwiched between anode and cathode, this conduction path corresponds to the electrolyte thickness. In SC-SOFCs with coplanar electrodes, the oxygen ions are transported from the cathode to the adjacent anode via surface ionic conduction through the electrolyte segment bridging the gap between the two electrodes [120]. The conduction path is composed of the interelectrode distance and the electrode width [5, 7]. The use of thin (< 200 μm) [9] or ultrathin (< 1 μm) [7] electrolytes is not mandatory, and thicker electrolyte substrates can be used, which are easier and cheaper to fabricate, exhibit sufficient mechanical strength to support the electrodes and enable the combination of various unit cells in a stack.

However, the exact mechanism of ionic conduction between adjacent coplanar electrodes is not completely understood. Surface ionic conduction seems to be the primary conduction mechanism, as the electrolyte surface roughness affects the ohmic resistance and cell performance, and as it permits the shortest conduction path [5, 17]. But there are neither established models nor conclusive evidence. The electrolyte thickness might still affect the ohmic cell resistance, depending on the depth at which the oxygen ions are conducted through the electrolyte. Except for one numerical approach [18], the effect of electrolyte thickness on the cell performance of SC-SOFCs with coplanar electrodes has not been investigated yet. In Ref. [18] the calculated cell power output was shown to increase with increasing electrolyte thickness from 10 to 40 μm, and to reach a plateau for a thickness of 40 μm and higher. The increase in cell performance was attributed to the decrease of the ohmic loss with increasing electrolyte

thickness. However, these electrolyte thicknesses are not representative of the thicknesses used in experimental studies (> 100 μm).

In a preliminary study, the performances of cells with an interdigitated pattern of five NiO-YSZ anode and five LSM-YSZ cathode lines on a 0.2 and 0.5 mm thick YSZ electrolyte substrate were compared. The average electrode width and interelectrode distance were ~400 and ~280 μm, respectively. The experimental procedure was similar to the one described in the previous chapters. As shown in Fig. 8.3, the maximum power almost doubled when increasing the electrolyte thickness from 0.2 to 0.5 mm. These results constitute the first experimental demonstration of a possible effect of electrolyte thickness on cell performance. Additional studies combined with modeling of the ionic conduction path will be necessary to further investigate the effect of electrolyte thickness on the cell performance of SC-SOFCs with coplanar electrodes.

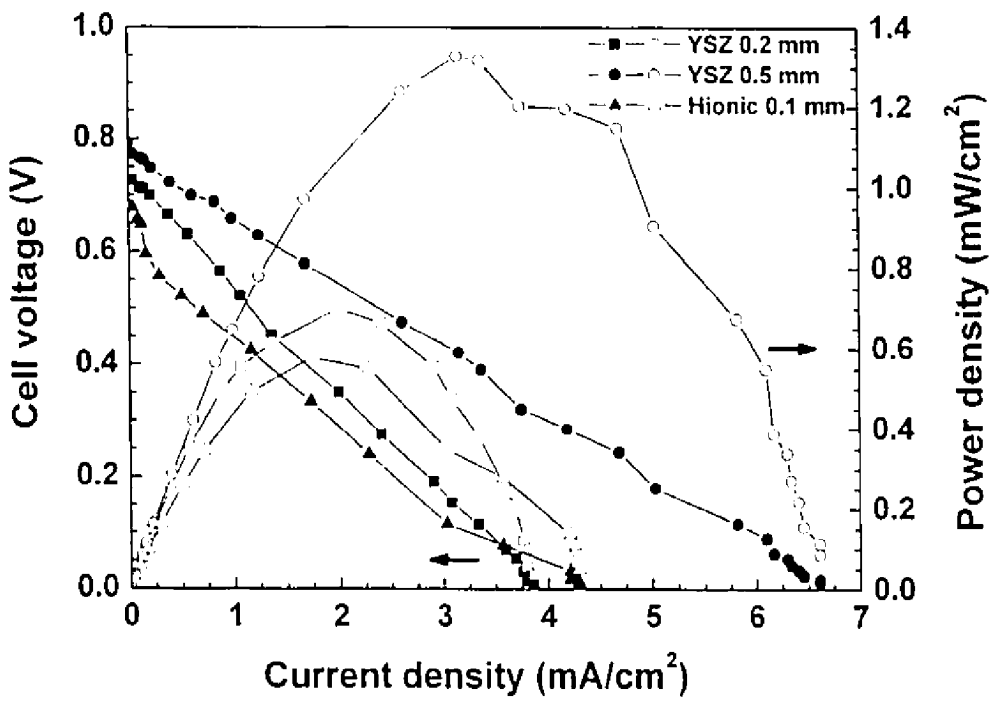

Figure 8.3: Cell voltage (closed symbols) and power density (open symbols) against current density for YSZ electrolytes of different thickness and a scandia stabilized zirconia electrolyte.

The effect of electrolyte material on cell performance was also investigated. The Hionic electrolyte is a new electrolyte material from NexTech Materials, which consists of scandia stabilized zirconia exhibiting higher mechanical strength and conductivity than YSZ [19]. Its thickness was ~0.1 mm. As compared to the cell with the 0.2 mm thick YSZ, no performance increase was obtained when using the new electrolyte material (Fig. 8.3). If the electrolyte thickness affects cell performance, then the expected lower performance of the cell with the thinner Hionic electrolyte might have been compensated by its higher conductivity in comparison to YSZ.

8.3 Cell performance calculations

As described in Chapter 1, the operating or measured cell voltage of a fuel cell is always lower than the reversible cell voltage. When current, I, is drawn from the cell, the voltage decreases with increasing current due to various losses (the terms overpotential and polarization are also used). One contribution to the voltage loss is the ohmic polarization resistance resulting from the ohmic resistance, R_{ohm}, to the transport of ions and electrons in the cell components. Additionally, a portion of the voltage is lost by activation polarization, η_{act}, as the reactants need to overcome a certain energy barrier, i.e., activation energy, in order to enable the electrode reactions to take place. Finally, concentration polarization, η_{conc}, at the electrodes occurs when mass transport effects impede the electrode reactions by slowing down the supply of reactants and the removal of reaction products. Thus, the operating cell voltage, E_{cell}, can be expressed as [9, 201]:

$$E_{cell} = OCV - R_{ohm} \cdot I - \eta_{act,a} - \eta_{act,c} - \eta_{conc,a} - \eta_{conc,c} \qquad (8.3)$$

In equation (8.3), the reversible cell voltage E_r from equations (1.6) and (1.7) has been replaced by the cell voltage under open circuit conditions, OCV, as differences between the open circuit voltage and the reversible voltage due to side reactions (E_L) (equation 1.7) are neglected [9]. $\eta_{act,a}$, $\eta_{act,c}$ and $\eta_{conc,a}$, $\eta_{conc,c}$ represent the activation and concentration polarization at anode and cathode, respectively.

The cell voltage can thus be calculated as a function of cell current according to equation (8.3) by determining the open circuit voltage and the different overpotentials. Although numerical analysis of the cell performance of conventional SOFCs has been

conducted in various studies [9, 201, 202], performance modeling for SC-μSOFCs with coplanar electrodes is still at a very early stage. Additionally, there are no established models on the ionic and electronic conduction, the gas transport around closely-spaced microscale electrodes and the electrode reaction kinetics under single-chamber conditions. The numerical modeling of the performance of SC-μSOFCs with coplanar electrodes has so far only been addressed in Ref. [18], where a three-dimensional finite element method based on macro modeling was employed for the computational simulation of the cell performance characteristics. As FEM modeling is a long and complex procedure, the aim of the cell performance calculation presented in this thesis was to use a simplified modeling approach that could serve as a simple tool for predicting the cell performance and establishing design guidelines for SC-μSOFCs with coplanar electrodes. Thus, careful utilization of this simplified model is required due to its many limitations as compared to real SC-μSOFC systems.

From the different SC-μSOFCs tested in this work, cells with one line and five lines per anode and cathode were chosen to compare the experimentally obtained cell performance with calculated cell voltage and power output. Cells with one pair of electrodes are represented by cells 11 to 15 from Table 4.2 (Chapter 4) and are denoted as cells C1L11_Ch4 to C1L15_Ch4. Cells with interdigitated patterns of five anode and cathode lines were selected from Chapter 4 (C5L_Ch4) and Chapter 7 (C5L_Ch7, the cell composed of NiO-YSZ anode and LSM-YSZ cathode). In the following sections, the different losses affecting the cell voltage were calculated for these cells based on a simplified electrochemistry model, so that the calculated voltage and power could be compared with the experimental data. Based on these calculations, challenges and problems for modeling the performance of SC-μSOFCs with coplanar electrodes are discussed. Finally, fuel utilization and cell efficiency of the tested cells were evaluated.

8.3.1 Calculation of the OCV

The generation of the OCV is due to the difference in oxygen partial pressure between cathode and anode and can be calculated using the Nernst equation (1.6) [9, 39, 105]. The number of electrons n in the Nernst equation represents the number of electrons being exchanged during the electrochemical reactions, notably the reduction

of oxygen, and is set equal to 4 [39, 105, 203]. The oxygen partial pressure at the cathode side corresponds to the initial O_2 content in the gas mixture, assuming that the cathode is completely inert to the fuel reactions [39]. The gas mixture is composed of methane and synthetic air (N_2 and O_2 in a ratio of 80:20). As an open testing chamber is used, the total pressure amounts to 1 atm and equals the sum of the partial pressures of CH_4, O_2 and N_2. With the ratio of nitrogen to oxygen in the synthetic air being equal to 4 and the ratio of methane to oxygen being given by the mixing ratio R_{mix}, the value of $p_{O2,cathode}$ can be calculated by:

$$p_{O2,cathode} = \frac{1\ atm}{R_{mix} + 5} \tag{8.4}$$

A typical range of $p_{O2,cathode}$ corresponds to $p_{O2,cathode} \leq 0.17\text{-}0.13$ atm for $R_{mix} = 1\text{-}2$ [105].

With the anode being catalytically active for the fuel reactions, the oxygen partial pressure at the anode corresponds to the gas composition of the reacted fuel-air mixture. Assuming an infinite reaction rate at the anode, the gas mixture will react to an equilibrium gas composition, which can be calculated using a thermodynamic database [39]. Here, the thermodynamic equilibrium for a CH_4-air gas mixture at different temperatures and R_{mix} was calculated by minimizing the Gibbs free energies of the gas components using the thermodynamic software FactSage™ (v6.0, Thermfact Ltd.) and the FS53 database. The calculated $p_{O2,anode}$ is shown as a function of temperature for three different R_{mix} in Fig. 8.4. $p_{O2,anode}$ increases with increasing temperature and decreasing R_{mix}.

The OCV is calculated using the Nernst equation (1.6) and is shown in Fig. 8.5 as a function of R_{mix} at 700°C, corresponding to the furnace temperature used throughout the experimental work of this thesis. The OCV increases with increasing R_{mix}. For low R_{mix} (< 0.6) this increase is very pronounced, whereas for $R_{mix} > 0.6$ the OCV continues to increase gradually. At 700°C and $R_{mix} = 2$, the calculated OCV (OCV_{calc}) is 1.089 V. This value was used for the following performance calculations. The measured OCVs obtained in this work for the same conditions were only in the range of 0.6-0.9 V and thus much lower than the calculated OCV. This difference can be attributed to insufficient selectivity of the electrode materials for the respective reactions [123] and to a non-equilibrium gas mixture present in real SC-SOFC systems [39].

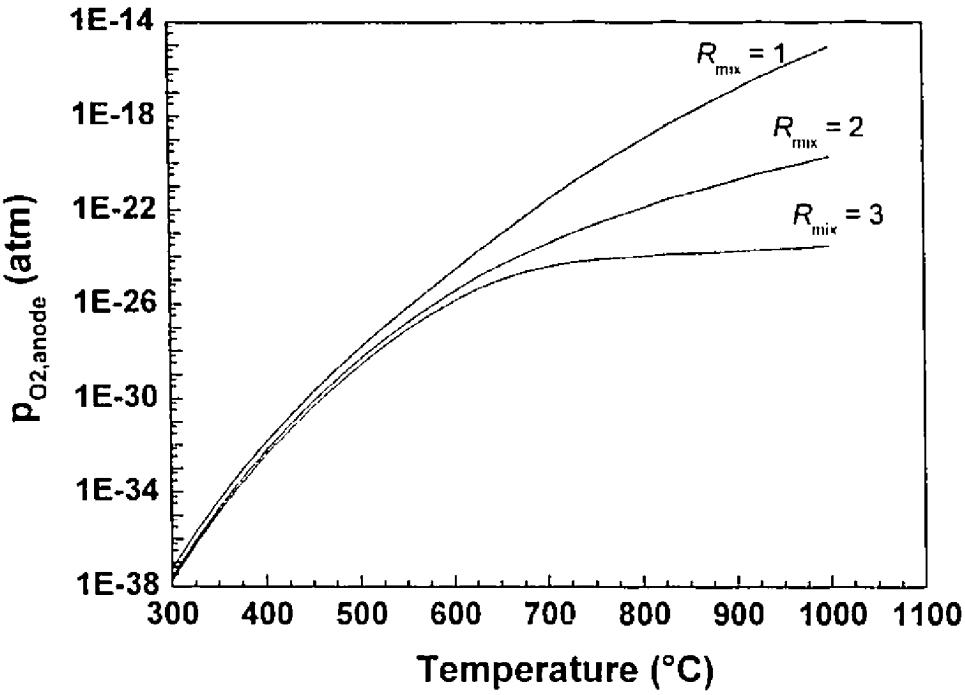

Figure 8.4: Oxygen partial pressure at the anode as a function of temperature for different methane-air gas mixture compositions.

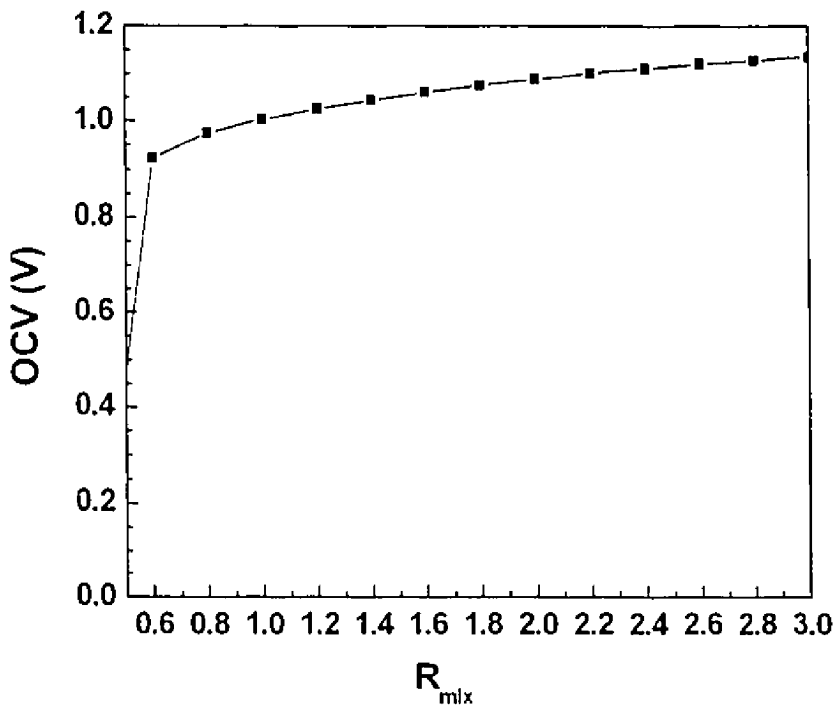

Figure 8.5: Open circuit voltage obtained from equilibrium gas calculations as a function of R_{mix} at 700°C for methane-air mixtures.

8.3.2 Calculation of the ohmic cell resistance

The ohmic cell resistance is composed of the contributions from the resistance of the electrolyte to the oxygen ion conduction, the resistance of the electrodes for the transport of electrons, interfacial resistances and the electronic resistance of the current collectors [3]. The study on current collection method presented in Chapter 6 of this thesis confirmed a non-negligible voltage loss in SC-μSOFCs with coplanar electrodes, resulting from current collection method and long electronic conduction paths in the electrode comb lines. However, the calculation of this voltage loss should consider the inhomogeneous current distribution in the electrodes [6, 13, 101], and no models representing the ohmic loss from electronic conduction in the coplanar electrodes have been established yet. Additionally, the ohmic cell resistance of SC-μSOFCs with coplanar electrodes was shown to primarily depend on the length of the ionic conduction path between adjacent anodes and cathodes for identical current collection conditions [5, 6, 21, 159]. Therefore, only the ohmic loss from ionic conduction was considered in the simplified model, and was calculated using the approach proposed by Fleig et al. [7] for SC-μSOFCs with coplanar electrodes. The ohmic resistance results from the conduction of the oxygen ions through the cross-section of a thin electrolyte between cathode and anode, according to equation (8.5):

$$R_{ohm} = \frac{p_{cond}}{\sigma_{ionic} \cdot t_{el} \cdot L} \tag{8.5}$$

where p_{cond} corresponds to the length of the ionic conduction path, σ_{ionic} to the ionic conductivity of the electrolyte, t_{el} to the electrolyte thickness and L to the electrode length [7]. A schematic representation of the different geometrical cell parameters used for calculating the ohmic loss according to equation (8.5) is given in Fig. 8.6. The electrode length L equals the overlapping length between adjacent anode and cathode lines, and the effect of the connecting segment in the case of interdigitated electrode structures is neglected [7]. The length of the ionic conduction path corresponds to the interelectrode gap, d, when only the edges of the electrodes are considered to be electrochemically active [7]. The ohmic resistance was therefore calculated using the interelectrode gap as the ionic conduction path, and the electrode width, w, was neglected. The thickness, t_{el}, was set equal to 0.2 mm, corresponding to the thickness of the YSZ substrates used for the different cells.

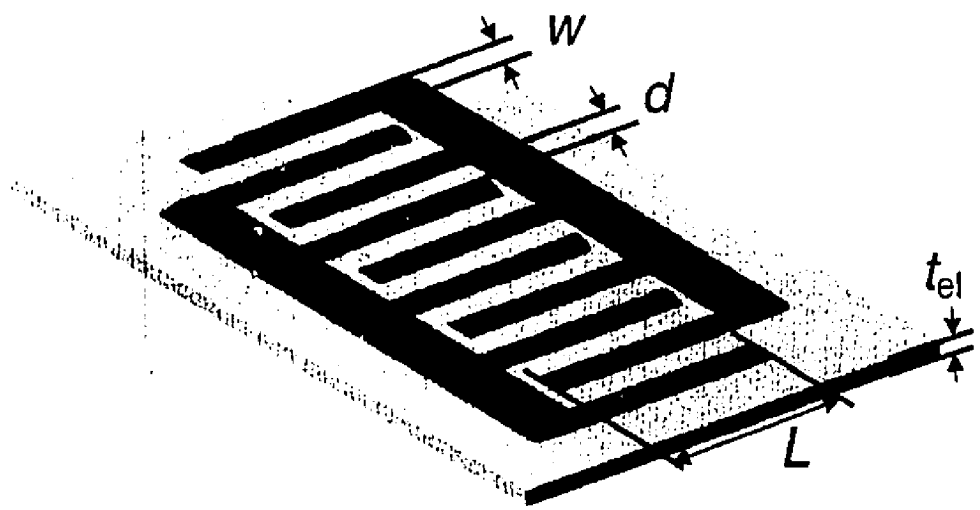

Figure 8.6: Definition of the geometrical cell parameters: w = electrode width, d = interelectrode gap, t_{el} = electrolyte thickness, L = overlapping electrode length.

As no data of the surface ionic conductivity for the YSZ substrates used throughout this work could be obtained from the supplier or be measured due to the lack of suitable equipment for conductivity measurements at elevated temperatures and in methane-air gas mixtures, the ohmic resistance calculations were performed based on the bulk conductivity of YSZ at 700°C (σ_{ionic} = 1 S/m [19]). The ohmic resistance for cells with interdigitated electrodes was also calculated using equation (8.5), as the electrolyte resistance is determined by the conduction between adjacent anode and cathode lines, independently from the number of lines.

The use of equation (8.5) for calculating the ohmic resistance, however, implies the following limitations. Assuming a constant ionic current through the cross-section, $t_{el} \cdot L$, of the electrolyte contradicts the concept of surface ionic migration between adjacent coplanar electrodes [5, 120]. The cross-sectional area for the ionic conduction should not depend on the whole electrolyte thickness, but the ions are rather transported on the electrolyte surface and/or until a certain depth, t_{el}^*, in the electrolyte bulk very close to the surface (see Fig. 8.7). Additionally, the ionic conduction path might be underestimated by only considering the interelectrode gap, as electrode width was shown to affect the ohmic cell resistance and the cell performance [5, 6].

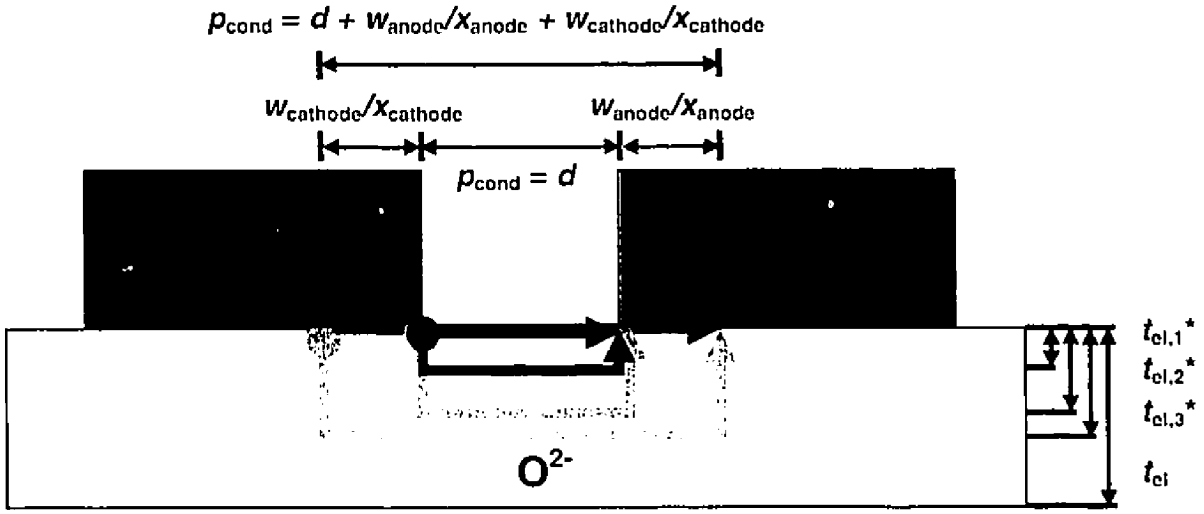

Figure 8.7: Schematics of possible ionic conduction paths.

However, it is not clear to which extent the electrode width contributes to the ohmic loss from ionic conduction. Experimental work on SC-SOFCs with coplanar electrodes showed that only the region of the electrodes closest to the interelectrode gap is involved in the electrochemical reactions [6, 13]. Instead of the whole electrode width, only a portion of the electrode width (w_{inv}/x) might therefore contribute to the conduction path p_{cond}, as shown in Fig. 8.7. Also, the contribution of the electrode width might not be the same for anode and cathode, resulting in different values of x for the electrodes. Finally, calculating the ohmic resistance based on surface ionic conduction requires reliable data of the surface ionic conductivity of the electrolyte material.

The experimentally measured ohmic resistance, $R_{ohm,m}$, was obtained from the experimental data by applying the method of least squares to fit the experimental *E-I* curves. Equation (8.6) represents the employed model function based on equation (8.3).

$$E_{cell} = OCV - R_{ohm,m} \cdot I - \frac{RT}{\alpha F} \sinh^{-1}\left(\frac{i}{2i_0}\right) \tag{8.6}$$

The OCV, current I and current density i were taken from the experimental data. R, T, α and F are constants (R = 8.314 J/(mol·K), T = 973 K, α = 0.5 [18], F = 96485 C/mol), whereas $R_{ohm,m}$ and the exchange current density, i_0, were the variable parameters. The third term on the right hand side of equation (8.6) represents the activation polarization

expressed by a one-term hyperbolic sine approximation of the Butler-Volmer equation [204]. Concentration losses were neglected. Activation and concentration polarization are discussed in detail in the following sections. The sum of the squared difference between the experimentally measured cell voltage and the cell voltage calculated by equation (8.6) was minimized.

Calculated and measured ohmic resistance, $R_{ohm,calc}$ and $R_{ohm,m}$, are listed in Table 8.1 for the different cells with one line per anode and cathode (C1L11_Ch4 to C1L15_Ch4) and the cells with interdigitated electrode patterns (C5L_Ch4 and C5L_Ch7). Despite the limitations of equation (8.5) for calculating the ohmic cell resistance of SC-μSOFCs with coplanar electrodes, the calculated ohmic cell resistance was in good agreement with respect to the experimental value for cells with one electrode pair and an electrode width of ~850 μm. However, in the case of cells with larger electrodes and cells with interdigitated electrode patterns, the calculated ohmic resistance is considerably lower than the measured resistance, due to the neglected effects of electrode width and resistance to electronic conduction, respectively. For these cells, correctly calculating the ohmic resistance necessitates a model of the exact conduction path of the ions from cathode to anode, and FEM modeling of the ohmic resistance from both ionic and electronic conduction.

Table 8.1: Comparison of measured and calculated ohmic resistance for the different cells.

Cell	L (mm)	d (μm)	w_{av} (μm)	$R_{ohm,m}$ (Ω)	$R_{ohm,calc}$ (Ω)
C1L11_Ch4	3.8	305	847	474	401
C1L12_Ch4	3.8	431	858	604	567
C1L13_Ch4	3.6	400	870	608	556
C1L14_Ch4	4.4	267	1303	938	303
C1L15_Ch4	4.4	275	1380	1017	313
C5L_Ch4	2.7	183	248	1479	339
C5L_Ch7	3.3	312	383	886	473

8.3.3 Calculation of activation and concentration polarization

8.3.3.1 Activation polarization

The activation polarization represents the voltage loss associated with the energy barrier that the reactants at the electrodes need to overcome [9, 201, 203, 205]. The activation polarization depends on the reaction kinetics at the electrode. Elevated reaction rates lead to low activation losses, whereas slow reaction kinetics cause high overpotentials. The electrochemical reaction rate can be represented by the current density, i, which is related to the overpotential, η_{act}, by the basic law of charge-transfer reactions, the Butler-Volmer equation [205]:

$$i = i_0\left(\exp\left(\frac{\alpha_1 F \eta_{act}}{RT}\right) - \exp\left(\frac{-\alpha_2 F \eta_{act}}{RT}\right)\right) \tag{8.7}$$

Equation (8.7) represents the anodic and cathodic current of an electrochemical reaction at an electrode-electrolyte interface. The overpotential describes the departure from the equilibrium electrode potential when the reaction takes place. The exchange current density, i_0, corresponds to the current density at equilibrium when the cathodic and anodic current densities are equal and the net current is zero. i_0 is a direct measure of the reaction rate, and high exchange current densities imply elevated reaction rates and lead to better cell performance. α_1 and α_2 are the anodic and cathodic charge transfer coefficients with $\alpha_1 + \alpha_2 = 1$.

The reactions at the electrodes involve multi-step reaction mechanisms of which the one with the slowest reaction kinetics is the rate determining step (rds). The transfer coefficients can thus be defined as [204, 205]:

$$\alpha_1 = \frac{n-\gamma}{\nu} - r\beta \tag{8.8}$$

$$\alpha_2 = \frac{\gamma}{\nu} + r\beta \tag{8.9}$$

where γ is the number of electrons transferred in the steps prior to the rds, n the number of electrons transferred in the overall reaction, ν the number of times the rds occurs, r the number of electrons transferred in the rds and β the symmetry factor. The Butler-Volmer equation (8.7) thus describes multistep overall electrodic reactions with possible electron transfer in steps other than the rds and with the rds occurring ν times

in the overall reaction [205]. Single-step reactions are rare in electrochemistry and reactions involving several electrons n are very unlikely to occur in a single step, but rather in n steps. However, due to the lacking knowledge of the exact reaction mechanism, one-step single-electron transfer processes are generally assumed. This is also the case in SOFC modeling, where four electrons are normally transferred in the oxygen reduction reaction [201, 203, 204]. By considering a single-step one-electron reaction ($\gamma = 0$, $\nu = n = r = 1$), the Butler-Volmer reaction can be simplified to:

$$i = i_0\left(\exp\left(\frac{(1-\beta)F\eta_{act}}{RT}\right) - \exp\left(\frac{-\beta F\eta_{act}}{RT}\right)\right) \tag{8.10}$$

Activation polarization results from the reactions at the electrode-electrolyte interface and the triple phase boundaries. Thus, both anode and cathode exhibit activation polarization, so that the total activation loss equals the sum of anode and cathode activation polarization according to:

$$\begin{aligned}\eta_{act} = \eta_{act,a} + \eta_{act,c} = {} & i_{0,a}\left(\exp\left(\frac{(1-\beta_a)F\eta_{act,a}}{RT}\right) - \exp\left(\frac{-\beta_a F\eta_{act,a}}{RT}\right)\right) \\ & + i_{0,c}\left(\exp\left(\frac{(1-\beta_c)F\eta_{act,c}}{RT}\right) - \exp\left(\frac{-\beta_c F\eta_{act,c}}{RT}\right)\right)\end{aligned} \tag{8.11}$$

For simplification, $\beta = 0.5$ is often assumed, so that $\alpha_{1,a} = \alpha_{2,a} = \beta_a = \alpha_a$ (= 0.5) and $\alpha_{1,c} = \alpha_{2,c} = \beta_c = \alpha_c$ (= 0.5) [201, 204, 205]. Although different values for the charge transfer coefficients of SOFC anode and cathode materials have also been reported in the literature [204, 206, 207], the assumption of $\alpha_a = \alpha_c = \alpha = 0.5$ was employed in this thesis in order to calculate the activation polarization as a function of current density by using the hyperbolic sine approximation of the Butler-Volmer equation (8.11) [201, 203, 204]:

$$\eta_{act} = \eta_{act,a} + \eta_{act,c} = \frac{RT}{\alpha F}\left(\sinh^{-1}\left(\frac{i}{2i_{0,a}}\right) + \sinh^{-1}\left(\frac{i}{2i_{0,c}}\right)\right) \tag{8.12}$$

The exchange current density depends on the electrode material, its catalytic activity, the electrolyte conductivity and the testing conditions. Different approaches were considered in the literature to determine i_0 from reactant concentrations [201], reactant and product partial pressures [204], impedance measurements [208, 209], curve fits on experimental data [206, 210] or single electrode polarization

measurements [211-214]. However, only a few values are available for the anode and cathode materials used in this work. For LSM and LSM-YSZ, values of i_0 range from 2 to 130 mA/cm^2 [201, 208, 210, 211, 213], whereas for NiO-YSZ anodes, exchange current densities between 118 and 400 mA/cm^2 can be found in the literature [201, 206]. No values have been reported for these materials under single-chamber conditions. Thus, the experimental data was used to determine i_0 for the NiO-YSZ anode and LSM-based cathode in methane-air mixtures with R_{mix} = 2 and at 700°C. Based on equation (8.3), the following curve fit was applied in combination with the method of least squares:

$$E_{cell} = OCV - R_{ohm,m} \cdot I - \frac{RT}{\alpha F}\left(\sinh^{-1}\left(\frac{i}{2i_{0,a}}\right) + \sinh^{-1}\left(\frac{i}{2i_{0,c}}\right)\right) \qquad (8.13)$$

where the hyperbolic sine approximation of the activation polarization of anode and cathode (equation 8.12) was used.

However, using the sum of anode and cathode activation polarization in the curve fit led to the same values for $i_{0,a}$ and $i_{0,c}$, and the exchange current density for each electrode could not be determined. Therefore, the activation polarization was reduced to a single term based on the assumption that only one electrode causes activation losses [204, 210]. The activation polarization associated with the other electrode can be neglected when its exchange current density is sufficiently larger than i_0 of the first electrode, thus enabling very fast reaction kinetics and minimizing the activation polarization. In SOFCs, the anode activation polarization is known to be lower than cathode activation losses due to much faster reaction kinetics of the hydrogen oxidation reaction in comparison with the sluggish oxygen reduction reaction [19]. Thus, the exchange current density for the anode reactions is in general much higher than the one for the cathode reactions. By neglecting the anode activation polarization, the exchange current density corresponding to the cathode, $i_{0,c}$, could then be determined from the experimental data using equation (8.6) for the curve fit.

Table 8.2 summarizes the calculated values of the cathode exchange current density for the different cells. Although, for cells C1L12_Ch4 and C1L14_Ch4, the values of $i_{0,c}$ are slightly higher as compared to the other cells, all values are within the range of data reported in the literature. For the following calculation of the activation

polarization, the mean value of the seven measured exchange current densities ($i_{0,c}^{*}$ = 5.71 mA/cm^2) was used. With the assumption that the anode activation polarization is negligible and with the lack of suitable data for $i_{0,a}$, the activation polarization was calculated based on equation (8.14), taking into account only the cathode activation polarization. Fig. 8.8 shows the cathode activation polarization as a function of current density.

$$\eta_{act} = \eta_{act,c} = \frac{RT}{\alpha F}\sinh^{-1}\left(\frac{i}{2i_{0,c}^{*}}\right) \tag{8.14}$$

Table 8.2: Values of $i_{0,c}$ obtained from the experimental data for the different cells.

Cell	C1L11 _Ch4	C1L12 _Ch4	C1L13 _Ch4	C1L14 _Ch4	C1L15 _Ch4	C5L _Ch4	C5L _Ch7
$i_{0,c}$ (mA/cm^2)	6.09	11.44	5.12	12.38	1.71	1.65	1.61

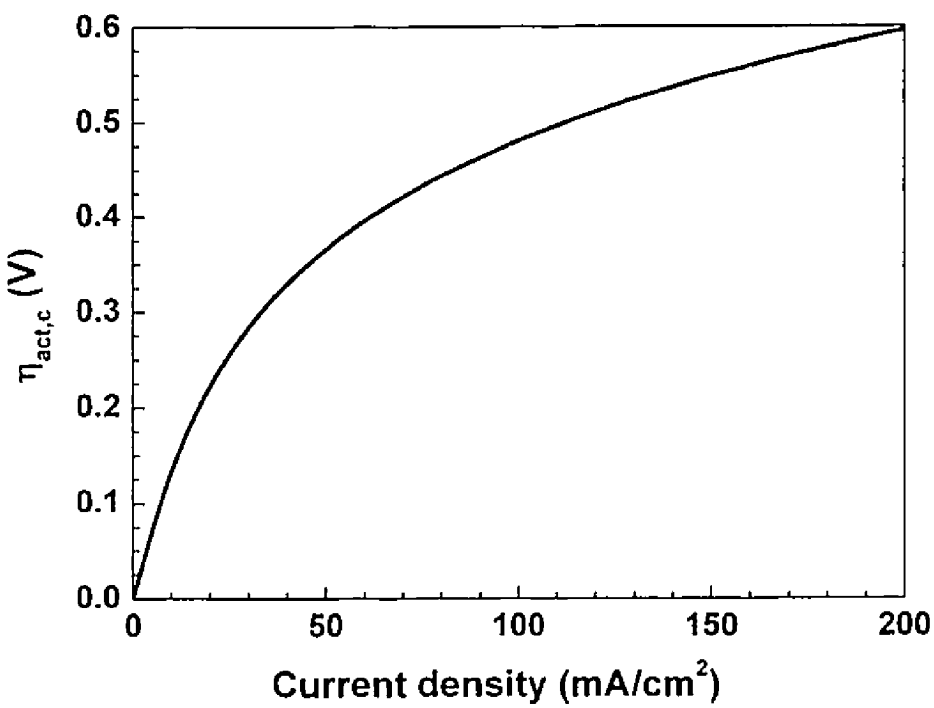

Figure 8.8: Cathode activation polarization as a function of current density.

8.3.3.2 Concentration polarization

Concentration polarization occurs when diffusion of reactants and reaction products to and from the reaction sites is limited at elevated current densities. However, at the elevated operating temperatures of SOFCs, the values of gaseous and surface diffusivities are high, thus avoiding any significant slow down of mass transfer [215]. Additionally, concentration overpotentials are negligible for thin electrodes (50 μm [201], 20 μm [18]). Therefore, voltage losses due to concentration polarization were not considered here.

8.3.4 Comparison between experimental and calculated cell performance

With the OCV, ohmic resistance and cathode activation polarization calculated in the previous sections, the cell voltage, $E_{cell,calc}$, and power density, P_{calc}, were then determined according to the following equations:

$$E_{cell,calc} = OCV_{calc} - R_{ohm,calc} \cdot I - \eta_{act,c} \tag{8.15}$$

$$P_{calc} = E_{cell,calc} \frac{I}{A_{electrode}} \tag{8.16}$$

where $A_{electrode}$ represents the average electrode area.

Fig. 8.9 and 8.10 show representative examples of the experimentally measured and the calculated cell voltage and power density as functions of current density for a cell with one and five lines per anode and cathode, respectively. Both measured and calculated voltage-current curves show a linear trend. For the cell with one pair of electrodes, the slope of the experimental curve is very similar to that of the calculated curve. However, the slope of the calculated *E-I* curve differs from that of the experimentally obtained curve for the cell with an interdigitated electrode pattern, indicating a lower calculated ohmic cell resistance. The comparison also shows that the calculated maximum power and current density are significantly higher than the measured values. Table 8.3 summarizes calculated and measured cell performance for the different cells and compares calculated and measured OCV, maximum current density, i_{max}, and maximum power density, P_{max}.

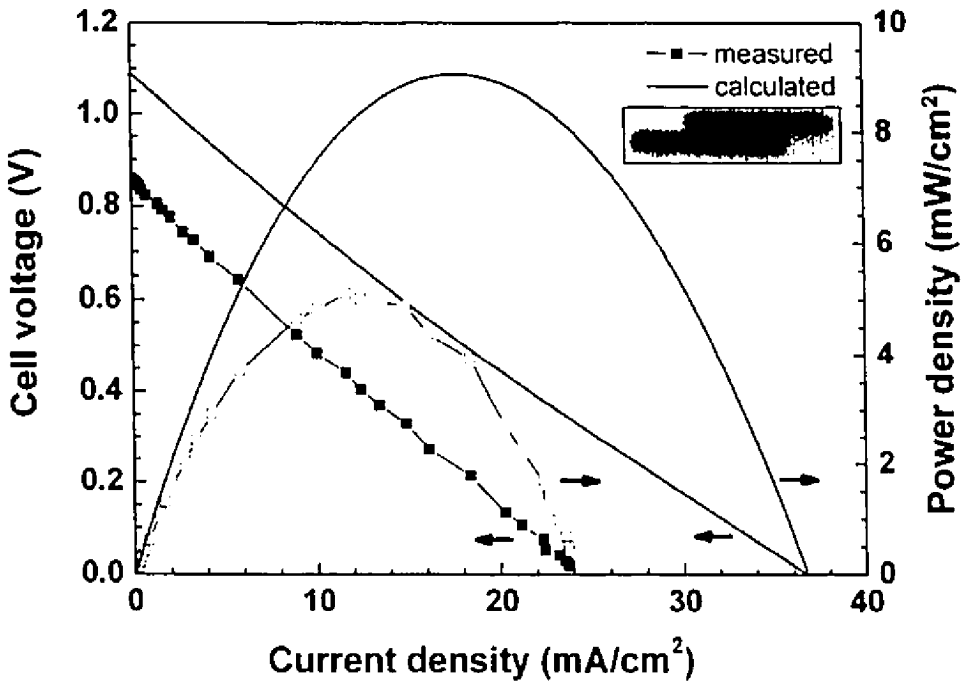

Figure 8.9: Measured and calculated cell voltage and power density as functions of current density for cell C1L11_Ch4 with one line per anode and cathode.

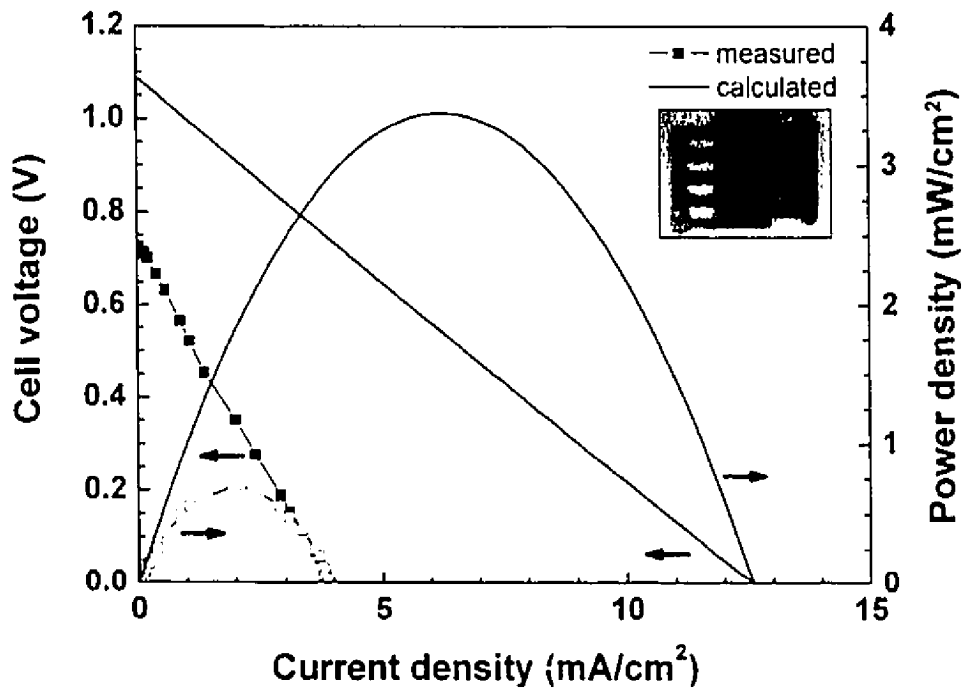

Figure 8.10: Measured and calculated cell voltage and power density as functions of current density for cell C5L_Ch7 with five lines per anode and cathode.

Table 8.3: Comparison of measured and calculated cell performance.

Cell	OCV_m (V)	OCV_{calc} (V)	$i_{max,m}$ (mA/cm^2)	$i_{max,calc}$ (mA/cm^2)	$P_{max,m}$ (mW/cm^2)	$P_{max,calc}$ (mW/cm^2)
C1L11_Ch4	0.860	1.089	23.76	36.7	5.11	9.07
C1L12_Ch4	0.865	1.089	21.99	27.6	4.89	7.03
C1L13_Ch4	0.816	1.089	17.41	27.4	3.59	6.99
C1L14_Ch4	0.819	1.089	9.52	32	2.06	8.03
C1L15_Ch4	0.808	1.089	6.29	29.3	1.24	7.33
C5L_Ch4	0.876	1.089	5.05	27.6	1.07	7.03
C5L_Ch7	0.727	1.089	3.86	12.5	0.70	3.37

For the cells composed of a single electrode pair with an average electrode width of ~850 μm, calculated maximum current and power density differ only by a factor of 1.25 to 2 from the measured values, indicating that the simplified model provides a good approximation of the cell performance for these cells. For the other cells, the calculated performance was significantly higher than the measured one. This difference is mainly attributed to the underestimation of the calculated ohmic resistance for these cells. In the case of cells C1L14_Ch4 and C1L15_Ch4, the contribution of the large electrode width to the ohmic resistance was neglected by only considering the interelectrode distance for the ionic conduction path. For the cells with interdigitated electrode patterns, the electronic conduction in the electrode comb lines affects the cell performance of real SC-SOFC systems.

The simplified model permits an approximate prediction of the cell performance in the case of SC-μSOFCs with a single pair of coplanar electrodes. It could therefore be used as a simple tool to evaluate the effect of cell size on cell performance and establish design guidelines for these fuel cells. When employing the measured value of the OCV for the cell performance calculation, the prediction can be improved and the calculated cell performance is in good agreement with the experimentally measured performance, as shown in Fig. 8.11 for cell C1L11_Ch4.

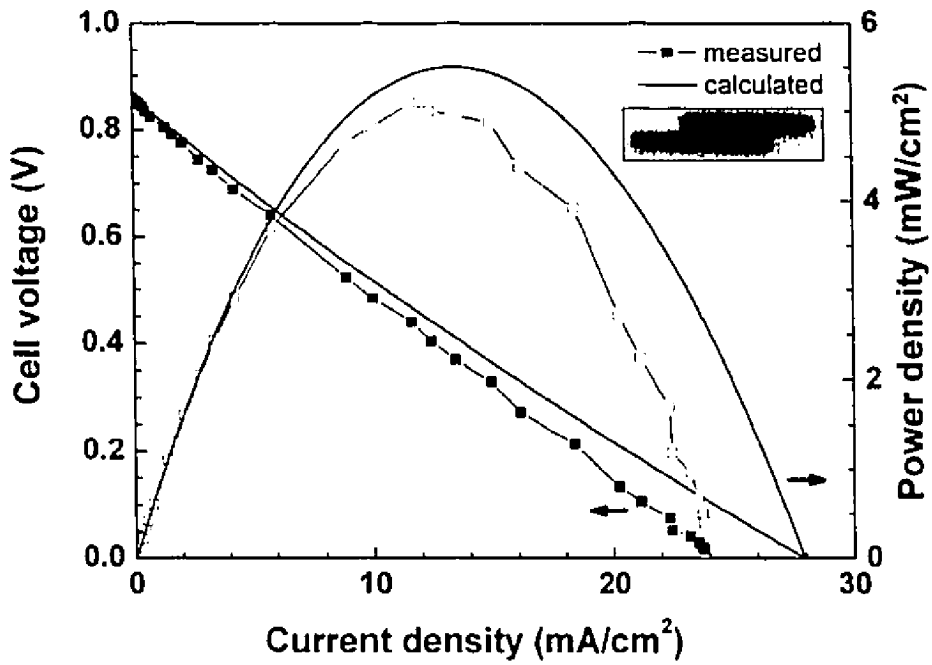

Figure 8.11: Comparison of measured and calculated cell voltage and power density as functions of current density for cell C1L11_Ch4 with one line per anode and cathode, using the measured OCV for calculating the cell performance.

8.3.5 Challenges of performance modeling

Although the work in this thesis was mainly of an experimental nature, simple calculations of the cell performance led to the identification of several challenges that will have to be addressed when modeling performance of SC-μSOFCs with coplanar electrodes:

- In SC-SOFC systems, the lack of selectivity of the electrode materials for the specific reactions affects the OCV. Thus differences between calculated and measured OCV will exist as long as selectivity issues are not solved through the development of more selective materials. Additionally, the OCV in real SC-SOFC systems can be affected by local temperature and gas composition changes.
- The necessity to develop a model for the correct ionic conduction path between adjacent anodes and cathodes.
- Such a model will also help to determine the exact conduction mechanism and determine the electrolyte conductivity to consider.

- If surface conduction is the main mechanism, values of the surface ionic conductivity of the electrolyte will have to be measured.
- The contribution of electronic conduction to the ohmic resistance needs to be considered.
- The lack of reliable values of the exchange current densities of anode and cathode materials under single-chamber conditions.

In this work, only a simplified electrochemical model, including OCV, ohmic resistance and electrode polarization, has been considered to obtain the cell voltage as a function of cell current. A complete numerical model for cell performance prediction will have to additionally integrate and couple effects of gas flow, heat transfer, transport in porous electrodes and catalytic chemistry. Such a model has been developed for anode-supported SC-SOFCs in Ref. [216]. However, establishing such a model is not simple and constitutes a research project on its own. Exact prediction of the actual catalytic reactions is impeded by the insufficient selectivity of current electrode materials. Moreover, in the case of SC-SOFCs with coplanar electrodes, modeling the gas flow around the electrodes might be especially difficult. The close vicinity of adjacent electrodes and possible intermixing of reactants and reaction products between the electrodes can lead to local concentration, temperature, gas composition and pressure gradients that will not only affect the gas flow but also the catalytic as well as electrochemical reactions.

8.3.6 Fuel utilization and cell efficiency

Fuel utilization is generally referred to as the current efficiency, ε_f, as the utilization and electrochemical conversion of the fuel lead to the generation of an electrical current [9]. The current efficiency is given by:

$$\varepsilon_f = \varepsilon_{FU} = \frac{I}{I_f} \tag{8.17}$$

where I corresponds to the current produced by the cell at the maximum cell power output. I_f represents the theoretical current generated for 100% electrochemical conversion of the fuel and can be calculated by Faraday's law [9]:

$$I_f = \frac{\dot{m}_F \cdot F \cdot n}{M} \tag{8.18}$$

where m'_F is the amount of fuel entering the cell per unit time (g/s), F the Faraday constant, n the number of electrons involved in the reactions and M the molar mass of the reacting fuel.

Although this approach has been commonly used for evaluating the fuel utilization of SC-SOFC systems [14, 151, 154], it does not take into account the utilization of the fuel for the generation of heat by the exothermic fuel reactions [10, 217]. The generated heat could be used for cogeneration [130], to effectively raise the cell temperature for improved cell performance [11] or to thermally self-sustain the single-chamber cells [15]. The fuel utilization should thus include the conversion of fuel both to current and heat. Therefore it has been defined in Ref. [217] as the ratio of the enthalpy drop of the fuel between cell inlet and outlet to the heat release generated by the oxidation of the incoming fuel:

$$\varepsilon_{FU} = 1 - \frac{\dot{m}_{F,out}\Delta H_{F,out}}{\dot{m}_{F,in}\Delta H_{F,in}} \tag{8.19}$$

The heat release by the inlet fuel equals the product of the mass flow rate of the incoming fuel $m'_{F,in}$ and its combustion enthalpy change $\Delta H_{F,in}$, whereas $m'_{F,out}$ and $\Delta H_{F,out}$ are the mass flow rate and combustion enthalpy change of the exhaust fuel.

Gas analysis of the exhaust gas stream is necessary in order to obtain the exact amount of unreacted fuel. Preliminary analysis on a SC-SOFC similar to the ones described in Chapter 6 for the study of current collection method was performed using the testing setup at the Hydro Québec research center in Varennes. The cell consisted of a comblike NiO-YSZ anode and a planar LSM cathode on opposite sides of a 1.6 x 2.5 cm^2 YSZ electrolyte substrate. The conversion of the fuel was very low and at the limit of detection of the used secondary ion mass spectrometer (Quadrupole model Prisma©, Pfeiffer-Balzers). This detection issue will also restrict the possibility of measuring the mass of unreacted fuel in the outlet gas stream of the SC-μSOFCs with coplanar electrodes considered in this work. These cells are of even smaller dimensions and even lower fuel conversion is expected. Additionally, measurement of the temperature in close vicinity of the SC-μSOFCs with coplanar electrodes only showed a small temperature increase (0-40°C) as compared to the furnace temperature, indicating little fuel conversion to heat.

Therefore the fuel utilization was calculated using equations (8.17) and (8.18) with methane ($M_{methane}$ = 16 g/mol) as fuel. For a total flow rate of methane and air of 150 sccm and a methane-to-oxygen ratio R_{mix} = 2, the flow rate of methane was 42.85 sccm. The cell current, I, was obtained from the experimental results at the maximum measured power. The fuel utilization was then estimated to be less than 0.1% for the cells listed in Table 8.3. This very low value is in accordance to current efficiencies reported in the literature for SC-SOFCs where anode-supported SC-SOFCs showed fuel utilization ranging from ~1% [14] to 2.4% [151] or 4-8% [154].

The fuel utilization or current efficiency of the cells tested in this work is affected by the very small electrode surface area (average electrode surface area < 0.3 cm^2) and thus the small amount of catalyst available for the fuel reactions. Only a very small amount of fuel from the incoming gas stream will be able to access the reaction sites and react. Although the flow rate of 150 sccm mainly used throughout this work is lower than flow rates reported in the literature for SC-SOFCs with coplanar electrodes [6, 13, 21], this flow rate might be too fast for the small cells. Very slow flow rates might, however, cause stagnation of reactants and reaction products in the reaction chamber, which could increase the risk of explosion, change the gas mixing ratio, and impede the supply of fresh reactants. Optimization of the gas flow rate will thus be necessary to improve fuel utilization and at the same time enable proper functioning of the cells. Gas intermixing between the closely-spaced microelectrodes might also contribute to the low fuel utilization [21].

The total cell efficiency is the product of thermodynamic, potential, system and current efficiency (equation 1.8). The thermodynamic efficiency, ε_{th}, was considered for the complete oxidation of methane and is equal to 1 [9]. The potential efficiency, ε_p, is given by the ratio of cell voltage under load to the equilibrium or open circuit voltage (equation 1.10) [9]. The cell voltage at the maximum measured power output was used for the cell voltage under load. For the cells from Table 8.3, ε_p ranged from 0.42 to 0.56. As fuel pretreatment and cell cooling were not employed during cell testing, the system efficiency was assumed to be 100%. With a current efficiency of less than 0.1%, the total efficiency of the single cells tested in this study was thus below 1%, corresponding to the estimated values of present SC-SOFCs [15].

The low fuel utilization and cell efficiency of current SC-SOFC systems can be attributed to the insufficient selectivity of the electrode materials for the respective electrode reactions [101]. A significant amount of fuel is utilized in direct fuel oxidation or other parasitic reactions and does thus not contribute to power generation and cell efficiency. With the development of more selective materials, fuel utilization and cell efficiency can therefore be increased. Moreover, fuel utilization and cell efficiency of current SC-SOFC systems are calculated with respect to one single cell. However, in practical applications, stacks of several cells would be used, enabling higher fuel cell efficiency for the whole stack. Fuel utilization could additionally be increased by arranging the cells in the fuel downstream so that unreacted fuel can react on the following cells of the stack, or by recirculating the unreacted fuel into the reaction chamber.

The low cell efficiency remains one of the main obstacles for the practical implementation of SC-SOFCs. Although the heat generated through the fuel oxidation reactions was shown to be sufficient to thermally self-sustain a SC-SOFC without any additional heating [15], the inherent low efficiency of the single-chamber design imposes a severe hurdle to the application of these cells as battery replacements. However, the intrinsic properties of SC-SOFCs such as their small, compact size and their capacity for heat generation and hydrocarbon reforming enable potential applications in other domains. Combined with conventional SOFCs, the generated heat from the SC-SOFC could be used to preheat gas streams or maintain the temperature of the conventional cell. Additionally, the SC-SOFC ahead of the conventional cell could be employed as a hydrocarbon reforming system. Without the need for reactant gas separation, SC-SOFCs could also work as gas, temperature or pressure sensors in mixed gas conditions. Furthermore, when SC-SOFCs are used in energy harvesting applications such as in exhaust gas streams at elevated temperatures, efficiency is a less important factor, as power is generated from waste fuels [16]. In the case of SC-SOFCs with coplanar electrodes, the small cell size, the possibility to create cell stacks on the same electrolyte substrate and the mechanical robustness of the cell due to the use of a thick, mechanically strong electrolyte substrate would be especially beneficial for sensor and energy harvesting applications in harsh environments.

Chapter 9 General discussion

9.1 Evaluation of the direct-writing technique for the fabrication of SC-μSOFCs with coplanar electrodes

9.1.1 Advantages of direct-write microfabrication

The fabrication of SC-μSOFCs with coplanar electrodes implies several fabrication challenges in addition to regular issues of fabricating at the microscale. Standard microfabrication techniques such as lithography-based methods possess sufficient resolution to create microscale electrode patterns, but dense electrode microstructures are generally obtained [160, 164]. Porous electrodes are, however, desired in order to increase the active surface area and enable gas diffusion to the reaction sites at the electrode-electrolyte interface [9]. Additionally, lithography-based techniques are limited with respect to creating electrode patterns of two different multicomponent materials on the same side of the electrolyte substrate. Combining microfabrication techniques with conventional ceramic forming methods, where electrode materials are used in the form of suspensions, seems most appropriate to face these fabrication challenges. Micromolding in capillaries [13] and microfluidic lithography [20] were successfully employed to fabricate interdigitated patterns of coplanar microscale porous electrodes. But, similarly to lithography, the versatility of these techniques depends on the necessity to fabricate and use molds.

Here robot-controlled direct-write microfabrication was investigated for creating SC-μSOFCs with coplanar electrodes. This method consists of the pressure-driven extrusion of electrode suspensions through micronozzles and their robot-controlled deposition on the electrolyte substrate in the desired shape. The main advantages of this fabrication technique can be summarized as:

- Versatility, permitting the fabrication of different electrode shapes by simply programming the robot-controlled deposition trajectory;
- Flexibility as to electrode size by using extrusion nozzles of different diameters;
- Flexibility as to electrode material: different electrode materials can be processed as long as they can be synthesized as inks;

- Rapidity because the deposition of one electrode takes a few tens of seconds (depending on deposition speed and number of electrode lines);
- Affordability as no molds have to be fabricated and the direct-writing system is simple;
- Porous electrode microstructures can be obtained by a suitable sintering step after deposition.

Different electrode materials can be used in direct-writing as long as the material can be synthesized in the form of an ink or suspension and be extruded through the micronozzle. Inks of the respective electrode material can be prepared by dispersing electrode powders in a liquid phase. Consequently, electrode suspensions were used similarly to ceramic forming techniques (e.g., screen printing, tape casting) where the electrode powders are mixed with solvent, binder and dispersant. By adjusting viscosity and particle loading of these inks to the direct-writing technique, coplanar microscale electrode patterns could be created with the direct-writing apparatus. Sintering of the deposited electrode patterns enabled tailoring of the electrode porosity. The versatility and flexibility of the technique permitted the successful fabrication of coplanar electrode structures of different shapes, sizes and material compositions.

9.1.2 Challenges of direct-write microfabrication of SC-μSOFCs with coplanar electrodes and possible solutions

Several challenges were faced for the direct-write microfabrication of SC-μSOFCs with coplanar electrodes:

- Control of ink rheology;
- Planarity of electrolyte substrate and substrate holder;
- Control of low extrusion pressures (< 2 bar);
- Alignment of electrodes;
- Precision of robotic deposition apparatus.

Uniformity and homogeneity of the deposited electrode structures were found to significantly depend on the rheology of the electrode inks. Uncontrolled ink spreading was notably one of the major drawbacks for the fabrication of coplanar electrodes of precise and repeatable dimensions, so that tailoring of extrusion pressure and deposition speed was necessary to obtain the desired electrodes. Ink composition, i.e.,

the amount of the respective ingredients, can also influence the ink spreading and an increased particle load was found to yield a higher viscosity for improved shape retention after deposition. However, the Newtonian flow behavior of the prepared inks did not permit complete elimination of the problem of ink spreading, even for optimized process parameters and ink composition, making it difficult to control the final electrode dimensions during direct-write fabrication. Additionally, size variations with respect to interelectrode distance and electrode width were observed when comparing electrode lines fabricated under identical conditions. Therefore, viscoelastic, gel-based inks were developed, where the viscosity depends on the shear stress level. The solid-like behavior of these inks at low shear stress significantly decreased spreading and enabled increased shape retention after deposition, whereas the liquid-like behavior at higher shear stress ensured a smooth flow through the extrusion nozzle. The dimensional uniformity and microstructural homogeneity of the deposited electrodes were considerably improved by using the viscoelastic inks. The elevated shape retention also enhanced the control over the electrode dimensions, as the electrode width was very close to the nozzle diameter, indicating very low ink spreading. The fabricated electrodes exhibited a cross-sectional thickness on the order of magnitude of the nozzle diameter, whereas the spreading of the Newtonian inks caused lens-like cross-sections of non-uniform, reduced thickness. Further optimization of these viscoelastic inks to reduce drying in air could be useful to avoid deposition in an oil bath. Also, the problem of anode detaching and breaking during sintering remains to be solved by investigating the effect of anode thickness, using anode materials with a thermal expansion coefficient closer to the one of the electrolyte or employing an anchoring technique of the porous anode on a porous YSZ layer previously deposited on the dense electrolyte substrate.

The following fabrication challenges were linked to the employed direct-writing apparatus. Variations in the planarity of substrate holder and electrolyte substrate have to be avoided, as a change in the distance between micronozzle and substrate changes the uniformity and width of the deposited structures for constant extrusion pressure and deposition speed. When depositing very short lines of a few millimeters only, the acceleration and deceleration of the micropositioning system reduce control over the homogeneity of the deposited structures. Low viscosity electrode inks necessitate very

low extrusion pressures (< 2 bar), which cannot be precisely adjusted with the available air-operated dispensing system. Observed pressure fluctuations during direct-write deposition can lead to variations in electrode dimensions such as width and thickness. Moreover, the I&J Fisnar micropositioning system has a minimum step size of 50 µm in x- and y-direction, making precise alignment and control of the interelectrode spacing difficult. Exact parallel alignment of the second electrode after the first one was already deposited and sintered was additionally complicated, as the electrolyte substrate had been removed from the micropositioning robot for the sintering of the first electrode, and the exact position of the substrate was lost. Therefore, immediate deposition of one electrode after another and cosintering were employed. This codeposition also enabled immediate reconstruction of the electrodes if the deposition was not satisfying.

9.1.3 Comparison of direct-write microfabrication of SC-µSOFCs with coplanar electrodes reported in the literature

Simultaneously to this project, a Korean group also proposed the direct-writing technique for SC-µSOFC fabrication [8, 21]. The main difference between their work and the work described in this thesis consists in the process characterization and tailoring. Detailed studies were presented in this thesis in order to characterize the effects of process parameters and ink rheology on homogeneity and uniformity of the deposited electrode patterns. A process map was established for identifying suitable combinations of extrusion pressure and deposition speed for the deposition of uniform electrode structures. Ink rheology was characterized as a function of particle loading, and for the viscoelastic inks, also for different ink compositions. Tailoring the ink viscosity and the process parameters permitted counterbalancing of the spreading of the Newtonian inks. The use of viscoelastic inks was proposed for the first time in this work for the direct-write microfabrication of coplanar microelectrodes and was shown to significantly improve the control of the dimensions of the deposited electrodes due to increased shape retention after deposition. Additionally, the direct-writing technique was employed to prove the feasibility of SC-µSOFCs with coplanar electrodes of complex geometries and to fabricate double-face cells with combilike anodes for studying the effects of current collection method. The smallest electrode widths achieved in this work

using the direct-writing technique were about six times smaller than the ones reported by the Korean group.

9.1.4 Alternative fabrication techniques

Direct-write microfabrication was shown to be a suitable technique for the creation of SC-μSOFCs with coplanar electrodes. Homogeneous electrode structures of controlled, uniform dimensions can be obtained when using viscoelastic inks. Another approach to achieve elevated shape retention and size control of the deposited structures consists of combining the direct-writing technique with micromachining. The electrode pattern could be micromachined into the electrolyte substrate by laser ablation, chemical etching, micromilling, etc. [129], and the created grooves could be filled with electrode inks by direct-writing. Newtonian inks could be suitable, as ink spreading is circumvented by retaining the deposited electrodes within the micromachined grooves. However, this approach adds another fabrication step, reduces the flexibility of direct-writing for creating different electrode shapes and sizes, and increases fabrication costs.

Deposition techniques such as thermal spraying or chemical vapor deposition could also be employed for fabricating SC-μSOFCs with coplanar electrodes. However, suitable masks are necessary not only for the desired electrode pattern but also to protect the already deposited electrode. Also thermal spraying techniques are generally used to deposited larger areas of material, and the small size of SC-μSOFCs might lead to a waste of material being deposited on the surrounding mask.

Finally, laser direct-writing could constitute an interesting approach for fabricating SC-μSOFCs with coplanar electrodes. As an alternative to lithography-based methods, laser direct-writing permits the creation of high-resolution patterns (down to 1-2 μm) and of porous microstructures [218]. Patterns of single component and multicomponent metal oxides were fabricated by laser direct-writing for electrochemical applications [218]. The problems of clogging and ink drying due to the use of an extrusion nozzle in conventional direct-writing are circumvented by employing a laser beam. Different variations of laser direct-writing exist where the laser is used to remove parts and shape deposited materials [218], to induce pyrolysis of a precursor film [219], to consolidate

dry powders deposited by direct-writing [220], or to pattern photoresponsive colloidal suspensions [221].

9.2 Discussion on SC-μSOFCs with coplanar electrodes

Although the concept of fuel cells with coplanar electrodes had already been proposed in 1965 [120], the first experimental proof of SC-SOFCs with coplanar electrodes was only provided in 1995 [157]. As a relatively recent technology, the number of studies reported in the literature is quite limited. Most of the studies focused on simple one electrode pair geometries and the effect of electrode width and interelectrode gap on cell performance [5, 6, 17, 21, 157]. Additionally, the influence of electrolyte roughness [5, 17], testing parameters such as gas mixing ratio [6, 13, 21], flow rate [21] and flow direction with respect to the electrode lines [6, 21] was investigated. Different microfabrication techniques were proposed to create patterns of interdigitated microelectrodes and the possibility to obtain a measurable power output from the fabricated micro cells was demonstrated [13, 20, 21, 98].

A variety of additional parameters affecting the functioning of SC-μSOFCs with coplanar electrodes was characterized in this work using the direct-writing technique for fabricating the necessary cells for the different studies. Notably, the observation of cell voltage and power stability issues with respect to electrode width led to the detection of miniaturization limits for SC-μSOFCs with a single pair of coplanar electrodes. For a constant electrode length, the electrode width principally determines the active electrode surface area. Under a certain size, the number of reaction sites is limited, and cell operation is not possible. Patterns of interdigitated, closely-spaced, microscale electrodes are to be employed in order to obtain stable cell performance with reduced ohmic losses. Furthermore, the effect of electrode shape and the feasibility of SC-μSOFCs with arbitrary, geometrically complex electrode structures were investigated. Due to the long conduction paths of the electrons within the comblike electrodes in interdigitated electrode geometries, current collection method significantly affects cell performance, and a quantitative study on its direct impact on ohmic resistance and power output was presented. For the first time the effect of electrolyte thickness on cell performance was investigated and preliminary results show that this parameter should not be neglected in cell design and fabrication. The effect of electrode and electrolyte

materials on the cell performance is difficult to be determined from studies presented in the literature because the use of different materials, cell sizes and testing conditions impedes direct comparison between the different studies. Therefore, a first study for cataloguing suitable material combinations of the three cell components was provided in this work by comparing different cells where only the material of one component was varied between each cell. This study also identified possible chemical interaction between adjacent anode and cathode materials during sintering.

The multitude of different parameters affecting the cell performance significantly complicates the understanding of the working principles of SC-μSOFCs with coplanar electrodes. Additionally, the effect of these parameters on the cell performance depends on cell component dimensions and compositions, as well as the testing setup and conditions. It is therefore difficult to compare results from one study reported in the literature to another. Instead of the exact impact of a parameter on cell functioning, a general behavior can be concluded from the different studies. For instance, cell power output increases with decreasing interelectrode gap.

To date, the working principles of SC-μSOFCs with coplanar electrodes are thus only vaguely understood because of the limited amount of comparable studies as well as the difficulties of fabrication and characterization. Exhaust gas analysis and impedance spectroscopy could give a further insight into the different mechanisms occurring in SC-μSOFCs with coplanar electrodes, but are handicapped because of the small size of these cells. A combination of both experimental work and modeling could be useful to further advance the understanding of this fuel cell technology. Future experimental work could continue exploring the different parameters affecting the cell performance that were identified in this thesis. Notably, current collection method needs to be improved, taking into account the small electrode size and the close vicinity of adjacent counter electrodes as well as the electrical conductivity of the electrode materials. Appropriate electrode and electrolyte material combinations should be identified in order to limit chemical interactions and enable stable cell performance. Further studies on the effect of electrolyte thickness on the cell performance should be conducted, while suitable models on the ionic conduction path between adjacent anodes and cathodes need to be developed. For more accurate performance predictions, FEM modeling of the ohmic polarization resistance and investigation of the

reaction kinetics, especially at the cathode side, under single-chamber operating conditions are necessary. Numerical models, that couple the gas flow around, over and between closely-spaced microelectrodes, the gas diffusion within the porous electrodes, the heterogeneous chemistry and the electrochemical reactions, should be established. Specifically, gas flow modeling could provide information on possible gas intermixing between adjacent anodes and cathodes and determine local gas composition, concentration, temperature and pressure gradients.

A major drawback of current SC-SOFCs is the lack of selective and stable electrode materials. Even in this thesis work, nickel-based anodes were shown to undergo oxidation-reduction cycles in methane-air mixtures during cell operation, and the loss of nickel is a problem known by the community. The catalytic activity of the electrode materials is currently studied in order to develop more selective materials that reduce the catalysis of undesired reactions and increase fuel utilization and cell efficiency of SC-SOFC systems. Cell efficiency and performance could also be improved by using cell stacks and employing the generated heat from the exothermic fuel reactions to thermally self-sustain the cells. If the use of fuel-air gas mixtures can be applied to solid electrolyte fuel cells operating at low temperatures, direct fuel oxidation reactions can be limited, allowing improved cell efficiency. In SC-μSOFCs with coplanar electrodes, the small electrode size and the small amount of available catalyst additionally reduce fuel utilization.

Potential applications of SC-μSOFCs with coplanar electrodes should benefit from the intrinsic properties of these cells, including their small size, the sealing-free cell design and the possibility of cell operation in fuel-air gas mixtures at elevated temperatures. The small size could enable integration with MEMS technology. Cells could be fabricated on the same silicon chip and directly power the adjacent electronic microdevices. Moreover, the cells could be employed as temperature, pressure or gas sensors in harsh industrial environments where gas mixtures at elevated temperatures are present. They could be placed as-fabricated inside gas tubes or chimneys by exposing the electrodes directly to the gas mixtures without any need for packaging design. Finally, energy harvesting applications such as in exhaust gas streams of vehicles could mitigate the low cell efficiency by producing energy from waste fuel gases.

Chapter 10 Conclusion and recommendations

SC-SOFCs with coplanar electrodes are a promising fuel cell design suitable for miniaturization and small-scale power applications. The use of closely-spaced microscale electrodes leads to a reduction of the ohmic cell resistance and increases the cell performance. However, the fabrication of SC-μSOFCs with coplanar microelectrodes needs to reconcile the small size of the electrodes, the construction of coplanar electrodes from multicomponent ceramic materials and the creation of porous electrode microstructures. In addition to the fabrication challenges, the working principles of these fuel cells are not completely explored.

In this thesis, a robot-controlled direct-write microfabrication method was used for the fabrication of SC-μSOFCs with coplanar electrodes. This technique circumvents the need for masks or molds and has the advantage of flexibility as to electrode material, size and shape. Direct-writing employs electrode inks or suspensions prepared from the respective electrode material in powder form and allows the creation of microscale electrode structures by extrusion of these inks through micronozzles and their robot-controlled deposition in the desired pattern on the electrolyte substrate. A subsequent sintering step leads to the consolidation of the deposited electrode patterns and enables tailoring of microstructure and porosity.

The objectives of this thesis have been realized through the achievement of the following original contributions:

Objective 1: *Fabrication of SC-μSOFCs with closely-spaced, interdigitated coplanar electrodes by robot-controlled direct-writing.* The suitability of the direct-writing technique for fabricating SC-μSOFCs with coplanar electrodes was demonstrated by the successful fabrication of coplanar microscale electrodes of different size and geometry. After sintering, the electrodes exhibited a homogeneous, porous microstructure. The direct-writing process was characterized in detail with respect to the effects of the process parameters, extrusion pressure and deposition speed, on the uniformity of the deposited electrode structures in the form of process maps. Additionally, the effect of particle loading and ink composition on ink rheology and extrusion behavior during direct-writing was investigated. Two sets of inks of different

rheological behavior, that is, Newtonian and viscoelastic inks, were fabricated, characterized and evaluated with respect to their applicability for the direct-write microfabrication of SC-μSOFCs with coplanar electrodes. The viscoelastic inks were shown to enable better shape retention of the deposited electrode structures as compared with Newtonian inks and led to enhanced control of the electrode dimensions.

Objective 2: *Electrochemical characterization of the fabricated SC-μSOFCs with coplanar electrodes.* The measurement of a power output in the mW range for the fabricated cells confirmed the feasibility of SC-μSOFCs with coplanar interdigitated electrodes by direct-writing and their suitability for small- and microscale fuel cell applications.

Objective 3: *Characterization of the effect of electrode size on cell performance.* SC-μSOFCs with single electrode pairs of different width were fabricated by direct-writing and their electrochemical testing enabled the identification of miniaturization limits with respect to the electrode width. A minimum or critical electrode width was observed for cells with one electrode pair, below which the available electrode surface area was too small to enable the generation of an open circuit voltage. Cells with electrode widths near the critical size exhibited a non-zero, but highly fluctuating OCV, whereas only larger electrodes delivered a stable voltage and power output. When combining electrode pairs with dimensions below the critical width in closely-spaced interdigitated electrode structures, the voltage instability could be overcome by the increased electrode area, while at the same time the small electrode widths and interelectrode gaps permit reduction of the ohmic cell resistance.

Objective 4: *Feasibility of SC-μSOFCs with coplanar electrodes of arbitrary, complex geometries.* The direct-write microfabrication and electrochemical characterization of SC-μSOFCs with electrodes of geometrically complex shape provided a proof of concept of the feasibility of nonconventional, arbitrary electrode

geometries. Additionally, cell performance was shown to be not significantly affected by electrode shape for similar electrode dimensions.

Objective 5: *Study of additional parameters affecting cell performance of SC-μSOFCs with coplanar electrodes.* The impact of current collection method on the cell performance of SC-μSOFCs with coplanar comblike electrodes was investigated by using a double-face cell configuration with planar cathode and comblike anode on opposite sides of the electrolyte. Collecting the current on the whole anode surface area led to a 50% higher power output as compared to current collection on the anode connecting line. Increasing the conductivity of the Ni-based anode by increasing the nickel content did not improve current collection and cell power output, but induced voltage instabilities and cell degradation due to enhanced oxidation-reduction cycles of the nickel-based anode and nickel loss.

In order to investigate the effect of electrode material on cell performance, cells with combinations of two different anode and two different cathode materials were characterized. Cells with NiO-YSZ anodes and LSM-based cathodes delivered the highest OCV and power output. However, chemical interaction between the closely-spaced anodes and LSM-based cathodes was observed due to the presence of manganese in the anode, which probably resulted from diffusion of manganese from the cathode into the anode during sintering.

Finally, a first experimental demonstration of electrolyte thickness affecting cell performance was provided. For cells with interdigitated electrode patterns of similar dimensions, the use of a 0.5 mm thick YSZ electrolyte substrate led to a twice as high peak power density as compared to a 0.2 mm thick electrolyte.

Objective 6: *Calculation of the theoretical cell performance with respect to performance prediction and establishing design guidelines.* The theoretical cell performance of SC-μSOFCs with coplanar electrodes was calculated using a simplified electrochemistry-based model, which permitted calculation of the cell performance in good agreement with the experimentally measured values for SC-μSOFCs with one pair of coplanar electrodes. However, this model does not enable reliable performance

prediction for cells with very large electrodes or interdigitated electrode patterns. A more complex model would be required where the ohmic voltage losses are determined by FEM modeling and the electrochemistry is coupled with gas transport around and through the electrodes. Additionally, existing models on the ionic conduction between coplanar electrodes need to be reviewed, and activation polarization under single-chamber operation conditions needs to be further investigated.

The obtained results on both fabrication and characterization of SC-μSOFCs with coplanar electrodes constitute an important step forward to improve the feasibility of these fuel cells and the understanding of their working principles. At the same time they also point out the necessity for further studies. With optimization of the existing and the development of new fabrication techniques, additional characterization of these fuel cells will be possible and permit improvement of their performance. Future direct-write fabrication should concentrate on the use of viscoelastic electrode inks in order to enable enhanced control of the electrode dimensions and interelectrode gaps. Experimental studies on SC-μSOFCs with coplanar electrodes should target the identification of the optimal electrode dimensions and geometries, find the general optimal operating conditions and establish efficient current collection methods. Modeling could provide backup for these studies in the form of cell performance prediction as a function of cell size and operating conditions. Ionic conduction and electrode reaction mechanisms could be determined by modeling. Selectivity of the electrode materials for the respective electrode reactions needs to be improved, and cell efficiency and potential applications will significantly depend on the development of more selective materials, which should also exhibit sufficient stability in both oxidizing and reducing environments. The low inherent cell efficiency and fuel utilization of current SC-SOFCs remains an important technical hurdle for their practical implementation. Potential applications could include preheating and reforming systems, sensors or energy harvesting devices where the following properties of SC-SOFCs could be valued: single gas chamber design, absence of gas-tight sealing, small size, thermally self-sustainable system, capacity for hydrocarbon reforming, and heat and power generation from gas mixtures at elevated temperatures and under harsh environments.

Although Jules Verne's visionary idea on the use of hydrogen from water as fuel for future energy production mainly referred to energy generation at the power plant scale or in transportation, where fossil fuels are still our primary energy sources, fuel cells generating electrical power by electrochemically combining hydrogen and oxygen are also very interesting candidates for small-scale applications. They promise ease for miniaturization, high volumetric energy densities and continuous operation with quick refueling. Single-chamber fuel cells especially meet the design criteria for compact, small-scale power generating devices. Today we are still far from completely replacing fossil fuel based energy sources by alternative, environmentally friendly energy systems and a combination of existing energy sources seems more realistic. SC-SOFCs could be used in combination with fossil fuel based energy generation, as exhaust gases are present everywhere, both at the larger and the smaller scale such as in industrial exhaust chimneys, residential gas exhaust systems and vehicle exhaust pipes. Harvesting energy from waste gases by using SC-SOFC technology could reduce the emission of green house gases like methane while simultaneously generating electricity for more efficient and cleaner energy production.

References

[1] C. K. Dyer, "Fuel cells for portable applications," *Journal of Power Sources*, vol. 106, pp. 31-34, 2002.

[2] S. Tasa and T. Aapro, "Fuel cells as energy sources for future mobile devices," in *Transactions of the ASME*, vol. 3, pp. 492-494, 2006.

[3] G. J. La O', H. J. In, E. Crumlin, G. Barbastathis, and Y. Shao-Horn, "Recent advances in microdevices for electrochemical energy conversion and storage," *International Journal of Energy Research*, vol. 31, pp. 548-575, 2007.

[4] T. Hibino and H. Iwahara, "Simplification of solid oxide fuel cell systems using partial oxidation of methane," *Chemistry Letters*, vol. 7, pp. 1131-1134, 1993.

[5] T. Hibino, K. Ushiki, and Y. Kuwahara, "New concept for simplifying SOFC system," *Solid State Ionics*, vol. 91, pp. 69-74, 1996.

[6] X. Jacques-Bedard, T. W. Napporn, R. Roberge, and M. Meunier, "Coplanar electrodes design for a single-chamber SOFC: Assessment of the operating parameters," *Journal of The Electrochemical Society*, vol. 154, pp. B305-B309, 2007.

[7] J. Fleig, H. L. Tuller, and J. Maier, "Electrodes and electrolytes in micro-SOFCs: A discussion of geometrical constraints," *Solid State Ionics*, vol. 174, pp. 261-270, 2004.

[8] S.-J. Ahn, Y.-B. Kim, J. Moon, J.-H. Lee, and J. Kim, "Co-planar type single chamber solid oxide fuel cell with micro-patterned electrodes," *Journal of Electroceramics*, vol. 17, pp. 689-693, 2006.

[9] N. Q. Minh and T. Takahashi, *Science and technology of ceramic fuel cells*, Amsterdam: Elsevier, 1995.

[10] T. Napporn, F. Morin, and M. Meunier, "Evaluation of the actual working temperature of a single-chamber SOFC," *Electrochemical and Solid-State Letters*, vol. 7, pp. A60-A62, 2004.

[11] M. Yano, A. Tomita, M. Sano, and T. Hibino, "Recent advances in single-chamber solid oxide fuel cells: A review," *Solid State Ionics*, vol. 177, pp. 3351-3359, 2007.

[12] X. Jacques-Bedard, T. W. Napporn, R. Roberge, and M. Meunier, "Performance and ageing of an anode-supported SOFC operated in single-chamber conditions," *Journal of Power Sources*, vol. 153, pp. 108-113, 2006.

[13] B. E. Buergler, M. Ochsner, S. Vuillemin, and L. J. Gauckler, "From macro- to micro-single chamber solid oxide fuel cells," *Journal of Power Sources*, vol. 171, pp. 310-320, 2007.

[14] M. Liu, Z. Lu, B. Wei, R. Zhu, X. Huang, K. Chen, G. Ai, and W. Su, "Anode-supported micro-SOFC stacks operated under single-chamber conditions," *Journal of The Electrochemical Society*, vol. 154, pp. B588-B592, 2007.

[15] Z. Shao, S. M. Haile, J. Ahn, P. D. Ronney, Z. Zhan, and S. A. Barnett, "A thermally self-sustained micro solid-oxide fuel-cell stack with high power density," *Nature*, vol. 435, pp. 795-798, 2005.

[16] M. Yano, M. Nagao, K. Okamoto, A. Tomita, Y. Uchiyama, N. Uchiyama, and T. Hibino, "A single-chamber SOFC stack operating in engine exhaust," *Electrochemical and Solid-State Letters*, vol. 11, pp. B29-B33, 2008.

[17] T. Hibino, A. Hashimoto, M. Suzuki, M. Yano, S.-I. Yoshida, and M. Sano, "A solid oxide fuel cell with a novel geometry that eliminates the need for preparing a thin electrolyte film," *Journal of the Electrochemical Society*, vol. 149, pp. A195-A200, 2002.

[18] C.-Y. Chung and Y.-C. Chung, "Performance characteristics of micro single-chamber solid oxide fuel cell: Computational analysis," *Journal of Power Sources*, vol. 154, pp. 35-41, 2006.

[19] S. M. Haile, "Fuel cell materials and components," *Acta Materialia*, vol. 51, pp. 5981-6000, 2003.

[20] S.-J. Ahn, J.-H. Lee, J. Kim, and J. Moon, "Single-chamber solid oxide fuel cell with micropatterned interdigitated electrodes," *Electrochemical and Solid-State Letters*, vol. 9, pp. A228-A231, 2006.

[21] S.-J. Ahn, Y.-B. Kim, J. Moon, J.-H. Lee, and J. Kim, "Influence of patterned electrode geometry on performance of co-planar type single chamber SOFC," *Journal of Power Sources*, vol. 171, pp. 511-516, 2007.

[22] J. A. Lewis, J. E. Smay, J. Stuecker, and J. Cesarano, "Direct ink writing of three-dimensional ceramic structures," *Journal of the American Ceramic Society*, vol. 89, pp. 3599-3609, 2006.

[23] J. A. Lewis, "Direct ink writing of 3D functional materials," *Advanced Functional Materials*, vol. 16, pp. 2193-2204, 2006.

[24] M. Kuhn, T. Napporn, M. Meunier, S. Vengallatore, and D. Therriault, "Direct-write microfabrication of single-chamber micro solid oxide fuel cells," *Journal of Micromechanics and Microengineering*, vol. 18, pp. 015005, 2008.

[25] M. Kuhn, T. Napporn, M. Meunier, D. Therriault, and S. Vengallatore, "Fabrication and testing of coplanar single-chamber micro solid oxide fuel cells with geometrically complex electrodes," *Journal of Power Sources*, vol. 177, pp. 148-153, 2008.

[26] M. Kuhn, T. W. Napporn, M. Meunier, and D. Therriault, "Experimental study of current collection in single-chamber micro solid oxide fuel cells with comblike electrodes," *Journal of The Electrochemical Society*, vol. 155, pp. B994-B1000, 2008.

[27] X. Li, *Principles of fuel cells,* New York: Taylor & Francis Group, 2006.

[28] J. Larminie and A. Dicks, *Fuel cell systems explained*, Chichester: John Wiley & Sons, 2000.

[29] K. Kordesch and G. Simader, *Fuel cells and their applications*, Weinheim: VCH, 1996.

[30] W. R. Grove, "On voltaic series and the combination of gases by platinum," *London and Edinburgh Philosophical Magazine and Journal of Sciences*, vol. 14, pp. 127-130, 1839.

[31] W. R. Grove, "On a gaseous voltaic battery," *London and Edinburgh Philosophical Magazine and Journal of Sciences*, vol. 3, pp. 417-420, 1842.

[32] E. Baur and H. Preis, "Ueber Brennstoff-Ketten mit Festleitern," *Zeitschrift fuer Elektrochimie und angewandte physikalische Chemie*, vol. 43, pp. 727-732, 1937.

[33] E. P. Murray, T. Tsai, and S. A. Barnett, "A direct-methane fuel cell with a ceria-based anode," *Nature*, vol. 400, pp. 649-651, 1999.

[34] B. C. H. Steele, "Running on natural gas," *Nature*, vol. 400, pp. 620-621, 1999.

[35] S. Park, J. M. Vohs, and R. J. Gorte, "Direct oxidation of hydrocarbons in a solid oxide fuel cell," *Nature*, vol. 404, pp. 265-267, 2000.

[36] W. Vielstich, A. Lamm, and H. A. Gasteiger, *Handbook of fuel cells: fundamentals, technology and applications. Volume 1, Fundamentals and survey of systems*, Chichester: Wiley, 2003.

[37] N. Q. Minh, "Solid oxide fuel cell technology - features and applications," *Solid State Ionics*, vol. 174, pp. 271-277, 2004.

[38] W. G. Coors, "Protonic ceramic fuel cells for high-efficiency operation with methane," *Journal of Power Sources*, vol. 118, pp. 150-156, 2003.

[39] B. E. Buergler, A. N. Grundy, and L. J. Gauckler, "Thermodynamic equilibrium of single-chamber SOFC relevant methane-air mixtures," *Journal of The Electrochemical Society*, vol. 153, pp. A1378-A1385, 2006.

[40] L. J. Gauckler, D. Beckel, B. E. Buergler, E. Jud, U. P. Muecke, M. Prestat, J. L. M. Rupp, and J. Richter, "Solid oxide fuel cells: Systems and materials," *Chimia*, vol. 58, pp. 837-850, 2004.

[41] J. W. Fergus, "Electrolytes for solid oxide fuel cells," *Journal of Power Sources*, vol. 162, pp. 30-40, 2006.

[42] A. Grosjean, O. Sanseau, V. Radmilovic, and A. Thorel, "Reactivity and diffusion between $La_{0.8}Sr_{0.2}MnO_3$ and ZrO_2 at interfaces in SOFC cores by TEM analyses on FIB samples," *Solid State Ionics*, vol. 177, pp. 1977-1980, 2006.

[43] A. Mitterdorfer and L. J. Gauckler, "$La_2Zr_2O_7$ formation and oxygen reduction kinetics of the $La_{0.85}Sr_{0.15}Mn_yO_3$, O_2(g) YSZ system," *Solid State Ionics*, vol. 111, pp. 185-218, 1998.

[44] J.-Y. Park, H. Yoon, and E. D. Wachsman, "Fabrication and characterization of high-conductivity bilayer electrolytes for intermediate-temperature solid oxide fuel cells," *Journal of the American Ceramic Society*, vol. 88, pp. 2402-2408, 2005.

[45] A. Tomita, T. Hibino, and M. Sano, "Surface modification of a doped $BaCeO_3$ to function as an electrolyte and as an anode for SOFCs," *Electrochemical and Solid-State Letters*, vol. 8, pp. 333-336, 2005.

[46] A. Weber and E. Ivers-Tiffee, "Materials and concepts for solid oxide fuel cells (SOFCs) in stationary and mobile applications," *Journal of Power Sources*, vol. 127, pp. 273-283, 2004.

[47] H. L. Tuller and A. S. Nowick, "Doped ceria as a solid oxide electrolyte," *Journal of The Electrochemical Society*, vol. 122, pp. 255-259, 1975.

[48] J. Pena-Martinez, D. Marrero-Lopez, J. C. Ruiz-Morales, C. Savaniu, P. Nunez, and J. T. S. Irvine, "Anodic performance and intermediate temperature fuel cell testing of $La_{0.75}Sr_{0.25}Cr_{0.5}Mn_{0.5}O_{3-\delta}$ at lanthanum gallate electrolytes," *Chemistry of Materials*, vol. 18, pp. 1001-1006, 2006.

[49] T. Ishihara, M. Honda, T. Shibayama, H. Minami, H. Nishiguchi, and Y. Takita, "Intermediate temperature solid oxide fuel cells using a new $LaGaO_3$ based oxide ion conductor," *Journal of The Electrochemical Society*, vol. 145, pp. 3177-3183, 1998.

[50] H. Iwahara, T. Hibino, and T. Yajima, "Studies on proton conducting ceramics based on perovskite-type oxides," *Nippon Kagaku Kaishi*, vol. 9, pp. 1003-1011, 1993.

[51] R. J. Gorte, "Recent developments towards commercialization of solid oxide fuel cells," *AIChE Journal*, vol. 51, pp. 2377-2381, 2005.

[52] L. Jia, Z. Lu, J. Miao, Z. Liu, G. Li, and W. Su, "Effects of pre-calcined YSZ powders at different temperatures on Ni-YSZ anodes for SOFC," *Journal of Alloys and Compounds*, vol. 414, pp. 152-157, 2006.

[53] D. W. Dees, T. D. Claar, T. E. Easler, D. C. Fee, and F. C. Mrazek, "Conductivity of porous Ni/ZrO_2-Y_2O_3 cermets," *Journal of The Electrochemical Society*, vol. 134, pp. 2141-2146, 1987.

[54] C. Sun and U. Stimming, "Recent anode advances in solid oxide fuel cells," *Journal of Power Sources*, vol. 171, pp. 247-260, 2007.

[55] C. M. Finnerty, N. J. Coe, R. H. Cunningham, and R. M. Ormerod, "Carbon formation on and deactivation of nickel-based/zirconia anodes in solid oxide fuel cells running on methane," *Catalysis Today*, vol. 46, pp. 137-145, 1998.

[56] J.-H. Koh, Y.-S. Yoo, J.-W. Park, and H. C. Lim, "Carbon deposition and cell performance of Ni-YSZ anode support SOFC with methane fuel," *Solid State Ionics*, vol. 149, pp. 157-166, 2002.

[57] M. D. Gross, J. M. Vohs, and R. J. Gorte, "Recent progress in SOFC anodes for direct utilization of hydrocarbons," *Journal of Materials Chemistry*, vol. 17, pp. 3071-3077, 2007.

[58] A. Lashtabeg and S. J. Skinner, "Solid oxide fuel cells - a challenge for materials chemists?," *Journal of Materials Chemistry*, vol. 16, pp. 3161-3170, 2006.

[59] D. M. Bastidas, T. Shanwen, and J. T. S. Irvine, "A symmetrical solid oxide fuel cell demonstrating redox stable perovskite electrodes," *Journal of Materials Chemistry*, vol. 16, pp. 1603-1605, 2006.

[60] Y.-H. Huang, R. I. Dass, Z.-L. Xing, and J. B. Goodenough, "Double perovskites as anode materials for solid-oxide fuel cells," *Science*, vol. 312, pp. 254, 2006.

[61] R. Kikuchi, N. Koashi, T. Matsui, K. Eguchi, and T. Norby, "Novel anode materials for multi-fuel applicable solid oxide fuel cells," *Journal of Alloys and Compounds: Proceedings of the Rare Earths'04 in Nara, Japan*, vol. 408-412, pp. 622-627, 2006.

[62] J. P. P. Huijsmans, "Ceramics in solid oxide fuel cells," *Current Opinion in Solid State and Materials Science*, vol. 5, pp. 317-323, 2001.

[63] F. S. Baumann, J. Fleig, M. Konuma, U. Starke, H.-U. Habermeier, and J. Maier, "Strong performance improvement of $La_{0.6}Sr_{0.4}Co_{0.8}Fe_{0.2}O_{3-\delta}$ SOFC cathodes by electrochemical activation," *Journal of The Electrochemical Society*, vol. 152, pp. 2074-2079, 2005.

[64] H.-C. Yu, F. Zhao, A. V. Virkar, and K.-Z. Fung, "Electrochemical characterization and performance evaluation of intermediate temperature solid oxide fuel cell with $La_{0.75}Sr_{0.25}CuO_{2.5-\delta}$ cathode," *Journal of Power Sources*, vol. 152, pp. 22-26, 2005.

[65] Z. Shao and S. M. Haile, "A high-performance cathode for the next generation of solid-oxide fuel cells," *Nature*, vol. 431, pp. 170-173, 2004.

[66] C. Xia, Y. Zhang, and M. Liu, "Composite cathode based on yttria stabilized bismuth oxide for low-temperature solid oxide fuel cells," *Applied Physics Letters*, vol. 82, pp. 901-904, 2003.

[67] N. Q. Minh, "Ceramic fuel cells," *Journal of the American Ceramic Society*, vol. 76, pp. 563-588, 1993.

[68] F. J. Gardner, M. J. Day, N. P. Brandon, M. N. Pashley, and M. Cassidy, "SOFC technology development at Rolls-Royce," *Journal of Power Sources*, vol. 86, pp. 122-129, 2000.

[69] M. Horiuchi, S. Suganuma, and M. Watanabe, "Electrochemical power generation directly from combustion flame of gases, liquids, and solids," *Journal of The Electrochemical Society*, vol. 151, pp. A1402-A1405, 2004.

[70] H. Kronemayer, D. Barzan, M. Horiuchi, S. Suganuma, Y. Tokutake, C. Schulz, and W. G. Bessler, "A direct-flame solid oxide fuel cell (DFFC) operated on methane, propane, and butane," *Journal of Power Sources*, vol. 166, pp. 120-126, 2007.

[71] K. Wang, R. Ran, Y. Hao, Z. Shao, W. Jin, and N. Xu, "A high-performance no-chamber fuel cell operated on ethanol flame," *Journal of Power Sources*, vol. 177, pp. 33-39, 2008.

[72] A. Kundu, J. H. Jang, J. H. Gil, C. R. Jung, H. R. Lee, S. H. Kim, B. Ku, and Y. S. Oh, "Micro-fuel cells--Current development and applications," *Journal of Power Sources*, vol. 170, pp. 67-78, 2007.

[73] V. T. Srikar, K. T. Turner, T. Y. A. Ie, and S. M. Spearing, "Structural design considerations for micromachined solid-oxide fuel cells," *Journal of Power Sources*, vol. 125, pp. 62-69, 2004.

[74] D. Nikbin, "Micro SOFCs: why small is beautiful," *Fuel Cell Review*, vol. 3, pp. 21-24, 2006.

[75] J. S. Wainright, R. F. Savinell, C. C. Liu, and M. Litt, "Microfabricated fuel cells," *Electrochimica Acta*, vol. 48, pp. 2869-2877, 2003.

[76] Y.-B. Kim, S.-J. Ahn, J. Moon, J. Kim, and H.-W. Lee, "Direct-write fabrication of solid oxide fuel cells," in *ECS Transactions - 9th International Symposium on Solid Oxide Fuel Cells, SOFC-IX, Québec, Canada, May 15-20, 2005*, vol. 2005-07, pp. 489-494, 2005.

[77] C. Finnerty and G. Spacht, "Solid oxide fuel cell development," *Fuel Cell Magazine*, vol. 6, pp. 28-32, 2006.

[78] D.-W. Shin, R.-H. Song, D.-H. Peck, D.-H. Jung, and D.-R. Shin, "Fabrication and performance of micro tube SOFC by coating nano suspension," in *Solid State Ionics: The Science and Technology of Ions in Motion, Proceedings of the 9th Asian Conference, Jeju Island, Republic of Korea, June 6-11, 2004*, pp. 271-279, 2004.

[79] P. Jasinski, "Micro solid oxide fuel cells and their fabrication methods," *Microelectronics International*, vol. 25, pp. 42-48, 2008.

[80] S. Rey-Mermet and P. Muralt, "Materials and design study for micromachined solid oxide fuel cells membranes," in *Materials Research Society Symposium Proceedings*, vol. 972, Solid-State Ionics-2006, pp. 217-223, 2007.

[81] H. Huang, M. Nakamura, P. Su, R. Fasching, Y. Saito, and F. B. Prinz, "High-performance ultrathin solid oxide fuel cells for low-temperature operation," *Journal of The Electrochemical Society*, vol. 154, pp. B20-B24, 2007.

[82] A. Bieberle-Hutter, D. Beckel, A. Infortuna, U. P. Muecke, J. L. M. Rupp, L. J. Gauckler, S. Rey-Mermet, P. Muralt, N. R. Bieri, N. Hotz, M. J. Stutz, D. Poulikakos, P. Heeb, P. Muller, A. Bernard, R. Gmur, and T. Hocker, "A micro-solid oxide fuel cell system as battery replacement," *Journal of Power Sources*, vol. 177, pp. 123-130, 2008.

[83] D. Beckel, A. Bieberle-Hutter, A. Harvey, A. Infortuna, U. P. Muecke, M. Prestat, J. L. M. Rupp, and L. J. Gauckler, "Thin films for micro solid oxide fuel cells," *Journal of Power Sources*, vol. 173, pp. 325-345, 2007.

[84] J. L. Hertz and H. L. Tuller, "Electrochemical characterization of thin films for a micro-solid oxide fuel cell," *Journal of Electroceramics*, vol. 13, pp. 663-668, 2004.

[85] C. D. Baertsch, K. F. Jensen, J. L. Hertz, H. L. Tuller, S. T. Vengallatore, S. M. Spearing, and M. A. Schmidt, "Fabrication and structural characterization of self-supporting electrolyte membranes for a micro solid-oxide fuel cell," *Journal of Materials Research*, vol. 19, pp. 2604-2615, 2004.

[86] H. L. Tuller, "Integration of solid state ionics and electronics: sensors and power sources," *Journal of the Ceramic Society of Japan*, vol. 112, pp. S1093-S1098, 2004.

[87] Y. Tang, K. Stanley, J. Wu, D. Ghosh, and J. Zhang, "Design consideration of micro thin film solid-oxide fuel cells," *Journal of Micromechanics and Microengineering*, vol. 15, pp. S185-S192, 2005.

[88] W. Vielstich, A. Lamm, and H. A. Gasteiger, *Handbook of fuel cells: fundamentals, technology and applications. Volume 3, Fuel cell technology and applications, part 1*, Chichester: Wiley, 2003.

[89] M. Mogensen and K. Kammer, "Conversion of hydrocarbons in solid oxide fuel cells," *Annual Review of Materials Research*, vol. 33, pp. 321-331, 2003.

[90] Z. Zhan, J. Liu, and S. A. Barnett, "Operation of anode-supported solid oxide fuel cells on propane-air fuel mixtures," *Applied Catalysis A: General*, vol. 262, pp. 255-259, 2004.

[91] B. E. Buergler, "Single chamber solid oxide fuel cells," Ph.D. thesis, ETH, Zurich, Switzerland, 2006.

[92] T. Hibino, S. Wang, S. Kakimoto, and M. Sano, "Single chamber solid oxide fuel cell constructed from an yttria-stabilized zirconia electrolyte," *Electrochemical and Solid-State Letters*, vol. 2, pp. 317-319, 1999.

[93] L. Bay, T. Horita, N. Sakai, M. Ishikawa, K. Yamaji, and H. Yokokawa, "Hydrogen solubility in Pr-doped and un-doped YSZ for a one chamber fuel cell," *Solid State Ionics*, vol. 113-115, pp. 363-367, 1998.

[94] K. Asano, T. Hibino, and H. Iwahara, "SOFC for chemical cogeneration using fuel-air mixed gas," in *ECS Transactions - 4th International Symposium on Solid Oxide Fuel Cells, SOFC-IV, Yokohama, Japan, 18-23 June*, 1995, pp. 58-66, 1995.

[95] N. X. P. Vo, S. P. Yoon, S. W. Nam, J. Han, T.-H. Lim, and S.-A. Hong, "Fabrication of an anode-supported SOFC with a sol-gel coating method for a mixed-gas fuel cell," *Key Engineering Materials*, vol. 277-279, pp. 455-462, 2005.

[96] S. Raz, M. J. G. Jak, J. Schoonman, and I. Riess, "Supported mixed-gas fuel cells," *Solid State Ionics*, vol. 149, pp. 335-341, 2002.

[97] I. Riess, "The significance of impeded reactions in solid state electrochemistry," *Solid State Ionics*, vol. 176, pp. 1667-1674, 2005.

[98] S. P. Yoon, H. J. Kim, B.-T. Park, S. W. Nam, J. Han, T.-H. Lim, and S.-A. Hong, "Mixed-fuels fuel cell running on methane-air mixture," *Journal of Fuel Cell Science and Technology*, vol. 3, pp. 83-86, 2006.

[99] G. A. Louis, J. M. Lee, D. L. Maricle, and J. C. Trocciola, "Solid electrolyte electrochemical cell," *US patent*, US4248941, 1981. [Online]. Available: http://patft.uspto.gov. [Consulted: May 20, 2006].

[100] A. K. Shukla, R. K. Raman, and K. Scott, "Advances in mixed-reactant fuel cells," *Fuel Cells*, vol. 4, pp. 436-447, 2005.

[101] I. Riess, "On the single chamber solid oxide fuel cells," *Journal of Power Sources*, vol. 175, pp. 325-337, 2008.

[102] M. A. Priestnall, V. P. Kotzeva, D. J. Fish, and E. M. Nilsson, "Compact mixed-reactant fuel cells," *Journal of Power Sources*, vol. 106, pp. 21-30, 2002.

[103] T. Hibino and S. Kakimoto, "Single room type solid electrolyte fuel cell and its manufacturing method," *Japanese patent*, JP2002280015A, 2002. [Online]. Available: http://ep.espacenet.com. [Consulted: June 6, 2006].

[104] M. Goedickemeier, D. Nussbaum, C. Kleinlogel, and L. J. Gauckler, "Solid oxide fuel cells with reaction-selective electrodes," in *192nd Meeting of the Electrochemical Society*, 1997.

[105] T. W. Napporn, X. Jacques-Bedard, F. Morin, and M. Meunier, "Operating conditions of a single-chamber SOFC," *Journal of The Electrochemical Society*, vol. 151, pp. A2088-A2094, 2004.

[106] T. Hibino, A. Hashimoto, T. Inoue, J.-i. Tokuno, S.-i. Yoshida, and M. Sano, "A solid oxide fuel cell using an exothermic reaction as the heat source," *Journal of The Electrochemical Society*, vol. 148, pp. A544-A549, 2001.

[107] B. Morel, R. Roberge, S. Savoie, T. W. Napporn, and M. Meunier, "Temperature and performance variations along single chamber solid oxide fuel cells," *Journal of Power Sources*, vol. 186, pp. 89-95, 2009.

[108] T. Hibino, A. Hashimoto, T. Inoue, J.-i. Tokuno, S.-i. Yoshida, and M. Sano, "A low-operating-temperature solid oxide fuel cell in hydrocarbon-air mixtures," *Science*, vol. 288, pp. 2031-2033, 2000.

[109] P. Jasinski, T. Suzuki, Z. Byars, F. Dogan, and H. U. Anderson, "Comparison of anode and electrolyte support configuration of single-chamber SOFC," in *ECS Transactions - 8th International Symposium on Solid Oxide Fuel Cells, SOFC-VIII, Paris, France, 27 Apr - 2 May, 2003*, vol. 2003-7, pp. 1101-1108, 2003.

[110] Z. Shao, C. Kwak, and S. M. Haile, "Anode-supported thin-film fuel cells operated in a single chamber configuration 2T-I-12," *Solid State Ionics*, vol. 175, pp. 39-46, 2004

[111] T. Hibino, A. Hashimoto, T. Inoue, J.-i. Tokuno, S.-i. Yoshida, and M. Sano, "Single-chamber solid oxide fuel cells at intermediate temperatures with various

hydrocarbon-air mixtures," *Journal of The Electrochemical Society*, vol. 147, pp. 2888-2892, 2000.

[112] M. Yano, T. Kawai, K. Okamoto, M. Nagao, M. Sano, A. Tomita, and T. Hibino, "Single-chamber SOFCs using dimethyl ether and ethanol," *Journal of The Electrochemical Society*, vol. 154, pp. B865-B870, 2007.

[113] T. Ishihara and Y. Takita, "Partial oxidation of methane into syngas with oxygen permeating ceramic membrane reactors," *Catalysis Surveys from Japan*, vol. 4, pp. 125-133, 2001.

[114] V. R. Choudhary, V. H. Rane, and A. M. Rajput, "Selective oxidation of methane to CO and H_2 over unreduced NiO-rare earth oxide catalysts," *Catalysis Letters*, vol. 22, pp. 289-297, 1993.

[115] D. Dissanayake, M. P. Rosynek, K. C. C. Kharas, and J. H. Lunsford, "Partial oxidation of methane to carbon monoxide and hydrogen over a Ni/Al_2O_3 catalyst," *Journal of Catalysis*, vol. 132, pp. 117-127, 1991.

[116] T. Hibino, A. Hashimoto, K. Asano, M. Yano, M. Suzuki, and M. Sano, "An intermediate-temperature solid oxide fuel cell providing higher performance with hydrocarbons than with hydrogen," *Electrochemical and Solid-State Letters*, vol. 5, pp. A242-A244, 2002.

[117] A. T. Ashcroft, A. K. Cheetham, J. S. Foord, M. L. H. Green, C. P. Grey, and et al., "Selective oxidation of methane to synthesis gas using transition metal catalysts," *Nature*, vol. 344, pp. 319, 1990.

[118] P. M. Torniainen, X. Chu, and L. D. Schmidt, "Comparison of monolith-supported metals for the direct oxidation of methane to syngas," *Journal of Catalysis*, vol. 146, pp. 1-10, 1994.

[119] W. Wang, L. Zhang, and S. P. Jiang, "Potential oscillation of methane oxidation reaction on $(La_{0.75}Sr_{0.25})(Cr_{0.5}Mn_{0.5})O_3$ electrodes of solid oxide fuel cells," *Journal of Power Sources*, vol. 178, pp. 92-96, 2008.

[120] W. van Gool, "The possible use of surface migration in fuel cells and heterogeneous catalysis," *Philips Research Reports*, vol. 20, pp. 81-93, 1965.

[121] T. Hibino, S. Wang, S. Kakimoto, and M. Sano, "One-chamber solid oxide fuel cell constructed from a YSZ electrolyte with a Ni anode and LSM cathode," *Solid State Ionics*, vol. 127, pp. 89-98, 2000.

[122] K. Asano, T. Hibino, and H. Iwahara, "A novel solid oxide fuel cell system using the partial oxidation of methane," *Journal of The Electrochemical Society*, vol. 142, pp. 3241-3245, 1995.

[123] I. Riess, P. J. van der Put, and J. Schoonman, "Solid oxide fuel cells operating on uniform mixtures of fuel and air," *Solid State Ionics*, vol. 82, pp. 1-4, 1995.

[124] M. G. Zabetakis, "Flammability characteristics of combustible gases and vapors," *U.S. Department of the Interior, Bureau of Mines*, Bulletin 627, 1965.

[125] D. A. Crowl, *Understanding explosions*, New York: Wiley-AIChE, 2003.

[126] H. C. Kim, J. K. Park, H. W. Lee, J. H. Lee, J. S. Kim, J. W. Son, and S. H. Choi, "Single chamber solid oxide fuel cell with isolated electrolyte," *Korean patent*, WO2007073015-A1, 2007. [Online]. Available: http://ep.espacenet.com. [Consulted: March 8, 2008].

[127] L. N. Van Rij, J. Le, R. C. Van Landschoot, and J. Schoonman, "A novel Ni-CERMET electrode based on a proton conducting electrolyte," *Journal of Materials Science*, vol. 36, pp. 1069-1076, 2001.

[128] A. Tomita, Y. Namekata, M. Nagao, and T. Hibino, "Room-temperature hydrogen sensors based on an In^{3+}-Doped SnP_2O_7 Proton Conductor," *Journal of The Electrochemical Society*, vol. 154, pp. J172-J176, 2007.

[129] J. Hertz and H. L. Tuller, "Single chamber solid oxide fuel cell comprises planar electrolyte layer; planar selectively active cathode contacting electrolyte layer and planar selectively active anode contacting electrolyte layer, all layers having specific thickness," *US patent*, WO2007024907-A2, 2007. [Online]. Available: http://apps.isiknowledge.com. [Consulted: April 19, 2007].

[130] B. Morel, R. Roberge, S. Savoie, T. W. Napporn, and M. Meunier, "An experimental evaluation of the temperature gradient in solid oxide fuel cells," *Electrochemical and Solid-State Letters*, vol. 10, pp. B31-B33, 2007.

[131] N. Uchiyama, "Single chamber type solid oxide fuel cell for motor vehicle, has solid oxide fuel cell unit accommodated inside exhaust-gas flow path of internal combustion engine," *Japanese patent*, JP2007220521-A, 2007. [Online]. Available: http://apps.isiknowledge.com. [Consulted: November 29, 2007].

[132] M. Nagao, M. Yano, K. Okamoto, A. Tomita, Y. Uchiyama, N. Uchiyama, and T. Hibino, "A single-chamber SOFC stack: Energy recovery from engine exhaust," *Fuel Cells*, vol. 8, pp. 322-329, 2008.

[133] H. Iwahara, "A one-chamber solid electrolyte fuel cell for chemical cogeneration," *Ionics*, vol. 4, pp. 409-414, 1998.

[134] R. B. Peterson, B. K. Paul, T. Palmer, Q. Wu, W. Jost, C.-H. T. Tseng, S. Tiwari, G. Patello, E. C. Buck, J. D. Holladay, R. Shimskey, P. Humble, P. MacFarlan, and J. Wainright, "Radiolytic microscale power generation based on single chamber fuel cell operation," *Journal of Micromechanics and Microengineering*, vol. 17, pp. S250-S256, 2007.

[135] C. Eyraud, J. Lenoir, and M. Gery, "Fuel cells using electrochemical properties of adsorbents - Piles a combustibles utilisant les proprietes electrochimiques des adsorbats," *C. R. Academie des Sciences, Paris*, vol. 252, pp. 1599-1600, 1961.

[136] C. K. Dyer, "A novel thin-film electrochemical device for energy conversion," *Nature*, vol. 343, pp. 547-548, 1990.

[137] T. Hibino, K. Asano, and H. Iwahara, "Improvement of Capcius cell using $SrCe_{0.95}Yb_{0.05}O_{3-\alpha}$ as a solid electrolyte," *Chemistry Letters*, vol. 3, pp. 485-488, 1994.

[138] K. Asano, T. Hibino, and H. Iwahara, "Studies on solid electrolytes for a new-type SOFC using methane-air mixture," *Denki kagaku oyobi kogyo butsuri kagaku*, vol. 64, pp. 649-653, 1996.

[139] K. Asano and H. Iwahara, "Performance of a one-chamber solid oxide fuel cell with a surface-modified zirconia electrolyte," *Journal of The Electrochemical Society*, vol. 144, pp. 3125-3130, 1997.

[140] T. Hibino, Y. Kuwahara, and S. Wang, "Effect of electrode and electrolyte modification on the performance of one-chamber solid oxide fuel cell," *Journal of The Electrochemical Society*, vol. 146, pp. 2821-2826, 1999.

[141] B. E. Buergler, M. E. Siegrist, and L. J. Gauckler, "Single chamber solid oxide fuel cells with integrated current-collectors," *Solid State Ionics*, vol. 176, pp. 1717-1722, 2005.

[142] P. Jasinski, T. Suzuki, F. Dogan, and H. U. Anderson, "Impedance spectroscopy of single chamber SOFC," *Solid State Ionics*, vol. 175, pp. 35-38, 2004.

[143] T. Hibino, A. Hashimoto, M. Yano, M. Suzuki, S.-I. Yoshida, and M. Sano, "High performance anodes for SOFCs operating in methane-air mixture at reduced temperatures," *Journal of The Electrochemical Society*, vol. 149, pp. A133-A136, 2002.

[144] M. Hori, K. Nagasaka, and M. Miyayama, "Evaluation of electrode performances of single-chamber solid oxide fuel cells," *Key Engineering Materials*, vol. 301, pp. 155-158, 2006.

[145] P. Jasinski, T. Suzuki, X. D. Zhou, F. Dogan, and H. U. Anderson, "Single chamber solid oxide fuel cell - investigation of cathodes," *Ceramic Engineering and Science Proceedings*, vol. 24, pp. 293-298, 2003.

[146] S. Asahara, D. Michiba, M. Hibino, and T. Yao, "Single chamber SOFC using $BaLaIn_2O_{5.5}$ solid electrolyte," *Electrochemical and Solid-State Letters*, vol. 8, pp. 449-451, 2005.

[147] I. C. Stefan, C. P. Jacobson, S. J. Visco, and L. C. De Jonghe, "Single chamber fuel cells: flow geometry, rate and composition considerations," *Electrochemical and Solid-State Letters*, vol. 7, pp. A198-A200, 2004.

[148] B. E. Buergler, Y. Santschi, M. Felberbaum, and L. J. Gauckler, "Influence of anode thickness on the electrochemical performance of single chamber solid oxide fuel cells," *Ceramic Engineering and Science Proceedings*, vol. 27, pp. 37-45, 2006.

[149] T. Suzuki, P. Jasinski, H. U. Anderson, and F. Dogan, "Single chamber electrolyte supported SOFC module," *Electrochemical and Solid-State Letters*, vol. 7, pp. A391-A393, 2004.

[150] B. Wei, Z. Lu, X. Huang, M. Liu, K. Chen, and W. Su, "Enhanced performance of a single-chamber solid oxide fuel cell with an SDC-impregnated cathode," *Journal of Power Sources*, vol. 167, pp. 58-63, 2007.

[151] T. Suzuki, P. Jasinski, V. Petrovsky, H. U. Anderson, and F. Dogan, "Anode supported single chamber solid oxide fuel cell in CH_4-air mixture," *Journal of The Electrochemical Society*, vol. 151, pp. A1473-A1476, 2004.

[152] Z. Shao, J. Mederos, W. C. Chueh, and S. M. Haile, "High power-density single-chamber fuel cells operated on methane," *Journal of Power Sources*, vol. 162, pp. 589-596, 2006.

[153] A. Tomita, D. Hirabayashi, T. Hibino, M. Nagao, and M. Sano, "Single-chamber SOFCs with a $Ce_{0.9}Gd_{0.1}O_{1.95}$ electrolyte film for low-temperature operation," *Electrochemical and Solid-State Letters*, vol. 8, pp. A63-A65, 2005.

[154] T. Suzuki, P. Jasinski, V. Petrovsky, H. U. Anderson, and F. Dogan, "Performance of a porous electrolyte in single-chamber SOFCs," *Journal of The Electrochemical Society*, vol. 152, pp. A527-A531, 2005.

[155] A. Nagata and T. Kimura, "Selective control of voltage polarity in a single-chamber solid-oxide fuel cell using the same catalytic electrodes with different sizes," in *IEEJ Transactions on Electrical and Electronic Engineering*, vol. 3, pp. 569-573, 2008.

[156] H. Kim, S. H. Choi, W. S. Kim, J. H. Lee, H. W. Lee, and J. Kim, "Development of single chamber solid oxide fuel cells with coplanar micro-electrode array," in *207th Meeting of the Electrochemical Society - Electrochemical Society Proceedings, Quebec, Canada, May 16-18, 2005*, pp. 1213, 2005.

[157] T. Hibino, K. Ushiki, T. Sato, and Y. Kuwahara, "A novel design for simplifying SOFC system," *Solid State Ionics*, vol. 81, pp. 1-3, 1995.

[158] C. Y. Chung, Y. C. Chung, J. Kim, J. Lee, and H. W. Lee, "Numerical modeling of micro single-chamber ceria-based SOFC," *Journal of Electroceramics*, vol. 17, pp. 959-964, 2006.

[159] T. Hibino, H. Tsunekawa, S. Tanimoto, and M. Sano, "Improvement of a single-chamber solid-oxide fuel cell and evaluation of new cell designs," *Journal of The Electrochemical Society*, vol. 147, pp. 1338-1343, 2000.

[160] E. J. Crumlin, G. J. La O, and Y. Shao-Horn, "Architectures and performance of high-voltage, microscale single-chamber solid oxide fuel cell stacks," in *ECS Transactions - 10th International Symposium on Solid Oxide Fuel Cells, SOFC-X, Nara, Japan, 3-8 June, 2007*, vol. 7, pp. 981-986, 2007.

[161] H. C. Kim, H. W. Lee, S. M. Kim, H. S. Song, J. H. Lee, J. S. Kim, J. W. Son, and S. J. Ahn, "Single-chamber solid oxide fuel cell using partition formed on one surface of electrolyte and interposed between two electrodes," *Korean patent*, KR724119-B1, 2008. [Online]. Available: http://apps.isiknowledge.com. [Consulted: June 9, 2008].

[162] J.-H. Min, S.-J. Ahn, J. Moon, J. Kim, and H.-W. Lee, "Single-chamber mini-solid oxide fuel cells operated at a lower temperature," in *ECS Transactions - 10th International Symposium on Solid Oxide Fuel Cells, SOFC-X, Nara, Japan, 3-8 June, 2007*, vol. 7, pp. 947-953, 2007.

[163] J.-W. Son, S.-J. Ahn, S. M. Kim, H. Kim, S.-H. Choi, J. Moon, H.-R. Kim, S. E. Kim, J.-H. Lee, H.-W. Lee, and J. Kim, "Fabrication and operation of co-planar type single chamber solid oxide fuel cells," in *Proceedings of the 7th European SOFC Forum, Lucerne, Switzerland, 3-7 July, 2006.*

[164] A. Bieberle-Huetter and H. Tuller, "Fabrication and structural characterization of interdigitated thin film $La_{(1-x)}Sr_xCoO_3$ (LSCO) electrodes," *Journal of Electroceramics*, vol. 16, pp. 151-157, 2006.

[165] T. Hibino, "Novel SOFC system free from a separator and gas seal," *Seramikkusu*, vol. 30, pp. 337-40, 1995.

[166] T. Hibino, K. Ushiki, and Y. Kuwabara, "Non-diaphragm solid electrolyte type fuel cell for co-generation," *Japanese patent*, JP8264195, 1996. [Online]. Available: http://ep.espacenet.com. [Consulted: February 2, 2007].

[167] B. Zhu, G. Meng, and B.-E. Mellander, "Non-conventional fuel cell systems: new concepts and development," *Journal of Power Sources*, vol. 79, pp. 30-36, 1999.

[168] T. Hibino, "Single-chamber SOFCs capable of operating in hydrocarbon-air mixtures," *Seramikkusu*, vol. 36, pp. 486-488, 2001.

[169] D. Rotureau, J. P. Viricelle, C. Pijolat, N. Caillol, and M. Pijolat, "Development of a planar SOFC device using screen-printing technology," *Journal of the European Ceramic Society*, vol. 25, pp. 2633-2636, 2005.

[170] J. Cesarano, R. Segalman, and P. Calvert, "Robocasting provides moldless fabrication from slurry deposition," *Ceramic Industry*, vol. 148, pp. 94-102, 1998.

[171] J. A. Lewis, "Direct-write assembly of ceramics from colloidal inks," *Current Opinion in Solid State and Materials Science*, vol. 6, pp. 245-250, 2002.

[172] D. B. Chrisey, "The power of direct-writing," *Science*, vol. 289, pp. 879-881, 2000.

[173] G. M. Gratson, M. Xu, and J. A. Lewis, "Direct writing of three-dimensional webs," *Nature*, vol. 428, pp. 386, 2004.

[174] R. B. Rao, K. L. Krafcik, A. M. Morales, and J. A. Lewis, "Microfabricated deposition nozzles for direct-write assembly of three-dimensional periodic structures," *Advanced Materials*, vol. 17, pp. 289-293, 2005.

[175] I. Grida and J. R. G. Evans, "Extrusion freeforming of ceramics through fine nozzles," *Journal of the European Ceramic Society*, vol. 23, pp. 629-635, 2003.

[176] D. Therriault, R. F. Shepherd, S. R. White, and J. A. Lewis, "Fugitive inks for direct-write assembly of three-dimensional microvascular networks," *Advanced Materials*, vol. 17, pp. 395-399, 2005.

[177] G. M. Gratson and J. A. Lewis, "Phase behavior and rheological properties of polyelectrolyte inks for direct-write assembly," *Langmuir*, vol. 21, pp. 457-464, 2005.

[178] J. A. Lewis and G. M. Gratson, "Direct writing in three dimensions," *Materials Today*, vol. 7, pp. 32-39, 2004.

[179] J. E. Smay, J. Cesarano III, and J. A. Lewis, "Colloidal inks for directed assembly of 3-D periodic structures," *Langmuir*, vol. 18, pp. 5429-5437, 2002.

[180] J. E. Smay, J. Cesarano III, B. A. Tuttle, and J. A. Lewis, "Directed colloidal assembly of linear and annular lead zirconate titanate arrays," *Journal of the American Ceramic Society*, vol. 87, pp. 293-295, 2004.

[181] G. M. Gratson, F. Garcia-Santamaria, V. Lousse, M. Xu, S. Fan, J. A. Lewis, and P. V. Braun, "Direct-write assembly of three-dimensional photonic crystals: conversion of polymer scaffolds to silicon hollow-woodpile structures," *Advanced Materials*, vol. 18, pp. 461-465, 2006.

[182] J. H. Moon, Y. B. Kim, and J. S. Kim, "Preparation method of electrochemical cell by preparing paste and substrate, and patterning the paste on the substrate by robo-dispensing, and solid oxide fuel cell prepared by the method," *Korean patent*, KR2007015731-A/KR760219-B1, 2007. [Online]. Available: http://apps.isiknowledge.com. [Consulted: November 29, 2007].

[183] Y.-B. Kim, S.-J. Ahn, J. Moon, J. Kim, and H.-W. Lee, "Direct-write fabrication of integrated planar solid oxide fuel cells," *Journal of Electroceramics*, vol. 17, pp. 683-687, 2006.

[184] N.-T. Nguyen and S. H. Chan, "Micromachined polymer electrolyte membrane and direct methanol fuel cells - a review," *Journal of Micromechanics and Microengineering*, vol. 16, pp. R1-R12, 2006.

[185] D.-J. Shim, H.-W. Sun, S. T. Vengallatore, and S. M. Spearing, "Damage and failure in silicon-glass-metal microfluidic joints for high-pressure MEMS devices," *Journal of Microelectromechanical Systems*, vol. 15, pp. 246-258, 2006.

[186] G. Grueneberg, "Electrochemical conversion of nuclear energy," in *Fuel cells: Modern processes for the electrochemical production of energy*, W. Vielstich and D. J. G. Ives, New York: Wiley-Interscience, 1965, pp. 374-376.

[187] M. Kuhn, T. Napporn, M. Meunier, D. Therriault, and S. Vengallatore, "Direct-write microfabrication of single-chamber solid oxide fuel cells with interdigitated electrodes," in *Materials Research Society Symposium Proceedings*, vol. 972, Solid-State Ionics-2006, pp. 211-216, 2007.

[188] D. Therriault, S. R. White, and J. A. Lewis, "Chaotic mixing in three-dimensional microvascular networks fabricated by direct-write assembly," *Nature Materials*, vol. 2, pp. 265-271, 2003.

[189] T. E. Karis, "An overview of rheology in the computer industry," *Journal of Applied Polymer Sciences*, vol. 59, pp. 1405-1416, 1996.

[190] X. Zhang, D. O. Hayward, and D. M. P. Mingos, "Further studies on oscillations over nickel wires during the partial oxidation of methane," *Catalysis Letters*, vol. 86, pp. 235-243, 2003.

[191] N. Nakagawa, H. Sakurai, K. Kondo, T. Morimoto, K. Hatanaka, and K. Kato, "Evaluation of the effective reaction zone at Ni(NiO)/zirconia anode by using an electrode with a novel structure," *Journal of The Electrochemical Society*, vol. 142, pp. 3474-3479, 1995.

[192] B. Morel, S. Savoie, R. Roberge, T. W. Napporn, and M. Meunier, "Ni-YSZ reduction process under CH_4 in a single-chamber SOFC," in *Proceedings of the 7th European SOFC Forum, Lucerne, Switzerland, 3-7 July, 2006*, 2006.

[193] M. Kuhn, T. W. Napporn, M. Meunier, S. Vengallatore, and D. Therriault, "Miniaturization limits for single-chamber micro solid oxide fuel cells with coplanar electrodes " *submitted to Journal of Power Sources*, 2009.

[194] T. Suzuki, P. Jasinski, H. U. Anderson, and F. Dogan, "Role of composite cathodes in single chamber SOFC," *Journal of The Electrochemical Society*, vol. 151, pp. A1678-A1682, 2004.

[195] A. Hartley, M. Sahibzada, M. Weston, I. S. Metcalfe, and D. Mantzavinos, "$La_{0.6}Sr_{0.4}Co_{0.2}Fe_{0.8}O_3$ as the anode and cathode for intermediate temperature solid oxide fuel cells," *Catalysis Today*, vol. 55, pp. 197-204, 2000.

[196] K. Ahn, H. Kim, Y.-C. Chung, J.-W. Son, H.-W. Lee, and J.-H. Lee, "Catalytic characteristics of perovskite-type oxides under mixed methane and oxygen gases," *Journal of the Korean Ceramic Society*, vol. 45, pp. 232-237, 2008.

[197] J. C. Fisher II and S. S. C. Chuang, "Investigating the CH_4 reaction pathway on a novel LSCF anode catalyst in the SOFC," *Catalysis Communications*, vol. 10, pp. 772-776, 2009.

[198] B. Morel, R. Roberge, S. Savoie, T. W. Napporn, and M. Meunier, "Catalytic activity and performance of LSM cathode materials in single chamber SOFC," *Applied Catalysis A: General*, vol. 323, pp. 181-187, 2007.

[199] C.-C. T. Yang, W.-C. J. Wei, and A. Roosen, "Reaction kinetics and mechanisms between $La_{0.65}Sr_{0.3}MnO_3$ and 8 mol% yttria-stabilized zirconia," *Journal of the American Ceramic Society*, vol. 87, pp. 1110-1116, 2004.

[200] Website of Polysciences Inc., www.polysciences.com.

[201] H. Zhu and R. J. Kee, "A general mathematical model for analyzing the performance of fuel-cell membrane-electrode assemblies," *Journal of Power Sources*, vol. 117, pp. 61-74, 2003.

[202] W. Vielstich, A. Lamm, and H. A. Gasteiger, *Handbook of fuel cells: fundamentals, technology and applications. Volume 4, Fuel cell technology and applications, part 2*, Chichester: Wiley, 2003.

[203] W. Vielstich, A. Lamm, and H. A. Gasteiger, *Handbook of fuel cells: fundamentals, technology and applications. Volume 2, Electrocatalysis*, Chichester: Wiley, 2003.

[204] D. A. Noren and M. A. Hoffman, "Clarifying the Butler-Volmer equation and related approximations for calculating activation losses in solid oxide fuel cell models," *Journal of Power Sources*, vol. 152, pp. 175-181, 2005.

[205] J. O. M. Bockris, A. K. N. Reddy, and M. E. Gamboa-Aldeco, *Modern electrochemistry 2A: Fundamentals of electrodics*, 2nd ed., New York: Kluwer Academic/Plenum Publishers, 2001.

[206] T. Kawada, N. Sakai, H. Yokokawa, M. Dokiya, M. Mori, and T. Iwata, "Characteristics of Slurry-Coated Nickel Zirconia Cermet Anodes for Solid Oxide Fuel Cells," *Journal of The Electrochemical Society*, vol. 137, pp. 3042-3047, 1990.

[207] J. I. Gazzarri and O. Kesler, "Electrochemical AC impedance model of a solid oxide fuel cell and its application to diagnosis of multiple degradation modes," *Journal of Power Sources*, vol. 167, pp. 100-110, 2007.

[208] A. C. Co, S. J. Xia, and V. I. Birss, "A kinetic study of the oxygen reduction reaction at $LaSrMnO_3$-YSZ composite electrodes," *Journal of The Electrochemical Society*, vol. 152, pp. A570-A576, 2005.

[209] Y. Hao, Z. Shao, J. Mederos, W. Lai, D. G. Goodwin, and S. M. Haile, "Recent advances in single-chamber fuel-cells: Experiment and modeling," *Solid State Ionics*, vol. 177, pp. 2013-2021, 2006.

[210] P. Leone, M. Santarelli, P. Asinari, M. Cali, and R. Borchiellini, "Experimental investigations of the microscopic features and polarization limiting factors of planar SOFCs with LSM and LSCF cathodes," *Journal of Power Sources*, vol. 177, pp. 111-122, 2008.

[211] K. Huang, M. Feng, J. B. Goodenough, and C. Milliken, "Electrode performance test on single ceramic fuel cells using as electrolyte Sr- and Mg-doped $LaGaO_3$," *Journal of The Electrochemical Society*, vol. 144, pp. 3620-3624, 1997.

[212] R. Maric, S. Ohara, T. Fukui, H. Yoshida, M. Nishimura, T. Inagaki, and K. Miura, "Solid oxide fuel cells with doped lanthanum gallate electrolyte and $LaSrCoO_3$ cathode, and Ni-samaria-doped ceria cermet anode," *Journal of The Electrochemical Society*, vol. 146, pp. 2006-2010, 1999.

[213] A. Touati and A. Hammou, "Determination of the exchange current in the SOFC composite cathode," *Ionics*, vol. 12, pp. 339-341, 2006.

[214] H. Uchida, M. Yoshida, and M. Watanabe, "Effect of ionic conductivity of zirconia electrolytes on the polarization behavior of various cathodes in solid fuel cells," *Journal of The Electrochemical Society*, vol. 146, pp. 1-7, 1999.

[215] C. G. Vayenas, S. I. Bebelis, I. V. Yentekakis, and S. N. Neophytides, "Electrocatalysis and electrochemical reactors," in *The CRC Handbook: Solid State Electrochemistry*, CRC Press, 1997, pp. 445-480.

[216] Y. Hao and D. G. Goodwin, "Numerical modeling of single-chamber SOFCs with hydrocarbon fuels," *Journal of The Electrochemical Society*, vol. 154, pp. B207-B217, 2007.

[217] Y. Hao and D. G. Goodwin, "Efficiency and fuel utilization of methane-powered single-chamber solid oxide fuel cells," *Journal of Power Sources*, vol. 183, pp. 157-163, 2008.

[218] C. B. Arnold, P. Serra, and A. Pique, "Laser direct-write techniques for printing of complex materials," *MRS Bulletin*, vol. 32, pp. 23-31, 2007.

[219] A. Watanabe, Y. Kobayashi, M. Konno, S. Yamada, and T. Miwa, "Direct drawing of submicron wiring by laser-induced pyrolysis of film prepared from liquid-dispersed metal nanoparticles," *Molecular Crystals and Liquid Crystals*, vol. 464, pp. 161-167, 2007.

[220] P. Kumar and S. Das, "Fabrication of meso- and micro-structured devices by direct-write deposition and laser processing of dry fine powders," in *ASME International Mechanical Engineering Congress and Exposition, Anaheim, CA, USA*, pp. 519-524, 2004.

[221] M. C. George, A. Mohraz, M. Piech, N. S. Bell, J. A. Lewis, and P. V. Braun, "Direct laser writing of photoresponsive colloids for microscale patterning of 3D porous structures," *Advanced Materials*, vol. 21, pp. 66-70, 2009.

Appendix I Direct-write microfabrication of single-chamber solid oxide fuel cells with interdigitated electrodes

M. Kuhn, T. Napporn, M. Meunier, D. Therriault, S. Vengallatore, *Materials Research Society Symposium Proceedings*, vol. 972, Solid-State Ionics-2006, pp. 211-216, 2007.

Abstract

Miniaturized single-chamber solid oxide fuel cells (SC-SOFCs) are a promising class of devices for portable power generation. Here we report the direct-write fabrication and structural characterization of SC-SOFCs in the single-face configuration, which consists of closely-spaced interdigitated electrodes on an electrolyte plate. The essential concepts underlying this technique are the fabrication of inks using electrode powders, pressure-driven extrusion through a micronozzle onto a robot-controlled platform, and sintering to form porous electrodes. As the first step in the development of detailed process-structure-performance correlations for the fuel cells, we studied the effects of extrusion pressure (in the range 30-40 bar) and stage velocity (in the range 0.2-2.0 mm/s) on the quality and size of electrodes for fixed suspension viscosity and nozzle diameter. An optimal combination of speed and pressure has been identified and catalogued in the form of process maps. Single-chamber SOFCs were fabricated with interdigitated electrodes with width and interelectrode spacings of 140 μm and 300 μm, respectively.

Introduction

Miniaturized solid oxide fuel cells (SOFCs) are gaining increasing interest as power generation technology for portable electronic devices such as notebooks, mobile phones and micromachined sensors [1-3]. In the conventional (dual-chamber) design, the fuel cell comprises an electrolyte "sandwiched" between anode and cathode layers. During operation, fuel (hydrogen or hydrocarbons) is supplied to the anode, oxygen to the cathode, and care is taken to ensure that the two gas streams do not mix. Thus, the dual-chamber design requires gas-tight, high-temperature microfluidic sealing

technology and thermal isolation schemes, both of which impose stringent manufacturing challenges [2]. Hence, there is increasing interest in exploring a different concept, namely single-chamber solid oxide fuel cells (SC-SOFCs). In this approach, the fuel and air are pre-mixed and flow over both electrodes of the fuel cell [4, 5]. SC-SOFCs are ideally suited for miniaturization because of their compact design, absence of any high-temperature microfluidic sealing requirements and potential ease of integration with micromachined sensors and actuators.

Three different types of SC-SOFCs are currently under investigation: (i) three-layer architecture with the electrolyte being "sandwiched" between the anode and cathode [5-8], (ii) single-face configuration with interdigitated electrodes situated on the same side of the electrolyte (as illustrated in Fig. A1.1a) [4, 9-13], and (iii) flow-through fuel cells with porous electrodes and electrolyte [14]. Our work is focused on the second configuration, for which the primary design requirements are: (i) minimization of interelectrode distance to micrometer dimensions (which is required to minimize polarization resistance and increase fuel cell efficiency), and (ii) fabrication of thick, porous electrodes to increase the number of triple phase boundaries [15, 16]. Achieving these designs using standard thin-film and photolithography-based microfabrication is a formidable challenge, and there is a need to develop alternate methods of microfabrication to synthesize micro fuel cells with interdigitated electrodes.

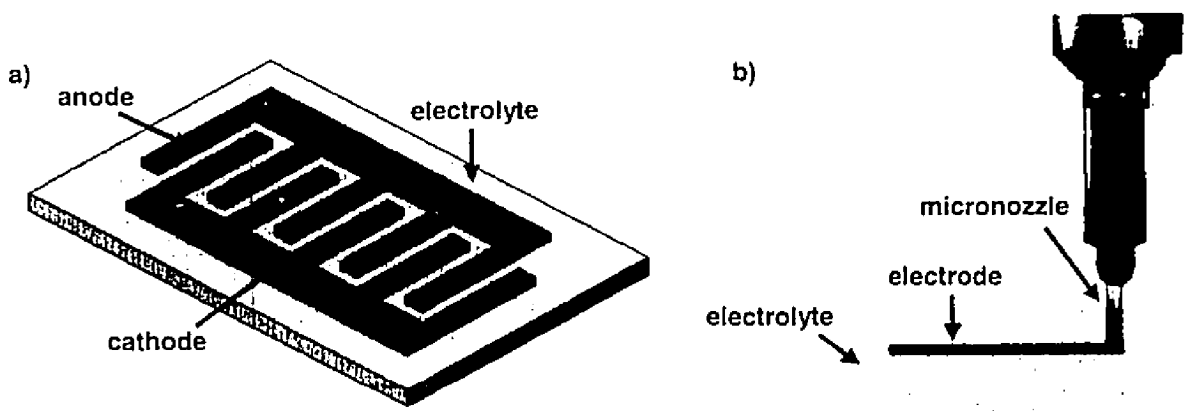

Figure A1.1: a) Schematic representation of single-chamber SOFC with interdigitated electrodes; b) Schematic representation of robot-controlled direct-write microfabrication.

In the early pioneering work of Hibino and co-workers [4, 12], the electrodes were created by manually smearing electrode inks on an electrolyte plate with a brush. The resulting interelectrode spacings ranged from 0.5 to 3.0 mm. Subsequently, more refined techniques based on microfluidic lithography [9] and robot-controlled direct-write microfabrication [11, 17] are being developed to reduce the interelectrode spacing to the range 50 to 300 μm. Of the two methods, direct-writing is more attractive because it obviates the need for any clean-room microfabrication, and therefore has the potential to permit low-cost and versatile manufacturing. The primary steps in direct-write manufacturing are as follows. First, the electrode powders are processed to fabricate suspensions (or inks) of the desired viscosity. Next, the inks are deposited onto an electrolyte plate by means of pressure-driven extrusion through a micronozzle, as shown in Fig. A1.1b. The plate is mounted on a robot-controlled mobile platform; this permits the deposition of electrode structures of different shapes and sizes. Finally, the structure is sintered to form porous electrodes. Thus, direct-writing involves numerous process parameters including particle size and size distribution, rheological properties of the suspension, extrusion pressure, nozzle size, stage velocity and sintering conditions. The effects of process parameters on fuel cell characteristics remain largely unexplored, which is the motivation for the present work.

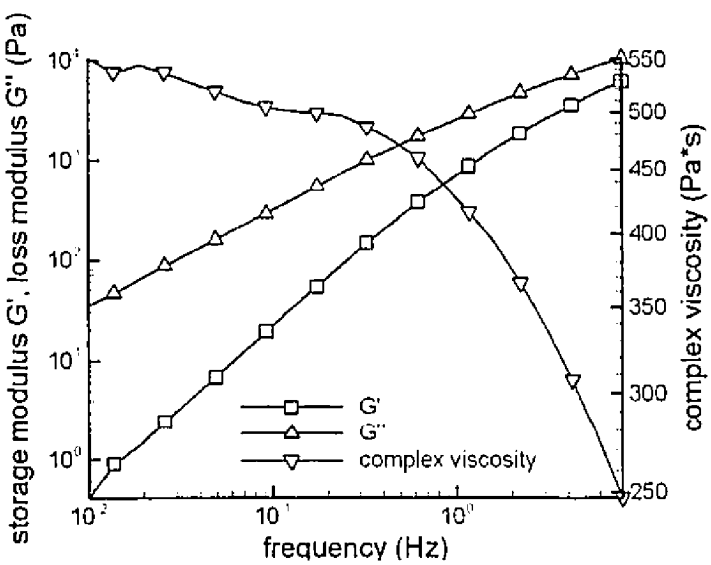

Figure A1.2: Storage modulus, *G'*, loss modulus, *G''*, and complex viscosity as functions of frequency for 60 wt% anode suspension.

Experimental details

Conventional SOFC materials - yttria-stabilized zirconia (YSZ), Ni/YSZ cermet and lanthanum strontium manganite (LSM) - were used as electrolyte, anode and cathode, respectively. YSZ (with 8 mol% yttria) electrolyte plates of thickness 0.5 mm were purchased from Marketech International. The electrode materials were obtained from NexTech Materials in the form of NiO-YSZ (8 mol% yttria) powder (median particle size of 0.9 μm, specific surface area (BET-surface) of 2.071 m^2/g, weight ratio of NiO:YSZ of 60:40) and $(La_{0.8}Sr_{0.2})_{0.98}MnO_3$ powders (median particle size of 0.6 μm and specific surface area (BET-surface) of 4.2438 m^2/g). Anode and cathode suspensions with 60 wt% and 55 wt% of powder, respectively, were prepared by ball milling for 1 h with YSZ balls (5-10 mm in diameter) in a Spex Mixer/Mill (Spex 8000 M).

The rheological properties of the suspension (including complex viscosity, η^*, and elastic and complex moduli, G' and G'') were measured by oscillatory-stress experiments using a stress-controlled rheometer (Bohlin CVO 120) with a parallel plate geometry. The diameter of the upper plate was 25 mm. Frequency sweeps were conducted at fixed shear stress amplitude of 20 Pa with frequencies ranging from 0.01 to 100 Hz. All measurements were made at a temperature of 22°C.

The deposition of the electrode structures on the YSZ electrolyte was realized using a robotic deposition apparatus (I & J 2200-4, I & J Fisnar Inc.) combined with a micro-extrusion system. A micronozzle with an inner diameter of 100 μm was used for all depositions. The extrusion pressure and stage velocities were varied in the range 30 to 40 bar and 0.2 to 2.0 mm/s, respectively.

The cathode and anode require different sintering temperature profiles. Therefore, the anode was deposited first and sintered at 1250°C for 3.75 h. Subsequently, the cathode was deposited between the anode structure using manual visual alignment, and the entire fuel cell assembly was sintered at 1100°C for 3.75 h. All sintering steps were conducted under ambient environment.

Electrode width and interelectrode spacing were obtained from optical micrographs analyzed with the image processing software Image-Pro Plus 5.1 and QCapture Pro 5.0. The optical micrographs were taken with an Olympus SZX12 stereomicroscope and an Evolution™ VF color camera with 1.4 million pixel resolution.

The sintered electrodes were observed on a Jeol JSM-840 scanning electron microscope (SEM).

Results and discussion

The preparation of electrode inks by colloidal processing of electrode powders is the first step in direct-write manufacturing. The particle size and load in the ink must be optimized to ensure satisfactory flow of the inks and avoid clogging inside the micronozzle during extrusion, and obtain a coherent electrode structure. By experimenting with different particle loads, it was found that 50 to 60 wt% suspensions were optimal for direct-writing of the electrodes. Fig. A1.2 shows the rheological properties (elastic modulus, storage modulus and complex viscosity as functions of frequency) for inks with 60 wt% anode powders. A shear-thinning behavior can be observed with a maximum viscosity of approximately 550 Pa·s.

Next, we investigated the effects of the key direct-writing parameters - extrusion pressure and stage velocity - on the size and uniformity of the electrodes. These results are catalogued in the form of a *process map* in Fig. A1.3.

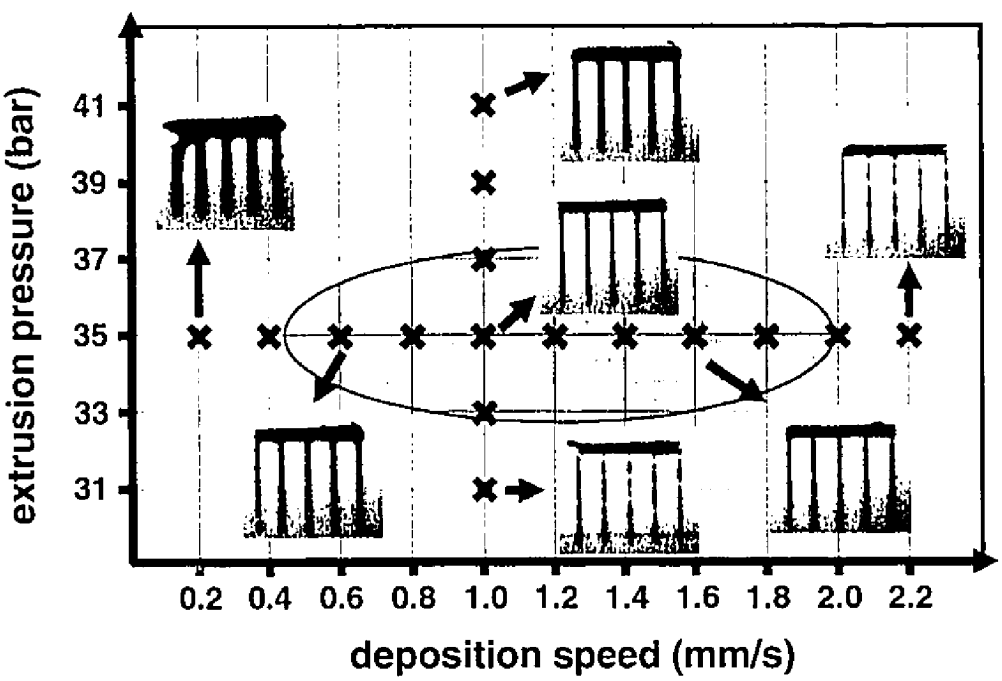

Figure A1.3: Effects of extrusion pressure and deposition speed on size and uniformity of direct-write deposition of 60 wt% anode suspension using a 100 μm diameter nozzle.

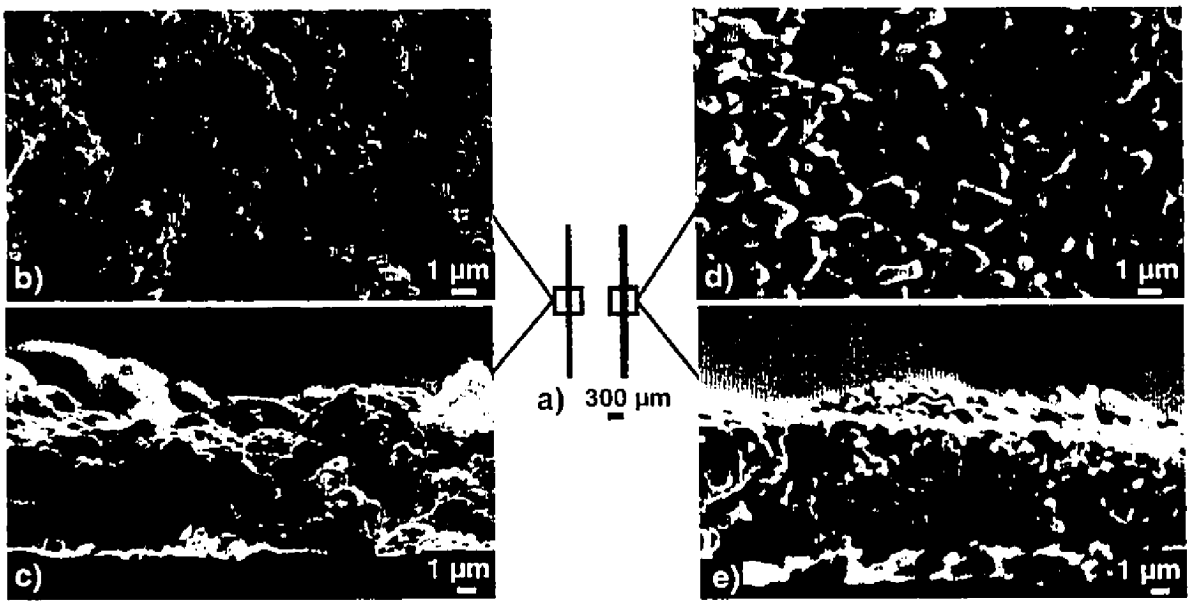

Figure A1.4: a) Optical micrograph of NiO-YSZ anode (left) and LSM cathode (right) lines on YSZ electrolyte; b) - e) SEM images of sintered direct-written electrode microstructures: b) anode, top surface; c) anode, cross-section; d) cathode, top surface; e) cathode, cross-section.

Thus, at a pressure of 35 bar, low velocity (0.2 mm/s) results in very broad electrodes, and high velocities (> 2.0 mm/s) lead to discontinuous structures. Similarly, for a given velocity of 1.0 mm/s, lower pressures lead to discontinuous structures and high pressures to broad electrodes. Based on these observations, an optimal range of pressures and stage velocities were identified, as highlighted in Fig. A1.3.

Fig. A1.4 shows the result of optical and scanning electron microscopy of the sintered electrodes. It is evident that direct-writing can be used to fabricate highly-porous electrodes with a thickness of several micrometers; both features are desirable in improving the performance of the fuel cell.

Finally, an optical micrograph of the SC-SOFC with interdigitated electrodes is shown in Fig. A1.5. The average width of the electrodes is 140 µm, and the average interelectrode spacing is 300 µm. For comparison, the interdigitated electrodes reported recently by Son et al. [11] had interelectrode spacings of 255, 443 and 743 µm. Our current work is focused on electrochemical testing of our SC-SOFCs, and continuing attempts to further reduce interelectrode spacings.

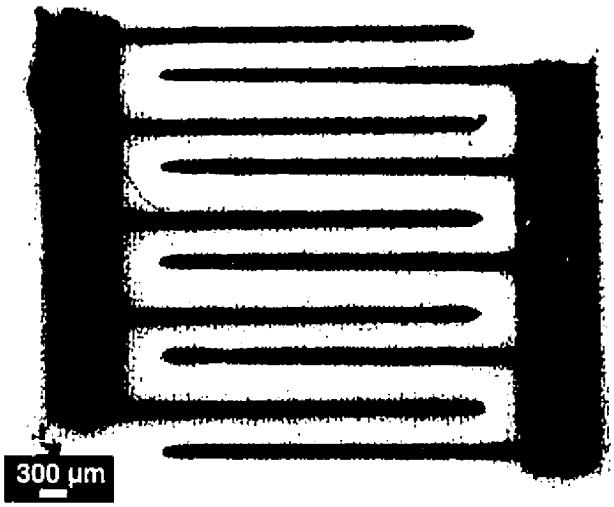

Figure A1.5: Optical micrograph of interdigitated LSM cathode (black) and NiO-YSZ anode (green) on YSZ electrolyte; average electrode width: 140 µm, average interelectrode spacing: 300 µm.

Conclusions

Direct-write microfabrication is a promising approach for creating single-chamber solid oxide fuel cells with interdigitated electrode structures at the microscale. Here, we reported the fabrication and characterization of SC-SOFCs with interdigitated electrodes such that the electrode width and interelectrode spacing are 140 µm and 300 µm, respectively. The effects of some process parameters on structural characteristics were evaluated in detail. These results establish the foundation for synthesizing the next generation of SC-SOFCs with interelectrode distances in the sub-50 micrometer range. Our future work includes: (i) evaluation of the effects of sintering conditions on electrode porosity, (ii) electrochemical testing of the fuel cell devices, and (iii) evaluation of the effects of electrode width, thickness and interelectrode spacing on power production.

References

[1] C. D. Baertsch, K. F. Jensen, J. L. Hertz, H. L. Tuller, S. T. Vengallatore, S. M. Spearing, and M. A. Schmidt, *J. Mater. Res.* 19, 2604 (2004).

[2] V. T. Srikar, K. T. Turner, T. Y. A. Ie, and S. M. Spearing, *J. Power Sources* 125, 62 (2004).

[3] D. Nikbin, *Fuel Cell Review* 3, 21 (2006).

[4] T. Hibino, K. Ushiki, and Y. Kuwahara, *Solid State Ionics* 91, 69 (1996).

[5] T. Hibino, A. Hashimoto, T. Inoue, J. Tokuno, S. Yoshida, and M. Sano, *Science* 288, 2031 (2000).

[6] T. W. Napporn, F. Morin, and M. Meunier, *Electrochem. Solid-State Lett.* 7, A60 (2004).

[7] T. W. Napporn, X. Jacques-Bedard, F. Morin, and M. Meunier, *J. Electrochem. Soc.* 151, A2088 (2004).

[8] Z. Shao, S. M. Haile, J. Ahn, P. D. Ronney, Z. Zhan, and S. A. Barnett, *Nature* 435, 795 (2005).

[9] S.-J. Ahn, J.-H. Lee, J. Kim, and J. Moon, *Electrochem. Solid-State Lett.* 9, A228 (2006).

[10] A. Bieberle-Huetter and H. Tuller, *J. Electroceram.* 16, 151 (2006).

[11] J.-W. Son, S.-J. Ahn, S. M. Kim, H. Kim, S.-H. Choi, J. Moon, H.-R. Kim, S. E. Kim, J.-H. Lee, H.-W. Lee, and J. Kim in *Fabrication and Operation of Co-Planar Type Single Chamber Solid Oxide Fuel Cells*, 7th European SOFC Forum, Lucerne, Switzerland, 2006.

[12] T. Hibino, H. Tsunekawa, S. Tanimoto, and M. Sano, *J. Electrochem. Soc.* 147, 1338 (2000).

[13] T. Hibino, A. Hashimoto, M. Suzuki, M. Yano, S. Yoshida, and M. Sano, *J. Electrochem. Soc.* 149, A195 (2002).

[14] A. K. Shukla, R. K. Raman, and K. Scott, *Fuel Cells* 4, 436 (2005).

[15] J. Fleig, H. L. Tuller, and J. Maier, *Solid State Ionics* 174, 261 (2004).

[16] C.-Y. Chung, Y.-C. Chung, *J. Power Sources* 154, 35 (2006).

[17] D. Therriault, S. R. White, and J. A. Lewis, *Nat. Mater.* 2, 265 (2003).

Appendix II Viscoelastic inks for direct-write microfabrication of single-chamber micro solid oxide fuel cells with coplanar thick electrodes

M. Kuhn, R. B. Rao, D. Therriault, *Materials Research Society Symposium Proceedings* (MRS Spring Meeting 2009), submitted March 16, 2009.

Abstract

Single-chamber micro solid oxide fuel cells (SC-μSOFCs) with coplanar electrodes were fabricated using a robotically controlled direct-write microfabrication approach. Viscoelastic, gel-based inks were employed to create homogeneous electrodes of controlled width and interelectrode distance as well as uniform cross-sectional thickness. Electrode powders, NiO-YSZ (yttria-stabilized zirconia) for the anode and $(La_{0.8}Sr_{0.2})_{0.98}MnO_3$-YSZ for the cathode, were first dispersed with a cationic polyethyleneimine solution. Polyacrylic acid was added to induce a fluid-to-gel transition. The rheology of the fabricated inks was characterized. The inks were then extruded through cylindrical micronozzles and deposited onto YSZ electrolyte substrates using a robotic deposition apparatus. Thickness and width of the sintered electrodes were close to the diameter of the extrusion nozzle. The improved shape retention of the deposited electrodes also enabled the fabrication of continuous electrodes with square cross-section. The cathode adhered very well to the electrolyte during sintering. However, the mismatch between the thermal expansion coefficient of anode and electrolyte seems to cause detaching and breaking of the anode so that electrochemical characterization of the fabricated cells was not yet possible.

Introduction

Single-chamber solid oxide fuel cells (SC-SOFCs) are operated in mixtures of fuel and oxidant gas, which simplifies fuel cell design and eliminates high-temperature gas-tight sealing issues of conventional dual-chamber SOFCs. The working principle of

these fuel cells is based on the selectivity of the electrodes for the respective reactions, that is, fuel oxidation at the anode and reduction of the oxidant at the cathode [1]. The single-chamber approach enables novel cell designs such as the single-face configuration, where both anode and cathode are located on the same side of the electrolyte (e.g., single parallel electrode pairs or interdigitated electrodes) [2]. Closely-spaced (< 1 mm), small (width < 1 mm) electrodes were found to reduce ohmic resistance and yield higher cell performance [2, 3]. Standard lithography-based microfabrication techniques have the resolution to fabricate microscale electrodes, but they do not permit to easily create structures of two different materials with porous microstructure on the same side of a substrate. Microfluidic lithography [4] and micromolding [5] were investigated for the fabrication of coplanar microscale electrodes. However, the versatility of these techniques is limited by the necessity to use molds and by low reproducibility when filling the microchannels in the mold [5].

Direct-write microfabrication was demonstrated as a suitable, fast and versatile technique for creating SC-microSOFCs (SC-μSOFCs) with coplanar electrodes [6-8]. This method consists of extruding inks of the respective electrode materials under constant pressure through a micronozzle and their deposition in the desired pattern on the electrolyte substrate. Anode and cathode inks were previously fabricated based on ceramic processing recipes for screen printing [3, 6-8].

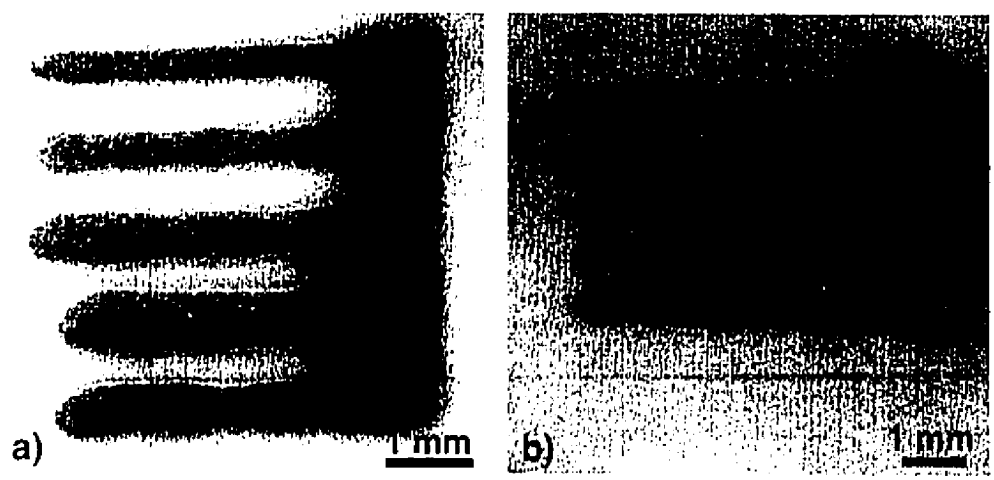

Figure A2.1: Optical micrograph of a) anode fabricated from Newtonian ink, featuring spreading and uniformity limitations, and b) homogenous cathode fabricated from viscoelastic ink using the direct-write microfabrication technique.

The Newtonian flow behavior of these inks enables homogeneous extrusion, but can lead to ink spreading after deposition, resulting in only moderate control over the interelectrode spacing and electrode width of the deposited electrode structures (Fig. A2.1a) [6, 8]. Additionally, the deposited electrodes exhibited lens-like shaped cross-sections of non-uniform thickness [7].

Colloidal gel-like inks with viscoelastic flow behavior have been reported in the literature [9, 10] to be well suited for direct-write microfabrication of ceramic structures, as they flow smoothly under applied shear through the deposition nozzle and show elevated shape retention after deposition. The viscoelastic response should therefore facilitate the fabrication of electrodes with controlled width and interelectrode spacing (Fig. A2.1b) for SC-SOFC applications.

Experimental details

NiO (specific surface area of 6.3 m^2/g, density of 6.7 g/cm^3 and mean particle size of 0.56 μm), YSZ (92 mol% ZrO_2, 8 mol% Y_2O_3) (specific surface area of 6.1 m^2/g, density of 5.9 g/cm^3 and mean particle size of 0.25 μm) and $(La_{0.8}Sr_{0.2})_{0.98}MnO_3$ (LSM)-YSZ (specific surface area of 9.7 m^2/g, density of 6.2 g/cm^3 and mean particle size of 0.56 μm) powders (NexTech Materials Ltd., Lewis Center, OH) were used for the fabrication of SC-μSOFCs with coplanar electrodes. A mixture of NiO and YSZ composed of 55 wt% NiO and 45 wt% YSZ was prepared by ball milling on a long roll jar mill (US Stoneware, East Palestine, OH) during 24 h. Zeta potential measurements were performed using a Zetasizer 3000 HSA (Malvern Instruments Ltd., Worcestershire, UK). All powders were negatively charged over a wide pH range (Fig. A2.2a). A cationic polyelectrolyte, polyethyleneimine (PEI), with a molecular weight of 1800 g/mol (Polysciences Inc., Warrington, PA), was used to stabilize the colloidal particles in an aqueous suspension with a pH of 7. The suspensions were thoroughly mixed by high-shear agitation (Thinky ARE-250 Conditioning Mixer, Thinky USA Inc., Laguna Hills, CA). 5 mg of methylcellulose (Methocel F4M, Dow Chemical Co., Midland, MI) per mL fluid was added as viscosifying agent. To induce the fluid-to-gel transition, polyacrylic acid (PAA, Polysciences Inc., Warrington, PA) with a molecular

weight of 1800 g/mol, supplied as a 65 wt% aqueous solution, was added. The final solids loading of the colloidal anode and cathode inks was ~30 vol%.

Rheological measurements were conducted on a controlled stress rheometer (Bohlin C-VOR, Cranbury, NJ) with a concentric cylinder measuring geometry (C-14, bob diameter of 14 mm and gap width of 0.7 mm). To avoid slip, the cup and bob had a roughened surface. The apparent viscosity was measured in controlled-stress viscometry mode over a shear rate range of 0.1 to 100 s^{-1} in descending order. Oscillatory measurements were performed at 1 Hz and a stress sweep was carried out in ascending order from 0.1 to 1000 Pa. To guarantee a uniform shear history and to ensure that the suspension was at equilibrium, a pre-shear of 50 s^{-1} was applied before each measurement during 120 s followed by a 600 s equilibrium time. All measurements were carried out at 25°C.

Anode and cathode structures were fabricated by direct-writing using a robotic deposition apparatus (ABL9000, Aerotech Inc., Pittsburgh, PA), and the motion of the robot axes in x-, y- and z-direction was controlled by a computer-aided program (RoboCAD 3.2, 3D Inks, LLC, Stillwater, OK). The electrode inks were housed in syringes (3 cc, EFD Inc., East Providence, RI) and extruded through cylindrical stainless steel dispensing tips (inner nozzle diameter of 0.1 mm, EFD Inc., East Providence, RI) using a pressure regulator (EFD Inc., East Providence, RI). Micronozzles with square cross-section were fabricated from square capillary tubing (Polymicro Technologies, Phoenix, AZ) with an inner square length of 0.1 mm. Approximately 1 cm long pieces were cut and fixed inside polypropylene needle hubs (Small Parts Inc., Miramar, FL) using 5-min Epoxy. The combination of the microextrusion system with the robotic deposition apparatus enabled the deposition of the extruded suspensions onto 0.2 mm thick YSZ electrolyte substrates (Marketech International Inc., Port Townsend, WA). To avoid ink drying and nozzle clogging during the fabrication process, deposition was performed in a reservoir filled with lamp oil. The deposited anode and cathode structures were dried in air and cosintered at 1200°C for 3 h. Optical and scanning electron microscope images were taken with an Olympus SZX12 stereomicroscope (Olympus Corporation, Tokyo, Japan) and a JEOL 6060LV SEM (JEOL-USA Inc., Peabody, MA), respectively.

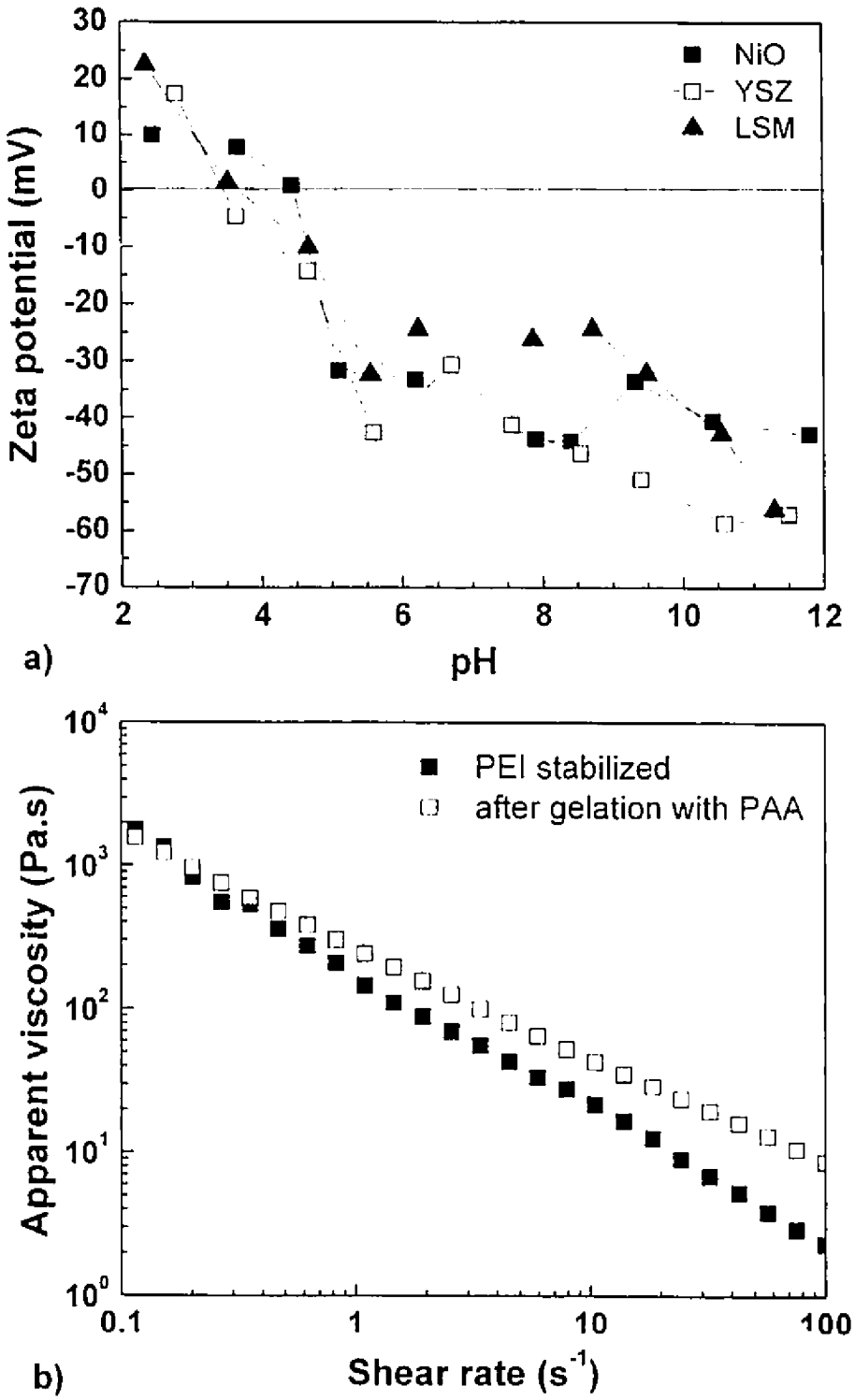

Figure A2.2: a) Zeta-potential as a function of pH for NiO, YSZ and LSM powders. b) Apparent viscosity as a function of shear rate for NiO-YSZ ink after stabilization of the powder with PEI in an aqueous suspension and after gelation.

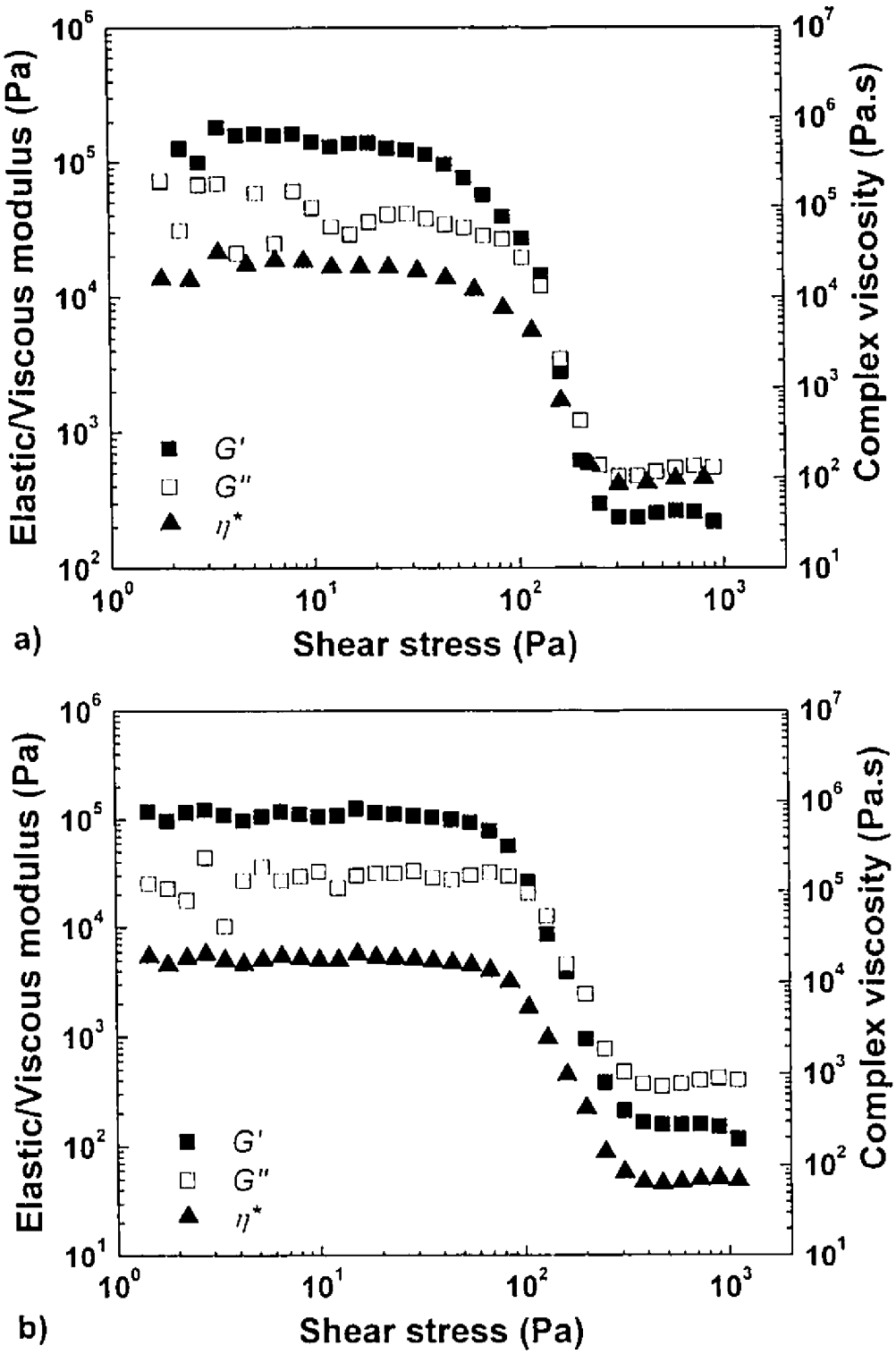

Figure A2.3: Shear stress amplitude sweeps of a) NiO-YSZ and b) LSM-YSZ electrode inks at 1 Hz and 25°C.

Discussion

To characterize the effect of PAA addition on the apparent viscosity, viscometry measurements were conducted on anode and cathode inks after stabilizing the powder with PEI in an aqueous suspension and after gelation with PAA. The viscometry measurements for the anode ink in Fig. A2.2b show that the gelation led to an increase in the apparent viscosity. Fig. A2.3 shows stress amplitude sweeps of the gel-based NiO-YSZ anode and LSM-YSZ cathode inks. Both inks exhibited a similar behavior, with an elastic modulus, G', of approximately 10^5 Pa in the linear viscoelastic regime. At low shear stress, solid-like behavior dominated, whereas at higher shear stress, the viscous modulus, G'', became more important. This viscoelastic behavior is beneficial for the direct-write fabrication of electrode structures, as a high G' yields elevated shape retention after deposition of the extruded ink filaments and a more liquid-like behavior ensures flow during extrusion.

The deposited and sintered electrode lines were of uniform shape (Fig. A2.1b), and exhibited a homogeneous surface and near-cylindrical rod dimensions very close to the inner nozzle diameter (Fig. A2.4a). Additionally, a constant cross-sectional thickness of approximately 100 μm was obtained. The electrode microstructure was homogeneous with fine pores (< 1 μm) (see inset in Fig. A2.4a).

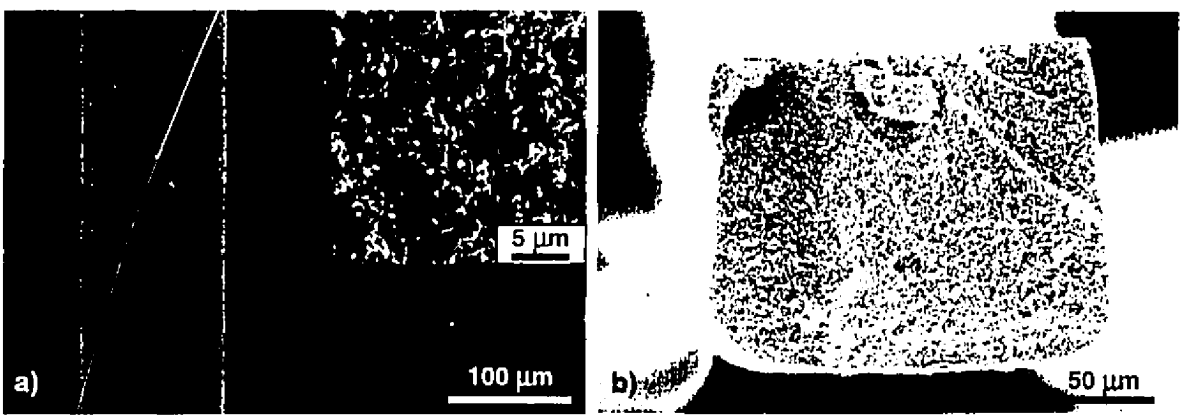

Figure A2.4: SEM images of deposited NiO-YSZ anode after sintering: a) Top view of cylindrical anode. The inset shows a close-up of the anode microstructure. b) Cross-sectional view of rectangular anode.

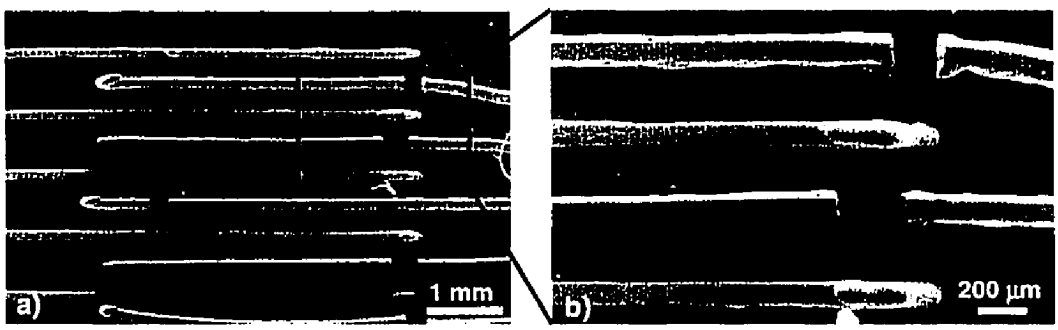

Figure A2.5: SEM images of a) anode and cathode lines in an interdigitated electrode structure, and b) close-up on broken anodes.

The high shape retention of the deposited electrode structures also permitted fabrication of electrodes with square cross-sections, which was not possible with the Newtonian inks, using square microcapillaries for extrusion (Fig. A2.4b).

Complete fuel cells composed of coplanar interdigitated anode and cathode structures were fabricated using the direct-writing technique. Fig. A2.5 shows that the electrode width was very close to the nozzle dimensions for both anode and cathode and that the interelectrode distance ranged between 240 and 270 µm. While the cathode lines adhered well to the YSZ substrate, the anode lines broke and detached from the electrolyte during sintering (Fig. A2.5b).

The difference between the thermal expansion coefficient (CTE) of NiO (14.6×10^{-6} K^{-1}) and YSZ (10.5×10^{-6} K^{-1}) is known to cause stress, cracking and anode delamination during SOFC fabrication and operation [11]. For comparison, the CTE of LSM (12.4×10^{-6} K^{-1}) is much closer to that of YSZ, and LSM sintering on YSZ is less a problem in SOFC fabrication [11]. Although the increased, uniform thickness of the deposited electrodes using viscoelastic gel-like inks compared to Newtonian inks could be beneficial for stable long-term cell operation [3], it also enhances the development of stresses induced by the thermal expansion coefficient mismatch and seems to cause cracking of the NiO-YSZ anode during sintering. Different heating and cooling rates between 1 to 4°C/min were applied, but did not lead to any improvement of the anode bonding. Using a weight to press the anodes firmly down on the YSZ during sintering did not avoid delamination and breakage either. The fabricated SC-µSOFCs could

therefore not be electrochemically tested yet. Further studies will be necessary to find a compromise electrode width that increases the tolerance to thermal stresses and at the same time enables stable long-term cell operation. The sintering issue could also be addressed by adding a porous YSZ layer between the dense YSZ electrolyte and the porous Ni-YSZ anode or by using anodes with a composition gradient along the electrode thickness. Additionally, anode materials with a thermal expansion coefficient similar to that of the electrolyte could be employed in order to avoid anode delamination during sintering. Ni-based anodes were shown to be not sufficiently selective for the fuel reactions during SC-operation [12]. Thus, the use of anode materials with both more compatible thermal expansion coefficient and higher selectivity could improve fabrication and performance of SC-SOFCs with coplanar electrodes.

Conclusions

Single-chamber micro solid oxide fuel cells (SC-μSOFCs) with coplanar electrodes were fabricated using a robot-controlled direct-write microfabrication technique. Compared to previously used electrode inks with Newtonian flow behavior, the use of gel-like, viscoelastic inks enabled the deposition of continuous electrode structures with enhanced control over electrode width, thickness and interelectrode distances. Although reproducibility and homogeneity of the fabricated electrodes could be significantly improved, the challenge of controlling stress-induced cracking and detaching of the anode from the electrolyte due to the thermal expansion mismatch between the two materials needs to be addressed. Nonetheless, the direct-write assembly from viscoelastic, gel-like electrode inks is a promising way to create coplanar electrodes with uniform thickness, improved homogeneity, and improved size and shape control for increased electrochemical performance and stability of SC-μSOFCs.

References

[1] T. Hibino and H. Iwahara, *Chem. Lett.* 7, 1131 (1993).

[2] T. Hibino, K. Ushiki, T. Sato, and Y. Kuwahara, *Solid State Ionics* 81, 1 (1995).

[3] X. Jacques-Bedard, T. W. Napporn, R. Roberge, and M. Meunier, *J. Electrochem. Soc.* 154, B305 (2007).

[4] S.-J. Ahn, J.-H. Lee, J. Kim, and J. Moon, *Electrochem. Solid-State Lett.* 9, A228 (2006).

[5] B. E. Buergler, M. Ochsner, S. Vuillemin, and L. J. Gauckler, *J. Power Sources* 171, 310 (2007).

[6] M. Kuhn, T. Napporn, M. Meunier, S. Vengallatore, and D. Therriault, *J. Micromech. Microeng.* 18, 015005 (2008).

[7] M. Kuhn, T. Napporn, M. Meunier, D. Therriault, and S. Vengallatore, *J. Power Sources* 177, 148 (2008).

[8] S.-J. Ahn, Y.-B. Kim, J. Moon, J.-H. Lee, and J. Kim, *J. Power Sources* 171, 511 (2007).

[9] J. A. Lewis, J. E. Smay, J. Stuecker, and J. Cesarano, *J. Am. Ceram. Soc.* 89, 3599 (2006).

[10] J. A. Lewis, *Curr. Opin. Solid State Mater. Sci.* 6, 245 (2002).

[11] N. Q. Minh, *J. Am. Ceram. Soc.* 76, 563 (1993).

[12] M. Mogensen and K. Kammer, *Annu. Rev. Mater. Res.* 33, 321 (2003).